Stochastic lattice-based models of diffusion in biological systems

Paul R. Taylor
New College
University of Oxford

A thesis submitted for the degree of
Doctor of Philosophy

Trinity 2016

Acknowledgements

I would like to sincerely thank my supervisors, Professor Ruth Baker and Dr Christian Yates. I have benefited enormously from their help and advice, to say nothing of their patience, which kept me on track even when the path to completion seemed insuperable. Both have been extremely generous with their time, especially in providing feedback to vastly improve and clarify earlier drafts of this thesis, and of other writings; I shall certainly remember that, while there are many things one may 'get', equations are not among them.

This work was made possible by a studentship from the Engineering and Physical Sciences Research Council, awarded through the Oxford University Systems Biology Doctoral Training Centre. Additional travel funding was provided by the European Society for Mathematical and Theoretical Biology; l'Institut de Mécanique des Fluides de Toulouse; New College, Oxford; and the Society for Industrial and Applied Mathematics. I acknowledge and appreciate all of these organisations for their financial support.

The Wolfson Centre for Mathematical Biology has provided a convivial and supportive environment for research, and I am grateful to all those who have contributed to its atmosphere. My contemporaries within the group, Lucy Hutchinson, Chris Lester, Marcin Paczkowski, and Robert Ross, deserve particular mention for being such excellent companions through doctoral study, sharing the travails and tribulations of research, as well as furnishing the latest gossip. Thanks are also due to my current and former officemates, Casper Beentjes, Liam Brown, Jochen Kursawe, Shuohao Liao, Aaron Lim, and Linus Schumacher, for their valuable advice, great tolerance, and solidarity against the pigeon menace. I am grateful to Sara Jolliffe for her help navigating Oxford's labyrinth of forms and procedures. Elsewhere in the Mathematical Institute, I have been fortunate to benefit from many fantastic opportunities for public engagement work: Rebecca Cotton-Barratt, Mareli Grady, and Thomas Woolley all have my gratitude for helping me to avoid doing research in a variety of exciting ways and places.

Almost all of the work in this thesis was carried out while living with four superb housemates: Matthew Ashford, Adam Berrington, James Mbewu, and Sam Tusk. Happily our research progressed with greater success than we enjoyed at the Port Mahon, and with more alacrity than we displayed with BSG. Matthew demands additional mention for helpful discussions on the mathematics of reaction rates.

For many other conversations and interactions, occasionally helpful but invariably enjoyable, I thank my friends. I am particularly grateful to Kathryn Atwell, for X5 commiserations; to Isabel Frost, for always providing a listening ear, and wine; to Michael Indian, for steadfastness, and continuing to let me crash on his floor; to Alistair Martin, for demonstrating how to lose most games; to Beth McMillan, for moral guidance; to Anna Muszkiewicz, for academic careers counselling; Will Smith, for demonstrating how to lose the remaining games; to and Ronja Woloszczuk, for providing a facade of culture. Their friendship has been a source of great joy, and I have been privileged to benefit from their support and encouragement.

Finally, but far from least, I remain indebted to my family for their unfailing love and support, and especially to my parents. It looks like they were right about the science thing after all.

Abstract

Diffusion is a universal phenomenon, throughout both biological and physical sciences, and a range of deterministic and stochastic models are available to interrogate diffusion-driven processes. Stochastic models are more computationally intensive to simulate, but may be necessary in situations where deterministic models lead to qualitatively different results.

Stochastic lattice-based position-jump (LBPJ) models are a popular framework for representing diffusion. Particles reside within discrete compartments, and may jump to other compartments or react with other particles sharing the same compartment. When the number of particles to be simulated becomes large, however, the computational costs may grow infeasibly large. In this thesis, we propose two modified LBPJ models, both of which are significantly less computationally intensive to simulate than the standard framework.

The first model uses non-local jumping, allowing particles to move with a distribution of longer but less frequent jumps, rather than jumping exclusively to nearest neighbour compartments. It is seen that boundary conditions must be formulated carefully to maintain agreement with equivalent partial differential equation models.

The second model focuses on LBPJ models incorporating volume exclusion. Two common approaches are 'fully-excluding' models, where at most one particle can occupy each compartment, and 'partially-excluding' models, where larger compartments can contain a finite number of particles. We reconcile these two frameworks, showing that they make similar predictions for the mean and variance of particle numbers. Later chapters extend this work to non-uniform lattices, and consider how reactions between particles can be incorporated into partially-excluding models.

Throughout the thesis, we present mathematical derivations, and support these with the results of computational simulation, validating the agreement of our models' results with results from established modelling frameworks, and demonstrating the reduced computational cost of our approaches in comparison to standard LBPJ models.

Contents

List of Acronyms

CME chemical master equation

CRDME convergent reaction-diffusion master equation

feRDME fully-excluding reaction-diffusion master equation

gRDME generalised reaction-diffusion master equation

HDE histogram distance error

LBPJ lattice-based position-jump

NRM next reaction method

ODE ordinary differential equation

PDE partial differential equation

peRDME partially-excluding reaction-diffusion master equation

RDME reaction-diffusion master equation

SSA stochastic simulation algorithm

vCME excluded volume chemical master equation

vRDME excluded volume reaction-diffusion master equation

wSSA weighted stochastic simulation algorithm

Chapter 1

Introduction

Chemical reactions and diffusion are fundamental to the continued existence of living organisms [1]. The reactions are typically non-linear and, as such, mathematical modelling is invaluable in understanding their behaviour [2]. Mathematical models have been applied to chemical kinetics since the mid-nineteenth century, when ordinary differential equations (ODEs) were used to describe reactant concentrations as continuous variables [3]. Such deterministic, non-spatial ODE descriptions were suitable for the systems studied at the time, which were typically well-mixed and contained large numbers of reactants. It was almost a century before the first probabilistic model of chemical reactions was published in 1940, describing the reacting particles as discrete entities that move and react randomly, and deriving equations to describe the mean and standard deviation of particle numbers [4].

Impetus was given to the development of stochastic modelling by developments in biology. Researchers observed that in processes where the numbers of some reactants are very low, such as gene regulation, the discreteness and stochasticity of the reactions could lead to qualitatively different outcomes to those predicted by a deterministic model. For example, the random time intervals observed between production of promotor proteins can lead to regulatory cascade circuits arriving at different outcomes [5]. Similarly, the importance of spatial effects to some biological systems came to be recognised, as particles cannot always be assumed to be well-mixed within the spatial domain of interest, especially within the crowded confines

of biological cells where mixing may be inhibited by volume-excluding effects [6, 7]. Some simple stochastic models can be solved analytically, but for larger models incorporating multiple reactions and species of particles it is often necessary to simulate the model numerically.

The first stochastic trajectories of a chemical reaction to be simulated and published were carried out in 1971 using a FACOM 230-60 computer, which filled a large room in Kyoto University and had less than a thousandth of the memory capacity and processing speed of a modern smartphone [3, 8]. Soon afterwards, Daniel Gillespie formulated the stochastic simulation algorithm (SSA), the first exact and general algorithm for stochastic simulation of chemical reaction systems [9]. Despite the exponential increase in computing power in the years since, stochastic simulation remains relatively computationally expensive. As the importance of stochastic and spatial effects in biology became more apparent, increasingly large and complex models have been devised, leading to higher computational costs, and growing interest in research into improving the efficiency of simulations [10].

Developing computationally efficient methods for the simulation of spatially-extended models in biology is the focus of this thesis. In the remainder of this chapter we further discuss the importance of stochasticity in biology, lattice-based modelling frameworks for spatially-extended models, and the challenge of simulating models with computationally efficient techniques. We conclude with an overview of the chapters in this thesis.

1.1 Stochastic modelling of reactions

An early application of stochastic approaches to biology modelled the well-studied genetic switch in the λ-phage, suggesting that stochastic fluctuations play an important role in regulating the actions of the phage [11]. More recent work has studied a number of other examples relating to gene-expression, often distinguishing between 'intrinsic noise', arising from the stochastic expression of the gene itself, and 'extrinsic noise', from environmental factors such as varying temperatures and levels of

other molecules in the cell [12, 13]. Some fluctuations can be extremely significant due to the small numbers of molecules involved [14]: a cell may only contain (on average) a few copies of some key reaction species, such as promoter sites for genes, and certain proteins [15].

Indeed, one of the fascinations of biology is the way in which natural selection has resulted in organisms that can not only survive and tolerate noise [16], but can actively regulate and exploit it for their benefit [17]. It has been suggested that biological cells can be considered 'antifragile', because they benefit from a certain level of randomness, with consequences for practitioners of synthetic biology [18]. Excessive levels of noise can be harmful, precluding the proper functioning of the organism, and potentially even leading to unwanted side-effects like cancerous growths, but moderate levels of noise allow the system to respond flexibly to unpredictable future circumstances [19].

From a mathematical perspective, noisy systems can exhibit very different properties and behaviours to deterministic systems. For example, we can observe stochastic bistability and bifurcations where, due to the effect of noise, fixed parameter regions exhibit varying numbers of equilibria with different values compared to the analogous deterministic system [20, 21]. Other examples include cases where stochastic fluctuations can make a gradual response mechanism behave like a threshold mechanism (stochastic focussing) [22], and can boost a weak input signal in a threshold system (stochastic resonance) [23, 24].

In this thesis we focus on the role of this stochasticity at the level of chemical reaction-diffusion systems, but randomness also plays an important role at higher levels, including the collective movement of organisms [25, 26], population dynamics [27, 28, 29], and biological evolution itself [30].

Many of the stochastic effects discussed so far can be observed in both spatial and non-spatial models, but other effects are distinctive to spatial models. Taking the well-studied case of Turing patterning as an example, it has been known for some time that the parameter space which allows for pattern formation is very restricted in the classical, deterministic version of the model, and this has been a common

criticism of its relevance to biology [31]. When stochastic versions are implemented, however, including both stochastic cell growth and noise intrinsic to the reactions, the resulting system can form a variety of patterns over a much wider range of parameter values [32, 33], but will not necessarily be so robust in the sense of reliably forming the same patterns [34]. It can therefore be important to use models capable of incorporating both stochastic effects and reactant concentrations that vary across the spatial domain of interest.

1.2 Lattice-based position-jump models

A range of modelling frameworks incorporating stochasticity have been applied to reaction-diffusion systems, including individual-based models [35] and stochastic differential equations [36]. In this thesis we develop lattice-based position-jump (LBPJ) models. In the LBPJ framework, described in greater detail in Section 2.1, the domain is divided into a lattice of discrete subdomains, or 'compartments'. It is assumed that each of these compartments is well-mixed, so that particles are uniformly distributed within the compartment they occupy. Molecules can move to adjacent compartments, or interact with other molecules sharing the same compartment. The evolution of the system is described by the reaction-diffusion master equation (RDME), and it can sometimes be valuable to take the continuum limit of the RDME to obtain a mean field description in terms of partial differential equations (PDEs) [37]. This deterministic limit should be interpreted with caution, however. There are cases where discretized, lattice-based models have been shown to produce qualitatively different results from the results of their corresponding continuous description [38], and when a continuous description is appropriate it must be chosen carefully to avoid error [39].

Their intuitive structure and relative ease of implementation make LBPJ models well suited for interdisciplinary research. Many of the examples in this thesis involve single-file diffusion, a volume-excluding LBPJ model in one spatial dimension. This class of model is of particular relevance to biological processes such as the diffusion

of αTAT1 within microtubules [40], the movement of flagellin in the formation of bacterial flagella [41], and the dispensing of proteins through in the nanochannels of drug delivery devices [42]. Other examples of single-file movement, where particles move non non-diffusively, are ion channels and the motion of motor proteins over microtubules; the motile particles in all these cases are approximately 1-10nm in diameter [43]. There has also been significant interest in the application of LBPJ models to processes such as embryonic development [44, 45], cancer metastasis [46], wound healing [47], tissue engineering [48] and biological invasions [49]. Similar models have also been applied to areas such as animal dispersal [50], and recently to the evolution of social behaviours [51].

Simultaneously, other researchers have worked on refining and extending the theoretical framework of LBPJ models. Developments include results for implementing particle diffusion on unstructured meshes and irregular geometries [52, 53, 54], and on dynamic, growing domains [55], as well as formulations of LBPJ systems incorporating bimolecular reactions that converge to analogous, spatially continuous models [56]. Hybrid methods combining LBPJ models with other frameworks, such as PDEs [57], and Brownian dynamics [58], have also been developed.

Since Gillespie first suggested how the SSA could be used to simulate an LBPJ model [9], there have been several developments along similar lines, implementing diffusive movement in slightly different ways [59, 60]. LBPJ models are a relatively efficient technique for implementing stochastic models of reaction and diffusion, but, as with all stochastic models, they become computationally intensive as the number of particles, reactant species and potential reactions increases. The challenge of simulating large stochastic models has led to significant work on computationally efficient stochastic simulation algorithms and models in recent years.

1.3 Efficient stochastic simulation

The computational time required to simulate a particular model can be thought of as the product of three factors: i) the number of instantiations of the stochastic model

necessary to produce sufficient results; ii) the number of events occurring in each instantiation of the stochastic model; and iii) the time taken to sample an individual event, implement it, and update event propensities accordingly. Existing work has sought to save time by reducing all three factors.

The first of these approaches, reducing the number of instantiations of the model required, is the least common. One recent significant development has been the introduction of multi-level simulation algorithms to discrete-state systems, including biological models. Multi-level algorithms estimate system statistics efficiently by combining the results from simulations of different accuracies in a telescoping sum: only a few computationally expensive, precise instantiations are used, supplemented by results from computationally cheap, less precise instantiations [61, 62, 63]. Another noteworthy development has been the introduction of the weighted stochastic simulation algorithm (wSSA) to study rare events [64]. By definition, it would normally be necessary to instantiate a model many times before a significant number of rare events are observed, and so estimating the probability of such an event occurring would be computationally expensive. The wSSA alters reaction propensities to bias the model towards the occurrence of rare events, then corrects for this bias in its final estimate of the event's likelihood, so that fewer instantiations of the model are required to observe a statistically significant number of events. Several refinements of the wSSA have been published, such as a version able to quantify the error associated with the predicted event probability [65].

Large time savings can also be obtained by making certain approximations, sacrificing the exact nature of the SSA for large reductions in computational cost. This is the second approach we consider here, reducing the number of individual events that are simulated over the course of the sample path. The earliest example of this approach is τ-leaping [66], which advances by discrete time steps, whose length is judged so that particle numbers do not change significantly over any single step, then estimating how many particles moved or reacted during that time.

Variations such as implicit τ-leaping [67], and improvements in efficient step size selection [68], have been proposed to further develop the τ-leaping approach. A less

common approach is R-leaping, which is similar to τ-leaping. Instead of jumping forward a given time step then determining which reactions occurred, R-leaping jumps forward a given number of reactions of a given reaction channel and then determines how large a time step was required [69]. The multinomial simulation algorithm combines τ-leaping with the SSA: in spatially-extended systems diffusion events are typically much more frequent than reaction events, so an approximate simulation algorithm is used for particles moving between compartments, while an exact algorithm is used for reactions within compartments [70]. Other innovations include cancelling opposing reaction and diffusion events [71], and using adaptive mesh refinements to focus computational resources efficiently on important regions of the domain [72].

The third and final approach to be considered here, reducing the computational cost of each event in a simulation, has led to a number of algorithms that are computationally cheaper than the original Gillespie SSA while remaining mathematically equivalent. One of the earliest and most successful algorithms proposed has been the next reaction method (NRM) [73]. The NRM drastically reduces the computational cost of a simulation by recalculating reaction propensities as seldom as possible, and reusing predicted times until reactions occur (scaled where necessary) rather than generating large numbers of random numbers whenever an event occurs. A related approach of particular applicability for spatially-extended systems is the next subvolume method, which combines the NRM with more traditional SSA techniques for LBPJ models where the reactants are divided between multiple spatial compartments [7]. Other algorithms have reduced the time required to check the list of possible reactions and determine which one is to be implemented next. The optimised direct method achieves this by running some preliminary instantiations of the model, then assembling a list of reactions in which the most frequently occurring ones are checked first [74]; the sorting direct method works similarly, but rearranges the list of reactions dynamically [75]. Meanwhile, the logarithmic direct method introduces binary searching, which finds entries at any position in a list relatively quickly [76]. Accelerations can also be achieved by recycling random numbers, which

are computationally expensive to generate [10].

The techniques listed in this section are far from exhaustive, and demonstrate the importance attached by researchers to developing computationally efficient stochastic simulation techniques. In this thesis, we focus on the second approach, reducing the number of events (specifically jump events) that occur in each instantiation of a stochastic model.

1.4 Thesis overview

The aim of this thesis is to develop computationally efficient methods for the simulation of stochastic LBPJ models of diffusion. We use a combination of analytical argument and numerical simulation to compare the predictions of our methods to those made by established models, confirming their agreement and demonstrating significant savings in computational time. We now highlight some open problems in the area, which this thesis aims to resolve.

1.4.1 Non-local jump models

At present most LBPJ models allow only purely local jumping, so that a particle can travel only to a nearest neighbour compartment [77], while others introduce a transition matrix approach, whereby any particle can jump to any compartment with some set probability [78]. The mean particle numbers predicted by local jumping models correspond to the results of the PDE diffusion equation, but results from the transition matrix approach cannot be reconciled with PDE models [78]. In Chapter 2 we investigate whether an intermediate approach is possible, wherein particles can make jumps of non-local but limited range, while still predicting results which are in agreement with a corresponding PDE model. This would significantly speed up the simulation of LBPJ models, since fewer jump events would need to be simulated. Since boundary conditions are integral to PDE models, it is also important to ask whether analogous conditions could be imposed on a non-local jumping LBPJ model.

We demonstrate that allowing particles to jump to non-nearest neighbour com-

partments can lead to shorter simulation times relative to an equivalent local jumping model, while generating results which are in agreement with both local jumping models and the corresponding PDE.[1] We also derive appropriate boundary conditions for LBPJ models that correspond to those for the corresponding PDE, and present simulation results showing the correspondence of non-local jumping models to both local jumping models and to the solutions of PDEs.

1.4.2 Reconciling exclusion effects at different spatial scales

Having considered how to replace frequent, short jumps with fewer, longer jumps in Chapter 2, we move on to compare LBPJ simulations at different spatial scales in Chapter 3, paying particular attention to volume exclusion effects. Existing LBPJ models incorporate volume exclusion in two different ways: 'fully-excluding' systems, where at most one particle can occupy each compartment, and 'partially-excluding' systems, which have a maximum capacity and reject incoming particles with some probability that is a function of its current capacity.

Coarser, partially-excluding models are computationally faster to simulate than fully-excluding models, because particles less frequently when compartments are larger. To date, there has been no attempt to reconcile the two modelling regimes. In this chapter, we therefore investigate whether both regimes make similar predictions about the mean and variance of particle numbers, to determine whether savings in computational time can be achieved by replacing fully-excluding models with partially-excluding ones.

Our contribution here is to reconcile, for the first time, the mathematical descriptions these different representations provide, and to demonstrate how the properties of coarser, partially-excluding lattices can be replicated by an aggregation of compartments on finer, fully-excluding lattices. Specifically, we present arguments for the mean and variance of particle numbers in partially-excluding compartments matching the mean and variance of particle number in a corresponding group of fully-

[1]The reported times taken to run particular simulations in Chapters 2, 3 and 4 were observed for code written in Matlab, running on an AMD Phenom^{TM} II X4 925 Processor.

excluding compartments. These conclusions are supported by simulations, where partially-excluding models are seen to run significantly faster than comparable fully-excluding models.

1.4.3 Hybrid fully/partially-excluding methods

Chapter 4 continues our work reconciling the mean and variance behaviour of particle numbers in fully- and partially-excluding models, extending and generalising results for uniform lattices to apply to non-uniform lattices. Many models of biological systems include spatial regions where fully-excluding compartments are necessary to maintain accuracy, but other regions where partially-excluding compartments could be adopted to save computational time without impacting on the accuracy of the model. It is therefore natural to ask whether the results obtained for uniform lattices in the previous chapter can be generalised to non-uniform lattices. Particular attention is given to interfacing distinct fully- and partially-excluding regions of a domain, using two different hybrid methods. We test the different models in a range of scenarios to confirm the agreement of their results, further supporting the value of partially-excluding models, both uniform and hybrid. A final set of simulations investigate a simple multi-species system, where different mixing behaviour leads to the fully- and partially-excluding models predicting different means and variances of particle numbers; both hybrid methods are seen to replicate the results of the fully-excluding model, however, while requiring less computational time.

1.4.4 Incorporating reactions

Our results in Chapters 3 and 4 are obtained for diffusive models of inert particles. In Chapter 5, we consider reactions, especially bi-molecular reactions between pairs of particles, and how they can be implemented within the framework of fully- and partially-excluding modelling. We are particularly motivated to determine the circumstances under which fully- and partially-excluding models predict similar average times until a reaction occurs. We begin by defining reaction rates for fully-excluding models, then use combinatorial arguments to obtain corresponding rates for reac-

tions within partially-excluding models, and within non-spatial models. Fully- and partially-excluding models are then compared to one another, and to non-spatial models, for a range of reactions, using a combination of analytical results and simulation. It is shown that, when particles diffuse quickly and remain well-mixed, all modelling frameworks give similar descriptions of reactive systems. We also study pathological examples, where fully-excluding models in one spatial-dimension predict longer inter-reaction periods due to a lack of particle mixing.

1.4.5 Concluding discussion

We conclude this thesis in Chapter 6 with a short discussion. We summarise the results obtained in the course of our work, and consider the opportunities for future work extending these results.

Chapter 2

Non-local jump models

In this chapter we extend the LBPJ approach to enable the approximation of large numbers of particle jumps between adjacent compartments with fewer, longer jumps, over more than one compartment. By reducing the number of jump events occuring, simulations can be accelerated. We begin by outlining the basic model, and then detail our extensions of it.

The majority of the work in this chapter, and in the corresponding appendices (A.1, A.2 and A.3), appears in the paper 'P.R. Taylor, R.E. Baker and C.A. Yates, Deriving appropriate boundary conditions of, and accelerating position-jump simulations of, diffusion using non-local jumping, *Physical Biology*, **12** (2015) 016006', and is reproduced with permission from IOP Publishing Ltd [79].

2.1 Local position-jump models

We begin by defining a spatial lattice over the one-dimensional domain $x \in [0, L]$ composed of K compartments of width $\Delta x = L/K$, as shown in Figure 2.1, such that the centre of the i^{th} compartment is located at $x_i = (2i-1)\Delta x/2$, for $i = 1, \ldots, K$. The number of particles in the i^{th} compartment at time t is denoted $n_i(t)$, and we assume that all particles are point particles with no physical extension, so that an unlimited number can reside in the same compartment. We write $M_i(t)$ to denote the expected value of $n_i(t)$, so that the mean of particle numbers over this domain

is given by the vector $\mathbf{M}(t) = [M_1(t), M_2(t), ..., M_K(t)]$.

A particle in any given compartment may only move to directly adjacent compartments, so for $2 \leq i \leq K-1$, particles in compartment i are permitted to jump to compartments $i-1$ or $i+1$, with non-negative rates per unit time of T_i^- and T_i^+, respectively. When the jump rates are independent of particle number, the mean

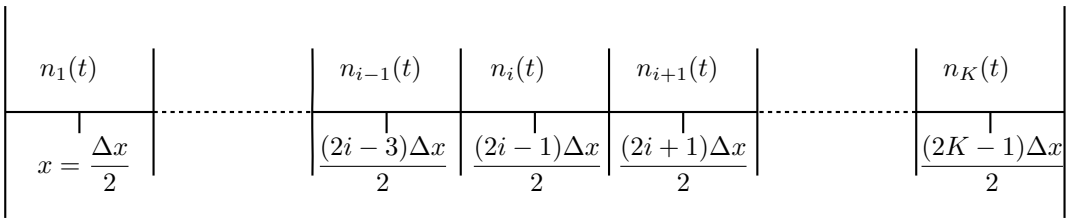

Figure 2.1: A representation of the spatial lattice for the individual-based stochastic model.

number of particles in compartment i evolves according to [37]

$$\frac{\mathrm{d}M_i}{\mathrm{d}t} = T_{i-1}^+ M_{i-1} - (T_i^+ + T_i^-)M_i + T_{i+1}^- M_{i+1}. \tag{2.1}$$

This is a standard result, and used without proof throughout this chapter, though we do discuss its derivation in Section 3.2.1.

2.1.1 Continuum approximations

We now introduce a continuous function $u(x,t)$ as a continuum approximation to these discrete values, such that

$$M_i(t) \approx u\left(x_i, t\right). \tag{2.2}$$

There are several factors that might cause the jump rates to vary spatially, such as the adhesive properties of particles in adjacent compartments, or (in the case of cell migration) the relative concentrations of signalling molecules [37, 80, 81]. In other models (such as the excluding processes discussed in Chapter 3) movement is restricted by blocking attempted jumps with a probability that is a function of the destination compartment's current occupancy, and usually limits the total number

of particles occupying each compartment to some predetermined maximum [82]. For now, however, we will assume that jump rates are independent of both time and position, and that any number of particles may share the same position, so we drop the subscripts and write simply T^+ and T^-. The right-hand side of equation (2.1) can be expanded using Taylor series about x, leading to

$$\frac{\partial u(x,t)}{\partial t} = \Delta x \frac{\partial u(x,t)}{\partial x}(T^- - T^+) + \frac{\Delta x^2}{2}\frac{\partial^2 u(x,t)}{\partial x^2}(T^- + T^+) + o((\Delta x)^2). \quad (2.3)$$

Note that in the unbiased case, where $T = T^- = T^+$, the first order terms cancel (we discuss biased jumping in Section 2.6). Defining $T = D/(\Delta x)^2$ is consistent with diffusive movement [83], and taking the limit $\Delta x \to 0$, we recover the diffusion equation,

$$\frac{\partial u}{\partial t} = D\frac{\partial^2 u}{\partial x^2}. \quad (2.4)$$

We note that the models considered for diffusion in this chapter are linear, and so an equivalent diffusion equation can be obtained to describe the probability density for the position of a diffusing particle. In later chapters, we consider non-linear volume-excluding models, where the diffusion equation can still be recovered as the limit of the mean equations, but does not accurately describe the probability density for the position of a given particle.

2.1.2 Chapter outline

We wish to find non-local jump rates (i.e. rates at which particles jump to non-neighbouring compartments) that will produce the same stochastic mean profile as the local jump rates when used in a simulation. Adopting these rates allows us to speed up simulations of motile particles since fewer events need to be simulated. In Section 2.2, we use Taylor expansions of the equations for mean particle numbers to find appropriate non-local jump rates. The use of these non-local jump rates is seen to have implications for the implementations of boundary conditions, and we consider how to implement Robin and flux boundary conditions in non-local jump

processes in Sections 2.3 and 2.4, respectively. In Section 2.5 we consider hybrid models, using non-local jump rates for particles in some compartments, while using local jump rates for particles elsewhere in the domain.

The majority of work in this chapter exclusively considers jumping without directional bias, but biased random walks are also valuable when modelling biological phenomena. We therefore consider biased movement in Section 2.6, and how directional bias affects our implementation of boundary conditions. In Section 2.7 we investigate the divergence of the predictions of non-locally jumping models from those of locally jumping and PDE models when the maximum jump length becomes excessively large, while in Section 2.8 we briefly investigate the effect of non-local jumping on the variances of particle number. Throughout the chapter, we use simulations to illustrate both the accuracy of our derivations, and the reduced computational cost of interrogating non-locally jumping models compared to an equivalent locally jumping model. The concluding discussion in Section 2.9 considers the potential for reduced computational costs in more detail.

2.2 Non-local jumping

To find appropriate non-local jump rates, we will Taylor expand the master equation for the mean number of particles in one compartment of a non-locally jumping system, and compare the second order terms (i.e. those $O((\Delta x)^2)$) to those of the local model.

For a non-local jump process, we write the rates of a jump q compartment-lengths to the left or to the right from position i as T_i^{-q} or T_i^{+q}, respectively. Jumps for which $q = 1$, i.e. jumps to adjacent compartments, are written $T_i^{\pm 1}$ to distinguish them from $T_i^{\pm}$, the rates for the local jump process. The mean number of particles in the i^{th} compartment, where $Q < i \leq K - Q$, will then evolve according to

$$\frac{\mathrm{d}M_i}{\mathrm{d}t} = \sum_{q=1}^{Q} T_{i-q}^{+q} M_{i-q} - \sum_{q=-Q, q\neq 0}^{Q} T_i^q M_i + \sum_{q=1}^{Q} T_{i+q}^{-q} M_{i+q}. \tag{2.5}$$

By assuming position independence again (i.e. $T_i^{\pm q} = T^{\pm q}$), and Taylor expanding about x, we obtain

$$\frac{\partial u(x,t)}{\partial t} = -\Delta x \frac{\partial u}{\partial x}(x,t) \left(\sum_{q=-Q, q\neq 0}^{Q} qT^q \right) + \frac{(\Delta x)^2}{2} \frac{\partial^2 u}{\partial x^2}(x,t) \left(\sum_{q=-Q, q\neq 0}^{Q} q^2 T^q \right) + o((\Delta x)^2). \tag{2.6}$$

Note again that in the unbiased case, where $T^{+q} = T^{-q} = T^q$, the first order terms cancel. We compare the second order term to that of equation (2.3) and obtain the equivalence condition

$$T = \sum_{q=1}^{Q} q^2 T^q. \tag{2.7}$$

For example, for a non-local jumping process with $Q = 2$, this condition is

$$T = T^1 + 4T^2. \tag{2.8}$$

Clearly there are an infinite number of rate choices that satisfy this relationship, but we will specify the basic non-local jumping rate as

$$T^q = \frac{T}{Qq^2}, \tag{2.9}$$

where T is the jumping rate from the equivalent, local process (we discuss some alternatives in Section 6.2.2). This satisfies equation (2.7) above, and also preserves the well-known relation that the mean squared displacement, $\langle x^2 \rangle$, of a particle scales linearly with time in a diffusion process. For example, doubling the jump distance reduces the rate at which jumps will occur by a factor of four. In Figure 2.2, we illustrate the jump rates for $Q = 2$ and $Q = 3$.

2.2.1 Example

To illustrate the accuracy of our non-local jumping model, and its potential to save computational time, we compare $1,000$ simulations of a local jump process to $1,000$ simulations of a non-local jump process where $Q = 5$. In each simulation, we used a Gillespie style algorithm, generating exponentially distributed times between jumps,

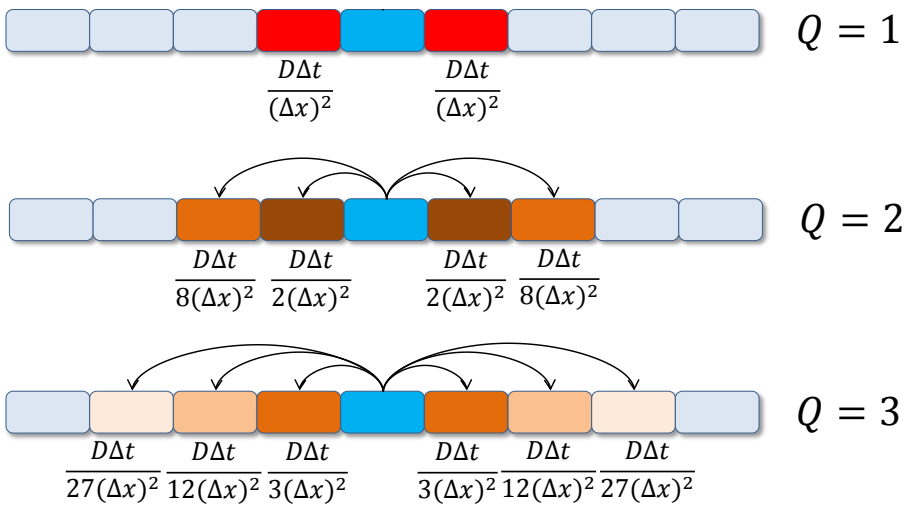

Figure 2.2: In the local jumping case, $Q = 1$, particles move to adjacent compartments in $(t, t + \Delta t]$ with jump probabilities $D\Delta t/(\Delta x)^2$, as shown in the first diagram. The equivalent non-local jump rates for $Q = 2$ and $Q = 3$ are illustrated in the second and third diagrams, respectively.

and uniformly distributed random numbers to select the jumping particle and determine its destination.

The domain $x \in [0, 5]$ was divided into 50 compartments of width $\Delta x = 0.1$. We imposed periodic boundary conditions, and set $D = 1$, initializing $1,800$ particles in a tent function centred around $x = 2.5$, so that our initial condition was

$$n_i(0) = \begin{cases} (i - 17) \times 25, & \text{for } 18 \leq i \leq 25, \\ 200 - ((i - 26) \times 25), & \text{for } 26 \leq i \leq 33, \\ 0, & \text{otherwise}, \end{cases} \tag{2.10}$$

as shown in Figure 2.3(a). These particles were then permitted to diffuse freely until time $t = 1$. Each repeat of the non-local simulation ran in an average of 11.7 seconds, compared to an average of 39.1 seconds for each repeat of the local simulation. Inspection of the mean compartment occupancies of the non-local and local simulations at $t = 1$, and comparison to the solution of the diffusion equation, (2.4), in Figure 2.3(c) shows the quality of the fit, with all three models matching well throughout the domain. We quantify this fit in Figure 2.3(b) using the histogram

distance error (HDE) metric, which is given by

$$\text{HDE} = \frac{1}{2}\sum_{k=1}^{K} |\tilde{M}_k - p_k|, \tag{2.11}$$

where $\tilde{M}_k$ is the mean number of particles in compartment k normalised against the total number of particles in the system, and p_k is the total number of particles predicted at $x = x_k$ by the PDE solution, normalised so that the sum of p_k over all integer values of k between 1 and K inclusive is equal to unity [84]. The HDE of two datasets will always therefore fall between zero and unity inclusive. Averaged simulation results were compared to the solution of the diffusive limit PDE (2.4), solved using Matlab's `pdepe` function. There is a small initial peak in the HDE of the results obtained from non-local jumping, but this diminishes by the end of the simulation. The final HDE for the non-local jumping results is small, both in absolute terms (less than 0.005, corresponding to less than 0.5% disagreement with the PDE) and relative to the HDE for the local jumping results, as can be observed in Figure 2.3(b). Having found a condition to match the mean results of a locally jumping process to those of a non-locally jumping process, and validated this condition with some preliminary simulations, we will now consider how to implement other, non-periodic, boundary conditions.

2.3 Implementing a Robin boundary condition

Boundaries appear in models of biological systems in a range of forms. An inert boundary, such as the edge of a petri dish, may be represented by a simple no-flux boundary condition [85]. By contrast, some biological boundaries, such as a cell membrane partially-covered with receptors, are reactive and may remove particles from the system upon contact [86].

The first-order reactive boundary condition for the diffusion equation at $x = 0$

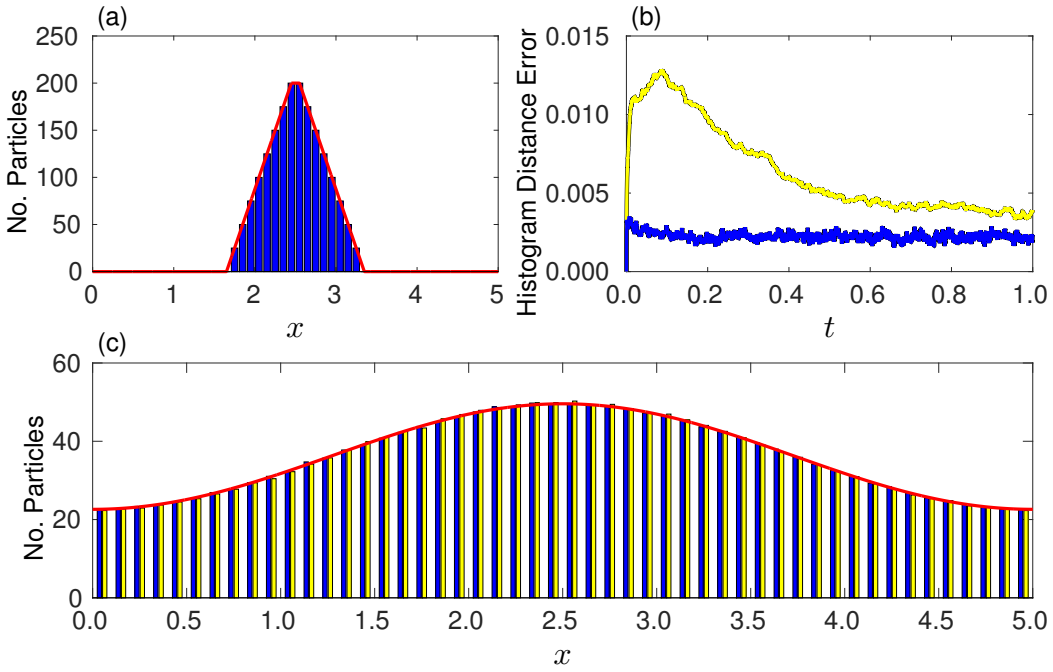

Figure 2.3: Averaged results of $1,000$ realisations of a local jump process and $1,000$ realisations of a non-local jump process with $Q = 5$, in the time interval $t \in [0, 1]$ with periodic boundary conditions at $x = 0$ and $x = 5$. (a) At time $t = 0$, we initialise $1,800$ particles in a tent function centred on $x = 2.5$. In (c), it can be seen that the mean occupancy of compartments in the non-local process (yellow bars) matches well to both the mean occupancy of compartments in the local process (blue bars) and the PDE solution (red line) at time $t = 1$. The accuracy is confirmed by a HDE comparison of the local and non-local simulations to the solution of the limiting PDE (b).

is given by the Robin (sometimes called 'radiation') boundary condition,

$$D\frac{\partial u}{\partial x}(0,t) = Ru(0,t), \tag{2.12}$$

where $R = 0$ describes a completely reflective boundary condition, $R = \infty$ a completely absorbing one, and intermediate values a boundary condition that sees some particles reflected and others absorbed.

2.3.1 The $Q = 1$ case

The constant jumping probability during some infinitessimally small time Δt is set to be $D\Delta t/(\Delta x)^2$ for the local case. A reactive boundary condition at the left-hand boundary is implemented by specifying that any particle at $x_1(t) = \Delta x/2$ that attempts to jump left is either reflected back to $\Delta x/2$ with probability $1 - P_{1,1}\Delta x$ or removed from the system with probability $P_{1,1}\Delta x$ (we write all adsorption probabilities in the form $P_{q,Q}\Delta x$, where q is the length of the jump and Q the maximum jump length of the system).

The mean number of particles in the first compartment at time $t + \Delta t$ is given by

$$M_1(t+\Delta t) = \left(1 - \frac{2D\Delta t}{(\Delta x)^2}\right) M_1(t) + \frac{D\Delta t}{(\Delta x)^2}\left[M_2(t) + (1 - P_{1,1}\Delta x)M_1(t)\right]. \tag{2.13}$$

After rearranging, and multiplying through by $\sqrt{\Delta t}$ this becomes

$$\sqrt{\Delta t}\left(\frac{M_1(t+\Delta t) - M_1(t)}{\Delta t}\right) = \frac{D\sqrt{\Delta t}}{\Delta x}\left(\frac{M_2(t) - M_1(t)}{\Delta x} - P_{1,1}M_1(t)\right). \tag{2.14}$$

Taking the diffusive limit (i.e. $\Delta t \to 0$, $\Delta x \to 0$ such that $\sqrt{\Delta t}/\Delta x$ remains constant), the left-hand side vanishes, and we arrive at

$$D\left.\frac{\partial u}{\partial x}\right|_{x=0} = DP_{1,1}u(0,t). \tag{2.15}$$

Comparison with equation (2.12) gives [87]

$$P_{1,1} = R/D. \tag{2.16}$$

2.3.2 Extending to the $Q = 2$ case

Using the formula stated in equation (2.9) to relate the diffusion constant, D, to the transition rates, in the case where $Q = 2$, we find that $D/2(\Delta x)^2$ describes the rate of jumping to a neighbouring lattice site, and $D/8(\Delta x)^2$ the rate of jumping two lattice sites. In this section, and for the rest of this chapter, we discuss implementing boundary conditions at the left-hand boundary without loss of generality.

We require two adsorption terms, $P_{1,2}$ for when a molecule hits the boundary as a result of a length-one jump, and $P_{2,2}$ for when the contact results from a length-two jump. Furthermore, as before, we consider that the actual boundary is located at $x = 0$, $\Delta x/2$ left of x_1. In the local case, particles moving left from x_1 will move $\Delta x/2$ left before hitting the boundary and being reflected back $\Delta x/2$ to the right, finishing at x_1 where they began. Analogously, in the non-local case, reflection therefore requires the particle to move leftwards as far as x_1, then to make a further move of total length Δx to the boundary and back. If this is less than the total length of the jump, all remaining movement takes place in the rightwards direction, as shown in Figure 2.4. So a leftwards length-two jump left from compartment 1 will end up in compartment 2, and a length-two jump from compartment 2 will end up in compartment 1 (assuming neither is adsorbed at the boundary). Then the equation for mean particle numbers at x_1 is given by

$$\begin{aligned} M_1(t+\Delta t) = \quad & \left(1 - \frac{2D\Delta t}{2(\Delta x)^2} - \frac{2D\Delta t}{8(\Delta x)^2}\right) M_1(t) + \frac{D\Delta t}{2(\Delta x)^2}\left(M_2(t) + (1 - P_{1,2}\Delta x)M_1(t)\right) \\ & + \frac{D\Delta t}{8(\Delta x)^2}\left(M_3(t) + (1 - P_{2,2}\Delta x)M_2(t)\right), \end{aligned} \tag{2.17}$$

which can be rearranged to give

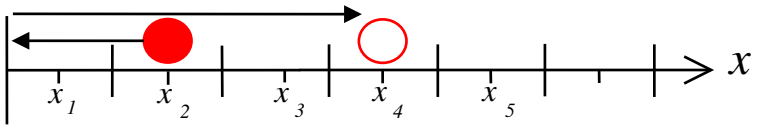

Figure 2.4: A particle (solid red circle) at x_2 attempts to make a length-five jump leftwards. After moving $3\Delta x/2$ to the left it hits the boundary and is reflected, travelling the remaining $7\Delta x/2$ to the right to finish in x_4 (empty red circle).

$$\frac{M_1(t+\Delta t)-M_1(t)}{\Delta t} = \frac{D}{(\Delta x)^2}\left[\left(\frac{-3-2P_{1,2}\Delta x}{4}\right)M_1(t) + \left(\frac{5-P_{2,2}\Delta x}{8}\right)M_2(t) + \frac{1}{8}M_3(t)\right]. \tag{2.18}$$

We then multiply through by $\sqrt{\Delta t}$, and rearrange the terms to arrive at

$$\begin{aligned}\sqrt{\Delta t}\left(\frac{M_1(t+\Delta t)-M_1(t)}{\Delta t}\right) = \; & D\left[\frac{\sqrt{\Delta t}}{8}\left(\frac{M_1(t)-2M_2(t)+M_3(t)}{(\Delta x)^2}\right)\right. \\ & -\frac{\sqrt{\Delta t}P_{2,2}}{8}\left(\frac{M_2(t)-M_1(t)}{\Delta x}\right) \\ & +\frac{7\sqrt{\Delta t}}{8h}\left(\frac{M_2(t)-M_1(t)}{\Delta x}\right) \\ & \left.+\frac{\sqrt{\Delta t}}{8h}\left(-P_{2,2}-4P_{1,2}\right)M_1(t)\right].\end{aligned} \tag{2.19}$$

We now take the limit as $\Delta t, \Delta x \to 0$ while keeping the ratio $\sqrt{\Delta t}/\Delta x$ constant. All the terms of equation (2.19) apart from the adsorption terms have been arranged into discretizations of exact derivatives, so the left-hand side, and the first two lines of the right-hand side vanish due to the presence of $\sqrt{\Delta t}$ terms. The remaining terms from the final line give

$$7\left.\frac{\partial u}{\partial x}\right|_{x=0} = (4P_{1,2}+P_{2,2})u(0,t). \tag{2.20}$$

Recalling the definition of the Robin boundary condition from equation (2.12), this reduces to

$$7R = D(4P_{1,2}+P_{2,2}). \tag{2.21}$$

Clearly this is not sufficient to specify $P_{1,2}$ and $P_{2,2}$ uniquely, so we examine the

dynamics at $M_2(t)$:

$$\begin{aligned} M_2(t+\Delta t) = & \left(\frac{D\Delta t}{2(\Delta x)^2} + (1 - P_{2,2}\Delta x)\frac{D\Delta t}{8(\Delta x)^2}\right) M_1(t) \\ & + \left(1 - \frac{2D\Delta t}{2(\Delta x)^2} - \frac{2D\Delta t}{8(\Delta x)^2}\right) M_2(t) \\ & + \frac{D\Delta t}{2(\Delta x)^2} M_3(t) + \frac{D\Delta t}{8(\Delta x)^2} M_4(t). \end{aligned} \tag{2.22}$$

Simplifying, we find

$$\begin{aligned} \frac{M_2(t+\Delta t) - M_2(t)}{\Delta t} = & \frac{D}{8}\frac{1}{(\Delta x)^2}\left[(5 - P_{2,2}\Delta x)M_1(t) - 10M_2(t) + 4M_3(t) + M_4(t)\right] \\ = & \frac{D}{8}\left(\frac{M_2(t) - 2M_3(t) + M_4(t)}{(\Delta x)^2}\right) \\ & + \frac{6D}{8}\left(\frac{M_1(t) - 2M_2(t) + M_3(t)}{(\Delta x)^2}\right) \\ & - \frac{P_{2,2}D}{8h}M_1(t) + \frac{D}{8h}\left(\frac{M_2(t) - M_1(t)}{\Delta x}\right). \end{aligned} \tag{2.23}$$

Again, upon multiplying by $\sqrt{\Delta t}$ and taking the diffusive limit as before, the left-hand side and the first two lines of the right-hand side go to zero. The remaining terms give

$$D\left.\frac{\partial u(x,t)}{\partial x}\right|_{x=0} = P_{2,2}Du(0,t), \tag{2.24}$$

which, recalling the Robin boundary condition in equation (2.12), gives us the adsorption rate for length-two jumps,

$$P_{2,2} = \frac{R}{D}. \tag{2.25}$$

Substituting this into the relationship derived by considering the dynamics at $M_1(t)$, equation (2.21) requires that the adsorption rate for length-one jumps be

$$P_{1,2} = \frac{3R}{2D}. \tag{2.26}$$

Since $P_{1,2}\Delta x$ is a probability, it must be between zero and one in value, and we

therefore note that this result imposes the constraint

$$0 \leq \Delta x \frac{R}{D} \leq \frac{2}{3}. \tag{2.27}$$

Hence for a given lattice and diffusion rate our choice of R is restricted or, conversely, if a value of R has been specified then our choice of compartment size, Δx, must be sufficiently small to satisfy this inequality. A similar constraint is observed in the local jumping implementation, but the condition becomes more restrictive in the non-local case as Q increases (in Section 4.6.2 of Chapter 3 we show how the Robin boundary condition can be reconceptualised to avoid this case in a locally jumping system).

We note that it is also possible to derive a non-local implementation of a Robin boundary condition in which the adsorption rates depend on the position that the reflecting particle is jumping from, rather than the length of the jump that took it to the boundary. In this $Q = 2$ case, we would then have to require that particles jumping from the first compartment be absorbed with probability $R\Delta x/D$, and particles from the second compartment with probability $3R\Delta x/D$. Since the larger of these probabilities here is greater than in the length-dependent case, it places a greater constraint on allowable values of R, D and Δx. We therefore proceed by assuming that adsorption probabilities depend on the distance a particle is travelling, and not on its compartment of origin.

2.3.3 Generalised adsorption rates for any value of Q

The method used to derive the adsorbing boundary condition in the $Q = 2$ case (i.e. rearranging terms into second derivatives that will vanish in the diffusive limit until only terms for x_1 and x_2 remain) can be used to derive a general result for the unbiased jump process with maximum jump length Q. At compartment k, where

$k \leq Q$, the dynamics are described by

$$\begin{aligned}\sqrt{\Delta t}\frac{\partial M_k}{\partial t} =& \frac{D\sqrt{\Delta t}}{Q(\Delta x)^2}\left[\sum_{j=1}^{Q}\left(\frac{\chi_{[0,k-1]}(j)}{(k-j)^2}M_j(t)\right) + \sum_{j=1}^{Q}\left(\frac{1}{j^2}M_{k+j}(t)\right)\right. \\ & - \sum_{j=1}^{Q}\left[\frac{\chi_{[0,k-1]}(j)}{(k-j)^2} + \frac{1}{j^2}\right]M_k(t) - \sum_{j=1}^{Q-k+1}\left[\frac{1}{(j+k-1)^2}\right]M_k(t) \\ & \left. + \sum_{j=1}^{Q-k+1}\left[\frac{1-P_{j+k-1,Q}\Delta x}{(j+k-1)^2}M_j(t)\right]\right], \end{aligned} \tag{2.28}$$

where $\chi_{[0,k-1]}(j)$ is an indicator function, equal to unity if $0 \leq j \leq k-1$, and zero otherwise. The two terms on the first line of the right-hand side represent particles jumping into the compartment centred at x_k from the left and right, respectively. The terms on the second line represents particles jumping from x_k, with the first set of brackets encompassing those particles that jump without being reflected, and the second those that jump and are reflected. The terms on the final line represent those particles that are reflected into the compartment at x_k, having avoided being adsorbed by the boundary. We assume that the lattice is sufficiently large so that no influence from the boundary conditions at the right-hand boundary need be considered, i.e. $K \geq 2Q$. This seems a reasonable constraint on the choice of Q, as in most cases it will be unrealistic to allow particles to travel more than half the width of the domain in a single jump.

The left-hand side of equation (2.28) will vanish in the diffusive limit, so we can focus on the right-hand side, rearranging it to the form,

$$\begin{aligned}\frac{D\sqrt{\Delta t}}{Q\Delta x^2}\left\{\sum_{j=1}^{Q-k+1}\left[\frac{1}{(j+k-1)^2}M_j(t)\right] - \left[\sum_{j=1}^{Q-k+1}\frac{1}{(j+k-1)^2}\right]M_k(t)\right. \\ + \sum_{j=1}^{Q}\left(\frac{1}{j^2}M_{k+j}(t)\right) + \left(\sum_{j=1}^{k-1}\frac{1}{(k-j)^2}M_j(t)\right) - \left(\sum_{j=1}^{k-1}\frac{1}{(k-j)^2} + \sum_{j=1}^{Q}\frac{1}{j^2}\right)M_k(t) \\ \left. - \sum_{j=1}^{Q-k+1}\left[\frac{P_{j+k-1,Q}\Delta x}{(j+k-1)^2}M_j(t)\right]\right\}. \end{aligned} \tag{2.29}$$

We have grouped the reflecting terms, non-reflecting terms, and adsorption events on separate lines. These three groupings are analysed separately in Appendices A.1,

A.2 and A.3, respectively. It can be shown that equation (2.28) can ultimately be rearranged, in the diffusive limit, to

$$0 = \frac{D}{Q}\left\{\left(\sum_{j=k}^{Q}\frac{j-2k+1}{j^2}\right)\left.\frac{\partial u}{\partial x}\right|_{x=0} + \left(\sum_{j=k}^{Q}\frac{1}{j}\right)\left.\frac{\partial u}{\partial x}\right|_{x=0} - \sum_{j=k}^{Q}\left[\frac{P_{j,Q}}{j^2}\right]u(0,t)\right\}. \tag{2.30}$$

Rearranging again we obtain

$$\sum_{j=k}^{Q}\left[\frac{P_{j,Q}}{j^2}\right]u(0,t) = \left(\sum_{j=k}^{Q}\frac{2j-2k+1}{j^2}\right)\left.\frac{\partial u}{\partial x}\right|_{x=0}. \tag{2.31}$$

Recalling that we wish to replicate the Robin boundary condition, equation (2.12), this gives us an expression determining the adsorption rates:

$$\sum_{j=k}^{Q}\left[\frac{P_{j,Q}}{j^2}\right] = \frac{R}{D}\sum_{j=k}^{Q}\left[\frac{2j-2k+1}{j^2}\right]. \tag{2.32}$$

By setting $k = Q$, we see that $P_{Q,Q} = R/D$ for any Q. For any other adsorption rate, $P_{k,Q}$ $(k \neq Q)$, we note that the left-hand side of equation (2.32) can be written

$$\frac{P_{k,Q}}{k^2} + \sum_{j=k+1}^{Q}\left[\frac{P_{j,Q}}{j^2}\right], \tag{2.33}$$

while the right-hand side can be written

$$\frac{R}{D}\left(\sum_{j=k+1}^{Q}\left[\frac{2j-2k-1}{j^2}\right] + \sum_{j=k+1}^{Q}\left[\frac{2}{j^2}\right] + \frac{1}{k^2}\right). \tag{2.34}$$

Since $k < Q$, and equation (2.32) holds for $1 \leq k \leq Q$, we can substitute k for $k+1$ to obtain

$$\sum_{j=k+1}^{Q}\left[\frac{P_{j,Q}}{j^2}\right] = \frac{R}{D}\sum_{j=k+1}^{Q}\left[\frac{2j-2k-1}{j^2}\right], \tag{2.35}$$

so these terms cancel from equations (2.33) and (2.34). Substituting q for k and

multiplying through by q^2 we obtain our final result for $q < Q$:

$$P_{q,Q} = \frac{R}{D}\left(1 + q^2 \sum_{j=q+1}^{Q} \left[\frac{2}{j^2}\right]\right). \tag{2.36}$$

Note that this equation implies

$$P_{1,2} = \frac{R}{D}\left(1 + \frac{2}{4}\right) = \frac{3R}{2D}, \tag{2.37}$$

as expected from equation (2.26).

2.3.4 Example

To confirm these analytic results we ran $1,000$ simulations (half using local jumping, and half using non-local jumping), with a Robin boundary condition ($R = 1$) at the left-hand boundary, and a zero-flux boundary condition at the right-hand boundary, comparing a local jump process to a non-local one with maximum jump length $Q = 5$. At time $t = 0$ we initialised $1,800$ particles in a peak centred on $x = 1$, as shown in Figure 2.5(a), so that for each repeat

$$n_i(0) = \begin{cases} (i-2) \times 25, & \text{for } 3 \leq i \leq 10, \\ 200 - ((i-11) \times 25), & \text{for } 11 \leq i \leq 18, \\ 0, & \text{otherwise.} \end{cases} \tag{2.38}$$

Each repeat was then run until time $t = 1$. As can be seen in Figure 2.5(c), the mean particle numbers obtained from the local and non-local jump processes match well, both with each other and to the solution of the diffusion equation, (2.4), with $D = 1$. We quantify this fit in Figure 2.5(b) using the HDE; the good agreement between the simulation results and the PDE demonstrated by the HDE confirms the approximation to the diffusive limit. Furthermore, the non-local simulations each took 7.9 seconds to run on average, while the local simulations required on average 26.7 seconds each. We also study the convergence of the non-local implementation as $\Delta x \to 0$ by solving the appropriate master equations describing the evolution

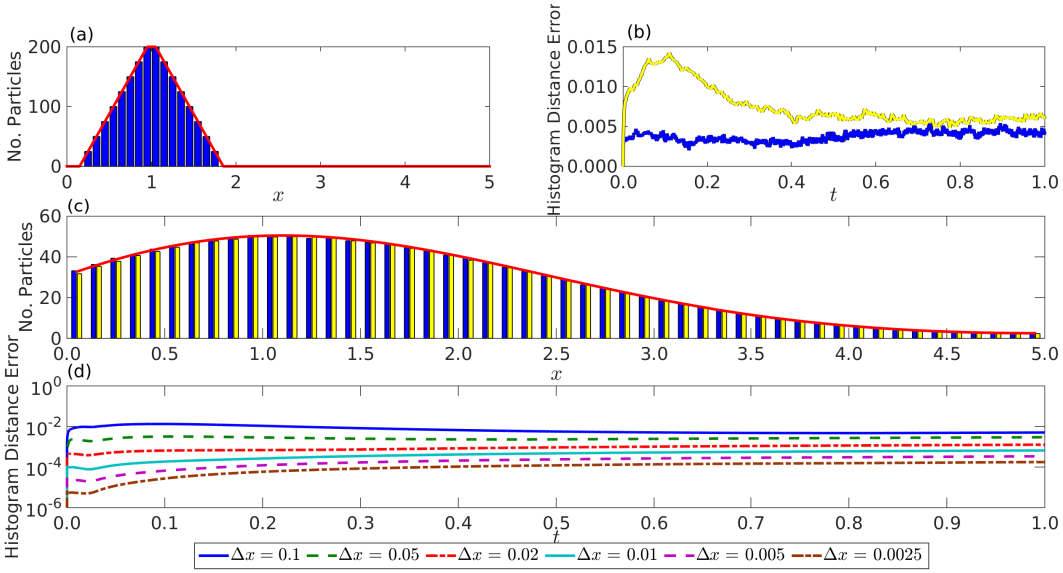

Figure 2.5: Averaged results of 500 realisations of a local jump process and 500 realisations of a non-local jump process with $Q = 5$, in the time interval $t \in [0, 1]$, with a zero-flux boundary condition at $x = 5$ and a Robin boundary condition with $R = 1$ at $x = 0$. Our parameters were $\Delta x = 0.1$ and $D = 1$. For our initial condition (a), we positioned $1,800$ particles in the system in a tent function centred around $x = 1$. The accuracy of our implementation of the boundary condition for the non-local jump process is confirmed in (b) by a HDE comparison to the solution of the limiting PDE. This is also illustrated in (c), where we demonstrate that the mean compartment occupancies observed for both the non-local (yellow bars) and local (blue bars) processes provide a good match to the PDE solution at $t = 1$. In panel (d), as Δx becomes smaller, we see the solution of the master equations describing the non-local system with Robin boundary condition becomes closer to the solution of the limiting PDE.

of mean particle numbers using the Euler method for decreasing values of Δx. We compare these results to the solution of the limiting PDE, and plot the HDE in Figure 2.5(d), showing the convergence of the solution as Δx becomes smaller.

2.4 Flux boundary conditions

It is possible to extend this work to derive flux boundary conditions (which correspond to inhomogeneous Neumann boundary conditions when jumping is unbiased). Suppose, for example, we wish to enforce the boundary condition

$$\left.\frac{\partial u}{\partial x}\right|_{x=0} = A. \tag{2.39}$$

We will treat A as a constant without loss of generality. Let us begin by considering only the case of positive flux into the system, i.e. $A < 0$.

2.4.1 Flux conditions for local jumping

In the local case we need to add a term to the master equation for compartment 1 to account for particle influx. We require the number of new particles entering the system between times t and $t + \Delta t$ to be proportional to Δt. Furthermore, we want the relative contribution of flux to the system to be independent of the choice of lattice size, so our term should be inversely proportional to the compartment size Δx. We will therefore write the contribution of the flux to the master equation as $B_{1,1}\Delta t/\Delta x$ for some constant $B_{1,1}$, where the subscripted numbers indicate the compartment in question and the maximum jump length of the system, respectively.

Starting with the purely local jumping process, and treating the boundary as completely reflecting to jumping particles (hence providing zero net flux), the master equation for compartment 1 is written

$$M_1(t + \Delta t) = \left(1 - \frac{D\Delta t}{(\Delta x)^2}\right) M_1(t) + \frac{D\Delta t}{(\Delta x)^2} M_2(t) + \frac{B_{1,1}\Delta t}{\Delta x}, \tag{2.40}$$

$$\Rightarrow \sqrt{\Delta t}\left(\frac{M_1(t + \Delta t) - M_1(t)}{\Delta t}\right) = \frac{\sqrt{\Delta t}}{\Delta x}\left(D\frac{M_2(t) - M_1(t)}{\Delta x} + B_{1,1}\right). \tag{2.41}$$

Taking the limit $\Delta t \to 0$, $\Delta x \to 0$ such that $\sqrt{\Delta t}/\Delta x$ remains constant, this becomes

$$\left.\frac{\partial u}{\partial x}\right|_{x=0} = -\frac{B_{1,1}}{D}. \tag{2.42}$$

Hence $A = -B_{1,1}/D$, and we can implement the Neumann boundary condition given by equation (2.39) by adding particles to compartment 1 at rate $-AD/\Delta x$. Figure 2.6 gives an example of this, confirming the accuracy of this implementation, starting from an initial distribution of

$$n_i(0) = \begin{cases} 105 - (10 \times i), & \text{for } i \leq 10, \\ 0, & \text{otherwise,} \end{cases} \tag{2.43}$$

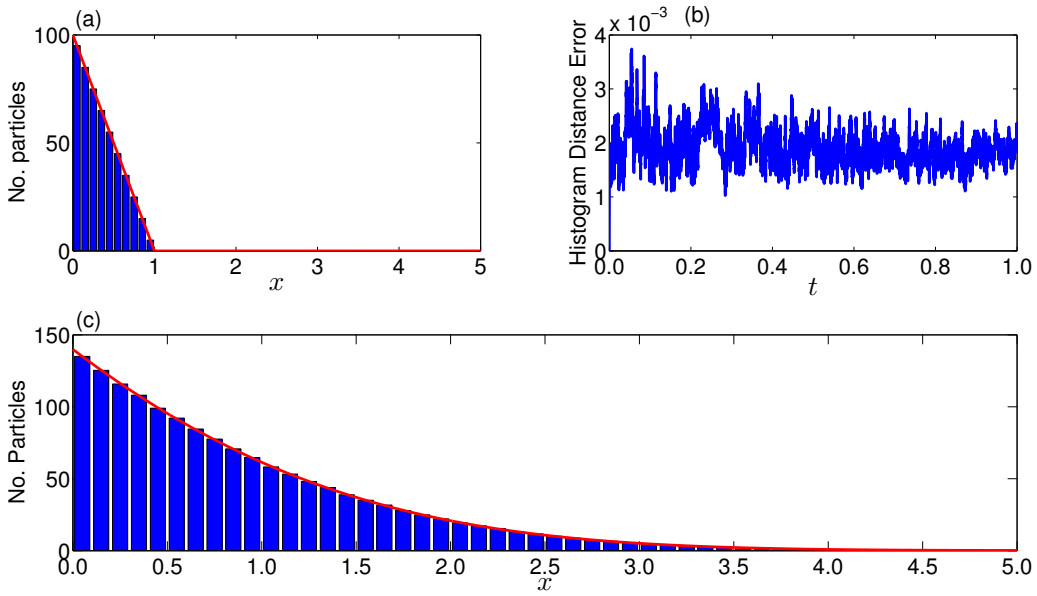

Figure 2.6: Average results from $1,000$ repeats of a diffusion simulation from $t = 0$ to $t = 1$, with a zero-flux boundary condition at $x = 5$ and an in-flux boundary condition with $A = -100$ at $x = 0$. At time $t = 0$, we initialise 500 particles in the first ten compartments of the system following a linearly decreasing distribution (a). In (c), it can be seen that the local simulation (blue bars) matches well to the PDE solution (red line). The accuracy is confirmed by a HDE comparison to the solution of the limiting PDE (b).

as shown in Figure 2.6(a). We set $D = 1$ as before, and impose boundary conditions

$$\left.\frac{\partial u}{\partial x}\right|_{x=0} = -100, \tag{2.44}$$

$$\left.\frac{\partial u}{\partial x}\right|_{x=5} = 0. \tag{2.45}$$

These boundary conditions imply that the simulation algorithm should add particles at the left-hand boundary of the domain. We note the good match between the local jumping simulation and the PDE at time $t = 1$, and the low value of the HDE, as shown in Figures 2.6(c) and (b), respectively.

2.4.2 Generalised flux boundary conditions for non-local jumps

For a system in which non-local jumps of maximum length Q are allowed, particles must be added, not simply to the first compartment, but to the first Q compartments,

with various weights (the reason for this will be illustrated in Section 2.4.3). These weights should preserve the total flux into the system, and the general result for their distribution is given below. We parametrised the input with $B_{1,1}\Delta t/\Delta x$ in the local case, so we will write the input term for the k^{th} compartment as $B_{k,Q}\Delta t/\Delta x$, in the non-local case.

Recalling that particles which jump into the boundary are reflected, the mean particle dynamics at x_k is given by

$$\begin{aligned}\sqrt{\Delta t}\frac{M_k(t+\Delta t)-M_k(t)}{\Delta t} &= \frac{D\sqrt{\Delta t}}{Q(\Delta x)^2}\left\{\left(\sum_{j=1}^{Q}\frac{\chi_{[0,k-1]}(j)}{(k-j)^2}M_j(t)\right)+\sum_{j=1}^{Q}\left(\frac{1}{j^2}M_{k+j}(t)\right)\right.\\ &\quad-\left(\sum_{j=1}^{Q}\frac{\chi_{[0,k-1]}(j)}{(k-j)^2}+\sum_{j=1}^{Q}\frac{1}{j^2}\right)M_k(t)\\ &\quad-\left[\sum_{j=1}^{Q-k+1}\frac{1}{(j+k-1)^2}\right]M_k(t)+\\ &\quad\left.+\sum_{j=1}^{Q-k+1}\left[\frac{1}{(j+k-1)^2}M_j(t)\right]\right\}+\frac{B_{k,Q}\sqrt{\Delta t}}{\Delta x}, \qquad (2.46)\end{aligned}$$

where $1 < k \leq Q$. We recognise this as the equation from the generalised Robin boundary case, but without adsorption and with an added input term $B_{k,Q}\sqrt{\Delta t}/\Delta x$. We can therefore reuse the results from Appendices A.1 and A.2, and see that in the diffusive limit

$$B_{k,Q} = -\frac{D}{Q}\left(\sum_{j=k}^{Q}\frac{j-2k+1}{j^2}+\sum_{j=k}^{Q}\frac{1}{j}\right)\left.\frac{\partial u}{\partial x}\right|_{x=0}. \qquad (2.47)$$

Consolidating, and imposing the Neumann boundary condition again, this gives us the general formula for the input term at x_k in the reflecting case:

$$B_{k,Q} = -\frac{AD}{Q}\left(\sum_{j=k}^{Q}\frac{2j-2k+1}{j^2}\right). \qquad (2.48)$$

We note that

$$\sum_{k=1}^{Q}B_{k,Q}/\Delta x = -AD/\Delta x, \qquad (2.49)$$

showing that the total rate at which particles are added to a system using the non-local boundary conditions recovers the total rate at which particles are added to a system using the local boundary conditions, as given in Section 2.4.1.

2.4.3 Example

In order to demonstrate the necessity of the derived non-local boundary conditions, rather than adding all new particles to the first compartment as we did for the local jumping simulation, we ran $1,000$ simulations of a non-locally jumping system with $Q = 5$. We adopted the initial condition and boundary conditions used in the local jumping simulation in Section 2.4.1, i.e. a no-flux boundary condition at $x = 5$, a Neumann condition with $A = -100$ at $x = 0$, and the inital distribution of particles illustrated by Figure 2.7(a) (the same distribution described in Section 2.4.1). Each simulation was run from $t = 0$ until $t = 1$, with $D = 1$. In half of these simulations we added new particles to the first five compartments, with rates as required by our result in equation (2.48) with $Q = 5$. The other half of these simulations were identical, except that all new particles were added to the first compartment with rate $-AD/\Delta x$. Figure 2.7(b) shows the superior fit of the data to the PDE limit in the first case, Figure 2.7(c) shows the final state of the system, with a close-up of the first five compartments, and illustrates how attempting to use the local implementation of a flux boundary condition rather than the derived non-local implementation leads to deviation from the PDE solution. Each repeat of the non-local simulation ran in an average of 6.7 seconds, compared to 21.9 seconds for the equivalent local simulations shown in Figure 2.6. As Δx becomes smaller, the non-local description can be seen in Figure 2.7(d) to converge to the solution of the corresponding PDE.

2.5 Hybrid diffusion models

Our non-local jumping method gives results that match well with the results of the local jumping method in most cases but, in the case of sharp spatial gradients in particle numbers, we have observed inaccurate results (see, for example, the simulation

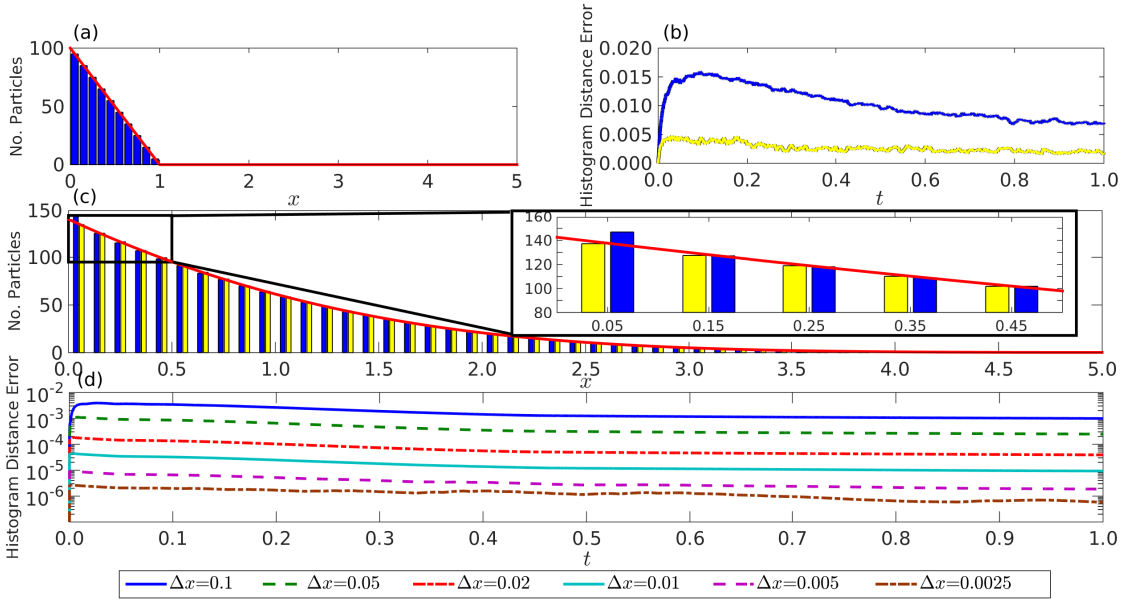

Figure 2.7: Average results from $1,000$ repeats of a diffusion simulation from $t = 0$ to $t = 1$, with a zero-flux boundary condition at $x = 5$ and an in-flux boundary condition with $A = -100$ at $x = 0$. At time $t = 0$, we initialise 500 particles in the first ten compartments of the system following a linearly decreasing distribution (a). In (c), it can be seen that the non-local simulation with $Q = 5$ and corresponding non-local boundary conditions (yellow bars) matches well to the PDE solution (red line), while the non-local simulation with local boundary conditions (i.e. all new particles added to the first compartment, shown by blue bars) deviates from this solution. The error is particularly evident in the first five compartments, as illustrated by the close-up. This difference in accuracy is confirmed by a HDE comparison of both implementations to the solution of the limiting PDE (b), where the non-local simulation with the derived non-local boundary conditions is shown in yellow and the non-local simulation with local boundary boundary conditions is shown in blue again. The apparent decline with time in the HDE for both implementations is an artefact of increasing particle numbers (compare with the increasing HDEs in Figure 2.11 as particle numbers fall). In panel (d), we see that the solution of the master equations describing the non-local system with flux boundary conditions becomes closer to the solution of the limiting PDE as Δx becomes smaller.

results shown in Figure 2.9, and further discussion in Section 2.7). In this light, it would therefore be useful if we could use non-local jumping in some regions of space to reduce the running time, but use local jumping in regions where the concentration changes rapidly in space so as to maintain accuracy.

We have already introduced an implementation of flux boundary conditions in non-locally jumping systems, and can therefore argue as follows. The lattice can be separated into two regions, with non-local jumping on the left region and local on the right (again, without loss of generality). We can use the local jump rates to calculate the particle flux from left-to-right, and also from right-to-left, based on the number of particles in the compartments to either side of the boundary. For left-to-right movement, we implement a constant flux boundary condition using our result in equation (2.48). Particles in the compartments concerned will otherwise continue to jump as normal, with any jump that would have taken them over the boundary reflecting instead: only the flux terms can take particles over the boundary to the right, and then only to the first local compartment. This means that additional, special jump rates for rightwards movement are required for particles in the Q compartments closest to the boundary (all continue to jump left with unchanged rates).

We now consider movement from right-to-left. Since the right region uses local jumping, we only have to implement special conditions in the first compartment to the right of the notional boundary. Particles in this compartment may jump right as normal, or jump left with the same probability. When jumping left, however, they may travel up to Q sites, with probabilities chosen to match the rates with which particles in those compartments are moving to the right.

An implementation of these conditions for $Q = 4$ is illustrated in Figure 2.8. We define $B_{k,Q}$, the rate with which a particle from a compartment $k \leq Q$ places to the left of the boundary will cross the boundary into the first compartment of the local domain, as

$$B_{k,Q} = -\frac{A_n D}{Q}\left(\sum_{j=k}^{Q}\frac{2j-2k+1}{j^2}\right), \tag{2.50}$$

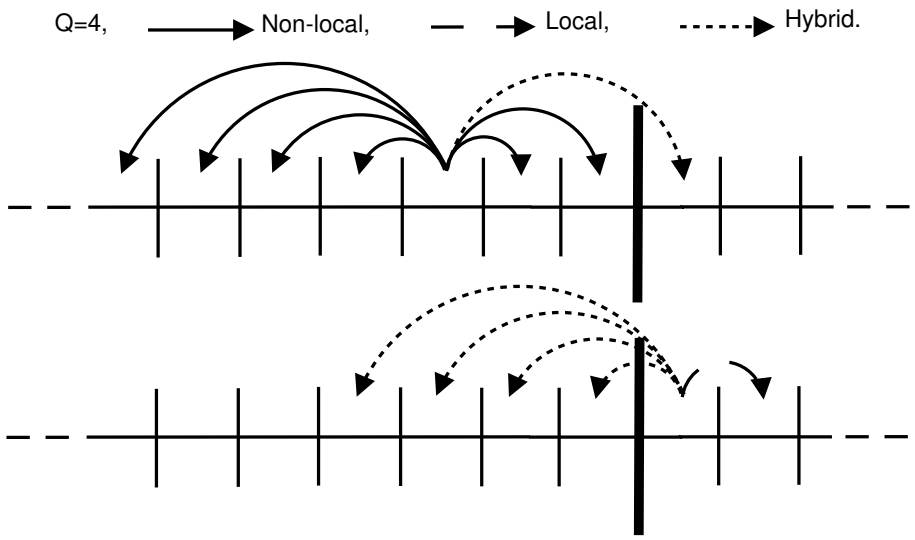

Figure 2.8: Example showing jumping options from compartments within the hybrid zone around the barrier for $Q = 4$. The non-local jumps denoted by solid lines all use standard non-local rates for their length; the dotted hybrid lines use Neumann based jumping rates. Reflecting particles are not shown.

where $A_n D$ is a measure of the expected flux over the boundary to the right, and is given by multiplying the number of particles in the cell closest to the boundary on the non-local side by the local jumping rate. Conversely, particles in the first local compartment to the right of the boundary can jump up to Q places to the left, with rates given by

$$B'_{k,Q} = -\frac{A_l D}{Q}\left(\sum_{j=k}^{Q}\frac{2j-2k+1}{j^2}\right), \tag{2.51}$$

where $A_l D$ is the multiple of the number of particles in the cell closest to the boundary on the local side and the local jumping rate (i.e. the expected jump rate over the boundary from right to left).

2.5.1 Example

We consider a simple morphogen gradient system. In the time interval $(t, t+\Delta t]$, particles are generated in each compartment in the left-half of the domain with probability $5,000\Delta t/\Delta x$, and decay with probability $100\Delta t$. In the diffusive limit

this corresponds to the PDE

$$\frac{\partial u}{\partial t} = \frac{\partial^2 u}{\partial x^2} + 5000H(2.5 - x) - 100u, \tag{2.52}$$

where $H(x)$ is the Heaviside function. Starting from an empty lattice at time $t = 0$, we ran 1,000 simulations until time $t = 1$ of a standard non-local implementation, and another 1,000 of a hybrid non-local model. In the hybrid model, non-local jumping was used in the first fifteen compartments and local jumping was used in the remainder of the domain, with an interface between these two regions at $x = 1.5$. The maximum jump length was $Q = 5$ in both cases. The results are shown in Figure 2.9. Figure 2.9(a) shows the averaged final state of the system, with the hybrid model (yellow bars) matching the PDE solution (red line) closely, while the unmodified non-local process deviates slightly around $x = 2.5$ where the particle concentration changes relatively sharply. The hybrid simulations each took on average 31.4 seconds to run, compared to 43.4 seconds for an equivalent local simulation (not shown), but clearly more significant time saving could be made for simulations with larger morphogen production regions, or higher equilibrium particle numbers in that region. Sharp spatial gradients can also be accomodated by using a finer grid, and Figure 2.9(d) shows how the master equations representing the non-local system converge to the solution of the PDE as Δx becomes smaller.

2.6 Boundary conditions for biased diffusion

So far, this chapter has only considered LBPJ models which are directionally unbiased, jumping to the left, or to the right, with equal probability. However, models of some biological phenomena, such as chemotactic movement, use biased random walks [88]. In this section, we therefore consider biased diffusion, and its implications for the implementation of boundary conditions.

To incorporate biased diffusion, we divide our probabilities of movement into a symmetric diffusion term, that can be treated non-locally, as usual, and an advection

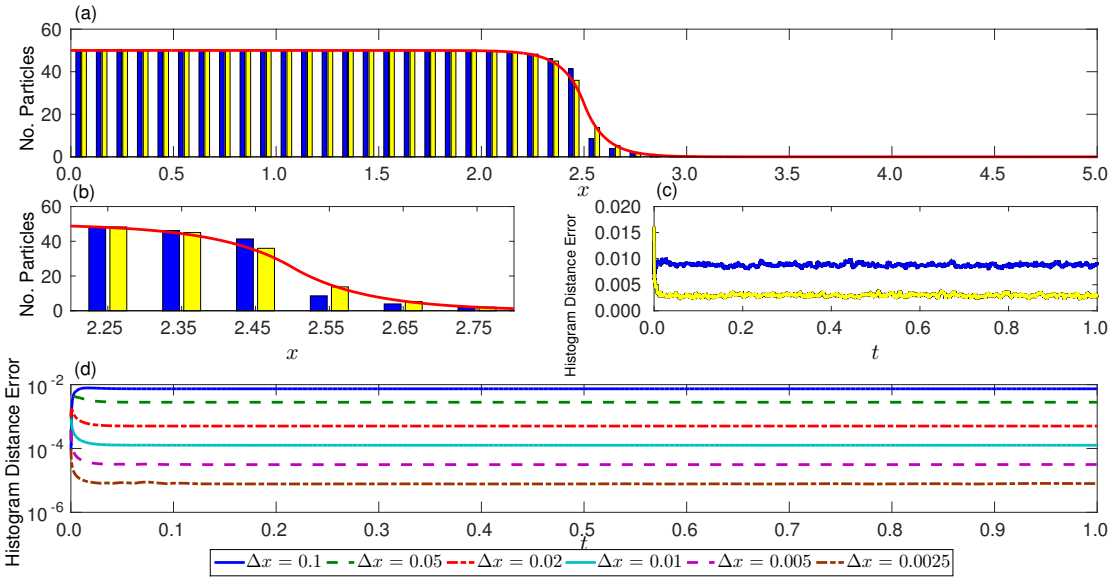

Figure 2.9: Panel (a) shows the state of a morphogen gradient system at time $t = 1$, starting from an initial state with no particles anywhere. Both simulations are non-local with $Q = 5$, but the results displayed using yellow bars were obtained using the hybrid method, with the interface positioned at $x = 1.5$, while the blue bars represent the standard non-local implementation. The red line shows the solution to the limiting PDE. It can be seen that the standard non-local simulations deviate slightly from the PDE solution around $x = 2.5$, and an enlarged image of this region is shown in (b). The goodness of fit of the hybrid method to the PDE solution is shown by the comparison of HDEs in (c). Another approach to ameliorate the effects of sharp gradients is to adopt a finer lattice. In panel (d) we see the solution of the master equations describing the non-local morphogen gradient system becoming closer to the solution of the limiting PDE as Δx becomes smaller, without use of our hybrid method.

term promoting movement in the favoured direction. The probability of jumping in either direction in the time interval $(t, t + \Delta t]$ as a result of diffusion is given by $D\Delta t/(\Delta x)^2$, as usual, while the additional probability of jumping in the favoured direction is given by $b\Delta t/\Delta x$, for some positive constant b. It can be shown that this will produce the advection-diffusion equation in the diffusive limit,

$$\frac{\partial u}{\partial t} = D\frac{\partial^2 u}{\partial x^2} \pm b\frac{\partial u}{\partial x}, \tag{2.53}$$

where a plus sign would correspond to a bias towards leftward movement, and a minus sign to a bias towards rightward movement. When deriving constant flux boundary conditions in the case of unbiased diffusion, the flux at $x = 0$ was given by $-D\partial u/\partial x$ in the diffusive limit, so we could implement constant flux boundary conditions with the Neumann boundary condition $-D\partial u/\partial x = -A$. In the biased case, we must adapt our flux term to incorporate the directional bias so it is given by $-D\partial u/\partial x + bu$ (assuming, without loss of generality, that the bias is towards rightward movement).

2.6.1 Local case

We begin by considering the local case, and write the master equation for the first lattice site, which includes particles being added to the system during timestep Δt with probability $J\Delta t/\Delta x$,

$$\begin{aligned} M_1(t+\Delta t) &= \left(1 - D\frac{\Delta t}{(\Delta x)^2} - b\frac{\Delta t}{\Delta x}\right) M_1(t) \\ &\quad + D\frac{\Delta t}{(\Delta x)^2} M_2(t) + J\frac{\Delta t}{\Delta x}, \\ \Rightarrow \sqrt{\Delta t}\frac{M_1(t+\Delta t) - M_1(t)}{\Delta t} &= D\frac{\sqrt{\Delta t}}{\Delta x}\frac{M_2(t) - M_1(t)}{\Delta x} \\ &\quad - b\frac{\sqrt{\Delta t}}{\Delta x} M_1(t) + J\frac{\sqrt{\Delta t}}{\Delta x}. \end{aligned} \tag{2.54}$$

In the diffusive limit, the left-hand side tends to zero, and all $\sqrt{\Delta t}/\Delta x$ terms tend to a constant and cancel. Therefore, we can rearrange to arrive at

$$J = \left(-D \left. \frac{\partial u}{\partial x} \right|_{x=0} + bu(0,t) \right) = -A. \tag{2.55}$$

This means that the unbiased implementation also works for biased jumping in the local jumping case. When the bias is towards leftward movement, it is easy to produce the same result by a very similar method.

2.6.2 Non-local case: first compartment

We assume the bias is away from the boundary at $x = 0$, and begin by deriving a result for the first compartment on the lattice, then proceed to derive results for the remaining $Q - 1$ compartments. We then show that the sum of all the terms added as a result of directional bias is zero, so total flux is conserved.

For the first compartment, we write the master equation,

$$\begin{aligned} \sqrt{\Delta t}\frac{M_1(t+\Delta t) - M_1(t)}{\Delta t} &= \frac{D\sqrt{\Delta t}}{Q(\Delta x)^2} \left\{ \left[-\sum_{j=1}^{Q} \frac{1}{j^2} - \sum_{j=2}^{Q} \frac{1}{j^2} \right] M_1(t) \right. \\ &\quad \left. + \sum_{j=1}^{Q} \left[\frac{1}{j^2} M_{j+1}(t) \right] + \sum_{j=2}^{Q} \left[\frac{1}{j^2} M_j(t) \right] \right\} \\ &\quad -b\frac{\sqrt{\Delta t}}{\Delta x} M_1(t) + J_{1,Q}\frac{\sqrt{\Delta t}}{\Delta x}. \end{aligned} \tag{2.56}$$

We ignore the left-hand side, which will vanish in the diffusive limit. On the right-hand side, the four summations represent, respectively, particles leaving compartment 1 by jumping to the right, particles leaving compartment 1 by jumping to the left and reflecting, particles jumping directly into compartment 1 from the right, and particles jumping into compartment 1 from the right by reflection. The terms outside of the brackets represent advection to the right and flux into the compartment from outside the system.

In our earlier work, we showed that the terms inside the brackets can be re-

arranged, collecting most into second derivative terms that vanish in the diffusive limit, and leaving

$$0 = \frac{D}{Q}\left(\sum_{j=1}^{Q}\frac{2j-1}{j^2}\right)\left.\frac{\partial u}{\partial x}\right|_{x=0} - bu(0,t) + J_{1,Q}. \tag{2.57}$$

Recalling the expression for flux in the advective case, we rearrange this to write

$$\begin{aligned} J_{1,Q} =& \frac{1}{Q}\left[\sum_{j=1}^{Q}\frac{2j-1}{j^2}\right]\left[-D\left.\frac{\partial u}{\partial x}\right|_{x=0} + bu(0,t)\right] \\ &+ \left(1 - \frac{1}{Q}\left[\sum_{j=1}^{Q}\frac{2j-1}{j^2}\right]\right)bu(0,t). \end{aligned} \tag{2.58}$$

We therefore use equation (2.55) to replace the terms in square brackets with $-A$, and arrive at

$$J_{1,Q} = \frac{-1}{Q}\left(\sum_{j=1}^{Q}\frac{2j-1}{j^2}\right)A + \left(1 - \frac{1}{Q}\left(\sum_{j=1}^{Q}\frac{2j-1}{j^2}\right)\right)bu(0,t). \tag{2.59}$$

2.6.3 Non-local case: all other compartments

For some compartment k, where $1 < k \leq Q$, we can apply similar reasoning, drawing on our previous work to write

$$0 = \frac{D}{Q}\left(\sum_{j=k}^{Q}\frac{2j-2k+1}{j^2}\right)\left.\frac{\partial u}{\partial x}\right|_{x=0} - b\sqrt{\Delta t}\frac{M_{k-1}-M_k}{\Delta x} + J_{k,Q}\frac{\sqrt{\Delta t}}{\Delta x}. \tag{2.60}$$

Having rearranged the bias terms into a first order derivative they vanish in the diffusive limit. In order to obtain an expression for flux at the boundary, we include balancing terms of M_1 in the equation, and arrive at our final expression for the flux,

$$J_{k,Q} = \frac{-1}{Q}\left(\sum_{j=k}^{Q}\frac{2j-2k+1}{j^2}\right)A - \frac{1}{Q}\left(\sum_{j=k}^{Q}\frac{2j-2k+1}{j^2}\right)bu(0,t). \tag{2.61}$$

We note that in the case $b = 0$ we recover our unbiased result. Drawing on our earlier work on boundary conditions, it can be seen that the sum of the advection-

dependent terms over all the compartments will be zero, so we can see that the flux at the boundary is still conserved when there is a bias in the jump rates. We also note that the new terms are independent of the boundary flux, A. They will therefore need to be incorporated into the system even for zero-flux boundary conditions where $A = 0$, or when a different boundary condition is implemented: it is easy to see that that these terms are also required for Robin boundary conditions. It therefore seems sensible, both for computational efficiency and for the conservation of particle numbers, to implement these terms as extra jumps between the first Q compartments, i.e. where these terms call for particles to be removed from the system, they should instead be moved to one of the sites (chosen with appropriate probability) where the additional terms require particles to be added. We note that if the bias instead favours movement towards the boundary then the signs of these extra terms will all be flipped.

2.6.4 Flux boundaries for biased jumping

To demonstrate the necessity for additional boundary flux terms for biased diffusion, given by equations (2.59) and (2.61), we simulated a biased system with $Q = 5$. In $1,000$ of these simulations we used the flux values derived above (shown as yellow bars in Figure 2.10(b) and (c)), while in the other $1,000$ we used the standard, non-local flux implementation for unbiased diffusion, from equation (2.48) (shown in blue). An in-flux boundary condition with $-A = 500$ was set at $x = 0$, and an outflux condition with $-A = 500$ at $x = 5$ (recalling from equation (2.55) that $-A$ corresponds to left-to-right flux). We use $D = 1$ as usual, and a bias towards rightward movement of $b = 5$. The limiting PDE and its boundary conditions are therefore

$$\frac{\partial u}{\partial t} = \frac{\partial^2 u}{\partial x^2} - 5\frac{\partial u}{\partial x}, \tag{2.62}$$

$$-\left.\frac{\partial u}{\partial x}\right|_{x=0} + 5u(0,t) = 500, \tag{2.63}$$

$$-\left.\frac{\partial u}{\partial x}\right|_{x=5} + 5u(5,t) = 500, \tag{2.64}$$

and it clear that the spatially homogeneous distribution $u(x,t) = 100$ is a steady-state solution to these equations.

The simulations started from the steady-state, with $5,000$ particles distributed uniformly across the domain as shown in Figure 2.10(a). Figure 2.10(c) shows the average state of the system at $t = 1$, with the unbiased boundary conditions giving rise to a density profile that deviates significantly from the steady-state (red line). However when the additional boundary fluxes for biased diffusion are incorporated our results correspond well to the steady-state. The quality of the fit is confirmed in Figure 2.10(b) by comparison of the HDEs. The non-local simulations ran in an average of 64.0 seconds, compared to 137.8 seconds for an equivalent, local simulation. Non-local jumping can therefore still deliver significant, albeit smaller, savings in computational time, even when more complicated boundary condition implementations are required. It can also be seen, in Figure 2.10(d), that the non-local description converges to the solution of the continuum PDE as Δx becomes small.

2.6.5 Robin boundaries for biased jumping

Recalling our notation from Section 2.3, we choose to let particles that hit the boundary as a result of the biased jumping term $b\Delta t/\Delta x$ be absorbed with probability $P_{1,Q}$ (particles hitting the boundary because of a diffusive term are still absorbed with probability $P_{1,Q}\Delta x$ as before, since such jumps scale with $\Delta t/(\Delta x)^2$). Using the reasoning from Section 2.6.1, and noting that the non-local Robin condition at the left-hand boundary is $D\partial u/\partial x + bu = Ru$ if the bias is towards leftward movement, and $D\partial u/\partial x - bu = Ru$ if towards rightward movement, it is easy to see that the local implementation of Robin conditions is unchanged, with $P_{1,1} = R/D$ when the bias moves particles away from the boundary, and $P_{1,1} = R/(D+b)$ when the bias moves them towards the boundary.

In the non-local case, we recall that the additional terms derived in Sections 2.6.2 and 2.6.3 must also be incorporated here, but when the bias favours movement away from the boundary it is clear that the adsorption terms will remain unchanged. When movement towards the boundary is favoured by the bias, adsorption rates $P_{k,Q}$

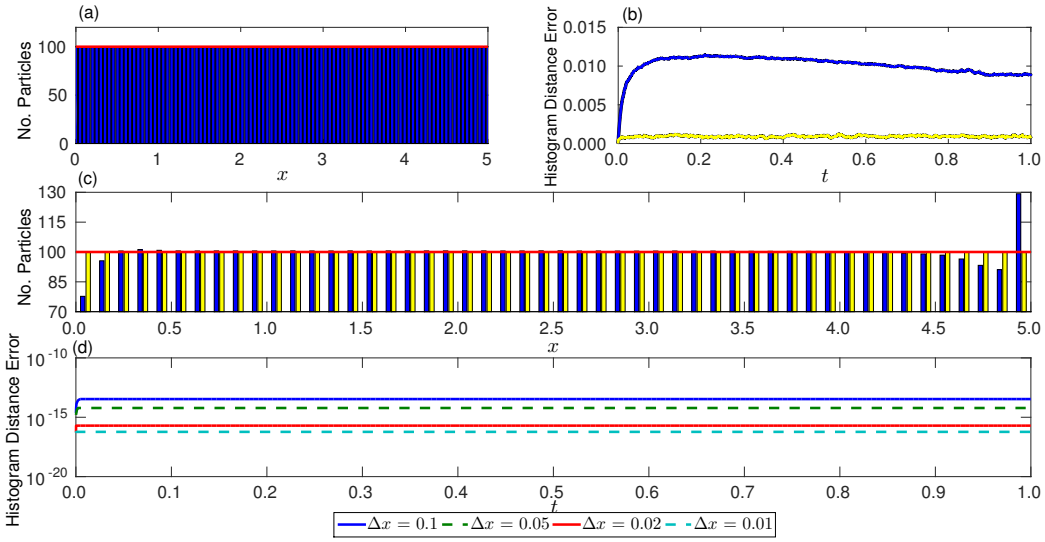

Figure 2.10: Panel (a) shows the initial state of the system (and also the steady-state) with 100 particles in each compartment. A comparison of HDEs for the derived asymmetric boundary conditions (yellow) and standard non-local boundary conditions (blue) is shown in (b), demonstrating the accuracy of the asymmetric implementation. In panel (c), the average state of the system at time t is shown: it can be seen that particles numbers around the boundary deviate significantly from the steady-state (red line), while the asymmetric implementation matches the steady-state well. As Δx becomes smaller, we see in panel (d) that the solution of the master equations describing the biased diffusion system with boundary fluxes becomes closer to the solution of the limiting PDE. We show results for fewer lattice spacings in this example because the error is very small, and rounding errors become significant for smaller Δx.

remain unchanged for $k \geq 2$, and it can be shown that for $k = 1$ the result derived in equation (2.32) becomes instead

$$P_{1,Q} + \frac{bQ}{D} P_{1,Q} + \sum_{j=2}^{Q} \left[\frac{P_{j,Q}}{j^2} \right] = \frac{R}{D} \sum_{j=1}^{Q} \left[\frac{2j-1}{j^2} \right]. \tag{2.65}$$

Using the same reasoning applied to the symmetric case, we obtain our new value for $P_{1,Q}$:

$$P_{1,Q} = \frac{R}{D + bQ} \left(1 + \sum_{j=2}^{Q} \left[\frac{2}{j^2} \right] \right). \tag{2.66}$$

We note that this result preserves the symmetric rates when $b = 0$, as expected. To illustrate this result we ran $1,000$ simulations, using the same parameters and initial condition as used in Figure 2.5, except for the addition of a bias towards leftward movement with $b = 2$. It can be seen in Figure 2.11 that our derived modifications to the adsorption rates result in a good match to the PDE solution by both local and non-local simulations. Each non-local jumping simulation ran in an average of 8.8 seconds, compared to an average of 23.8 seconds, showing that, even in this complicated case, non-local jumping can accelerate stochastic simulations of LBPJ models. Figure 2.11(d) shows the convergence of the non-local system to the limiting PDE for small Δx.

These results complete our work on boundary conditions for non-local jumping. To conclude this chapter, we briefly illustrate the dangers of choosing excessively large values of Q in Section 2.7, and consider whether we should expect the variances of non-local simulations to match those of local jumping simulations in Section 2.8. A brief closing discussion of potential time-savings may be found in Section 2.9.

2.7 The limits of non-local jumping

We have already noted (in Section 2.5) that the accuracy of non-local jumping simulations can deteriorate in the prescence of sharp spatial gradients. This results from non-local models slightly underestimating the rate at which particles depart

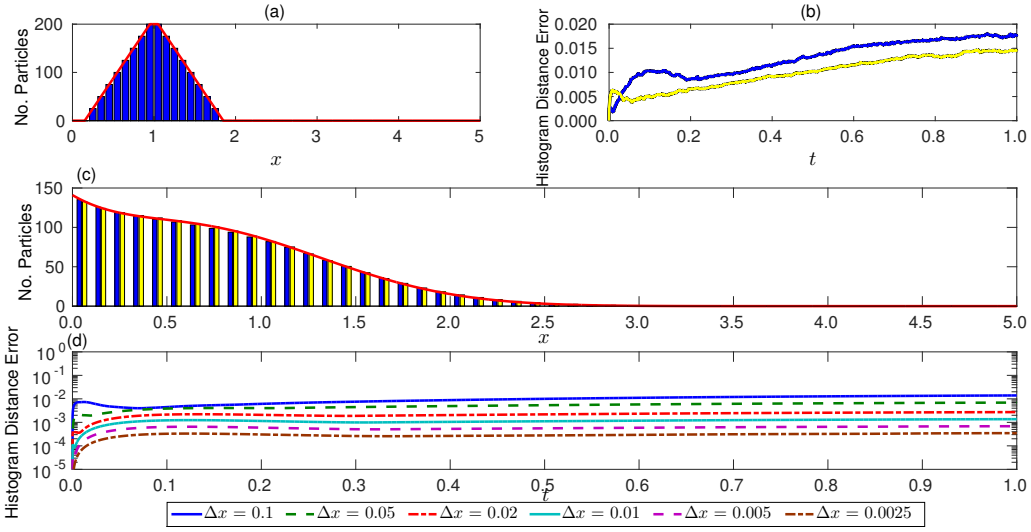

Figure 2.11: (a) shows the initial state of the system with $1,800$ particles placed in a peaked profile about $x = 1$. In (c) we see the averaged system state at time $t = 0.2$, averaged over $1,000$ simulations, with a good match between both local (blue bars) and non-local (yellow bars) simulations, and the PDE solution (red line). The HDEs confirm this match in (b) their rising values resulting from the rapidly dropping number of particles in the system. In (d) we see the solution of the master equations describing the biased diffusion system with Robin boundary condition becoming closer to the solution of the limiting PDE as Δx becomes smaller.

from their initial positions. For the scenarios we have studied so far where $Q = 5$ this does not lead to significant deviations from either the corresponding local jumping model or from the PDE solution, but in this section we run a simple diffusion simulation with large values of $Q = 15$ and $Q = 25$, and a sharply peaked initial condition, to illustrate the resulting error. We also perform some basic error analysis to quantify the divergence of model predictions as Q increases.

At time $t = 0$ we initialise our domain with initial condition

$$n_i(0) = \begin{cases} 100, & \text{for} \quad i = 25, 26; \\ 0, & \text{otherwise;} \end{cases} \tag{2.67}$$

as illustrated in Figure 2.12(a), and allow the particles to diffuse until $t = 1$ with $D = 1$, for a local jumping simulation, and for non-local jumping simulations with $Q = 5, 15$ and 25. We compare the results of these simulations to the solution of the corresponding PDE, and plot the resulting HDE values in Figure 2.12(b), observing

that the HDE values for $Q = 15$ and $Q = 25$ are significantly higher than those for $Q = 5$ and for the local simulation. This is confirmed by considering snapshots of the simulation results at $t = 0.3$ and $t = 1$ in Figures 2.12(c) and (d), respectively, which confirm that the errors arise from large values of Q underestimating the rate at which particles diffuse from their starting positions. This example confirms that caution must be taken when using non-local jumping to accelerate simulations, as inaccuracy can result when inappropriately large values of Q are chosen.

For suitable choices of Q, however, error analysis suggests that the deviation of a non-locally jumping model from a locally jumping model will remain small. We note that, in the discrete, local jumping case, we approximate a second partial derivative with respect to x as

$$\begin{aligned} D\frac{\partial^2 u}{\partial x^2} &= Du''(x,t) \\ &\approx D\frac{u(x-\Delta x,t) - 2u(x,t) + u(x+\Delta x,t)}{(\Delta x)^2}, \end{aligned} \tag{2.68}$$

where we use dashes to denote partial derivatives with respect to x, e.g. $\partial u/\partial x = u'(x,t)$. Expanding the terms from equation (2.68), we arrive at

$$\begin{aligned} Du''(x,t) &\approx \frac{D}{(\Delta x)^2}\left(\begin{array}{c} \left[u(x,t) - (\Delta x)u'(x,t) + \frac{(\Delta x)^2}{2}u''(x,t)\right. \\ \left. -\frac{(\Delta x)^3}{6}u'''(x,t) + \frac{(\Delta x)^4}{24}u''''(x,t) + ...\right] \\ -2u(x,t) \\ +\left[u(x,t) + (\Delta x)u'(x,t) + \frac{(\Delta x)^2}{2}u''(x,t)\right. \\ \left. +\frac{(\Delta x)^3}{6}u'''(x,t) + \frac{(\Delta x)^4}{24}u''''(x,t) + ...\right] \end{array}\right) \\ &\approx Du''(x,t) + \frac{D}{12}(\Delta x)^2 u''''(x,t) + o\left((\Delta x)^2\right). \end{aligned} \tag{2.69}$$

The error for the local jumping model is thus approximately $D(\Delta x)^2 u''''(x,t)/12$.

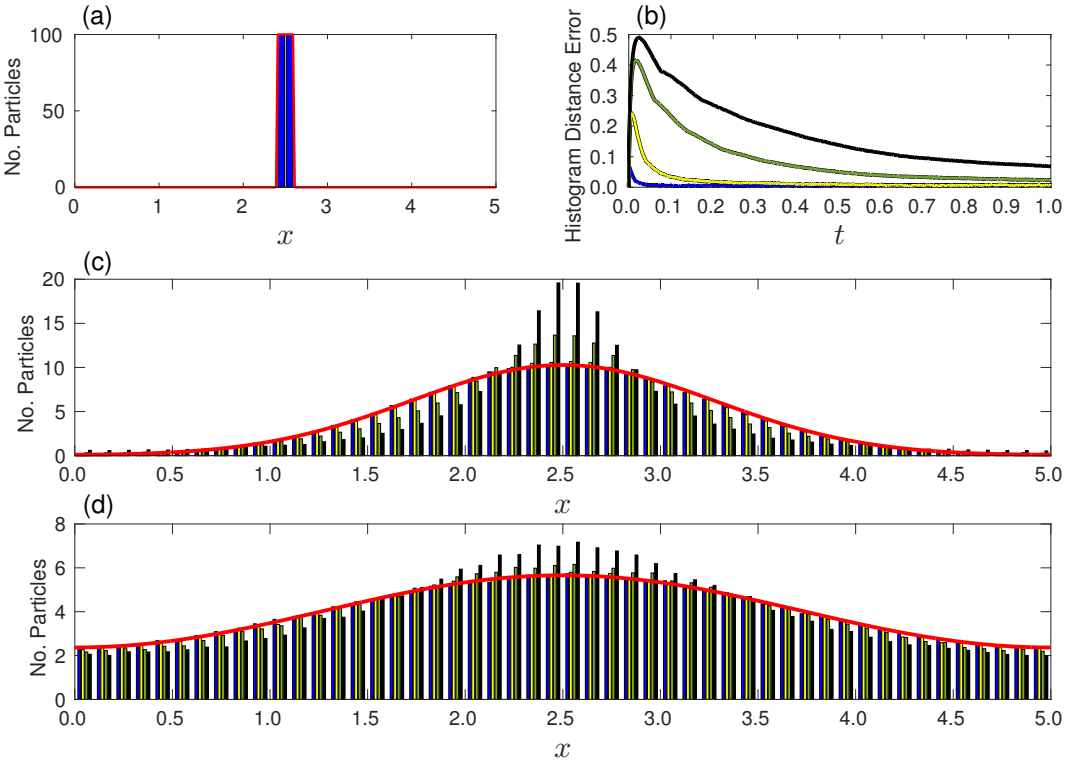

Figure 2.12: Average results from $1,000$ repeats of a diffusion simulation from $t = 0$ to $t = 1$, with a zero-flux boundary conditions at $x = 0$ and $x = 5$. At time $t = 0$, we initialise 200 particles in the centre of the domain (a). In (c) and (d), it can be seen that the non-local simulation with $Q = 5$ (yellow bars) matches well to the locally jumping simulation (blue bars) and to the PDE solution (red line) at times $t = 0.3$ and $t = 1$, respectively, while the non-local simulations with $Q = 15$ (green bars) and $Q = 25$ (black bars) deviate from this solution. As the maximum jump length Q is increased, the resulting simulations overestimate the number of particles at the centre of the domain, and underestimate movement away from the starting position. This difference in accuracy is confirmed by a HDE comparison of results from all four stochastic simulations to the solution of the limiting PDE (b), where poor accuracy is observed for large values of Q.

For the non-local jumping model, we write instead

$$\begin{aligned}
D\frac{\partial^2 u}{\partial x^2} &= Du''(x,t) \\
&\approx \frac{D}{Q}\frac{\sum_{q=1}^{Q} u(x-q\Delta x,t)/q^2 - 2u(x,t) + \sum_{q=1}^{Q} u(x+q\Delta x,t)/q^2}{(\Delta x)^2} \\
&\approx \frac{D}{Q(\Delta x)^2}\left(\begin{array}{c}
\sum_{q=1}^{Q}\left[u(x,t) - q\Delta x u'(x,t) + \frac{(q\Delta x)^2}{2}u''(x,t)\right. \\
\left. -\frac{(q\Delta x)^3}{6}u'''(x,t) + \frac{(q\Delta x)^4}{24}u''''(x,t) + ...\right]/q^2 \\
-2u(x,t) \\
+\sum_{q=1}^{Q}\left[u(x,t) + q\Delta x u'(x,t) + \frac{(q\Delta x)^2}{2}u''(x,t)\right. \\
\left. + \frac{(q\Delta x)^3}{6}u'''(x,t) + \frac{(q\Delta x)^4}{24}u''''(x,t) + ...\right]/q^2
\end{array}\right) \\
&\approx \frac{D}{Q}\sum_{q=1}^{Q} u''(x,t) + \frac{D}{12Q}\sum_{q=1}^{Q}(q\Delta x)^2 u''''(x,t) + o\left((\Delta x)^2\right) \\
&\approx Du''(x,t) + \frac{D}{12Q}\frac{2Q^3+3Q^2+Q}{6}(\Delta x)^2 u''''(x,t) + o\left((\Delta x)^2\right) \\
&\approx Du''(x,t) + D\frac{2Q^2+3Q+1}{72}(\Delta x)^2 u''''(x,t) + o\left((\Delta x)^2\right). \qquad (2.70)
\end{aligned}$$

We therefore obtain an error term which is approximately

$$D(2Q^2+3Q+1)(\Delta x)^2 u''''(x,t)/72, \qquad (2.71)$$

which recapitulates the local jumping error term from equation (2.69) when $Q = 1$. As Q becomes large the error term will therefore scale by approximately Q^2, so very long jumps will clearly be inappropriate, as was illustrated in Figure 2.12. However, for smaller maximum jump lengths the error term remains relatively small: for example, when $Q = 5$ we find an error term of $11D(\Delta x)^2 u''''(x,t)/12$, while providing significant decreases in computational time.

2.8 An aside on variances

This chapter has focussed solely on matching mean particle numbers between non-locally and locally jumping systems. However, in some cases the variance of particle numbers in each compartment may also be important. In this section we briefly sketch a proof that the variance of particle numbers in each compartment at steady-state is independent of our choice of non-local transition rates, at least in a system with no-flux boundary conditions and without any directional bias.

It is possible to derive an ODE for the evolution of the variance of particle number in each compartment, and we explain the method in more detail in Section 3.2.3. Consider some compartment j, such that $Q < j < (K - Q)$ (recalling that K is the number of compartments on the lattice). For unbiased diffusion we can obtain the equation

$$\begin{aligned}\frac{\mathrm{d}V_j}{\mathrm{d}t} &= -4\sum_{q=1}^{Q} T^q V_j + 2\sum_{q=1}^{Q} T^q V_{j-q,j} + 2\sum_{q=1}^{Q} T^q V_{j,j+q} \\ &\quad + \sum_{q=1}^{Q} T^q M_{j-q} + 2\sum_{q=1}^{Q} T^q M_j + \sum_{q=1}^{Q} T^q M_{j+q}, \end{aligned} \tag{2.72}$$

where V_j is the variance of particle numbers in compartment j, and $V_{i,j}$ the covariance of particle numbers between compartments i and j. Similar expressions can be derived for the compartments closer to the boundaries, and for the evolution of covariance values, although they are not presented here. Suppose that there are N particles in the system, so that we can find a steady-state mean value for each compartment,

$$\hat{M} = \frac{N}{K}. \tag{2.73}$$

To find a steady-state value for the variances, $\hat{V}$, we note that the steady-state value of each covariance must be $-\hat{V}/(K-1)$ (since the sum of all variances and covariances gives the variance of particle numbers across the whole system, which must be zero since the number of particles is held constant). We can then substitute

these steady-state values into the ODE to find

$$\begin{aligned} 0 &= -4\sum_{q=1}^{Q} T^q\hat{V} - \frac{2}{K-1}\sum_{q=1}^{Q} T^q\hat{V} - \frac{2}{K-1}\sum_{q=1}^{Q} T^q\hat{V} \\ &\quad + \sum_{q=1}^{Q} T^q\frac{N}{K} + 2\sum_{q=1}^{Q} T^q\frac{N}{K} + \sum_{q=1}^{Q} T^q\frac{N}{K} \\ &= -4\frac{K}{K-1}\hat{V}\sum_{q=1}^{Q} T^q + 4\frac{N}{K}\sum_{q=1}^{Q} T^q \\ &= -4\frac{K}{K-1}\hat{V} + 4\frac{N}{K}, \qquad (2.74) \\ \Rightarrow \hat{V} &= \frac{N(K-1)}{K^2}, \qquad (2.75) \end{aligned}$$

so the steady-state variance values will be the same for any (non-zero) choice of transition rates. Although this does not prove that the variances of a non-locally jumping system will necessarily match those of a locally jumping one away from the steady-state, we did not observe any significant differences in our simulation results.

2.9 Discussion

Computational time can provide a barrier to the use of exact SSAs such as the Gillespie algorithm and its extensions. Our non-local diffusion model suggests a new avenue of research in the acceleration of such simulations, by reducing computational time, as illustrated by comparisons throughout this chapter, while retaining the option of tracking individual particles, and remaining relatively simple to implement and explain. These time savings arise from the need to simulate fewer diffusion events, which outweighs the increased number of possible events to be checked, at least when implemented in an efficiently sorted, next subvolume method style algorithm [7].

How much time is saved by moving to a non-local jump model? We assume that the time taken to run a simulation is proportional to the number of jump events. If in a given time period the locally jumping system would simulate N_l events, then

the equivalent non-locally jumping system would simulate

$$\frac{N_l}{Q}\left(\sum_{q=1}^{Q}\frac{1}{q^2}\right), \tag{2.76}$$

events. Using Euler's well-known solution to the Basel problem, i.e.

$$\sum_{n=1}^{\infty}\frac{1}{n^2}=\frac{\pi^2}{6}, \tag{2.77}$$

we can establish upper and lower limits on the number of jump events simulated by the equivalent non-locally jumping system, such that

$$\frac{N_l}{Q}<N_n\leq\frac{N_l\pi^2}{6Q}. \tag{2.78}$$

We would therefore expect simulations of a non-local jumping model to finish at least $(6Q/\pi^2)\approx 0.6Q$ times faster than, and not more than Q times faster than, simulations of the equivalent local jumping model. These bounds are provided only as a rough estimate, but are consistent with the simulation durations observed in this chapter.

It is also interesting to consider whether non-local jumping models can be employed to investigate first passage time distributions, and whether these distributions would agree with those obtained using local jumping models. In the diffusive limit, non-local jumping models recapitulate the PDE diffusion equation, so it is reasonable to assume that when the distance to be travelled is significantly larger than the maximum jump distance, $Q\Delta x$, similar first passage time distributions will be observed. Over shorter distances, however, no such agreement can be expected, as can be illustrated by a simple example. Suppose we wish to investigate the time taken for a particle to travel Δx from its initial position, i.e. making any jump out of its starting compartment. A locally jumping particle, jumping in either direction with rate $D/(\Delta x)^2$, will have an expected first passage time of $(\Delta x)^2/2D$. A non-locally jumping particle with maximum jump length $Q=2$ will jump some

distance in either direction with total rate $5D/8(\Delta x)^2$, and hence will have an expected first passage time of $4(\Delta x)^2/5D$. The expected time taken to travel Δx is therefore longer for the non-local model, and this difference would be exacerbated for larger choices of Q. The first passage time distributions predicted by the two models can be expected to converge when the distance to be traversed is large, but over relatively short distances the two models will not agree.

We have presented a framework for using non-local jumping to accelerate stochastic diffusion simulations, developing the initial theory to incorporate hybrid systems and asymmetric jumping. We have also derived generalised boundary conditions for local and non-local jumping, corresponding to flux and Robin boundary conditions in the diffusive limit. Simulations have demonstrated the accuracy with which these models correspond to their locally, jumping and PDE equivalents, and have also shown the time-saving potential these methods offer.

Having seen that LBPJ simulations can be accelerated by replacing large numbers of short jumps with fewer, longer jumps, it is natural to ask whether even greater time savings can be made by replacing the many compartments on a fine-grained lattice with fewer, wider compartments, forming a coarser-grained lattice. In particular, we wish to investigate how volume-excluding effects, which we have so far ignored, would be implemented equivalently at the different scales.

In the next chapter we demonstrate a deep connection between LBPJ simulations incorporating volume exclusion on fine- and coarse-grained lattices. We show that the mean and variance of particle numbers in each coarse compartment can be derived from the mean and variance of total particle numbers across a number of compartments on the fine-grained lattice.

Chapter 3

Reconciling exclusion effects at different spatial scales

Models of diffusion that incorporate volume-excluding effects have a wide range of applications in biology and elsewhere [29, 89]. Coarse-grained LBPJ models, where large compartments can hold multiple particles, can be far more computationally efficient than fine-grained LBPJ models, where smaller compartments can hold at most one particle, and suffice when fine-grained detail is not required. Although both models are used ubiquitously in the literature, there has previously been no attempt to demonstrate that both give similar descriptions of the mean and variance of particle numbers. In this chapter we demonstrate a deep connection between volume-excluding diffusion processes on lattices with different compartment sizes.

The majority of work in this chapter appears in the Rapid Communication 'P.R. Taylor, C.A. Yates, M.J. Simpson and R.E. Baker, Reconciling transport models across scales: the role of volume exclusion, *Physical Review E*, **92** (2015) 040701(R)', and is reproduced with permission from the American Physical Society [90].

3.1 Modelling diffusive transport on different scales

Many phenomena of interest to theoretical biologists have been modelled as LBPJ systems, in which the domain is divided into discrete compartments, and particles

may jump between compartments, or interact with other particles in their vicinity [46]. LBPJ simulations can become computationally expensive, especially when the system is large, or when diffusive jumps are significantly more common than reaction events [70].

3.1.1 Non-excluding models

So far we have considered only LBPJ models that are 'non-excluding', and so allow unlimited numbers of particles to occupy the same compartment [55]. Apart from LBPJ models, the two most common models applied to describe non-excluding diffusive particles are off-lattice random walks and PDEs. These three formulations are profoundly linked. The location of a particle undergoing a simple Brownian motion is described by a probability density function that evolves following the PDE diffusion equation. In one dimension, the diffusion equation itself can be used to derive jump rates for a LBPJ, as can a Brownian motion, and a random walk on a lattice can be used to recover either a Brownian motion or the diffusion equation in the limit as the compartment size goes to zero [83].

Less attention has been given to reconciling LBPJ models when volume-excluding effects are taken into account. However, biological cells are crowded places, with up to 40% of their volume occupied by large macromolecules, so it is valuable to incorporate volume exclusion into models of diffusion in this context [6].

3.1.2 Fully-excluding and partially-excluding models

Many LBPJ models attempt to incorporate volume exclusion by imposing a maximum capacity on each compartment of the lattice to account for the physical extension of the particles in question [45]. We define a 'partially-excluding' process to be a LBPJ system in which at most $0 < m < \infty$ particles can occupy the same compartment at any given time, and attempts by particles to move into a given destination compartment may fail with a probability that is a function of the current occupancy of the destination compartment [91]. We further define a 'fully-excluding' process to be the special case where $m = 1$. Although both fully-excluding and partially-

excluding models are ubiquitous in the literature on diffusive processes [80, 81], there has not previously been any attempt to unify the two modelling paradigms.

In particular, in this chapter we focus on the jump rates of particles in a LBPJ model, moving without directional bias. We expect these jump rates to scale inversely with the square of the compartment size [92]. By considering the total number of particles across contiguous groups of m fully-excluding compartments of size h, where particles jump with rate D/h^2, we seek to match the number of particles within partially-excluding compartments of capacity m and size mh, where particles jump with rate D/m^2h^2. We will confirm the agreement of these two descriptions of particle movement, conditional upon the correct choice of probability for jumps to fail due to volume exclusion, by deriving and comparing master equations for the evolution of the mean and variance of particle numbers in both fully-excluding and partially-excluding models.

Since the fully-excluding description defines each particle's position as precisely as is possible in a LBPJ model, we shall consider it to be the most 'accurate' description. In this chapter, we clarify the relationship between partially- and fully-excluding models, demonstrating for the first time that a partially-excluding model on a coarse grid can accurately approximate the aggregated behaviour of a fully-excluding model on a finer grid, as illustrated in Figure 3.1. This unification of the two approaches will assist practitioners in making informed judgements on the most appropriate and efficient modelling framework for their simulations, and allow them to justify the use of more efficient techniques when finely detailed results are not required. This is an important development because, as we shall demonstrate, adopting partially-excluding models instead of fully-excluding models can reduce the computational time required for simulations by orders of magnitude.

3.1.3 Chapter outline

In Section 3.2, we derive master equations for the mean and variance of particle numbers in each compartment, in both fully- and partially-excluding systems. We find that fully-excluding and non-excluding models return similar equations for the

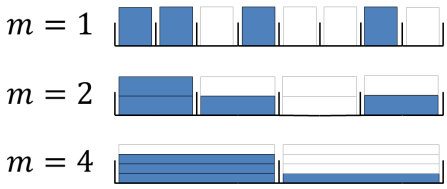

Figure 3.1: When we discuss aggregated fully-excluding compartments, we mean that they are grouped into notional, coarser compartments of greater capacity. In this figure, we see how this would apply to one possible particle distribution, with fully-excluding compartments at the top, and partially-excluding compartments below, with blue boxes representing particles and white spaces representing unused capacity. The total number of particles in each aggregated, coarse compartment is the total number of particles across all the finer compartments covering the same region of the domain.

evolution of mean particle numbers, and show that, in order to obtain analogous master equations for mean particle numbers in a partially-excluding model, attempted jumps into a compartment containing n particles must fail with probability n/m. Previous work has adopted this blocking probability [80], but to our knowledge this is the first demonstration that this is the only possible choice which returns a linear equations for the evolution of mean particle numbers.

In Section 3.3 we use these results to demonstrate the relationship between partially-excluding processes, and suitably aggregated fully-excluding processes (see Figure 3.1). We begin this section by showing that the partially-excluding steady-state values for both means and variances match those for an appropriately aggregated set of fully-excluding compartments. Having demonstrated an agreement between steady-state values, we then show that the equation for the evolution of the mean population of a compartment in a partially-excluding system, and the equation for the evolution of the population of m aggregated fully-excluding compartments, are equivalent (a previous attempt to reconcile these equations in the literature is shown to overestimate partially-excluding jump rates). An analogous approach is used to show the agreement of the variance equations. To verify these results, in Section 3.4 we present simulations of a system containing sharp gradients in particle density, demonstrating accuracy and a better than sixtyfold increase in computational speed by using coarser, partially-excluding systems in the place of

fully-excluding ones.

The implications of volume exclusion for the implementation of boundary conditions are discussed in Section 3.5, with a combination of error analysis and numerical simulation. The chapter then concludes with a short discussion of the potential for savings of computational time in Section 3.6. In Section 3.6 we also look forward to the development of hybrid modelling in Chapter 4, combining partially- and fully-excluding models for the purpose of obtaining computational time savings where possible while preserving accuracy where necessary.

3.2 Deriving master equations

We wish to demonstrate the correspondence of particle numbers in the partially-excluding compartments to the sum of particle numbers across multiple fully-excluding compartments (as illustrated in Figure 3.1). To show this correspondence, we use ODE master equations for the mean and variances of particle numbers. We consider the domain $x \in [0, L]$, and discretise it into a spatial lattice of K compartments. Each compartment is defined to have maximum particle capacity m, and the maximum capacity of the domain is therefore $\kappa = mK$.

For simplicity, we will work with one-dimensional processes for the remainder of this chapter, although our results can be extended to processes in two and three dimensions.

3.2.1 Mean particle numbers

The distribution of particles over the domain of K compartments is given by the vector $\mathbf{n}(t) = [n_1(t), n_2(t), ..., n_K(t)]$, where $n_i(t)$ denotes the number of particles in the i^{th} compartment at time t. We will work on a partially excluding system with capacity m, but in the interests of clarity will initially omit the superscript $^{(m)}$ from the variables. Particles in compartment i may *attempt* to jump to compartments $i-1$ or $i+1$ with rates T_i^- and T_i^+, respectively. In this chapter we consider exclusively unbiased movement over a uniform lattice, i.e. $T_i^{\pm} = d$ for all i, but provide a more

general derivation here as similar techniques are required for non-uniform lattices in Chapter 4. We define two operators, $J_i^+ : \mathbb{R}^K \to \mathbb{R}^K$, for $i = 1, ..., K-1$, and $J_i^- : \mathbb{R}^K \to \mathbb{R}^K$, for $i = 2, ..., K$, as

$$J_i^+ : [n_1, ..., n_i, ..., n_K] \to [n_1, ..., n_{i-2}, n_{i-1}, n_i + 1, n_{i+1} - 1, n_{i+2}, ..., n_K],$$
$$J_i^- : [n_1, ..., n_i, ..., n_K] \to [n_1, ..., n_{i-2}, n_{i-1} - 1, n_i + 1, n_{i+1}, n_{i+2}, ..., n_K].$$

Both operators move a particle into compartment i, taken from the compartment to the right or left, respectively. Assume that attempted jumps into compartment j fail with probability $f(n_j)$, where $j = 1, \ldots, K$, due to volume-excluding effects. We can then write

$$\begin{aligned}\frac{\mathrm{dPr}(\mathbf{n},t)}{\mathrm{d}t} = & \sum_{i=1}^{K-1} T_i^+ \quad \left\{(n_i+1)\left[1-f(n_{i+1}-1)\right]\mathrm{Pr}(J_i^+\mathbf{n},t)\right. \\ & \qquad \left. - n_i\left[1-f(n_{i+1})\right]\mathrm{Pr}(\mathbf{n},t)\right\} \\ & + \sum_{i=2}^{K} T_i^- \quad \left\{(n_i+1)\left[1-f(n_{i-1}-1)\right]\mathrm{Pr}(J_i^-\mathbf{n},t)\right. \\ & \qquad \left. -n_i\left[1-f(n_{i-1})\right]\mathrm{Pr}(\mathbf{n},t)\right\}. \end{aligned} \tag{3.1}$$

We define the mean vector $\mathbf{M} = [M_1, ..., M_K]$, where

$$M_j = \sum_{n_1=1}^{m}\sum_{n_2=1}^{m}\cdots\sum_{n_K=1}^{m} n_j \mathrm{Pr}(\mathbf{n},t) = \sum_{n_1,n_2,...,n_K=0}^{\mathcal{N}} n_j \mathrm{Pr}(\mathbf{n},t), \tag{3.2}$$

where we use $\sum^{\mathcal{N}}$ to denote summing over all possible values of n_i for all values of i such that $1 \leq i \leq K$. Multiplying equation (3.1) by n_j and summing over all

possible values that the vector $\mathbf{n}(t)$ can take, this expression becomes

$$\frac{\mathrm{d}M_j}{\mathrm{d}t} = \sum_{n_1,n_2,\ldots,n_K=0}^{\mathcal{N}} n_j \left(\sum_{i=1}^{K-1} T_i^+ \left\{ (n_i+1)\left[1-f(n_{i+1}-1)\right] \Pr(J_i^+\mathbf{n},t) \right.\right.$$
$$\left. - n_i\left[1-f(n_{i+1})\right]\Pr(\mathbf{n},t)\right\}$$
$$+ \sum_{i=2}^{K} T_i^- \left\{ (n_i+1)\left[1-f(n_{i-1}-1)\right] \Pr(J_i^-\mathbf{n},t) \right.$$
$$\left.\left. - \; n_i\left[1-f(n_{i-1})\right]\Pr(\mathbf{n},t)\right\} \right). \qquad (3.3)$$

We begin by considering only the first term of this expression, with $Pr(J_i^+ n,t)$ expanded explicitly to give

$$\sum_{n_1,n_2,\ldots,n_K=0}^{\mathcal{N}} n_j \sum_{i=1}^{K-1} T_i^+ (n_i+1)\left[1-f(n_{i+1}-1)\right] Pr(n_1,n_2,...,n_i+1,n_{i+1}-1,...n_K,t). \qquad (3.4)$$

When $i \neq j, j-1$ each term of this expression reduces to

$$T_i^+ \langle n_j n_i \rangle - T_i^+ \langle n_j n_i f(n_{i+1}) \rangle , \qquad (3.5)$$

where $\langle n_j n_i \rangle$ indicates the mean of the product. When $i = j$,

$$\begin{aligned}
& \sum_{n_1,n_2,\ldots,n_K=0}^{\mathcal{N}} n_j T_j^+ (n_j+1)\left[1-f(n_{j+1}-1)\right] Pr(n_1,n_2,...,n_j+1,n_{j+1}-1,...n_K,t) \\
= & \sum_{n_1,n_2,\ldots,n_K=0}^{\mathcal{N}} T_j^+ (n_j+1)^2\left[1-f(n_{j+1}-1)\right] Pr(n_1,n_2,...,n_j+1,n_{j+1}-1,...n_K,t) \\
& -T_j^+ (n_j+1)\left[1-f(n_{j+1}-1)\right] Pr(n_1,n_2,...,n_j+1,n_{j+1}-1,...n_K,t) \\
= & \; T_j^+ [\langle n_j n_j \rangle - \langle n_j n_j f(n_{j+1}) \rangle - M_j + \langle n_j f(n_{j+1}) \rangle]. \qquad (3.6)
\end{aligned}$$

Similarly for $i = j-1$,

$$\begin{aligned}
& \sum_{n_1,n_2,\ldots,n_K=0}^{\mathcal{N}} T_{j-1}^+ n_j (n_{j-1}+1)\left[1-f(n_j-1)\right] Pr(n_1,n_2,...,n_{j-1}+1,n_j-1,...n_K,t) \\
= & \; T_{j-1}^+ [\langle n_{j-1} n_j \rangle - \langle n_{j-1} n_j f(n_j) \rangle + M_{j-1} - \langle n_{j-1} f(n_j) \rangle]. \qquad (3.7)
\end{aligned}$$

By combining expressions (3.5)-(3.7), we can write expression (3.4) as

$$\sum_{i=1}^{K-1} T_i^+ \left[\langle n_j n_i\rangle - \langle n_j n_i f(n_{i+1})\rangle\right] + T_{j-1}^+ M_{j-1} - T_{j-1}^+ \langle n_{j-1} f(n_j)\rangle - T_j^+ M_j + T_j^+ \langle n_j f(n_{j+1})\rangle \,.$$

We then consider the second term of equation (3.3),

$$- \sum_{n_1,n_2,\ldots,n_K=0}^{\mathcal{N}} n_j \sum_{i=1}^{K-1} T_i^+ n_i \left[1 - f(n_{i+1})\right] Pr(n_1, n_2, ..., n_i, ..., n_K, t). \tag{3.8}$$

This simplifies to

$$- \sum_{i=1}^{K-1} T_i^+ \left[\langle n_i n_j\rangle - \langle n_i f(n_{i+1}) n_j\rangle\right]. \tag{3.9}$$

When combined with the expressions derived from the first term these give a contribution of

$$- T_j^+ M_j + T_j^+ \langle n_j f(n_{j+1})\rangle + T_{j-1}^+ M_{j-1} - T_{j-1}^+ \langle n_{j-1} f(n_j)\rangle \,, \tag{3.10}$$

to equation (3.3). Applying the same approach to the third and fourth terms, we obtain a contribution of

$$- T_j^- M_j + T_j^- \langle n_j f(n_{j-1})\rangle + T_{j+1}^- M_{j+1} - T_{j+1}^- \langle n_{j+1} f(n_j)\rangle \,. \tag{3.11}$$

In this chapter, we only consider directionally-unbiased movement on uniform lattices, so we set $T_i^{\pm} = d$ for all values of i. Adding equations (3.11) to (3.10) with this substitution, and including the superscript $^{(m)}$ terms again, we arrive at

$$\begin{aligned} \frac{\mathrm{d}M_j^{(m)}}{\mathrm{d}t} = \quad & d \quad \left[-M_j^{(m)} + \left\langle n_j^{(m)} f\left(n_{j+1}^{(m)}\right)\right\rangle + M_{j-1}^{(m)} - \left\langle n_{j-1}^{(m)} f\left(n_j^{(m)}\right)\right\rangle\right] \\ + \quad & d \quad \left[-M_j^{(m)} + \left\langle n_j^{(m)} f\left(n_{j-1}^{(m)}\right)\right\rangle + M_{j+1}^{(m)} - \left\langle n_{j+1}^{(m)} f\left(n_j^{(m)}\right)\right\rangle\right], \end{aligned} \tag{3.12}$$

for $1 < j < K$. Similar reasoning can be applied to the probability master equations for $M_1^{(m)}$ and $M_K^{(m)}$ to obtain

$$\begin{aligned}\frac{\mathrm{d}M_1^{(m)}}{\mathrm{d}t} &= d\left[-M_1^{(m)} + \left\langle n_1^{(m)} f\left(n_2^{(m)}\right)\right\rangle \right. \\ &\qquad \left. + M_2^{(m)} - \left\langle n_2^{(m)} f\left(n_1^{(m)}\right)\right\rangle\right], \qquad (3.13)\\ \frac{\mathrm{d}M_K^{(m)}}{\mathrm{d}t} &= d\left[-M_K^{(m)} + \left\langle n_K^{(m)} f\left(n_{K-1}^{(m)}\right)\right\rangle \right. \\ &\qquad \left. + M_{K-1}^{(m)} - \left\langle n_{K-1}^{(m)} f\left(n_K^{(m)}\right)\right\rangle\right]. \qquad (3.14)\end{aligned}$$

In a fully-excluding model, we write

$$f^{(1)}\left(n_j^{(1)}\right) = n_j, \qquad (3.15)$$

while for a non-excluding model, we write

$$f^{(\infty)}\left(n_j^{(\infty)}\right) = 0. \qquad (3.16)$$

By substituting either of these blocking probabilities into equation (3.12) we recover a discretised version of the diffusion equation,

$$\frac{\mathrm{d}M_j}{\mathrm{d}t} = d\big(M_{j-1} - 2M_j + M_{j+1}\big). \qquad (3.17)$$

3.2.2 Derivation of blocking probabilities

We now wish to find a general formula for the blocking probability in the partially-excluding case that recovers this same discretised diffusion equation, (3.17), while satisfying three other conditions:

1. when the compartment is empty, the blocking probability must be zero, i.e. $f^{(m)}(0) = 0$;

2. when the compartment is full to capacity, the blocking probability must be equal to unity, i.e. $f^{(m)}(m) = 1$;

3. the blocking probability should be exclusively a function of the current occupancy of the target compartment.

The only possible blocking probability that satisfies all these conditions is the natural choice

$$f^{(m)}(n_j^{(m)}) = n_j^{(m)}/m, \tag{3.18}$$

where the blocking probability depends linearly on occupancy. To prove this, we use standard results for the expectation of a function of two variables to write

$$\left\langle n_i^{(m)} f(n_j^{(m)}) \right\rangle \approx M_i^{(m)} f^{(m)}\left(M_j^{(m)}\right) + f^{(m)\prime}\left(M_j^{(m)}\right) V_{i,j}^{(m)}, \tag{3.19}$$

where $V_j^{(m)}$ describes the variance of particle numbers in the j^{th} compartment, and $V_{i,j}^{(m)}$ the covariance of particle numbers between the i^{th} and j^{th} compartments. Substituting this expression into equation (3.12), we write

$$\begin{aligned}\frac{\mathrm{d}M_j}{\mathrm{d}t} \approx \frac{D}{m^2h^2} \quad & \Big[M_{j-1} - 2M_j + M_{j+1} \\ & + M_j f^{(m)}(M_{j-1}) + M_j f^{(m)}(M_{j+1}) - M_{j-1} f^{(m)}(M_j) - M_{j+1} f^{(m)}(M_j) \\ & + V_{j-1,j}\left(f^{(m)\prime}(M_{j-1}) - f^{(m)\prime}(M_j)\right) \\ & + V_{j,j+1}\left(f^{(m)\prime}(M_{j+1}) - f^{(m)\prime}(M_j)\right)\Big],\end{aligned} \tag{3.20}$$

where in the interests of clarity we do not include $^{(m)}$ superscripts after each M and V term. To recover the diffusion equation, all the lines of this equation except for the first must evaluate to zero. In order for the third and fourth lines to evaluate to zero, we require

$$f^{(m)\prime}(M_{j\pm1}) - f^{(m)\prime}(M_j) = 0. \tag{3.21}$$

Since M_j and $M_{j\pm1}$ can be chosen independently, we find $f^{(m)\prime}(M_j) = A$, and hence $f^{(m)}(M_j) = AM_j + B$ for some constants A and B. Setting $M_j = 0$, our first condition (that $f^{(m)}(0) = 0$) requires that $B = 0$. Then, by setting $M_j^{(m)} = m$, the second condition (that $f^{(m)}(m) = 1$) requires that $A = 1/m$. In order to match

equation (3.12), it is therefore necessary to choose a blocking probability of the form $f^{(m)}(M_j) = M_j/m$.

3.2.3 Variance of particle numbers

Using the same techniques applied to derive the mean equations in Section 3.2.1, and making use of the derived blocking probability, we can obtain ODEs describing the evolution of the variances of particle numbers in the compartments. In this case, we begin from the definition of the variance of particle numbers in the j^{th} compartment,

$$V_j^{(m)}(t) = \sum_{n_1,n_2,\ldots,n_K=0}^{\mathcal{N}} \left[\left(n_j^{(m)}\right)^2 \Pr(\mathbf{n},t)\right] - \left(M_j^{(m)}(t)\right)^2. \tag{3.22}$$

It can be shown that

$$\begin{aligned}\frac{\mathrm{d}}{\mathrm{d}t}\sum_{n_1,n_2,\ldots,n_K=0}^{\mathcal{N}}\left(n_j^{(m)}\right)^2 P(\mathbf{n}) &= d\left\{2\left(1-\frac{1}{m}\right)\left\langle n_{j-1}^{(m)}n_j^{(m)}\right\rangle - 4\left\langle\left(n_j^{(m)}\right)^2\right\rangle\right. \\ &\quad \left. +2\left(1-\frac{1}{m}\right)\left\langle n_j^{(m)}n_{j+1}^{(m)}\right\rangle + M_{j-1}^{(m)} + 2M_j^{(m)} + M_{j+1}^{(m)}\right\}.\end{aligned} \tag{3.23}$$

By using $\langle n_i n_j\rangle = V_{i,j} + M_i M_j$, we can then write

$$\begin{aligned}\frac{\mathrm{d}V_j^{(m)}}{\mathrm{d}t} &= \frac{\mathrm{d}}{\mathrm{d}t}\sum_{n_1,n_2,\ldots,n_K=0}^{\mathcal{N}}\left(n_j^{(m)}\right)^2 P(\mathbf{n}) - \frac{\mathrm{d}}{\mathrm{d}t}(M_j^{(m)})^2 \\ &= \frac{\mathrm{d}}{\mathrm{d}t}\sum_{\mathcal{N}}\left(n_j^{(m)}\right)^2 P(\mathbf{n}) - 2d\left(M_{j-1}^{(m)}M_j^{(m)} - 2(M_j^{(m)})^2 + M_j^{(m)}M_{j+1}^{(m)}\right) \\ &= d\left[2\left(\frac{m-1}{m}\right)V_{j,j-1}^{(m)} - 4V_j^{(m)} + 2\left(\frac{m-1}{m}\right)V_{j,j+1}^{(m)}\right. \\ &\qquad +M_{j-1}^{(m)}\left(1-\frac{M_j^{(m)}}{m}\right) + M_j^{(m)}\left(1-\frac{M_{j-1}^{(m)}}{m}\right) \\ &\qquad \left. +M_j^{(m)}\left(1-\frac{M_{j+1}^{(m)}}{m}\right) + M_{j+1}^{(m)}\left(1-\frac{M_j^{(m)}}{m}\right)\right],\end{aligned} \tag{3.24}$$

for $1 < j < K$, with similar results obtainable for $j = 1$ and $j = K$:

$$\begin{aligned}
\frac{\mathrm{d}V_1^{(m)}}{\mathrm{d}t} &= d\left[-2V_1^{(m)} + 2\left(\frac{m-1}{m}\right)V_{1,2}^{(m)}\right. \\
&\quad \left. + M_1^{(m)}\left(1 - \frac{M_2^{(m)}}{m}\right) + M_2^{(m)}\left(1 - \frac{M_1^{(m)}}{m}\right)\right]; \qquad (3.25) \\
\frac{\mathrm{d}V_K^{(m)}}{\mathrm{d}t} &= d\left[2\left(\frac{m-1}{m}\right)V_{K-1,K}^{(m)} - 2V_K^{(m)}\right. \\
&\quad \left. + M_K^{(m)}\left(1 - \frac{M_{K-1}^{(m)}}{m}\right) + M_{K-1}^{(m)}\left(1 - \frac{M_K^{(m)}}{m}\right)\right]. \qquad (3.26)
\end{aligned}$$

When considering the covariance of particle numbers between two adjacent compartments, we find that its evolution is described by

$$\begin{aligned}
\frac{\mathrm{d}V_{j-1,j}^{(m)}}{\mathrm{d}t} &= d\left[\left(\frac{2}{m} - 4\right)V_{j-1,j}^{(m)} + V_j^{(m)}\right. \\
&\quad + V_{j-1}^{(m)} + V_{j-2,i}^{(m)} + V_{j-1,j+1}^{(m)} \qquad (3.27) \\
&\quad \left. - M_{j-1}^{(m)}\left(1 - \frac{M_j^{(m)}}{m}\right) - M_j^{(m)}\left(1 - \frac{M_{j-1}^{(m)}}{m}\right)\right],
\end{aligned}$$

where $2 < j < K$. Similar expressions can be found for the evolution of $V_{1,2}^{(m)}$ and $V_{K-1,K}^{(m)}$,

$$\begin{aligned}
\frac{\mathrm{d}V_{1,2}^{(m)}}{\mathrm{d}t} &= d\left[\left(\frac{2}{m} - 3\right)V_{1,2}^{(m)} + V_1^{(m)} + V_2^{(m)} + V_{1,3}^{(m)}\right. \\
&\quad \left. - M_1^{(m)}\left(1 - \frac{M_2^{(m)}}{m}\right) - M_2^{(m)}\left(1 - \frac{M_1^{(m)}}{m}\right)\right], \qquad (3.28) \\
\frac{\mathrm{d}V_{K-1,K}^{(m)}}{\mathrm{d}t} &= d\left[\left(\frac{2}{m} - 3\right)V_{K-1,K}^{(m)} + V_{K-1}^{(m)} + V_K^{(m)} + V_{K-2,K}^{(m)}\right. \\
&\quad \left. - M_{K-1}^{(m)}\left(1 - \frac{M_K^{(m)}}{m}\right) - M_K^{(m)}\left(1 - \frac{M_{K-1}^{(m)}}{m}\right)\right]. \qquad (3.29)
\end{aligned}$$

Equations for the evolution of particle number covariance between non-adjacent compartments can also be obtained,

$$\frac{\mathrm{d}V_{i,j}^{(m)}}{\mathrm{d}t} = d\left(-4V_{i,j}^{(m)} + V_{i-1,j}^{(m)} + V_{i+1,j}^{(m)} + V_{i,j-1}^{(m)} + V_{i,j+1}^{(m)}\right), \qquad (3.30)$$

where $1 < i < j-1 < K$, and for $1 < j+1 < i < K$. Slightly modified terms can be found for the boundaries, so that we have

$$\frac{\mathrm{d}V_{1,j}^{(m)}}{\mathrm{d}t} = d\left(-3V_{1,j}^{(m)} + V_{2,j}^{(m)} + V_{1,j-1}^{(m)} + V_{1,j+1}^{(m)}\right), \text{ for } 2 < j < K, \tag{3.31}$$

$$\frac{\mathrm{d}V_{1,K}^{(m)}}{\mathrm{d}t} = d\left(-2V_{1,K}^{(m)} + V_{2,K}^{(m)} + V_{1,K-1}^{(m)}\right), \tag{3.32}$$

$$\frac{\mathrm{d}V_{K,j}^{(m)}}{\mathrm{d}t} = d\left(-3V_{K,j}^{(m)} + V_{K-1,j}^{(m)} + V_{K,j-1}^{(m)} + V_{K,j+1}^{(m)}\right), \text{ for } 1 < j < K-1 \tag{3.33}$$

We note that none of these derivations require any closure assumptions about expressions of the form $\left\langle n_i^{(m)} n_j^{(m)} \right\rangle$ or $\left\langle n_i^{(m)} n_j^{(m)} n_k^{(m)} \right\rangle$: all such terms are either cancelled out or subsumed into the variance and covariance terms, just as they are in the non-excluding case [93].

3.3 Reconciling the different scales

Having derived results for the evolution of means and variances of particle numbers for fully-excluding and partially-excluding systems, we now seek conditions under which $M_i^{(m)}$ and $V_i^{(m)}$, the mean and variance values for the number of particles in one partially-excluding lattice site with capacity m, will match the mean and variance of the total number of particles in m contiguous fully-excluding lattice sites.

We therefore define $S_j^{(m)}$ to be the total number of particles in m contiguous fully-excluding lattice sites,

$$S_j^{(m)} = \sum_{i=(j-1)m+1}^{jm} n_i^{(1)}. \tag{3.34}$$

We further define $\mu_j^{(m)} = \left\langle S_j^{(m)} \right\rangle$ to be the mean total number of particles in those m contiguous fully-excluding lattice sites,

$$\mu_j^{(m)} = \left\langle \sum_{i=(j-1)m+1}^{jm} n_i^{(1)} \right\rangle = \sum_{i=(j-1)m+1}^{jm} M_i^{(1)}, \tag{3.35}$$

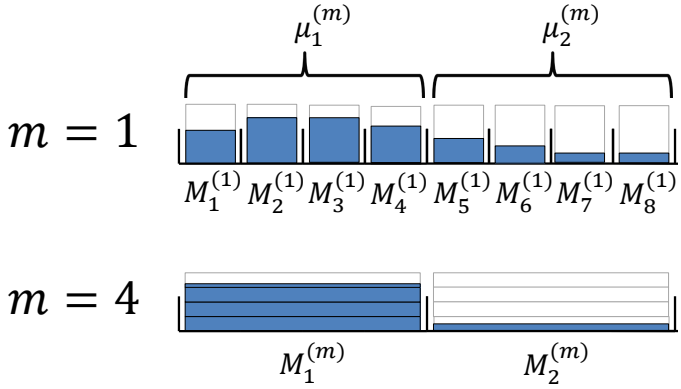

Figure 3.2: The aggregated fully-excluding compartments described by each $\mu_j^{(m)}$ and $v_j^{(m)}$ term are specified so that they occupy the same region of domain as that underlying $M_j^{(m)}$ and $V_j^{(m)}$. Because $M_j^{(m)}$ and $\mu_j^{(m)}$ describe mean occupancies they can take non-integer values, as illustrated in this figure.

and $v_j^{(m)}$ to be the variance of particle numbers across those lattice sites,

$$\begin{aligned} v_j^{(m)} &= \left\langle \left(\sum_{i=(j-1)m+1}^{jm} n_i^{(1)} \right)^2 \right\rangle - \left\langle \sum_{i=(j-1)m+1}^{jm} n_i^{(1)} \right\rangle^2 \\ &= \sum_{i=(j-1)m+1}^{jm} \sum_{l=(j-1)m+1}^{jm} V_{i,l}^{(1)}. \end{aligned} \tag{3.36}$$

In both cases, the indices of aggregated fully-excluding lattice sites are chosen so that $\mu_j^{(m)}$ and $v_j^{(m)}$ will correspond to $M_j^{(m)}$ and $V_j^{(m)}$, respectively, as is illustrated for $\mu_j^{(m)}$ in Figure 3.2.

3.3.1 Agreement at steady-state

The mean and variance evolution equations together form a degenerate system. However, if we impose zero-flux boundary conditions and fix the number of particles at some constant N, then the variance of total particle numbers in the domain will be zero. This provides an additional constraint

$$\sum_{i=1}^{K} V_i^{s,(m)} + 2 \sum_{i=1}^{K-1} \sum_{j=i+1}^{K} V_{i,j}^{s,(m)} = 0. \tag{3.37}$$

With this condition we can find unique steady-state values for the means, variance and covariances

$$\hat{M}_i^{(m)} = m\left[\frac{N}{\kappa}\right], \tag{3.38}$$

$$\hat{V}_i^{(m)} = m\left[\frac{N}{\kappa}\left(1-\frac{N}{\kappa}\right)\right] - m(m-1)\left[\frac{N}{\kappa(\kappa-1)}\left(1-\frac{N}{\kappa}\right)\right], \tag{3.39}$$

$$\hat{V}_{i,j}^{(m)} = -m^2\left[\frac{N}{\kappa(\kappa-1)}\left(1-\frac{N}{\kappa}\right)\right], \ \forall i \neq j, \tag{3.40}$$

where we use the hat to denote a steady-state value. Notice that, within the square brackets, all K and m terms occur only in the product $mK = \kappa$, i.e. the fixed total capacity of the domain. When comparing two different lattices partitioning the same domain $x \in [0, L]$, although the number of compartments and the capacities of those compartments will vary, consistency requires that the value of κ will remain constant. For example, if we are considering a domain of 256 fully-excluding lattice sites, and wish to replicate the model's behaviour with partially-excluding lattice-sites of capacity $m = 8$, then we must use $K = 32$ such sites to maintain the same total capacity.

It is therefore trivial to note the agreement between the mean particle numbers of the fully-excluding and partially-excluding systems at steady-state:

$$\hat{\mu}_j^{(m)} = \sum_{i=(j-1)m+1}^{jm} \hat{M}_i^{(1)} = m\left[\frac{N}{\kappa}\right] = \hat{M}_j^{(m)}. \tag{3.41}$$

Similarly,

$$\begin{aligned}
\hat{v}_j^{(m)} &= \sum_{i=(j-1)m+1}^{jm} \sum_{l=(j-1)m+1}^{jm} \hat{V}_{i,l}^{(1)} \\
&= m\hat{V}_i^{(1)} + m(m-1)\hat{V}_{i,l}^{(1)}, \quad i \neq l, \\
&= \hat{V}_j^{(m)}.
\end{aligned} \tag{3.42}$$

So the steady-state values for both the mean and the variance of total particle numbers across m fully-excluding compartments of width h match those for the

number of particles in a partially-excluding compartment of capacity m and width mh.

We note that the steady-state variance and covariance terms for the fully-excluding system can be confirmed using an alternative approach. To find the variance, we exploit the fact that $n_i^{(1)}$ can only take the values zero or unity, and hence $\left\langle n_i^{(1)} n_i^{(1)} \right\rangle = \left\langle n_i^{(1)} \right\rangle = M_i^{(1)}$. This allows us to write

$$\begin{aligned} \hat{V}_i^{(1)} &= \widehat{\left\langle n_i^{(1)} n_i^{(1)} \right\rangle} - \hat{M}_i^{(1)} \hat{M}_i^{(1)} \\ &= \hat{M}_i^{(1)} - \hat{M}_i^{(1)} \hat{M}_i^{(1)} \\ &= \frac{N}{\kappa}\left(1 - \frac{N}{\kappa}\right), \end{aligned} \tag{3.43}$$

which matches our master equation steady-state value for the variance. Similarly for a covariance term, we note that in the fully-excluding system the expression $\left\langle n_i^{(1)} n_j^{(1)} \right\rangle$ is simply the probability that both the i^{th} and j^{th} compartments are occupied. We can therefore use a simple conditioning to argue that

$$\begin{aligned} \hat{V}_{i,j}^{(1)} &= \widehat{\left\langle n_i^{(1)} n_j^{(1)} \right\rangle} - \hat{M}_i^{(1)} \hat{M}_j^{(1)} \\ &= \frac{N}{\kappa}\frac{N-1}{\kappa-1} - \frac{N}{\kappa}\frac{N}{\kappa} \\ &= -\frac{N}{\kappa(\kappa-1)}\left(1 - \frac{N}{\kappa}\right), \end{aligned} \tag{3.44}$$

which matches the steady-state covariance value obtained from the master equations. We can thus be confident in the accuracy of our model at its steady-state, and proceed to consider how fully-excluding and partially-excluding systems can be matched as they evolve in time.

3.3.2 Time evolution: mean equations

To obtain an expression for the evolution of $\mu_j^{(m)}$, we note that it can be obtained from the sum of the master equations for the mean particle numbers in each indi-

vidual fully-excluding compartment,

$$\begin{aligned}\frac{\mathrm{d}\mu_j^{(m)}}{\mathrm{d}t} &= \sum_{i=(j-1)m+1}^{jm} \frac{\mathrm{d}M_i^{(1)}}{\mathrm{d}t} \\ &= \frac{D}{h^2} \sum_{i=(j-1)m+1}^{jm} \left(M_{i-1}^{(1)} - 2M_i^{(1)} + M_{i+1}^{(1)}\right) \\ &= \frac{D}{h^2} \left(M_{(j-1)m}^{(1)} - M_{(j-1)m+1}^{(1)} - M_{jm}^{(1)} + M_{jm+1}^{(1)}\right), \end{aligned} \tag{3.45}$$

where we have used $d = D/h^2$, to relate the jump rate on the fully-excluding lattice d to the diffusion coefficient of the limiting PDE. We compare this to

$$\frac{\mathrm{d}M_j^{(m)}}{\mathrm{d}t} = \frac{D}{m^2h^2}\left(M_{j-1}^{(m)} - 2M_j^{(m)} + M_{j+1}^{(m)}\right), \tag{3.46}$$

noticing the jump rate differs between the two expressions since it scales with the inverse square of the compartment width. Importantly, we note that it is not possible to compare the $M^{(1)}$ and $M^{(m)}$ terms by assuming that particles are uniformly distributed within any given partially-excluding compartment, an approach used in some previous work [91]. This would lead us to write $M_{(j-1)m+1}^{(1)} = \mu_j^{(m)}/m$ etc., and equation (3.45) would become

$$\frac{\mathrm{d}\mu_j^{(m)}}{\mathrm{d}t} = \frac{D}{mh^2}\left(\mu_{j-1}^{(m)} - 2\mu_j^{(m)} + \mu_{j+1}^{(m)}\right), \tag{3.47}$$

which would imply a jump rate m times faster than we would expect from the partially-excluding equation, since we anticipate a jump rate of $D/(mh)^2$. A detailed analysis of this increased jump rate, deriving expected leaving times and locations for a random walker on a square lattice, is presented in Appendix B.1, and Appendix B.2 connects these results to the properties of Brownian motion, emphasising why the assumption of uniform distribution within each partially-excluding compartment cannot be used to obtain jump rates.

We proceed instead by making the assumption that the mean values of the fully-excluding compartments can be approximated by linearly interpolating the aggre-

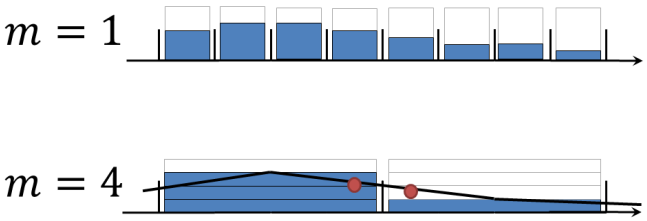

Figure 3.3: Schematic of the interpolation process for $m = 4$. The upper diagram depicts the mean occupancies of fully-excluding compartments, $M^{(1)}$, while the lower diagram shows the mean occupancy of the corresponding aggregated compartments, $\mu^{(m)}$ where $m = 4$. Note that, since we are dealing with mean occupancies, neither of these terms will (in general) be integer-valued. The red dots mark the locations at which values are being interpolated.

gated means described by $\mu_j^{(m)}$, as illustrated in Figure 3.3. Let the i^{th} aggregated, coarse compartment be centred on $x = mh(i-1/2)$, and the j^{th} fine compartment be centred on $x = h(j-1/2)$. It is then possible to make the following approximations:

$$M^{(1)}_{(j-1)m} \approx \frac{1}{2m}\frac{m+1}{m}\mu^{(m)}_{j-1} + \frac{1}{2m}\frac{m-1}{m}\mu^{(m)}_{j}; \tag{3.48}$$

$$M^{(1)}_{(j-1)m+1} \approx \frac{1}{2m}\frac{m-1}{m}\mu^{(m)}_{j-1} + \frac{1}{2m}\frac{m+1}{m}\mu^{(m)}_{j}; \tag{3.49}$$

$$M^{(1)}_{jm} \approx \frac{1}{2m}\frac{m+1}{m}\mu^{(m)}_{j} + \frac{1}{2m}\frac{m-1}{m}\mu^{(m)}_{j+1}; \tag{3.50}$$

$$M^{(1)}_{jm+1} \approx \frac{1}{2m}\frac{m-1}{m}\mu^{(m)}_{j} + \frac{1}{2m}\frac{m+1}{m}\mu^{(m)}_{j+1}. \tag{3.51}$$

With these approximations, equation (3.45) becomes

$$\frac{\mathrm{d}\mu_j^{(m)}}{\mathrm{d}t} = \frac{D}{m^2h^2}\left(\mu^{(m)}_{j-1} - 2\mu^{(m)}_{j} + \mu^{(m)}_{j+1}\right). \tag{3.52}$$

This means that whenever equations (3.48)-(3.51) are valid, we predict that the mean evolution of the aggregated fully-excluding system will match the mean values of the partially-excluding system. A physical interpretation of the linear interpolations is given in Appendix B.3.

3.3.3 Time evolution: variance equations

The values of the covariance matrix cannot, in general, be interpolated in the same way that we interpolated the mean values, since the elements of the covariance matrix will be positive on the diagonal and negative everywhere else. We can use interpolation arguments away from the diagonal, however, and then apply similar reasoning to argue that the variances $v_j^{(m)}$ and $V_j^{(m)}$ will also match. We begin by recalling equation (3.30),

$$\frac{\mathrm{d}V_{i,j}^{(m)}}{\mathrm{d}t} = \frac{D}{m^2h^2}\left(-4V_{i,j}^{(m)} + V_{i-1,j}^{(m)} + V_{i+1,j}^{(m)} + V_{i,j-1}^{(m)} + V_{i,j+1}^{(m)}\right), \qquad |i-j| > 1, \quad i,j \neq 1, K;$$

noting that the form of this equation is analogous to a two-dimensional version of equation (3.46). From our definition of $v_{i,j}^{(m)}$, we can write

$$\frac{\mathrm{d}v_{i,j}^{(m)}}{\mathrm{d}t} = \sum_{p=(i-1)m+1}^{im} \sum_{q=(j-1)m+1}^{jm} \frac{\mathrm{d}V_{p,q}^{(1)}}{\mathrm{d}t}; \quad |i-j| > 1; \quad i,j \neq 1, K. \tag{3.53}$$

We evaluate each of the ODE terms on the right-hand side of equation (3.53) to obtain

$$\begin{aligned}\frac{\mathrm{d}v_{i,j}^{(m)}}{\mathrm{d}t} = \frac{D}{h^2} \Bigg[& \sum_{p=(i-1)m+1}^{im} \left(V_{p,(j-1)m}^{(1)} - V_{p,(j-1)m+1}^{(1)}\right) \\ & + \sum_{p=(i-1)m+1}^{im} \left(V_{p,jm+1}^{(1)} - V_{p,jm}^{(1)}\right) \\ & + \sum_{q=(j-1)m+1}^{jm} \left(V_{(i-1)m+1,q}^{(1)} - V_{(i-1)m,q}^{(1)}\right) \\ & + \sum_{q=(j-1)m+1}^{jm} \left(V_{im+1,q}^{(1)} - V_{im,q}^{(1)}\right) \Bigg],\end{aligned} \tag{3.54}$$

where these four groups of terms represent transport over the bottom, top, left and right boundaries of $v_{i,j}^{(m)}$ as illustrated in Figure 3.4, respectively. By analogy with the linear interpolation approximations for mean values described in equations

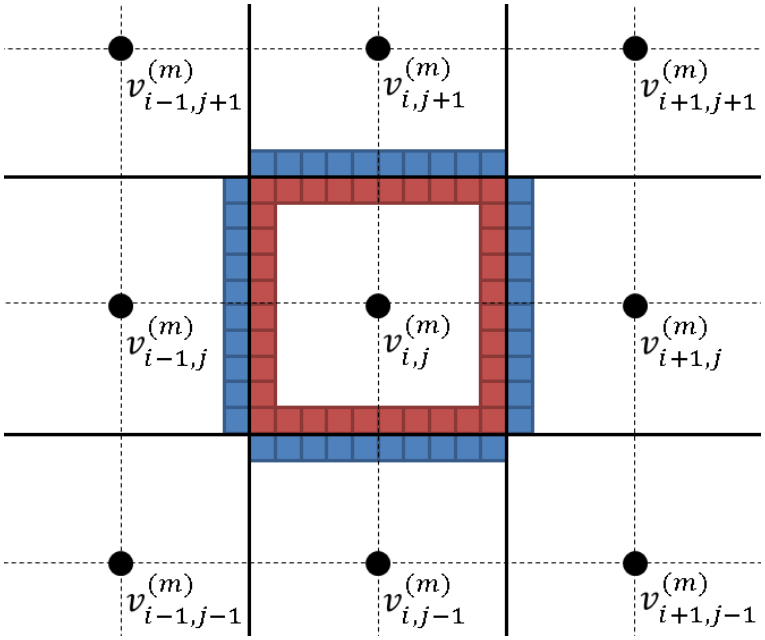

Figure 3.4: The red and blue compartments represent those $V^{(1)}$ terms which contribute explicitly to the evolution of $v^{(m)}_{i,j}$, with the inner, red compartments representing the negative terms of equation (3.54), and the outer, blue compartments the negative terms.

(3.48)-(3.51), we conjecture that

$$\begin{aligned}
\frac{1}{m}\sum_{p=(i-1)m+1}^{im}\left(V^{(1)}_{p,(j-1)m}-V^{(1)}_{p,(j-1)m+1}\right) &\approx \frac{1}{m^2}\left(\left[\frac{1}{2}\frac{m+1}{m}v^{(m)}_{i,j-1}+\frac{1}{2}\frac{m-1}{m}v^{(m)}_{i,j}\right]\right.\\
&\quad\left.-\left[\frac{1}{2}\frac{m-1}{m}v^{(m)}_{i,j-1}+\frac{1}{2}\frac{m+1}{m}v^{(m)}_{i,j}\right]\right)\\
&= \frac{1}{m^3}\left(v^{(m)}_{i,j-1}-v^{(m)}_{i,j}\right), \qquad (3.55)\\
\frac{1}{m}\sum_{p=(i-1)m+1}^{im}\left(V^{(1)}_{p,jm+1}-V^{(1)}_{p,jm}\right) &\approx \frac{1}{m^3}\left(v^{(m)}_{i,j+1}-v^{(m)}_{i,j}\right), \qquad (3.56)\\
\frac{1}{m}\sum_{q=(j-1)m+1}^{jm}\left(V^{(1)}_{(i-1)m+1,q}-V^{(1)}_{(i-1)m,q}\right) &\approx \frac{1}{m^3}\left(v^{(m)}_{i-1,j}-v^{(m)}_{i,j}\right), \qquad (3.57)\\
\frac{1}{m}\sum_{q=(j-1)m+1}^{jm}\left(V^{(1)}_{im+1,q}-V^{(1)}_{im,q}\right) &\approx \frac{1}{m^3}\left(v^{(m)}_{i+1,j}-v^{(m)}_{i,j}\right), \qquad (3.58)
\end{aligned}$$

where we have assumed that the average difference between the fully-excluding covariance values across each boundary of $v^{(m)}_{i,j}$ can be expressed as a linear interpola-

tion of two $v^{(m)}$ terms. Substituting these values into equation (3.54), we obtain

$$\frac{\mathrm{d}v_{i,j}^{(m)}}{\mathrm{d}t} = \frac{D}{m^2h^2}\left(-4v_{i,j}^{(m)} + v_{i-1,j}^{(m)} + v_{i+1,j}^{(m)} + v_{i,j-1}^{(m)} + v_{i,j+1}^{(m)}\right), \qquad |i-j| > 1, \\ i,j \neq 1, K;$$

which matches equation (3.53) as expected. We conclude that, away from the diagonal of the covariance matrix, the covariances of the partially-excluding system will evolve similarly to those of the summed-excluding system.

To consider the behaviour around the variance values, and adjacent covariances, we begin by noting that with $m = 1$, equations (3.24) and (3.27) become

$$\begin{aligned} \frac{\mathrm{d}V_i^{(1)}}{\mathrm{d}t} &= \frac{D}{h^2}\left[-4V_i^{(1)} + M_{i-1}\left(1 - M_i^{(1)}\right) + M_i^{(1)}\left(1 - M_{i-1}^{(1)}\right)\right. \\ &\quad \left. + M_i^{(1)}\left(1 - M_{i+1}^{(1)}\right) + M_{i+1}^{(1)}\left(1 - M_i^{(1)}\right)\right], \quad 1 < i < K, \end{aligned} \tag{3.59}$$

$$\begin{aligned} \frac{\mathrm{d}V_{i-1,i}^{(1)}}{\mathrm{d}t} &= \frac{D}{h^2}\left[-2V_{i-1,i}^{(1)} + V_i^{(1)} + V_{i-1}^{(1)} + V_{i-2,i}^{(1)} + V_{i-1,i+1}^{(1)}\right. \\ &\quad \left. + M_{i-1}^{(1)}\left(1 - M_i^{(1)}\right) + M_i^{(1)}\left(1 - M_{i-1}^{(1)}\right)\right], \quad 2 < i < K-1. \end{aligned} \tag{3.60}$$

By the standard equation for the variance of the sum of random variables, we find

$$\frac{\mathrm{d}v_j^{(m)}}{\mathrm{d}t} = \sum_{k=(j-1)m+1}^{jm}\left(\frac{\mathrm{d}V_k^{(1)}}{\mathrm{d}t}\right) + 2\sum_{p=(j-1)m+1}^{jm-1}\sum_{q=p+1}^{jm}\left(\frac{\mathrm{d}V_{p,q}^{(1)}}{\mathrm{d}t}\right). \tag{3.61}$$

We use equation (3.30) to substitute covariances for each of the ODE terms on the

right-hand side of equation (3.61), to obtain

$$\begin{aligned}\frac{\mathrm{d}v_j^{(m)}}{\mathrm{d}t} &= \frac{D}{h^2}\Bigg[\sum_{p=(j-1)m+1}^{jm}\left(V^{(1)}_{p,(j-1)m+1}+V^{(1)}_{p,jm}\right)\\ &\quad-\sum_{p=(j-1)m+2}^{jm}\left(V^{(1)}_{p,(j-1)m}+V^{(1)}_{p,jm+1}\right)\\ &\quad+\sum_{q=(j-1)m+1}^{jm}\left(V^{(1)}_{(j-1)m+1,q}+V^{(1)}_{jm,q}\right)\\ &\quad-\sum_{q=(j-1)m+2}^{jm}\left(V^{(1)}_{(j-1)m,q}+V^{(1)}_{jm+1,q}\right)\\ &\quad+M^{(1)}_{(j-1)m}\left(1-\frac{M^{(1)}_{(j-1)m+1}}{m}\right)+M^{(1)}_{(j-1)m+1}\left(1-\frac{M^{(1)}_{(j-1)m}}{m}\right)\\ &\quad+M^{(1)}_{jm}\left(1-\frac{M^{(1)}_{jm+1}}{m}\right)+M^{(1)}_{jm+1}\left(1-\frac{M^{(1)}_{jm}}{m}\right)\Bigg].\end{aligned} \tag{3.62}$$

We may draw an analogy to the mean equations, when after summation only those fine compartments on the borders of the notional coarse compartment make a contribution to the dynamics; we wish to show that $v_j^{(m)}$ evolves in the same way as $V_j^{(m)}$ does in equation (3.24), recapitulated for reference:

$$\begin{aligned}\frac{\mathrm{d}V_i^{(m)}}{\mathrm{d}t} = \quad &\frac{d}{m^2}\Bigg[2\left(\frac{m-1}{m}\right)V^{(m)}_{i,i-1}-4V_i^{(m)}+2\left(\frac{m-1}{m}\right)V^{(m)}_{i,i+1}\\ &+M^{(m)}_{i-1}\left(1-\frac{M^{(m)}_i}{m}\right)+M^{(m)}_i\left(1-\frac{M^{(m)}_{i-1}}{m}\right)\\ &+M^{(m)}_i\left(1-\frac{M^{(m)}_{i+1}}{m}\right)+M^{(m)}_{i+1}\left(1-\frac{M^{(m)}_i}{m}\right)\Bigg].\end{aligned}$$

The contributions of the variance terms are illustrated in Figure 3.5. It can be seen that they represent a simple diffusion pattern in two dimensions, similar to the expressions seen in the covariance equations away from the diagonal. The only deviation from this is seen in the top-left and bottom-right corners, where there is outflow to the external compartments but no inflow from them. Since the affected region on each edge is $1/m$ of the total edge length, it seems intuitive that this

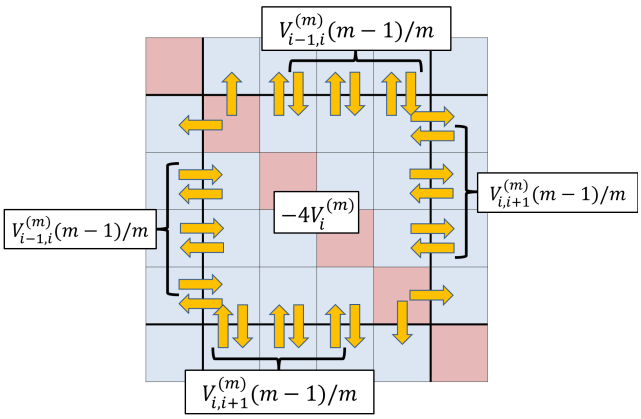

Figure 3.5: The red compartments represent the variances of the fully-excluding system (i.e. the central diagonal of the covariance matrix), while the blue compartments represent the covariances. It can be seen that particles are leaving the central compartment at every edge (accounting for the $-4V_i^{(m)}$ term in the partially-excluding model), and are entering from the surrounding compartments at each edge except for the two in the top-left corner and the two in the bottom-right corner (those adjacent to the fine grid variance terms). This explains why the input terms are $V_{i-1,i}^{(m)}(m-1)/m$ and $V_{i,i+1}^{(m)}(m-1)/m$ respectively.

corresponds to the partially-excluding system, where the input terms from the surrounding compartments all scale with $(m-1)/m$. A similar argument can be made for the $v_{j-1,j}^{(m)}$ off-diagonal terms, where outflow scales with $(4-2/m)$. We also note that in our expression for $v_j^{(m)}$, the contributions from mean terms simply represent the propensity for a move occuring, just as they do in the partially-excluding case. On this basis, and considering the strong agreements in numerical investigations we present in Section 3.4, it seems reasonable to expect the variance of the total number of particles across m fully-excluding compartments to match that of a partially-excluding compartment with capacity m.

3.4 Numerical investigations

In order for the mean equations of the fully-excluding and partially-excluding systems to match we made the assumption that there is an approximately linear distribution of particles across each compartment. In this section we simulate a system where this

assumption does not hold, to show that partially-excluding models can still predict the dynamics of fully-excluding models accurately.

The spatial domain used was $x \in [0, L]$, with $L = 1$, and we compared the averaged results from 5,000 simulations of a fully-excluding system with 128 compartments, to those from 5,000 simulations of a partially-excluding system with 16 compartments of capacity 8. We chose our diffusion coefficient to be $D = 10^3/128^2$, and initialised the system at $t = 0$ such that 16 particles were placed at the left-hand boundary of the domain (occupying the first 16 fully-excluding compartments, and filling the first two partially-excluding compartments to capacity, respectively). In Figures 3.6 and 3.7 we observe good agreement between both the means and variances of the fully-excluding and partially-excluding systems at $t = 1$, and also see a good fit of the mean values to those of the corresponding diffusion equation, solved using Matlab's `pdepe` function. It took 21.6 seconds to simulate 5,000 repeats of the partially-excluding system, compared to 1395.3 seconds to simulate an equal number of repeats of the fully-excluding system. The partially-excluding simulation therefore ran around 64 times faster, as might be expected since the fully-excluding simulation will feature, on average, $m^2 = 64$ times more attempted jumps than the partially-excluding one due to the higher jump propensity.

To compute error measures, we solved the master equations for both means and variances numerically using Matlab's `ode45` function, comparing the results from $m = 2$, $m = 4$ and $m = 8$ to those from the fully-excluding system using the HDE metric, described in Section 2.2.1. Note that in the previous chapter the HDE was used to compare the mean of simulation results to the solution to a PDE. In this chapter, however, we use the HDE to compare mean and variances obtained from ODE master equations for partially-excluding models to the corresponding aggregated mean and variance obtained from ODE master equations for the fully-excluding model.

In Figures 3.8 and 3.9 we observe how the HDEs vary between $t = 0$ and $t = 1$ for different values of m, observing strong agreement between the partially-excluding system and the aggregated fully-excluding system. We therefore see that, even in

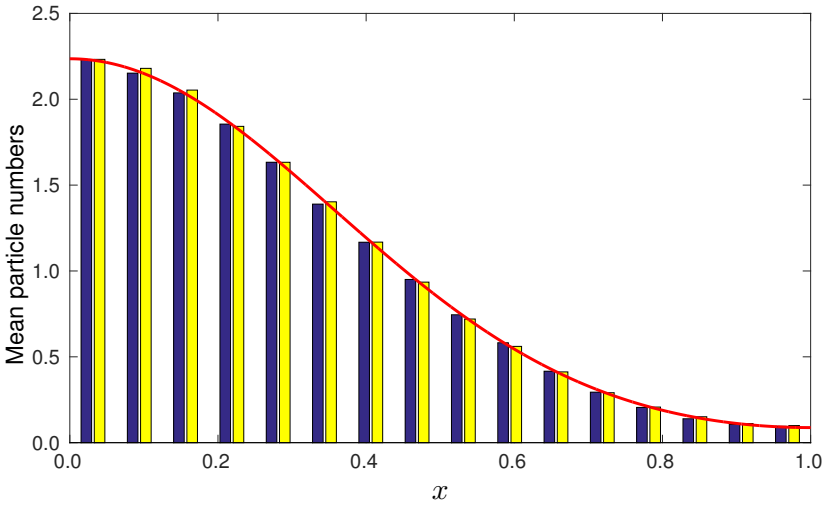

Figure 3.6: The mean particles number resulting from aggregating fully-excluding compartments of size 1/128 are shown as blue bars, while those from the partially-excluding compartments with capacity $m = 8$ and size 1/16 are shown as yellow bars. The solution of the limiting PDE is shown as a red line for comparison.

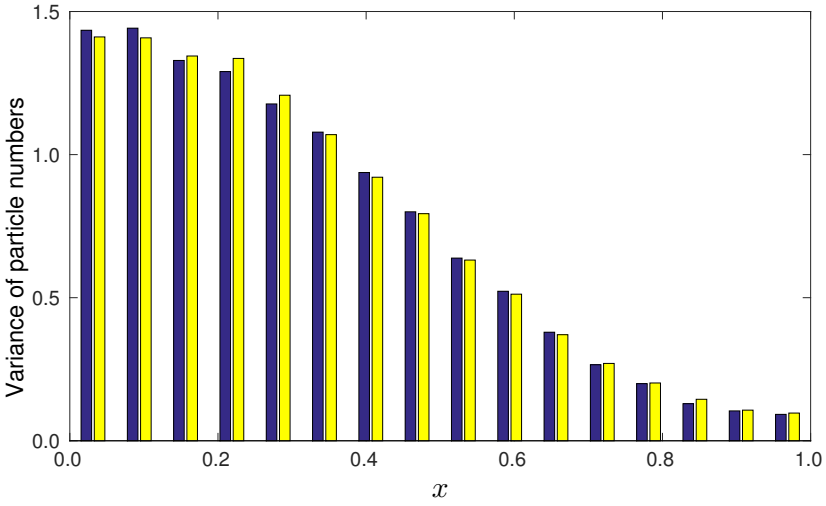

Figure 3.7: As in Figure 3.6, but showing the variance of particle numbers rather than the mean.

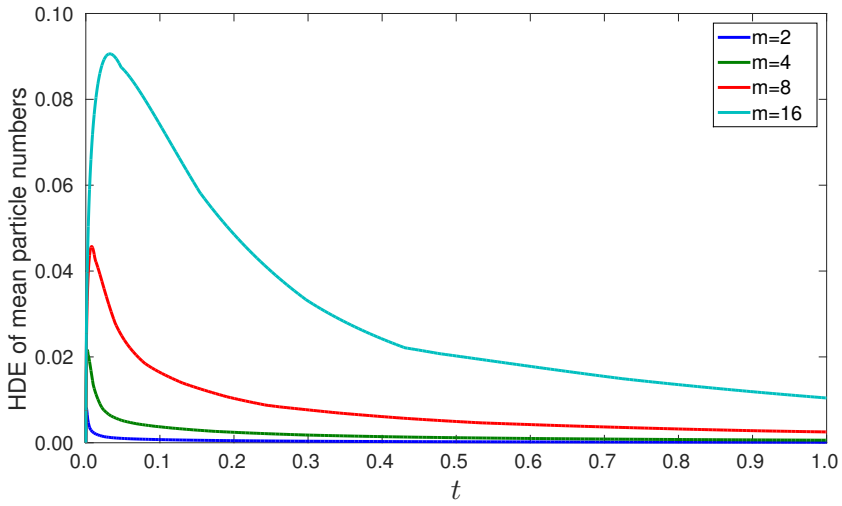

Figure 3.8: We observe good agreement between the solution to the mean evolution equations for the partially-excluding system, and the mean of aggregated particle numbers across m compartments of the fully-excluding system, for a range of values of m.

a potentially difficult case where particle concentrations cannot be assumed to vary linearly over each coarse compartment, partially-excluding models provide accurate predictions while requiring only a fraction of the computational time required to simulate fully-excluding models.

Further numerical investigations, comparing the results of fully- and partially-excluding models in a variety of scenarios, are presented in Sections 4.3 and 4.4 of the following chapter. In the remainder of this chapter, we consider how volume-excluding effects may affect the implementation of boundary conditions, then conclude with a brief discussion of the results obtained so far.

3.5 Volume exclusion and boundary conditions

In Sections 2.3 and 2.4 of Chapter 2, we derived boundary conditions for LBPJ models, so that we could match the results of our simulations to the solution of a limiting PDE. Those results were only derived for uniform, non-excluding lattices. In the following chapter we will use a flux boundary condition in an excluding model (in Section 4.3.3) to create a morphogen gradient, so in this section we generalise

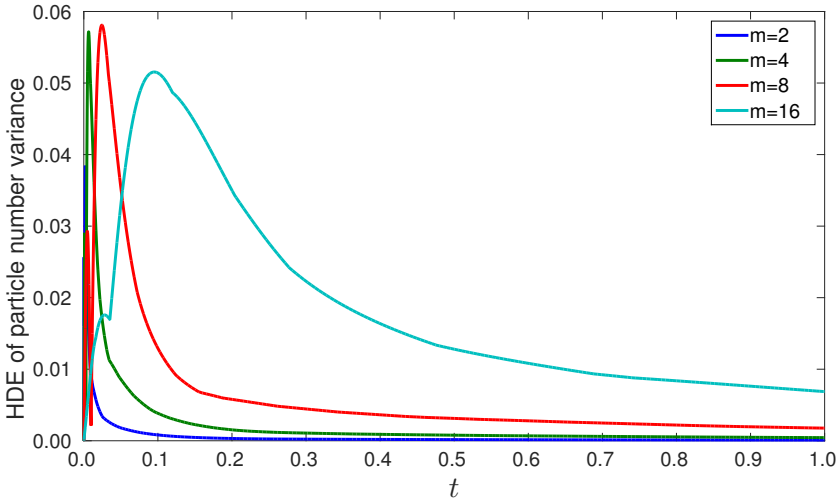

Figure 3.9: The master equations for the evolution of variances in the partially-excluding system match the variances of the aggregated fully-excluding system well. We observe initial peaking as an artefact of normalising the data, since the variances are zero at $t = 0$, with subsequent peaks for $m = 8$ and $m = 16$ apparently following from the peaks observed in the HDE for the mean values.

our previous results to discuss the implementation of boundary conditions in models incorporating volume exclusion.

Previously, we described PDE boundary conditions in terms of a continuous function $u(x, t)$, defined to agree with mean particle numbers at the centre of each compartment, as described in equation (2.2) which we restate for convenience:

$$u(x_i, t) = M_i(t). \tag{3.63}$$

In the context of this chapter's work on reconciling descriptions at different spatial scales, it makes more sense to work with a continuous concentration value, $c(x, t)$ instead, such that for $1 < i < K$,

$$c(x_i, t) = \frac{M_i(t)}{mh} = \frac{1}{mh} u(x_i, t). \tag{3.64}$$

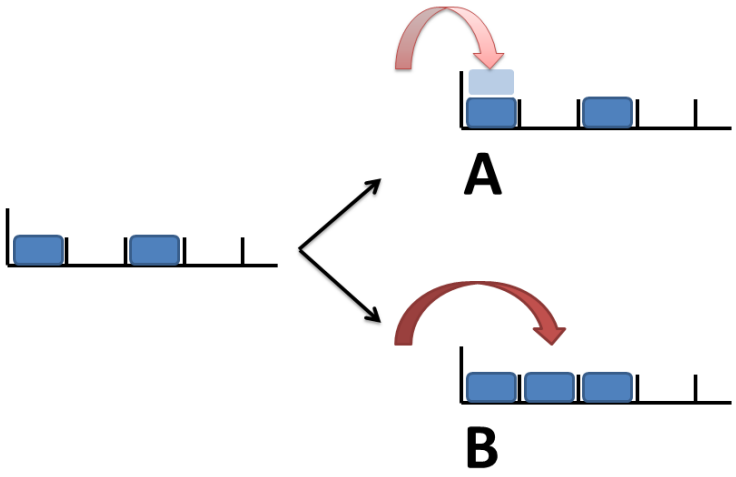

Figure 3.10: Two options for implementing an influx boundary condition in a model incorporating volume exclusion. To the left, we see a fully-excluding lattice, with the first and third compartments from the boundary occupied. When an influx event occurs it is not possible to add a new particle to the first compartment, as this is already at capacity, so two implementation options are to queue the event until the first compartment becomes empty (A), or to immediately add a new particle to the closest available compartment to the boundary (B).

3.5.1 Flux boundary conditions for a fully-excluding, uniform lattice

Implementing an in-flux boundary condition in an volume-excluding system is a challenging problem: the stochasticity of the process may lead to a particle attempting to enter the system when the boundary compartment is fully occupied. Conversely, implementing an out-flux condition is non-trivial in any stochastic system, whether excluding or non-excluding, since there may not be a particle present in the boundary compartment to be removed when the event occurs.

One possibility is to queue up flux events. If such an event is scheduled to occur at a time when it cannot be implemented in the system it is stored instead, and implemented as soon as the system changes to make it possible (a particle moving out of the full, in-flux boundary compartment, or a particle moving into an empty, out-flux boundary compartment). This possibility is illustrated in Figure 3.10 as option A. Unfortunately when simulated this leads to major inaccuracies around the boundaries of the system.

Instead, this chapter's work on reconciling particle behaviours between scales suggests a solution. Having already worked on showing the agreement of mean particle numbers within coarse, partially-excluding compartments of capacity m with mean numbers within the aggregation of m fully-excluding compartments, it is natural to ask how this translates to boundary conditions. Specifically, we wish to use $\mu_1^{(m)}$ and $\mu_2^{(m)}$ to approximate the concentration gradient at the boundaries, $\partial c/\partial x$. If $\mu^{(m)}$ can be used at the boundary in this way, then we could use this to justify adding particles to any of the first m fully-excluding compartments, rather than just the first one. This option is illustrated in Figure 3.10 as option B.

To test this approach, we will first apply some error analysis to determine how accurate these approximations would be to the actual derivative at the boundary, and follow up with numerical simulation of a test system with both in-flux and out-flux boundary conditions. If the width of each fully-excluding compartment is h, then the gradient at the boundary is approximated as

$$\begin{aligned}
\left.\frac{\partial c}{\partial x}\right|_{x=0} &\approx \frac{\frac{M_2^{(m)}(t)}{mh} - \frac{M_1^{(m)}(t)}{mh}}{mh} && (3.65)\\
&\approx \frac{c(\frac{3h}{2},t) - c(\frac{h}{2},t)}{mh} && (3.66)\\
&\approx \frac{\left(c(0,t) + \frac{3mh}{2}c'(0,t) + \frac{9m^2h^2}{8}c''(0,t)\right) - \left(c(0,t) + \frac{mh}{2}c'(0,t) + \frac{m^2h^2}{8}c''(0,t)\right)}{mh}\\
&\approx \left.\frac{\partial c}{\partial x}\right|_{x=0} + mh\left.\frac{\partial^2 c}{\partial x^2}\right|_{x=0}, && (3.67)
\end{aligned}$$

where we have assumed that the $O(h^2)$ terms of the expansion are neglible in comparison to the first and second derivative terms. The local error therefore scales with the partially-excluding compartment size mh. Suppose instead we consider two coarse compartments comprised of m fine compartments (each of width h), i.e. $S_1^{(m)}$

and $S_2^{(m)}$. Then we can write

$$\left.\frac{\partial c}{\partial x}\right|_{x=0} \approx \frac{\frac{\mu_2^{(m)}(t)}{mh} - \frac{\mu_1^{(m)}(t)}{mh}}{mh} \tag{3.68}$$

$$\approx \frac{\frac{1}{mh}\sum_{i=m+1}^{2m}[m_i(t)] - \frac{1}{mh}\sum_{i=1}^{m}[m_i(t)]}{mh} \tag{3.69}$$

$$\approx \frac{\sum_{i=m+1}^{2m}\left[c(ih-\frac{1}{2},t)\right] - \sum_{i=1}^{m}\left[c(ih-\frac{1}{2},t)\right]}{m^2h} \tag{3.70}$$

$$\approx \frac{1}{m^2h}\left[h\sum_{i=m+1}^{2m}(i-\frac{1}{2}) - h\sum_{i=1}^{m}(i-\frac{1}{2})\right]\left.\frac{\partial c}{\partial x}\right|_{x=0} + \frac{1}{2m^2h}\left[h^2\sum_{i=m+1}^{2m}(i-\frac{1}{2})^2 - h^2\sum_{i=1}^{m}(i-\frac{1}{2})^2\right]\left.\frac{\partial^2 c}{\partial x^2}\right|_{x=0} \tag{3.71}$$

$$\approx \left.\frac{\partial c}{\partial x}\right|_{x=0} + \frac{h}{2m^2}\left[\sum_{i=m+1}^{2m}(i^2-i+\frac{1}{4}) - \sum_{i=1}^{m}(i^2-i+\frac{1}{4})\right]\left.\frac{\partial^2 c}{\partial x^2}\right|_{x=0}$$

$$\approx \left.\frac{\partial c}{\partial x}\right|_{x=0} + \frac{h}{2m^2}\left[\sum_{i=1}^{2m}(i^2) - 2\sum_{i=1}^{m}(i^2) - \sum_{i=1}^{m}(m)\right]\left.\frac{\partial^2 c}{\partial x^2}\right|_{x=0} \tag{3.72}$$

$$\approx \left.\frac{\partial c}{\partial x}\right|_{x=0} + \frac{h}{2m^2}\left[\frac{2(2m)^3+3(2m)^2+(2m)}{6} - 2\frac{2m^3+3m^2+m}{6} - m^2\right]\left.\frac{\partial^2 c}{\partial x^2}\right|_{x=0}$$

$$\approx \left.\frac{\partial c}{\partial x}\right|_{x=0} + mh\left.\frac{\partial^2 c}{\partial x^2}\right|_{x=0}, \tag{3.73}$$

so the local error again scales with mh. It therefore seems reasonable to add particles to, or remove them from, the closest available compartment to the boundary.

As an aside, we note that our derivation of the Robin condition is not affected by the introduction of volume exclusion effects.

3.5.2 Simulation results

As a test case for flux boundary conditions in the models incorporating volume exclusion, we define a system with an in-flux boundary condition at the left of the domain, and an out-flux boundary condition at the right, using method B from Figure 3.10. The resulting system has a linear, non-uniform steady-state. We define a domain $x \in [0, 50]$, with flux conditions to maintain a linear gradient steady-state,

such that the mean occupancy at the left boundary is 0.9, and at the right boundary is 0.1, i.e.

$$c(x,t) = 0.9 - \frac{(0.9-0.1)}{50}x = 0.9 - 0.016x. \tag{3.74}$$

This deliberately extreme case has been chosen to ensure that there will be many occasions when the flux events must be implemented several compartments away from the boundary.

We set $D = 10^3/128^2$, and run each simulation until time $t = 1$, using a fully-excluding grid in all cases with varying grid spacings (normally we would seek to maintain the total capacity of the system, but in this case we are only interested in the effect of the grid size on the accuracy of the results). To set the initial state in each repeat of the simulation, we generate a random number between zero and one for each compartment: if the number is less than the analytic steady-state solution for that compartment then that compartment begins the simulation occupied, otherwise it begins the simulation unoccupied.

In Figure 3.11 we plot the mean occupancy of each compartment in the system as obtained from multiple realisations of the model, and compare this to the analytic solution: as expected, the mean occupancy values match more closely with the expected, steady-state solution as the grid becomes finer. This can be observed clearly in Figure 3.12, which contains a plot of the absolute differences between the analytic solution and the average compartment occupancies from the simulations.

3.6 Discussion

As has previously been discussed, exact stochastic simulation is relatively computationally expensive. Chapter 2 demonstrated how speed-ups could be achieved by approximating large numbers of short jumps with fewer, variable-length jumps, and this chapter has presented another means of speeding up simulations, by coarse-graining the spatial locations of particles.

We began by deriving equations for the evolution of the mean and variance of particle numbers in fully-excluding and partially-excluding compartments. Mean

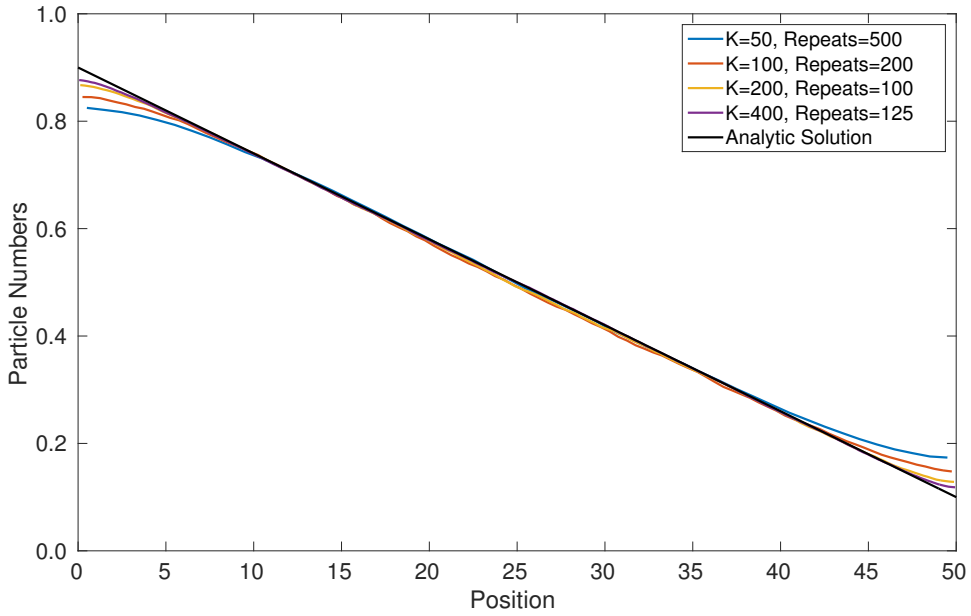

Figure 3.11: Average state of a system at time $t = 1$, with a constant influx boundary condition at the left of the domain and a constant outflux boundary condition at the right. We vary the particle length h, and hence the number of compartments K, to observe how the error varies as the lattice becomes finer. The deviation of simulation results from the analytic solution can be observed near the boundaries, and it is also clear that this error is reduced for finer grid spacings.

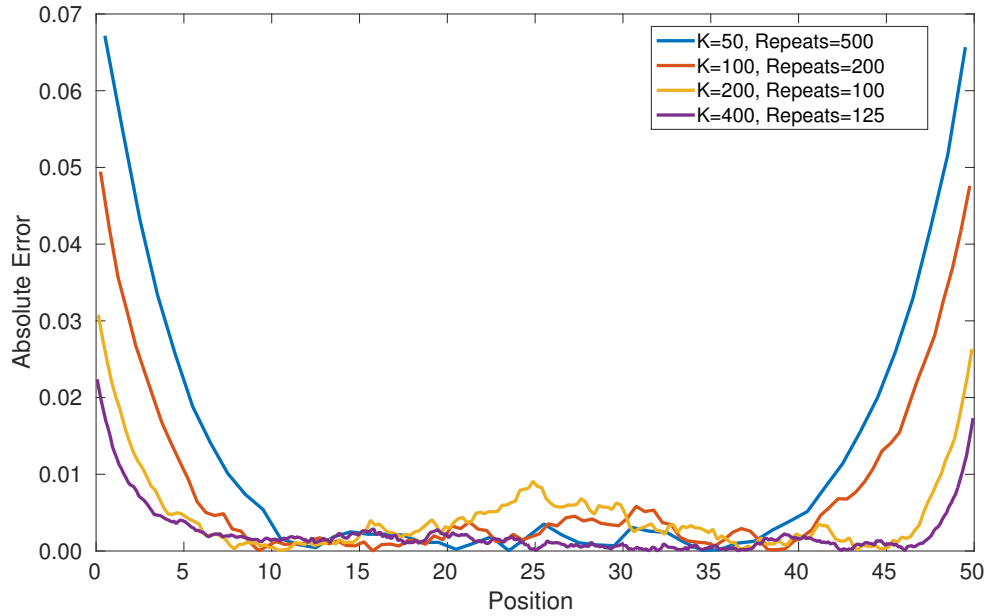

Figure 3.12: The absolute difference between the average occupancy at each lattice site and the analytic solution is highest at the boundaries, and is reduced for finer lattice spacings.

and variance equations for non-excluding LBPJ models had been published previously [93], but the equations for volume-excluding models are novel. By requiring the mean equations for partially-excluding compartments to recapitulate the diffusion equation, it was possible to establish a unique form for the blocking probability. We presented further novel results, demonstrating through steady state analysis and interpolation arguments that the predictions of fully-excluding and partially-excluding mean and variance equations can be reconciled. The remainder of the chapter presented the results of numerical investigation, and discussed the implications of volume exclusion for the implementation of boundary conditions.

The computational time savings demonstrated in this chapter are significant, and we have seen partially-excluding models being simulated in only $1/m^2$ of the time required to simulate the equivalent fully-excluding model. Since the speed-ups are a result of fewer jumps being simulated, they will be equally effective for systems in two or three dimensions. Although the precise time taken by a simulation will depend on the algorithm used, there is no reason to expect the computational cost of implementing a jump event to be higher in a partially-excluding model compared to a fully-excluding model. In some cases, such as a simple implementation using a linear search rather than a binary search to find event locations, the smaller number of compartments in the partially-excluding model could lead to additional time savings, in addition to those already obtained by only simulating a fraction of the jump events occuring in the equivalent fully-excluding model.

It may be noted that there are some arrangements of particles in which the fully-excluding and partially-excluding models do not appear to agree precisely. For example, consider a small domain of six fully-excluding boxes, with the middle four occupied by particles and the two boundary compartments unoccupied. Consider also the equivalent partially-excluding model with $m = 3$: i.e. two partially-excluding compartments, each containing two particles, with capacity for one more. The partially-excluding model would allow for jumping between the two compartments, but the crowding at the middle of the domain would prohibit such movement between the two halves of the domain in the fully-excluding model. This is not a

problem for models containing a single species of particle (although the following two chapters explore several multi-species models where the results of fully-excluding and partially-excluding models are not reconcilable in one spatial dimension). Because jumps occur m^2 times more frequently in the fully-excluding model compared to the partially-excluding model, it is to be expected that the particles occupying a partially-excluding compartment will explore multiple configurations, some of which permit movement between the corresponding partially-excluding compartments and others prohibiting such movement. The partially-excluding jump rates and blocking probabilities can therefore be considered as representing average properties of the ensemble, rather than corresponding to any given combination of fully-excluding compartment occupancies (the questions of particle mixing and probabilistic arrangements are revisited in our work on reactions in Chapter 5).

It should also be noted that, as argued in Appendices B.1 and B.2, it is not possible to make a one-to-one correspondence linking jumps between partially-excluding compartments and jumps between fully-excluding compartments, for reasons related to the fractal properties of Brownian motion. It is for this reason that we have employed linear interpolations in this chapter, and we discuss the physical interpretation of these interpolations in Appendix B.3.

So far we have only considered volume exclusion on uniform lattices. Recent years have seen increasing interest in hybrid models, capable of spatially-precise simulation within small spatial regions of interest, while using less computationally intensive methods elsewhere on the domain [94, 57, 95]. In the next chapter, we present two methods by which a fully-excluding region can be interfaced with a partially-excluding region where $m > 1$, resulting in a non-uniform lattice. We compare the resulting hybrid models against models using uniform fully- and partially-excluding lattices in a range of scenarios.

Chapter 4

Hybrid methods to couple excluding models at different scales

Many processes in biology are multiscale, incorporating events at varying spatial and temporal scales [96]. In this chapter, we outline and test hybrid models that include volume exclusion. These hybrid models use fully-excluding compartments in regions of the domain where precision is necessary, while using computationally efficient partially-excluding compartments elsewhere.

The majority of the work in this chapter appears in the paper 'P.R. Taylor, R.E. Baker, M.J. Simpson and C.A. Yates, Coupling volume-excluding compartment-based models of diffusion at different scales: Voronoi and pseudo-compartment approaches, *Journal of the Royal Society: Interface*, **13** (2016) 0336', and is reproduced with permission from Royal Society Publishing [97].

4.1 Non-uniform lattices

As discussed in Chapter 3, volume exclusion (crowding) can be incorporated into compartment-based models by assigning a maximum particle capacity, m, to each compartment, where m varies linearly with compartment size. Attempted moves into

any given compartment are blocked with some probability. Of particular interest is the case where this probability scales linearly with compartment occupancy, such that the blocking probability is equal to zero when empty and to unity when full to capacity, m [80, 81, 91]. Recall that we describe such a model as 'partially-excluding' or 'coarse-grained' when $m > 1$, and as 'fully-excluding' or 'fine-grained' when $m = 1$.

In the previous chapter, we showed that the descriptions of a system given by fully-excluding and partially-excluding models can be reconciled. Specifically, we demonstrated that the mean and variance of particle numbers within each partially-excluding compartment of capacity m is an accurate predictor of the mean and variance of the total number of particles across the m corresponding contiguous fully-excluding compartments.

So far our work has considered uniform lattices, where every compartment is of the same size and capacity. In many cases, it may be necessary to incorporate events occurring across a wide range of spatial and temporal scales [98]. This means that it may be desirable to, for example, simulate the diffusion of particles with precision in a small spatial region of interest, such as the area around receptors on a cell membrane [99], or around an ion channel [100], while using less computationally intensive methods elsewhere on the domain. As a result, recent years have seen the development of multiple hybrid approaches for linking compartment-based models to off-lattice models of diffusion [101, 102, 95], off-lattice models to PDE models of diffusion [94], and PDE models to compartment models of diffusion [57, 103, 104]. To our knowledge, however, there have been no attempts to develop a hybrid system interfacing volume-excluding compartment-based models at different levels of spatial resolution.

4.1.1 Chapter outline

In this chapter, we consider how to interface a uniform region of partially-excluding compartments with another uniform region of fully-excluding compartments, and in Section 4.2 we present two hybrid approaches capable of accurately simulating

diffusion in such systems. Both approaches will be of value to researchers working on multi-scale systems, as they can speed up simulations while preserving precision where needed.

The first hybrid method we present extends to diffusion on non-uniform, Voronoi lattices the previous results reconciling fully-excluding and partially-excluding systems. We use these results to present one simple and elegant means of connecting two uniformly partitioned regions of differing compartment capacity. The second hybrid method we present defines a small area between the fine- and coarse-grained regions of the domain, where particle behaviour exhibits some characteristics of both regions. We term this area a pseudo-compartment, and the modelling framework a pseudo-compartment method, by analogy to a recent paper using similar techniques to couple a PDE model to a compartment-based model [57].

To determine the accuracy of these hybrid approaches, in Section 4.3 we apply each one to three scenarios, comparing the correspondence of the means and variances of particle numbers in the hybrid system to the corresponding moments in non-hybrid fine-grained and coarse-grained systems, as well as to PDE solutions when appropriate. The first scenario confirms that the hybrid systems are capable of maintaining a uniform steady-state. The second compares their accuracy in a simple case of particle spreading from an initially inhomogeneous particle distribution. In the third scenario, we examine a morphogen gradient formation system, incorporating particle decay and influx of particles at the left-hand boundary, $x = 0$. Morphogen gradients are a common example of a multi-scale system in biology, as they incorporate both regions of low particle density where models with high spatial resolution are often desirable, and regions of high particle density where such detailed modelling is computationally infeasible and unnecessary [105, 106]. In all three cases, we observe that the mean and variance of particle numbers in each compartment of the hybrid models agree with those obtained from simulations run on uniform fully-excluding and partially-excluding lattices.

Having shown the accuracy of our hybrid approaches in three test cases, we next consider a scenario which illustrates the need for hybrid modelling. In Section 4.4

we therefore consider a simple multi-species scenario, where the simulated results of a partially-excluding model fail to match those of a fully-excluding model. We demonstrate that both hybrid systems are capable of matching the accuracy of the fully-excluding model in this scenario, while requiring only between a third and a seventh of the computational time to simulate.

The main focus of this chapter is on connecting two uniform lattices of differing compartment capacity, and so our study of Voronoi lattices is generally restricted to the special cases needed to achieve this end. We have also obtained more general results, however, that reconcile the mean and variance behaviours of a uniform fully-excluding model with those of any non-uniform Voronoi lattice (subject to integer-valued compartment values). These results are presented in Section 4.5.

Finally, we extend our work on flux and Robin boundary conditions from Chapter 2. Our original derivations were made for uniform lattices, and in Section 4.6 we therefore reexamine the implementation of boundary conditions, presenting results for models incorporating Voronoi-partitioned lattices. The chapter then concludes with a brief discussion in Section 4.7.

4.2 Hybrid fully-/partially-excluding systems

Recalling the reasoning used to match descriptions of uniform lattices at different spatial scales in Chapter 3, we proceed to outline two hybrid models using non-uniform lattices. In both cases, we justify the correspondence of mean particle numbers in each compartment of the hybrid model to the mean particle numbers in the accurate, $m = 1$ uniform lattice.

4.2.1 Voronoi method

Jump rates between compartments can be derived from the assumption of underlying Brownian motion of particles using first-passage time arguments (the method is outlined in Appendix C.1) [55]. Particles are assumed to begin from a fixed point within their current compartment, the 'residence point', and are deemed to have

jumped to a neighbouring compartment when they first reach that compartment's residence point. For a uniform lattice, these residence points are located at the centre of each compartment.

For a non-uniform Voronoi lattice, we let the compartment residence points be at $[x_1, \ldots, x_K]$ on the domain $[0, L]$, then define $\Delta x_j = x_j - x_{j-1}$, for $1 < j \leq K$. Compartment edges are then placed so as to be equidistant between neighbouring residence points, so that the j^{th} compartment covers the interval $x \in [x_j - \Delta x_j/2, x_j + \Delta x_{j+1}/2]$ (an example is given in Figure 4.1). Recall that the capacity of each compartment varies linearly with its length, and that the capacity of compartments on a uniform lattice is given by $m = L/(Kh)$, or the compartment length divided by particle length, h. Similarly, we obtain capacities $[m_1, \ldots, m_K]$ for the K Voronoi compartments by dividing their lengths by h, obtaining

$$m_1 = \frac{2x_1 + \Delta x_2}{2h}, \tag{4.1}$$

$$m_j = \frac{\Delta x_j + \Delta x_{j+1}}{2h}, \quad 1 < j < K, \tag{4.2}$$

$$m_K = \frac{2(L - x_K) + \Delta x_K}{2h}. \tag{4.3}$$

The positioning of residence points is restricted by a requirement that every compartment should have an integer-valued capacity. Inverting the conditional expected exit times obtained in Appendix C.1, and factoring in the relative probabilities of moving left or right, the following transition rates for a particle in the j^{th} compartment can be obtained [55, 83]:

$$T_j^- = \frac{2D}{\Delta x_j(\Delta x_j + \Delta x_{j+1})} = \frac{D}{\Delta x_j m_j h}, \tag{4.4}$$

$$T_j^+ = \frac{2D}{\Delta x_{j+1}(\Delta x_j + \Delta x_{j+1})} = \frac{D}{\Delta x_{j+1} m_j h}, \tag{4.5}$$

where T_j^- and T_j^+ are transition rates for leftward and rightward jumps, respectively. The following equation for the evolution of mean particle number can then

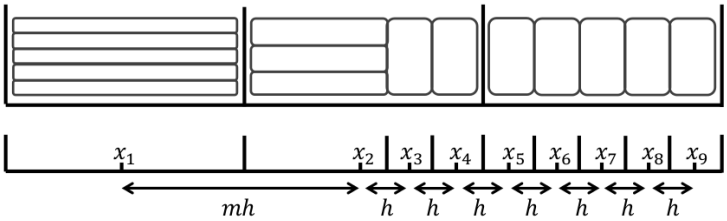

Figure 4.1: The locations of a Voronoi lattice's residence points are chosen $(x_1, \ldots, x_9)$, and then compartment edges are positioned equidistant between neighbouring residence points. This particular arrangement demonstrates how a compartment of capacity $(m+1)/2$ can be used to interface regions where $m > 1$ with regions where $m = 1$. In this case, $\Delta x_2 = mh$, and $\Delta x_j = h$ for $j = 3, \ldots, 9$. When grouped, we would find $S_1^{(v)}(t) = n_1^{(v)}(t)$, $S_2^{(v)}(t) = \sum_{i=2}^{4} n_i^{(v)}(t)$ and $S_3^{(v)}(t) = \sum_{i=5}^{9} n_i^{(v)}(t)$.

be obtained:

$$\begin{aligned}\frac{\mathrm{d}M_j^{(v)}}{\mathrm{d}t} &= T_{j-1}^{+}\left(M_{j-1}^{(v)} - \frac{1}{m_j}\langle n_{j-1}^{(v)} n_j^{(v)}\rangle\right) - T_j^{-}\left(M_j^{(v)} - \frac{1}{m_{j-1}}\langle n_{j-1}^{(v)} n_j^{(v)}\rangle\right) \\ &\quad -T_j^{+}\left(M_j^{(v)} - \frac{1}{m_{j+1}}\langle n_j^{(v)} n_{j+1}^{(v)}\rangle\right) + T_{j+1}^{-}\left(M_{j+1}^{(v)} - \frac{1}{m_j}\langle n_j^{(v)} n_{j+1}^{(v)}\rangle\right),\end{aligned} \tag{4.6}$$

where we use $n_j^{(v)}$, $M_j^{(v)}$ and $V_j^{(v)}$ to denote the number, mean and variance respectively of particles in the j^{th} Voronoi compartment. From the definitions of the transition rates given in equations (4.4) and (4.5) we note that $T_{j-1}^{+}/m_j = T_j^{-}/m_{j-1}$, and $T_j^{+}/m_{j+1} = T_{j+1}^{-}/m_j$, and hence equation (4.6) simplifies to

$$\frac{\mathrm{d}M_j^{(v)}}{\mathrm{d}t} = T_{j-1}^{+} M_{j-1}^{(v)} - \left(T_j^{-} + T_j^{+}\right) M_j^{(v)} + T_{j+1}^{-} M_{j+1}^{(v)}. \tag{4.7}$$

In the same way, we can obtain equations for the evolution of variances,

$$\begin{aligned}\frac{\mathrm{d}V_j^{(v)}}{\mathrm{d}t} &= -2\left(T_j^{-} + T_j^{+}\right) V_j^{(v)} + 2T_{j-1}^{+}\left(1 - \frac{1}{m_j}\right) V_{j-1,j}^{(v)} + 2T_{j+1}^{-}\left(1 - \frac{1}{m_j}\right) V_{j,j+1}^{(v)} \\ &\quad +T_{j-1}^{+} M_{j-1}^{(v)}\left(1 - \frac{M_j^{(v)}}{m_j}\right) + T_j^{-} M_i^{(v)}\left(1 - \frac{M_{j-1}^{(v)}}{m_{j-1}}\right) \\ &\quad +T_j^{+} M_j^{(v)}\left(1 - \frac{M_{j+1}^{(v)}}{m_{j+1}}\right) + T_{j+1}^{-} M_{j+1}^{(v)}\left(1 - \frac{M_j^{(v)}}{m_j}\right).\end{aligned} \tag{4.8}$$

The derivation of equations (4.6) and (4.8) have been outlined in Sections 3.2.1 and 3.2.3. In the previous section, we summarised previous work showing that $M_j^{(m)}(t)$ and $V_j^{(m)}(t)$ are accurate predictors of $\mu_j^{(m)}(t)$ and $v_j^{(m)}(t)$, respectively. We now wish to show that particle behaviour is similarly conserved between scales when using a Voronoi partitioned lattice.

Suppose that the Voronoi lattice consists of p compartments of capacity $m > 1$ at the left of the domain, followed by a single compartment of capacity $(m+1)/2$, and then the remainder of the domain is partitioned into fine compartments of capacity one (as illustrated in Figure 4.1, for $p = 1$ and $m = 5$). To avoid non-integer compartment capacities, our choice of m must be odd-valued. Recall that, to aggregate compartments on a fully-excluding uniform lattice, we wrote

$$S_j^{(m)}(t) = \sum_{i=(j-1)m+1}^{jm} n_i^{(1)}(t). \tag{4.9}$$

By analogy, we define $S_j^{(v)}(t)$ such that

$$S_j^{(v)}(t) = \begin{cases} n_j^{(v)}(t) & \text{if} \quad j < p+1, \\ \displaystyle\sum_{i=p+1}^{p+(m+1)/2} n_i^{(v)}(t) & \text{if} \quad j = p+1, \\ \displaystyle\sum_{i=p+(m+3)/2+m(j-p-1)}^{p+(m+1)/2+m(j-p)} n_i^{(v)}(t) & \text{if} \quad j > p+1. \end{cases} \tag{4.10}$$

These groupings are illustrated in Figure 4.1 for $p = 1$ and $m = 5$. As in the previous section, we write $\mu_j^{(v)}(t)$ and $v_j^{(v)}(t)$ to denote the mean and variance of $S_j^{(v)}(t)$, and seek to show a connection between: (i) $\mu_j^{(v)}(t)$ and $\mu_j^{(m)}(t)$; and (ii) $v_j^{(v)}(t)$ and $v_j^{(m)}(t)$. Recall from the previous chapter that the evolution of $\mu_j^{(m)}(t)$ is described by equation (3.52) which we restate here for convenience:

$$\frac{\mathrm{d}\mu_j^{(m)}}{\mathrm{d}t} = \frac{D}{m^2h^2}\left(\mu_{j-1}^{(m)} - 2\mu_j^{(m)} + \mu_{j+1}^{(m)}\right). \tag{4.11}$$

We begin by examining the equation for the evolution of $\mu_j^{(v)}$. For $j < p$, we write

$$\frac{\mathrm{d}\mu_j^{(v)}}{\mathrm{d}t} = \frac{\mathrm{d}M_j^{(v)}}{\mathrm{d}t} = \frac{D}{m^2h^2}\left(\mu_{j-1}^{(v)} - 2\mu_j^{(v)} + \mu_{j+1}^{(v)}\right), \tag{4.12}$$

which clearly matches equation (4.11). For $j > p+1$, a similar match can be obtained using the same linear interpolation applied in the previous section.

When $j = p, p+1$ we use equations (4.4) and (4.5) to obtain

$$\begin{aligned}
\frac{\mathrm{d}\mu_p^{(v)}}{\mathrm{d}t} &= \frac{D}{m^2h^2}M_{p-1}^{(v)} - 2\frac{D}{m^2h^2}M_p^{(v)} + \frac{D}{mm_{p+1}h^2}M_{p+1}^{(v)}, &(4.13)\\
\frac{\mathrm{d}\mu_{p+1}^{(v)}}{\mathrm{d}t} &= \sum_{i=p+1}^{p+(m+1)/2}\frac{\mathrm{d}M_i^{(v)}}{\mathrm{d}t}(t)\\
&= \frac{D}{m^2h^2}M_p^{(v)} - \frac{D}{mm_{p+1}h^2}M_{p+1}^{(v)}\\
&\quad -\frac{D}{h^2}M_{p+(m+1)/2}^{(v)} + \frac{D}{h^2}M_{p+(m+3)/2}^{(v)}. &(4.14)
\end{aligned}$$

As before, we make the substitutions $M_{p-1}^{(v)} = \mu_{p-1}^{(v)}$ and $M_p^{(v)} = \mu_p^{(v)}$, and make the assumption that values of $M_{p+(m+1)/2}^{(v)}$ and $M_{p+(m+3)/2}^{(v)}$ can be interpolated from $\mu_{p+1}^{(v)}$ and $\mu_{p+2}^{(v)}$ using equations (3.48)-(3.51). Finally, we observe that the residence point of the $(p+1)^{th}$ Voronoi compartment coincides with the centre of the $(p+1)^{th}$ aggregated compartment (as illustrated in Figure 4.1), so the interpolated value for $M_{p+1}^{(v)}$ is simply

$$M_{p+1}^{(v)} = \frac{m_{p+1}}{m}\mu_{p+1}^{(v)}. \tag{4.15}$$

Using the above substitutions, it is possible to write equations (4.13) and (4.14) in terms of $\mu^{(v)}$, rather than $M^{(v)}$, and we arrive at

$$\begin{aligned}
\frac{\mathrm{d}\mu_p^{(v)}}{\mathrm{d}t} &= \frac{D}{m^2h^2}\left(\mu_{p-1}^{(v)} - 2\mu_p^{(v)} + \mu_{p+1}^{(v)}\right), &(4.16)\\
\frac{\mathrm{d}\mu_{p+1}^{(v)}}{\mathrm{d}t} &= \frac{D}{m^2h^2}\left(\mu_p^{(v)} - 2\mu_{p+1}^{(v)} + \mu_{p+2}^{(v)}\right), &(4.17)
\end{aligned}$$

so we can expect the values of $\mu^{(v)}$ to match those of $\mu^{(m)}$. Although we do not show them here, analogous treatments can be applied to matching $v^{(v)}$ with $v^{(m)}$.

Voronoi partitioned lattices provide one method of interfacing two regions partitioned by uniform lattices of differing compartment capacities, but only for certain compartment capacity values. It is not possible, for example, to interface a region where $m = 1$ with a region where $m = 2$, as any intermediate sized compartment would have non-integer-valued capacity. In such situations, it is useful to have another hybrid method capable of interfacing the regions.

4.2.2 Pseudo-compartment method

Pseudo-compartment methods have previously been used to interface compartment-based models with PDE models. In such models, the domain consists of a region in which diffusion is modelled using a discrete model, another region in which diffusion is modelled using a continuum PDE model, and a pseudo-compartment that combines both models. Specifically, although particle concentration in the pseudo-compartment is modelled in a spatially continuous manner using PDEs, discrete jump events between the pseudo-compartment and the neighbouring compartment-based region can take place, by adjusting the particle concentration profile appropriately [57]. In this section, we discuss using similar ideas to interface one region of the domain, partitioned by a coarse lattice with compartment capacity $m > 1$, with another region, partitioned with a fine lattice where $m = 1$.

We assume, without loss of generality, that the coarse region is to the left-hand side of the domain, and that it consists of p compartments of capacity $m > 1$. The first m fully-excluding compartments, i.e. those of index $p + 1$ through to $p + m$, are then said to collectively comprise the pseudo-compartment (this is illustrated for $p = 1$ and $m = 5$ in Figure 4.2). Particles in compartments 1 through to p may attempt to jump to neighbouring compartments in this range with rate D/m^2h^2, while particles in compartments $p+1$ through to K may attempt to jump to neighbouring compartments in this range with rate D/h^2. In both cases, these jumps fail with blocking probability,

$$\left(1 - \frac{n_j^{(c)}}{m_j}\right), \tag{4.18}$$

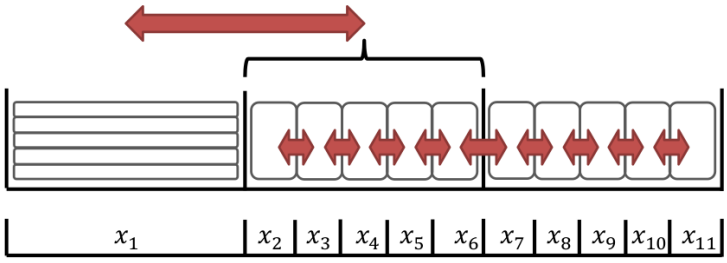

Figure 4.2: Pseudo-compartment method, with $m = 5$ and $p = 1$. The compartments of index 2 through to 6 form the pseudo-compartment. Particles in these compartments may attempt to jump to neighbouring compartments with rate D/h^2, or into compartment 1 with propensity D/m^2h^2, subject to the standard blocking probability arising from volume exclusion. Particles in compartment 1 may jump into any unoccupied compartment with index 2 through to 6 with propensity D/mh^2. When grouped, we have $S_1^{(c)}(t) = n_1^{(c)}(t)$, $S_2^{(c)}(t) = \sum_{i=2}^{6} n_i^{(c)}(t)$ and $S_3^{(c)}(t) = \sum_{i=7}^{11} n_i^{(c)}(t)$.

where j is the index of the destination compartment, and we use $n_j^{(c)}$, and later $M_p^{(c)}$, to denote, respectively, the number of particles and the mean number of particles in compartment j of the lattice.

In addition, it is possible for a particle in compartment p to move into the pseudo-compartment with jump propensity D/m^2h^2. When this happens, one of the compartments that comprise the pseudo-compartment is selected uniformly at random, and if it is unoccupied a particle jumps into it from compartment p (if it is occupied then the jump is terminated). Equivalently, volume-excluding effects can be incorporated by multiplying the jump propensity by the fraction of compartments in the pseudo-compartment currently unoccupied, and selecting a destination from among the unoccupied compartments uniformly at random.

Similarly, a particle residing within any part of the pseudo-compartment may jump into compartment p, with propensity

$$\frac{D}{m^2h^2}\left(1 - \frac{n_p^{(c)}}{m}\right). \tag{4.19}$$

All of the possible particle jumps for an example lattice are illustrated by arrows in Figure 4.2. Suppose that the p^{th} compartment is the last partially-excluding compartment, so that all compartments of index greater than p will be fully-excluding.

Within the partially-excluding region, we write the usual equations for the evolution of mean particle numbers

$$\frac{\mathrm{d}M_1^{(c)}}{\mathrm{d}t} = \frac{D}{m^2h^2}\left(-M_1^{(c)} + M_2^{(c)}\right), \tag{4.20}$$

$$\frac{\mathrm{d}M_i^{(c)}}{\mathrm{d}t} = \frac{D}{m^2h^2}\left(M_{i-1}^{(c)} - 2M_i^{(c)} + M_{i+1}^{(c)}\right), \quad 1 < i < p. \tag{4.21}$$

The equation for compartment p, the final partially-excluding compartment, is modified to account for the incoming particles it can receive from all fully-excluding compartments within the pseudo-compartment:

$$\frac{\mathrm{d}M_p^{(c)}}{\mathrm{d}t} = \frac{D}{m^2h^2}\left(M_{p-1}^{(c)} - 2M_p^{(c)} + \sum_{j=p+1}^{p+m} M_j^{(c)}\right). \tag{4.22}$$

Similarly, the equations for mean particle number in the m fully-excluding compartments comprising the pseudo-compartment region must also account for particles moving to, and arriving from, the partially-excluding region, as well as for movement over the fully-excluding lattice,

$$\frac{\mathrm{d}M_{p+1}^{(c)}}{\mathrm{d}t} = \frac{D}{h^2}\left(\frac{1}{m}\frac{1}{m^2}M_p^{(c)} - \left[1 + \frac{1}{m^2}\right]M_{p+1}^{(c)} + M_{p+2}^{(c)}\right), \tag{4.23}$$

$$\frac{\mathrm{d}M_i^{(c)}}{\mathrm{d}t} = \frac{D}{h^2}\left(\frac{1}{m}\frac{1}{m^2}M_p^{(c)} + M_{i-1}^{(c)} - \left[2 + \frac{1}{m^2}\right]M_i^{(c)} + M_{i+1}^{(c)}\right), \quad p+1 < i \leq p+m, \tag{4.24}$$

and, finally, beyond the pseudo-compartment, the evolution of mean particle number is described using the standard equations for the evolution of mean particle numbers with $m = 1$,

$$\frac{\mathrm{d}M_i^{(c)}}{\mathrm{d}t} = \frac{D}{h^2}\left(M_{i-1}^{(c)} - 2M_i^{(c)} + M_{i+1}^{(c)}\right), \quad p+m < i < K, \tag{4.25}$$

$$\frac{\mathrm{d}M_K^{(c)}}{\mathrm{d}t} = \frac{D}{h^2}\left(M_{K-1}^{(c)} - M_K^{(c)}\right). \tag{4.26}$$

To compare the description of particle diffusion given by the pseudo-compartment

model to the description given by the fully-excluding model where $m = 1$ we must aggregate the compartments, writing

$$S_j^{(c)}(t) = \begin{cases} n_j^{(c)}(t) & \text{if } j < p+1, \\ \sum_{i=p+1}^{p+m} n_i^{(c)}(t) & \text{if } j = p+1, \\ \sum_{i=p+1+m(j-p-1)}^{p+m(j-p)} n_i^{(c)}(t) & \text{if } j > p+1. \end{cases} \tag{4.27}$$

As before, we write $\mu_j^{(c)}(t) = \langle S_j^{(c)}(t) \rangle$, and seek to show the agreement of $\mu_j^{(c)}(t)$ with $\mu_j^{(m)}(t)$. This is trivial for $j < p$ and for $j > p+1$, as these are sections of uniformly partitioned compartments where $m > 1$ and $m = 1$, respectively, and so the previously obtained results apply. When $j = p$, we use equation (4.22) to write

$$\begin{aligned} \frac{\mathrm{d}\mu_p^{(c)}}{\mathrm{d}t} = \frac{\mathrm{d}M_p^{(c)}}{\mathrm{d}t} &= \frac{D}{m^2h^2}\left(M_{p-1}^{(c)} - 2M_p^{(c)} + \sum_{j=p+1}^{p+m} M_j^{(c)} \right), \\ &= \frac{D}{m^2h^2}\left(\mu_{p-1}^{(c)} - 2\mu_p^{(c)} + \mu_{p+1}^{(c)} \right), \end{aligned} \tag{4.28}$$

which is the expected form needed for agreement of $\mu_p^{(c)}$ with $\mu_p^{(m)}$. Similarly, for $j = 1$ we use equations (4.23) and (4.24) to write

$$\begin{aligned} \frac{\mathrm{d}\mu_{p+1}^{(c)}}{\mathrm{d}t} = \sum_{j=p+1}^{p+m} \frac{\mathrm{d}M_j^{(c)}}{\mathrm{d}t} &= \frac{D}{m^2h^2} M_p^{(c)} - \frac{D}{m^2h^2} \sum_{j=p+1}^{p+m} M_j^{(c)} - \frac{D}{h^2} M_{p+m}^{(c)} + \frac{D}{h^2} M_{p+m+1}^{(c)}, \\ &= \frac{D}{m^2h^2}\mu_p^{(c)} - \frac{D}{m^2h^2}\mu_j^{(c)} - \frac{D}{h^2} M_{p+m}^{(c)} + \frac{D}{h^2} M_{p+m+1}^{(c)}. \end{aligned} \tag{4.29}$$

Interpolating values of $M_{p+m}^{(c)}$ and $M_{p+m+1}^{(c)}$ using equations (3.48)-(3.51), we finally arrive at

$$\frac{\mathrm{d}\mu_{p+1}^{(c)}}{\mathrm{d}t} = \frac{D}{m^2h^2}\left(\mu_p^{(c)} - 2\mu_{p+1}^{(c)} + \mu_{p+2}^{(c)} \right), \tag{4.30}$$

so we expect the values of $\mu_j^{(c)}$ to accurately predict those of $\mu_j^{(m)}$.

Similar reasoning can be used to analyse the variance of, and covariances between, groupings of compartments. Away from the pseudo-compartment, we can call upon previous results for uniform lattices (as presented in Section 3.3.3). The agreement of

(i) $v_p^{(v)}$ with $v_p^{(m)}$, (ii) $v_{p+1}^{(v)}$ with $v_{p+1}^{(m)}$, and (iii) $v_{p,p+1}^{(v)}$ with $v_{p,p+1}^{(m)}$ (i.e. the variance of particle number in the last partially-excluding compartment, the variance of particle number in the pseudo-compartments, and the covariance of particle numbers between the two compartments) is less obvious, but we consider each of the three cases in Appendices C.2, C.3 and C.4, respectively. There are also a large number of special cases to be considered (e.g. $v_{i,j}^{(v)}$, for $i < p < j$) but these resolve very similarly, so in the interests of space we do not include details of them here.

Having presented two hybrid methods for interfacing partially-excluding with fully-excluding regions, we now apply them both to a number of test systems to check their correspondence to the fully-excluding model where $m = 1$.

4.3 Numerical investigations

In this section we consider three single-species test cases: maintaining a uniform steady-state in a purely diffusive system; particle redistribution from a non-uniform initial state; and a morphogen gradient. For each case we compare four different models:

1. uniform fully excluding ($m = 1$): 105 compartments of capacity one and length 0.2;

2. uniform partially excluding ($m = 7$): 15 compartments of capacity seven and length 1.4;

3. hybrid Voronoi: five compartments of capacity seven and length 1.4, one box of capacity four and length 0.8, and 66 compartments of capacity one and length 0.2;

4. hybrid pseudo-compartment: five compartments of capacity seven and length 1.4, and 70 of capacity one and length 0.2. The first seven fully-excluding compartments form the pseudo-compartment.

In each case we use these four models to obtain, respectively, numerical values for $\mu_j^{(m)}$ and $v_j^{(m)}$, for $M_j^{(m)}$ and $V_j^{(m)}$, for $\mu_j^{(v)}$ and $v_j^{(v)}$, and for $\mu_j^{(c)}$ and $v_j^{(c)}$, aggregating

compartments from the finer grids into regions of capacity $m = 7$. In each case we set $h = 0.2$, $L = 21$, and hence $\kappa = 105$. We choose diffusion constant $D = 2$ for all test cases, and perform $50,000$ realisations of each case over the time interval $t \in [0, 25]$.

The agreement of these four models with a comparison data set was quantified using the HDE, defined in Section 2.2.1. Since we consider the fully-excluding model as 'accurate', in the sense that it specifies each particle's location precisely rather than making assumptions about its position within a larger compartment, a further $50,000$ realisations of the fully-excluding model were generated to provide an independent estimate for $\mu_j^{(m)}$ and $v_j^{(m)}$, and these values were used as our comparison data set.

To generate these realisations we used an algorithm based on Gillespie's Direct Method [107]. In each of the three test cases, we also record the time taken to simulate 50,000 realisations of each model. All simulations were performed using Matlab code, parallelised using parfor.

4.3.1 Test Case 1: Maintaining a spatially uniform steady-state

In this simplest test, for each realisation we initialise 15 uniformly distributed particles over the lattice, let them diffuse freely, then record their final positions to ensure they remain uniformly distributed. This is the most basic test, and is performed to confirm that the hybrid interfaces do not interfere with a homogeneous particle distribution.

The mean and variance of particle numbers in each aggregated box at $t = 25$ are plotted in Figure 4.3, showing good agreement between all four models. This agreement is quantified in Table 4.1, where we observe that in each model, mean values deviate from the comparison data by less than 0.25%, and variance values deviate by less than 0.5%. The inclusion of HDE values for the fully-excluding model provides a measure of the effect of noise on reproducibility, quantifying the difference between the results of two identically defined stochastic processes. It is also possible to demonstrate the steady-state agreement of all four models by analysing

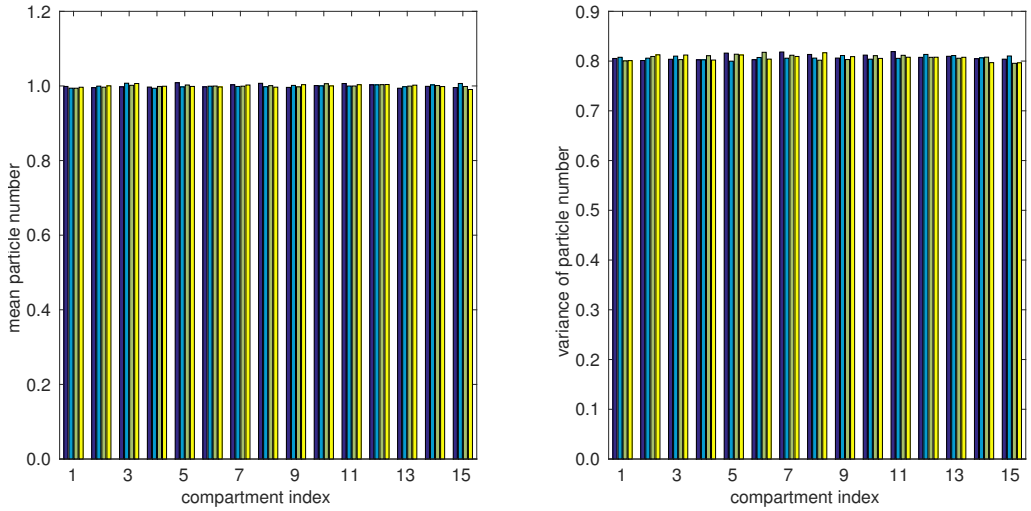

Figure 4.3: Results from 50,000 repeats of the uniform steady-state simulation at time $t = 25$. Fifteen particles were uniformly distributed at time $t = 0$ and then diffused freely. From left to right, each set of four bars shows results from the fully-excluding (dark blue), partially-excluding (light blue), Voronoi (green) and pseudo-compartment (yellow) models.

their master equations for the evolution of means and variances, and we show this for more general Voronoi models in Section 4.5.2.

We find that the hybrid models are faster to simulate than the fully-excluding model. However, the decrease in computational time is modest, and we anticipate that significant computational savings will only be achieved when the majority of particle motion is concentrated in the partially-excluding region.

Table 4.1: Details of uniform distribution simulation.

Model	Mean HDE at $t = 25$	Variance HDE at $t = 25$	Time to simulate (seconds)	Acceleration relative to fully-excluding
Fully-excluding	0.0023	0.0046	28741	-
Partially-excluding	0.0022	0.0036	582	49.4 times faster
Voronoi	0.0020	0.0035	19738	1.5 times faster
Pseudo-compartment	0.0017	0.0033	26361	1.1 times faster

4.3.2 Test Case 2: Particle redistribution

The second test case examines the ability of our hybrid models to accommodate a net particle flux over the interface. Our initial state consists of thirty-five particles collected at the left of the domain. For the uniform fully-excluding model, this means that the first thirty-five compartments are occupied. For all the other models, the first five compartments, each of capacity seven, are full to capacity.

We compare the agreement of mean and variance values at $t = 1, 2, 3 \ldots, 25$ in Figure 4.4. As anticipated, all four models perform well, although the Voronoi method performs somewhat better than the pseudo-compartment method. A possible explanation of this is that, with particle concentrations in the pseudo-compartment higher to the left and lower to the right, particles jumping into the pseudo-compartment from compartment p will disproportionately arrive in the more numerous vacant compartments to the right of the pseudo-compartment, slightly lengthening the average jump length. We note though that, even in this case of strongly asymmetric flux, the HDE remains below 0.008 throughout the simulation.

We also plot the means and variances of particle numbers at $t = 25$ in Figure 4.5, and for consistency with the other test cases list the HDE values at time $t = 25$ in Table 4.2. We also record the time taken to simulate each model in Table 4.2, noting again that the hybrid models run faster than the fully-excluding model, with the Voronoi method taking only half as much time to simulate.

4.3.3 Test Case 3: Morphogen gradient

In the final single-species test case, a simple morphogen gradient system is simulated. Starting from an empty initial state, particles enter the domain at the left-hand boundary with rate r_1. As well as moving diffusively, particles decay with rate r_2. In the absence of volume exclusion, a flux boundary condition can be implemented

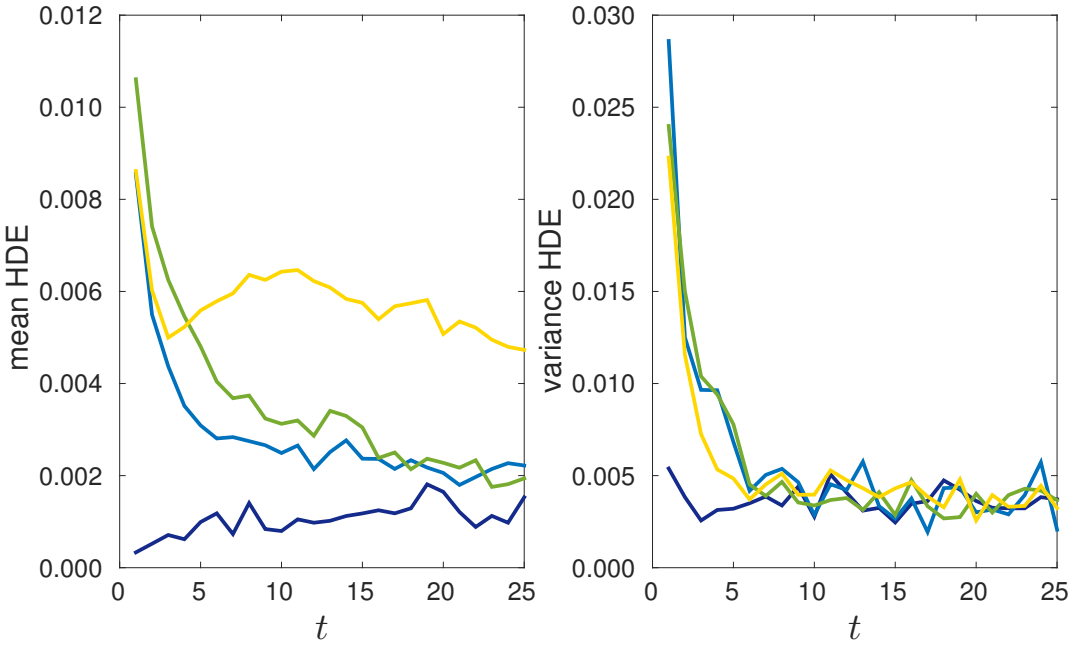

Figure 4.4: HDE values for the mean and variance of the particle redistribution simulation results at discrete times $t = 1, 2, \ldots, 25$. Values for the fully-excluding, partially-excluding, Voronoi and pseudo-compartment models are shown in dark blue, light blue, green and yellow, respectively.

Table 4.2: Details of particle redistribution simulation.

Model	Mean HDE at $t = 25$	Variance HDE at $t = 25$	Time to simulate (seconds)	Acceleration relative to fully-excluding
Fully-excluding	0.0015	0.0037	40775	-
Partially-excluding	0.0022	0.0021	752	54.2 times faster
Voronoi	0.0019	0.0037	20884	2.0 times faster
Pseudo-compartment	0.0047	0.0032	31330	1.3 times faster

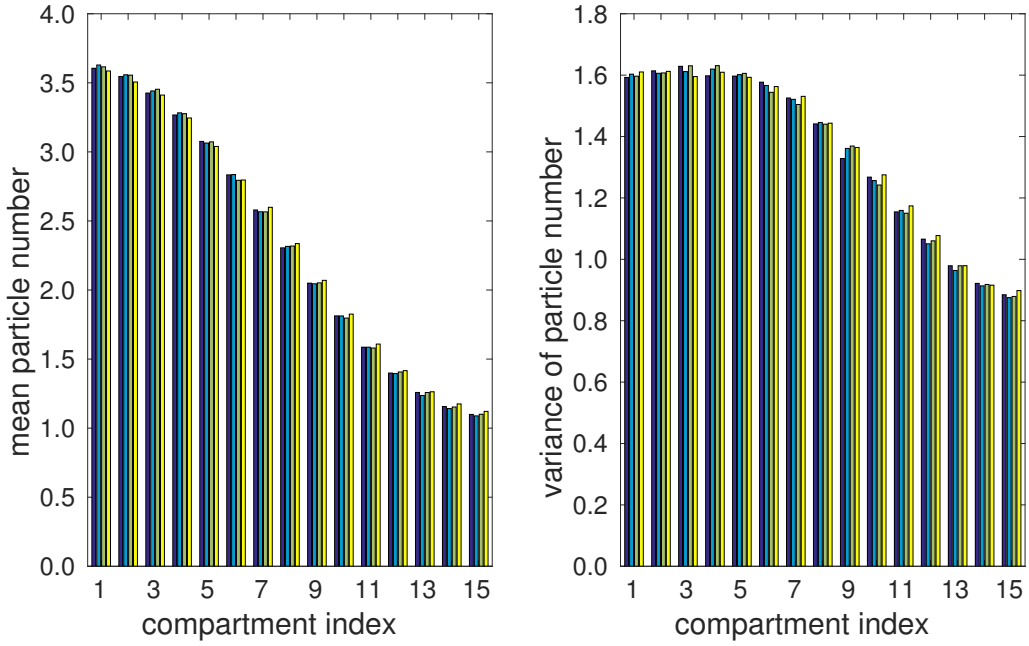

Figure 4.5: Results from 50,000 repeats of the particle redistribution simulation at time $t = 25$. Thirty-five particles were initialised at the left of the domain at time $t = 0$, and then diffused freely. From left to right, each set of four bars shows results from the fully-excluding (dark blue), partially-excluding (light blue), Voronoi (green) and pseudo-compartment (yellow) models.

Table 4.3: Details of morphogen gradient simulation.

Model	Mean HDE at $t = 25$	Variance HDE at $t = 25$	Time to simulate (seconds)	Acceleration relative to fully-excluding
Fully-excluding	0.0015	0.0050	16622	-
Partially-excluding	0.0023	0.0060	385	43.2 times faster
Voronoi	0.0032	0.0059	3438	4.8 times faster
Pseudo-compartment	0.0077	0.0105	4847	3.4 times faster

by adding or removing particles in the closest compartment to the boundary at a specified rate [79]. When volume exclusion is incorporated, however, it will sometimes be the case that the closest compartment to the boundary is already filled to capacity, in which case no more particles may be added to it. When this occurred in simulations, we added particles to the first compartment from the boundary with available capacity (as discussed in Section 3.5 of the previous chapter).

The means and variances of particles at time $t = 25$ are illustrated in Figure 4.6, while HDE values and the computational time required to simulate each model are presented in Table 4.3. In this case, the hybrid simulations are significantly faster than the equivalent fully-excluding simulations. This is because the majority of particles are located in the first third of the domain, where the hybrid models use computationally efficient partially-excluding compartments. Simulations of the Voronoi method ran more than four times faster than the fully-excluding model, while simulations of the pseudo-compartment method ran more than three times faster than the fully-excluding model.

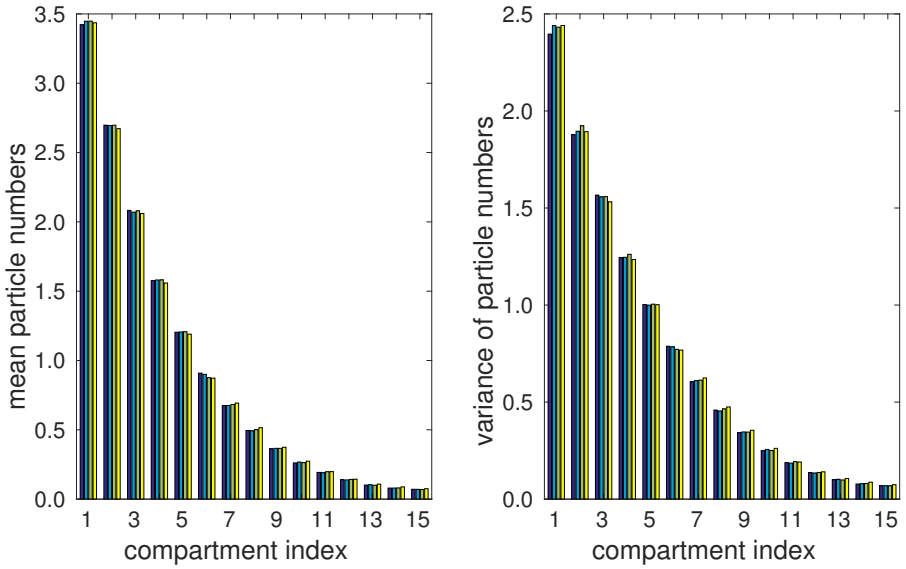

Figure 4.6: Results from 50,000 repeats of the morphogen gradient scenario at time $t = 25$. Particles are added to the system with rate $r_1 = 1$, and are placed into the closest compartment to the left-hand boundary that is not full to capacity, while each particle decays with rate $r_2 = 0.05$. From left to right, each set of four bars shows results from the fully-excluding (dark blue), partially-excluding (light blue), Voronoi (green) and pseudo-compartment (yellow) models.

4.4 Application to a simple multi-species exclusion system

Having established the accuracy of the hybrid methodologies in the test cases of the previous section, we now apply them to a simple model system where the results of the partially-excluding model deviate from those of the fully-excluding model.

We consider a simple multi-species system containing two species of particle, A and B [108]. Neither species is reactive, and particles do not interact with each other except through volume exclusion effects. The initial state of the system consists of 21 particles of species A at the left of the domain, and 21 particles of species B at the right of the domain, as illustrated in Figure 4.7 (so that for the fully-excluding model, the first and last 21 compartments are occupied, and for the other models the first and last three compartments are filled to capacity). When simulated using a partially-excluding model, this system will eventually reach a homogeneous steady-state, with both A and B particles intermixed since the coarsened lattice description

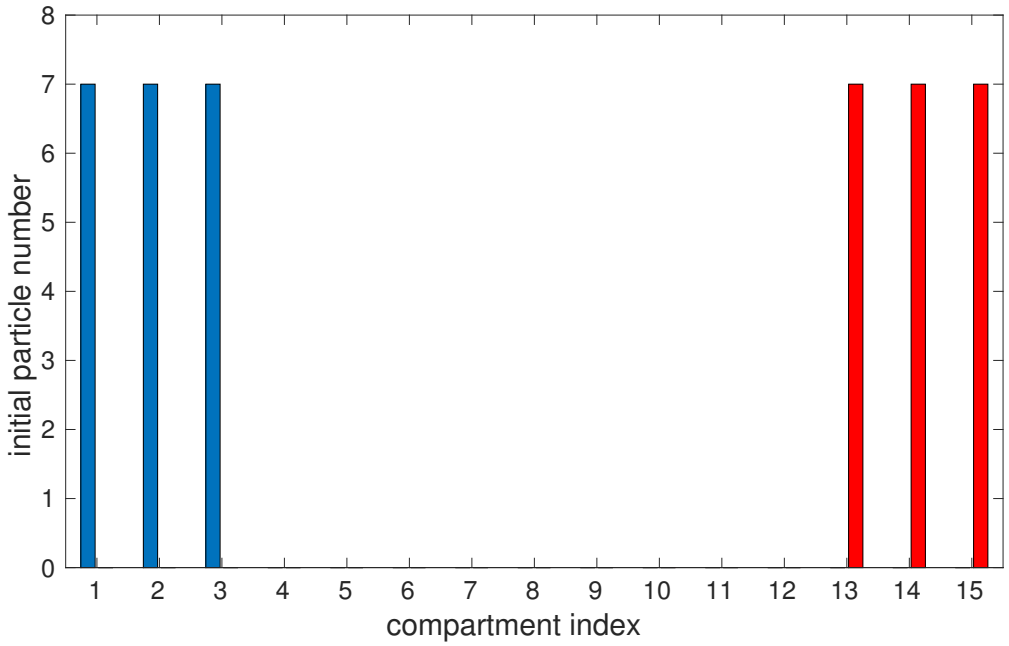

Figure 4.7: At time $t = 0$, 21 particles of species A (blue) are initialised at the left of the domain, and 21 particles of species B (red) are initialised at the right.

allows particles to move past each another. In contrast, the fully-excluding model does not allow particles to pass one another, and hence the two species will remain separated. Our hybrid methods can improve the efficiency of simulations by including a small interface region in the model, where it is possible for the two species meet, using a fully-excluding lattice, while using a computationally efficient, partially-excluding lattice elsewhere in the domain.

Figures 4.8 and 4.9 illustrate how such regions can be arranged for Voronoi and pseudo-compartment methods where $m = 5$, and how the interfaces can be shifted left or right to prevent particles of species A and B from passing one another. Shifting the interface imposes a small computational cost, but this is more than compensated for by the decreased number of jump events occurring due to the coarser lattice partitioning.

We adopt the same values of κ, h, L and D used in Section 4.3, and perform $50,000$ realisations of each model over the time interval $t \in [0, 25]$. For the Voronoi and pseudo-compartment methods, we begin each realisation with six compartments

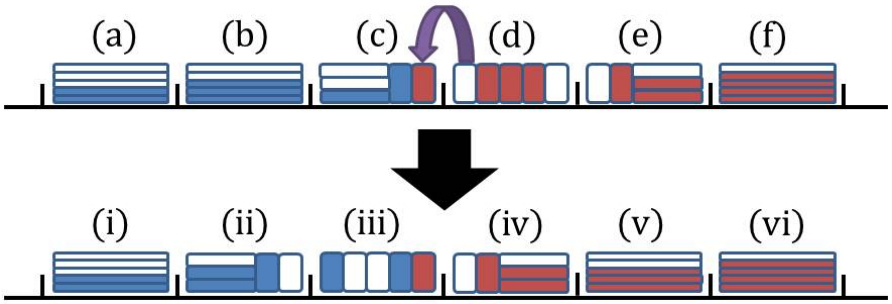

Figure 4.8: An illustration of an adaptive Voronoi domain partition. Particles of species A and B are shown in blue and red, respectively. The upper image shows the lattice before the hybrid region shifts left, where the areas marked (a), (b) and (f) are partially-excluding, those marked (c) and (e) are a combination of fully-excluding and partially-excluding, and the one marked (d) is a section of fully-excluding compartments. When a B particles enters compartment (c), the interface shifts left as illustrated in the lower image, where the areas marked (i), (v) and (vi) are partially-excluding, those marked (ii) and (iv) are a combination of fully-excluding and partially-excluding, and the one marked (iii) is a section of fully-excluding compartments. Where a partially-excluding compartment is replaced with a finer partition (i.e. (b) and the left part of (c)), the particles within it are assigned to the replacing compartments with probabilities proportional to the compartment lengths. When a section of compartments is replaced by a coarser partition (i.e. (e) and the right of (d)) the occupancy of the new compartments is found from the total number of particles across that section.

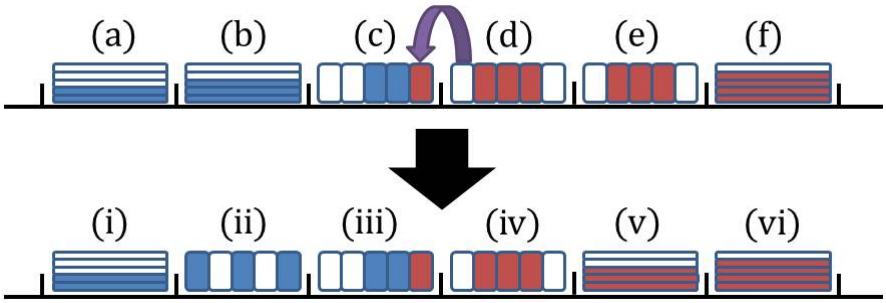

Figure 4.9: An illustration of an adaptive domain partition using the pseudo-compartment model. Particles of species A and B are shown in blue and red, respectively. The upper image shows the lattice before the hybrid region shifts left, where the areas marked (a), (b) and (f) are partially-excluding, those marked (c) and (e) are pseudo-compartments, and the one marked (d) is a section of fully-excluding compartments. When a B particles enters compartment (c), the interface shifts left as illustrated in the lower image, where the areas marked (i), (v) and (vi) are partially-excluding, those marked (ii) and (iv) are pseudo-compartments, and the one marked (iii) is a section of fully-excluding compartments. The positions of any particles in compartment (b) are uniformly randomised across (ii), while the occupancy of (v) is given by the total number of particles across (e).

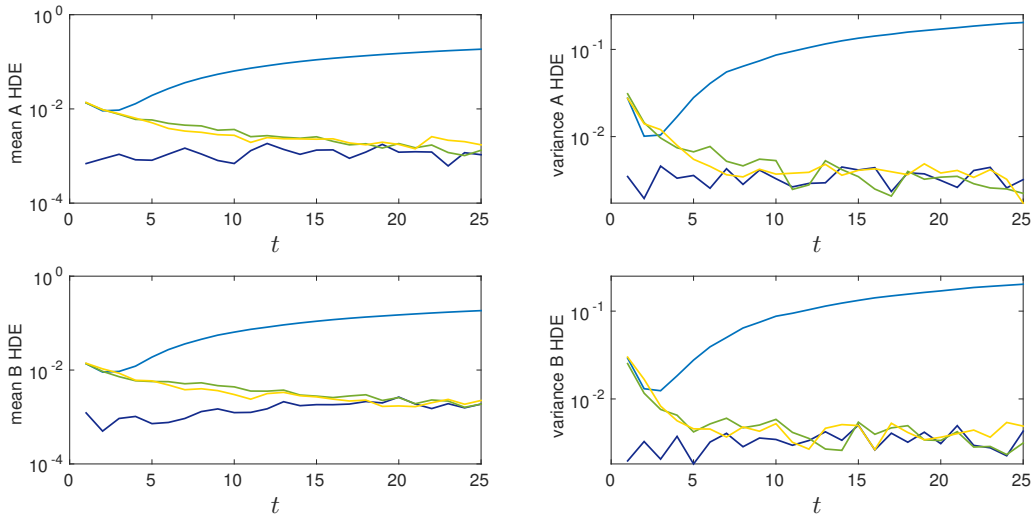

Figure 4.10: HDE values for the mean and variance of the multi-species simulation results at discrete times $t = 1, 2, \ldots, 25$. The growing deviation of the partially-excluding model (plotted in light blue) from the other three models can be clearly seen.

of capacity $m = 7$ at the left-hand side and at the right-hand side of the domain, with an intermediate region at the centre of the domain of the form illustrated in Figures 4.8 and 4.9.

We compare mean and variance values at $t = 1, 2, 3, \ldots, 25$, and plot the resulting HDEs in Figure 4.10. As anticipated, the results generated using the partially-excluding model deviate significantly from those generated using the fully-excluding and hybrid models. This deviation is illustrated by plots of the means and variances of particle numbers at $t = 25$ in Figure 4.11. The HDE values at time $t = 25$ are listed in Table 4.4 together with the time taken to simulate each system. It can be seen that the Voronoi and pseudo-compartment methods run 6.9 and 3.2 times faster, respectively, than the fully-excluding system without losing accuracy.

In the chapter so far, we have shown how Voronoi partitions can be used to connect uniform regions of fully- and partially-excluding compartments. It is also possible to obtain more general results, showing that the behaviour of more general Voronoi partitions can be matched by aggregations of fully-excluding compartments, and we present these in the following section.

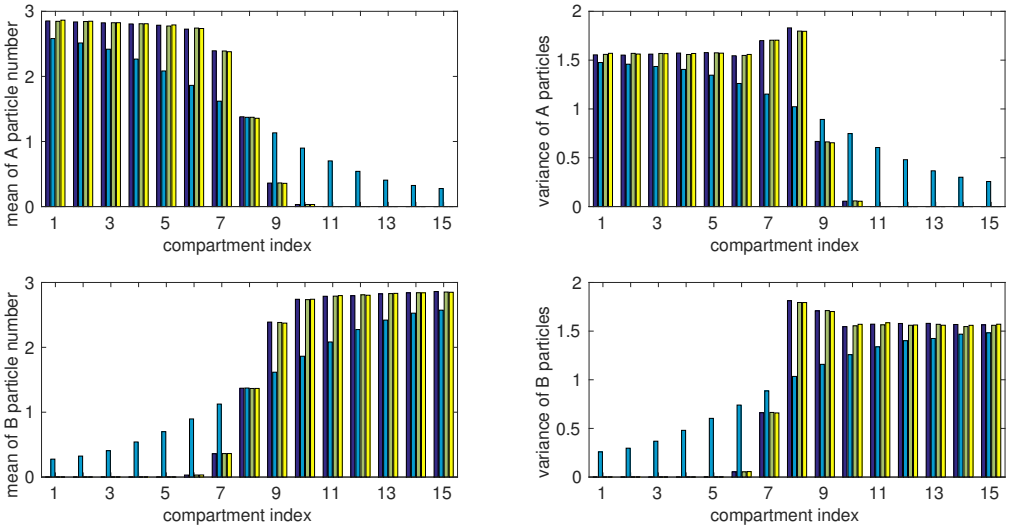

Figure 4.11: Results from 50,000 repeats of the multi-species simulation. Results taken from final state at time $t = 25$. From left to right, each set of four bars shows results from the fully-excluding (dark blue), partially-excluding (light blue), Voronoi (green) and pseudo-compartment (yellow) models. The fully-excluding and hybrid model results display strong agreement, but the results of the partially-excluding model differ as this model cannot prevent the particles of differing species from moving past one another.

Table 4.4: Details of multi-species simulation.

Model	Mean HDE at $t = 25$ (A/B)	Variance HDE at $t = 25$ (A/B)	Time to simulate (seconds)	Acceleration relative to fully-excluding
Fully-excluding	0.0011/0.0019	0.0032/0.0043	53663	-
Partially-excluding	0.1853/0.1844	0.2034/0.2023	902	59.5 times faster
Voronoi	0.0013/0.0019	0.0022/0.0031	7722	6.9 times faster
Pseudo-compartment	0.0017/0.0023	0.0017/0.0049	16755	3.2 times faster

4.5 Generalising results for Voronoi partitioned lattices

In this section we extend to Voronoi partitioned lattices the results obtained for uniform, partially-excluding lattices. As in Section 4.2.1, we define residence points for the K boxes of the Voronoi partition at $[x_1, \ldots, x_K]$, with capacities $[m_1, \ldots, m_K]$. Recalling equations (4.1)-(4.3), we restrict choices of x_j to those that result in integer-valued capacities, but otherwise permit them to be chosen freely. For $1 \leq i \leq K$, we will seek to show the agreement of the mean and variance of particle numbers in the i^{th} Voronoi compartment, $M_i^{(v)}$ and $V_i^{(v)}$, to the mean and variance of total particle numbers across m_i corresponding fully-excluding compartments (this is illustrated in Figure 4.12).

4.5.1 Aside on partitioning

Recall that we are considering particles of length h. Both a Voronoi partition and a fully-excluding partition of the domain $x \in [0, L]$ will have the same total capacity $\kappa = L/h$. In one dimension, this implies that the area covered by any compartment in a Voronoi partition of the domain can be expressed as the area covered by a union of contiguous compartments from the fully-excluding lattice, provided each compartment on the Voronoi partition has integer-valued capacity.

We can therefore use the same technique that we applied to uniform lattices in Section 3.3.2, representing each partially-excluding Voronoi compartment as the sum of several fully-excluding compartments on the uniform lattice, and showing that we recover the same ODE for the mean evolution of this sum as we would expect for the partially-excluding compartment. Let us define q_j to be the sum of capacities of all compartments with index less than or equal to j, such that

$$q_j = \begin{cases} 0, & \text{for} \quad j = 0; \\ \sum_{i=1}^{j} m_i, & \text{otherwise.} \end{cases} \tag{4.31}$$

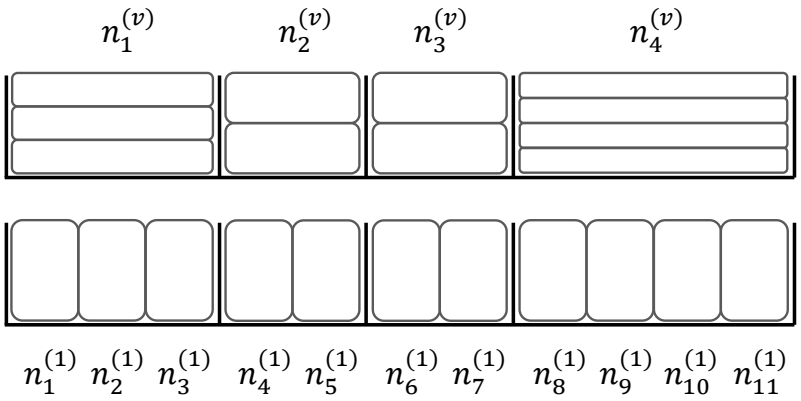

Figure 4.12: In this example, we have a domain comprised of four Voronoi compartments with capacities $m_1 = 3$, $m_2 = m_3 = 2$ and $m_4 = 4$, and we illustrate the corresponding groupings of compartments on a fully-excluding lattice.

We can then define the total number of particles in the fully-excluding compartments corresponding to the j^{th} Voronoi compartment at time t as $S_j^{(gv)}(t)$, where

$$S_j^{(gv)}(t) = \sum_{i=q_{j-1}+1}^{q_j} n_i^{(1)}(t), \tag{4.32}$$

This is illustrated in Figure 4.12, for a domain of four Voronoi compartments with capacities $m_1 = 3$, $m_2 = m_3 = 2$ and $m_4 = 4$, respectively. From the capacities of the Voronoi compartments, we use equation (4.31) to obtain $q_1 = 3$, $q_2 = 5$, $q_3 = 7$ and $q_4 = 11$, and so, when the fully-excluding compartments are grouped, we find

$$\begin{aligned}
S_1^{(gv)}(t) &= \sum_{i=1}^{3} n_i^{(1)}(t), \\
S_2^{(gv)}(t) &= \sum_{i=4}^{5} n_i^{(1)}(t), \\
S_3^{(gv)}(t) &= \sum_{i=6}^{7} n_i^{(1)}(t), \\
S_4^{(gv)}(t) &= \sum_{i=8}^{11} n_i^{(1)}(t).
\end{aligned}$$

By analogy to the work in previous sections we write $\mu_j^{(gv)}(t)$ and $v_j^{(gv)}(t)$ to denote the mean and variance values of $S_j^{(gv)}(t)$, and seek to match these values to $M_j^{(v)}(t)$

and $V_j^{(v)}(t)$.

4.5.2 Matching steady-state values

By analogy to the steady-state values obtained for uniform lattices, given in equations (3.38)-(3.40), we conjecture that the steady-state mean, variance and covariance values for particle numbers in compartments of the Voronoi model will be given by

$$\hat{M}_i^{(v)} = m_i \left[\frac{N}{\kappa}\right], \tag{4.33}$$

$$\hat{V}_i^{(v)} = m_i \left[\frac{N}{\kappa}\left(1-\frac{N}{\kappa}\right)\right] - m_i(m_i-1)\left[\frac{N}{\kappa(\kappa-1)}\left(1-\frac{N}{\kappa}\right)\right], \tag{4.34}$$

$$\hat{V}_{i,j}^{(v)} = -m_i m_j \left[\frac{N}{\kappa(\kappa-1)}\left(1-\frac{N}{\kappa}\right)\right], \ \forall i \neq j, \tag{4.35}$$

where we recall that $\kappa = L/h$. In the interests of brevity, we note that equations (4.33)-(4.35) can be written

$$\hat{M}_i^{(v)} = m_i \hat{M}^{(1)}, \tag{4.36}$$

$$\hat{V}_i^{(v)} = m_i \hat{V}^{(1)} - m_i(m_i-1)\hat{CV}^{(1)}, \tag{4.37}$$

$$\hat{V}_{i,j}^{(v)} = -m_i m_j \hat{CV}^{(1)}, \tag{4.38}$$

where $\hat{M}^{(1)}$, $\hat{V}^{(1)}$ and $\hat{CV}^{(1)}$ denote, respectively, the mean of a single fully-excluding compartment, the variance of a single fully-excluding compartment, and the covariance between two fully-excluding compartments. Written in this form, it is clear that if our conjectured values for $\hat{M}_i^{(v)}$, $\hat{V}_i^{(v)}$ and $\hat{V}_{i,j}^{(v)}$ in equations (4.33)-(4.35) are correct, then they must match the values of $\hat{\mu}_i^{(gv)}$, $\hat{v}_i^{(gv)}$ and $\hat{v}_{i,j}^{(gv)}$ (Figure 4.13 gives a graphical explanation of why the variances and covariances take this form). For $2 < i < K-1$, we can substitute equation (4.33) into the mean evolution equations

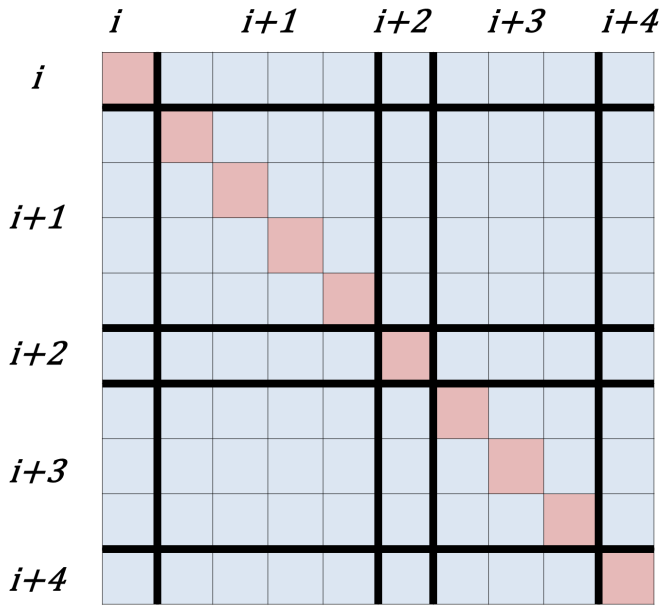

Figure 4.13: The variances and covariances of the aggregated values $S_j^{(gv)}(t)$ can be constructed from those of the fully-excluding grid, in a modified version of the argument presented in Figure 3.5. In this diagram, the corresponding Voronoi compartment capacities are $m_i = m_{i+2} = m_{i+4} = 1$, $m_{i+1} = 4$ and $m_{i+3} = 3$. The red squares indicate variances and the blue squares covariances for fully-excluding compartments. The thick black lines demarcate the values that can be summed to obtain variance and covariance values for $S_j^{(gv)}(t)$, and the shape of these regions explains the forms of equations (4.37) and (4.38).

given in equation (4.7) and observe that they imply $\mathrm{d}M_i/\mathrm{d}t = 0$:

$$\begin{aligned}
\frac{\mathrm{d}M_i^{(v)}}{\mathrm{d}t} &= T_{i-1}^{+}\hat{M}_{i-1}^{(v)} - \left(T_i^{-} + T_i^{+}\right)\hat{M}_i^{(v)} + T_{i+1}^{-}\hat{M}_{i+1}^{(v)}, \\
&= \frac{D}{\Delta x_i m_{i-1} h} m_{i-1}\left[\frac{N}{\kappa}\right] \\
&\quad - \left(\frac{D}{\Delta x_i m_i h} + \frac{D}{\Delta x_{i+1} m_i h}\right) m_i \left[\frac{N}{\kappa}\right] \\
&\quad + \frac{D}{\Delta x_{i+1} m_{i+1} h} m_{i+1}\left[\frac{N}{\kappa}\right] \qquad (4.39) \\
&= \left[\frac{D}{\Delta x_i h} - \frac{D}{\Delta x_i h} - \frac{D}{\Delta x_{i+1} h} + \frac{D}{\Delta x_{i+1} h}\right]\frac{N}{\kappa} = 0, \qquad (4.40)
\end{aligned}$$

where we recalled the Voronoi transition rates from equations (4.4) and (4.5). This demonstrates that equation (4.33) correctly describes the steady-state mean occupancy of each Voronoi compartment (the proof is completed by considering the boundary cases, $i = 1$ and $i = K$, which resolve very similarly and are not shown here).

We approach the variance evolution equations in a similar manner, substituting equations (4.37) and (4.38), and the mean steady-state values previously obtained, into equation (4.8), we obtain

$$\begin{aligned}
\frac{\mathrm{d}V_j^{(v)}}{\mathrm{d}t} &= -2\left(T_j^{-} + T_j^{+}\right)\hat{V}_j^{(v)} + 2T_{j-1}^{+}\left(1 - \frac{1}{m_j}\right)\hat{V}_{j-1,j}^{(v)} + 2T_{j+1}^{-}\left(1 - \frac{1}{m_j}\right)\hat{V}_{j,j+1}^{(v)} \\
&\quad + T_{j-1}^{+}\hat{M}_{j-1}^{(v)}\left(1 - \frac{\hat{M}_j^{(v)}}{m_j}\right) + T_j^{-}\hat{M}_i^{(v)}\left(1 - \frac{\hat{M}_{j-1}^{(v)}}{m_{j-1}}\right) \\
&\quad + T_j^{+}\hat{M}_j^{(v)}\left(1 - \frac{\hat{M}_{j+1}^{(v)}}{m_{j+1}}\right) + T_{j+1}^{-}\hat{M}_{j+1}^{(v)}\left(1 - \frac{\hat{M}_j^{(v)}}{m_j}\right) \qquad (4.41) \\
&= -2\left(\frac{D}{\Delta x_j m_j h} + \frac{D}{\Delta x_{j+1} m_j h}\right)\left(m_j\hat{V}^{(1)} - m_j(m_j - 1)C\hat{V}^{(1)}\right) \\
&\quad - 2\frac{D}{\Delta x_j m_{j-1} h}\left(1 - \frac{1}{m_j}\right) m_{j-1} m_j C\hat{V}^{(1)} \\
&\quad - 2\frac{D}{\Delta x_j m_{j+1} h}\left(1 - \frac{1}{m_j}\right) m_j m_{j+1} C\hat{V}^{(1)} \\
&\quad + \frac{D}{\Delta x_j h}\frac{N}{\kappa}\left(1 - \frac{N}{\kappa}\right) + \frac{D}{\Delta x_j h}\frac{N}{\kappa}\left(1 - \frac{N}{\kappa}\right) \\
&\quad + \frac{D}{\Delta x_{j+1} h}\frac{N}{\kappa}\left(1 - \frac{N}{\kappa}\right) + \frac{D}{\Delta x_{j+1} h}\frac{N}{\kappa}\left(1 - \frac{N}{\kappa}\right). \qquad (4.42)
\end{aligned}$$

Considering the last two lines, we recall from equation (3.39) that

$$\hat{V}^{(1)} = \frac{N}{\kappa}\left(1 - \frac{N}{\kappa}\right), \tag{4.43}$$

and use this to write, after some cancellation,

$$\begin{aligned}
\frac{\mathrm{d}V_j^{(v)}}{\mathrm{d}t} &= -2\left(\frac{D}{\Delta x_j h} + \frac{D}{\Delta x_{j+1} h}\right)\left(\hat{V}^{(1)} - (m_j - 1)C\hat{V}^{(1)}\right) \\
&\quad -2\frac{D}{\Delta x_j h}\left(1 - \frac{1}{m_j}\right) m_j C\hat{V}^{(1)} - 2\frac{D}{\Delta x_j h}\left(1 - \frac{1}{m_j}\right) m_j C\hat{V}^{(1)} \\
&\quad +2\left(\frac{D}{\Delta x_j h} + \frac{D}{\Delta x_{j+1} h}\right)\hat{V}^{(1)} \qquad (4.44) \\
&= -2\left(\frac{D}{\Delta x_j h} + \frac{D}{\Delta x_{j+1} h}\right)\left(\hat{V}^{(1)} - (m_j - 1)C\hat{V}^{(1)}\right) \\
&\quad -2\left(\frac{D}{\Delta x_j h} + \frac{D}{\Delta x_j h}\right)(m_j - 1)\, C\hat{V}^{(1)} \\
&\quad +2\left(\frac{D}{\Delta x_j h} + \frac{D}{\Delta x_{j+1} h}\right)\hat{V}^{(1)} \qquad (4.45) \\
&= 0, \qquad (4.46)
\end{aligned}$$

as expected. By considering the covariance equations, and variance equations for $j = 1, K$, we complete the proof and determine that our conjectured steady-state values for variances and covariance of particle number in Voronoi compartments are correct (these other cases are numerous but resolve very similarly so are not shown here).

4.5.3 Agreement of master equations

Having shown the agreement of the *steady-state* values $\hat{M}_j^{(v)}$, $\hat{V}_j^{(v)}$ and $\hat{V}_{i,j}^{(v)}$ with $\hat{\mu}_j^{(gv)}$, $\hat{v}_j^{(gv)}$ and $\hat{v}_{i,j}^{(gv)}$, respectively, we turn our attention to the agreement of Voronoi model with the aggregated fully-excluding model dynamically. We recall the mean evolution equation used in the previous section, equation (4.39), which we restate

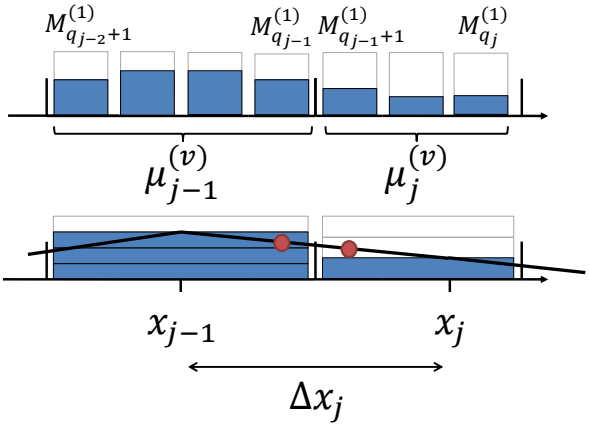

Figure 4.14: A graphical representation of the interpolations described in equations (4.50) and (4.51), for $m_{j-1} = 4$ and $m_j = 3$. Meanwhile, the ratio $\Delta x_j/h$ replaces m in the fraction $(m \pm 1)/m$ in equation (4.49).

here for convenience

$$\begin{aligned}\frac{\mathrm{d}M_i^{(v)}}{\mathrm{d}t} &= \frac{D}{\Delta x_i m_{i-1} h} M_{i-1}^{(v)} - \left(\frac{D}{\Delta x_i m_i h} + \frac{D}{\Delta x_{i+1} m_i h}\right) M_i^{(v)} \\ &\quad + \frac{D}{\Delta x_{i+1} m_{i+1} h} M_{i+1}^{(v)}. \end{aligned} \tag{4.47}$$

Recalling from equation (4.32) that $S_j^{(gv)}$ corresponds to the total number of particles in the fully-excluding compartments indexed $(q_{j-1}+1)$ to q_j, we can therefore write

$$\frac{\mathrm{d}\mu_j^{(gv)}}{\mathrm{d}t} = \frac{D}{h^2}\left(M^{(1)}_{q_{j-1}} - M^{(1)}_{q_{j-1}+1} - M^{(1)}_{q_j} + M^{(1)}_{q_j+1}\right). \tag{4.48}$$

We can then use a linear interpolation argument. In the previous chapter, where we considered uniform lattices, we used substitutions from equations (3.48)-(3.51), e.g.

$$M^{(1)}_{j-1} = \frac{1}{2m}\frac{m+1}{m}\mu^{(m)}_{i-1} + \frac{1}{2m}\frac{m-1}{m}\mu^{(m)}_{i}. \tag{4.49}$$

In the equation above, m was used in two distinct ways: in the fraction $1/2m$ it represented the capacities of the partially-excluding compartments relative to the fully-excluding one, but in the fraction $(m \pm 1/m)$ it was used as a measure of distance between the residence points of compartment $(i-1)$ and of compartment i. In the former case, we therefore replace m with m_{i-1} or m_i, respectively, while

in the second we replace it with $\Delta x_i/h$. The equivalent interpolation for a Voronoi partitioned lattice is therefore

$$\begin{aligned} M^{(1)}_{q_{j-1}} &= \frac{1}{2m_{j-1}} \frac{\frac{\Delta x_j}{h}+1}{\frac{\Delta x_j}{h}} \mu^{(gv)}_{j-1} + \frac{1}{2m_j} \frac{\frac{\Delta x_j}{h}-1}{\frac{\Delta x_j}{h}} \mu^{(gv)}_{j} \\ \Rightarrow M^{(1)}_{q_{j-1}} &= \frac{\Delta x_j + h}{2\Delta x_j m_{j-1}} \mu^{(gv)}_{j-1} + \frac{\Delta x_j - h}{2\Delta x_j m_j} \mu^{(gv)}_{j}. \end{aligned} \tag{4.50}$$

This interpolation is illustrated in Figure 4.14, and we can obtain expressions for the remaining terms in the same manner,

$$M^{(1)}_{q_{j-1}+1} = \frac{\Delta x_j - h}{2\Delta x_j m_{j-1}} \mu^{(gv)}_{j-1} + \frac{\Delta x_j + h}{2\Delta x_j m_j} \mu^{(gv)}_{j}, \tag{4.51}$$

$$M^{(1)}_{q_j} = \frac{\Delta x_{j+1} + h}{2\Delta x_{j+1} m_j} \mu^{(gv)}_{j} + \frac{\Delta x_{j+1} - h}{2\Delta x_{j+1} m_{j+1}} \mu^{(gv)}_{j+1}, \tag{4.52}$$

$$M^{(1)}_{q_j+1} = \frac{\Delta x_{j+1} - h}{2\Delta x_{j+1} m_j} \mu^{(gv)}_{j} + \frac{\Delta x_{j+1} + h}{2\Delta x_{j+1} m_{j+1}} \mu^{(gv)}_{j+1}. \tag{4.53}$$

We can substitute these values into equation (4.48), arriving at

$$\begin{aligned} \frac{\mathrm{d}\mu^{(gv)}_j}{\mathrm{d}t} &= \frac{D}{h^2}\left(M^{(1)}_{q_{j-1}} - M^{(1)}_{q_{j-1}+1} - M^{(1)}_{q_j} + M^{(1)}_{q_j+1} \right) \\ &= \frac{D}{h^2}\left(\frac{h}{\Delta x_j m_{j-1}} \mu^{(gv)}_{j-1} - \frac{h}{\Delta x_j m_j} \mu^{(gv)}_{j} - \frac{h}{\Delta x_{j+1} m_j} \mu^{(gv)}_{j} + \frac{h}{\Delta x_{j+1} m_{j+1}} \mu^{(gv)}_{j+1} \right) \\ &= T^+_{i-1} \mu^{(m_{i-1})}_{i-1} - \left(T^-_i + T^+_i \right) \mu^{(m_i)}_i + T^-_{i+1} \mu^{(m_{i+1})}_{i+1}. \end{aligned} \tag{4.54}$$

Hence, when the linearly interpolated values are accurate, we expect the mean evolution of the aggregated fully-excluding compartments to match the mean evolution of an equivalently sized partially-excluding compartment on a one-dimensional, Voronoi partitioned lattice. As before, interpolations cannot be easily applied to variance and covariance terms (for the reasons discussed in Section 3.3.3), though some analogous results can be obtained in special cases.

4.6 Boundary conditions for Voronoi partitioned lattices

In the preceding chapters, we have shown how flux and Robin boundary conditions can be implemented for non-excluding models (Sections 2.3 and 2.4) and how flux boundary conditions can be implemented for volume-excluding models (Section 3.5). In both cases, only uniformly partitioned lattices were considered. In this section, we extend these results to Voronoi partitioned lattices.

As in Section 3.5, we will work with a continuous concentration value, $c(x,t)$, so for a Voronoi model we write

$$c(x_i,t) = \frac{M_i^{(v)}(t)}{m_i h} = \frac{1}{m_i h} u(x_i,t), \tag{4.55}$$

for $1 < i < K$, where $u(x,t)$ was used in Chapter 2 to to agree with mean particle numbers at the centre of each compartment, as described in equation (2.2) which we restate for convenience:

$$u(x_i,t) = M_i(t). \tag{4.56}$$

4.6.1 Flux boundaries for a Voronoi partitioned lattice

Suppose we wish to recover the flux boundary condition,

$$\left.\frac{\mathrm{d}c}{\mathrm{d}x}\right|_{x=0} = -A. \tag{4.57}$$

The natural implementation of a constant flux boundary condition is to add particles to the first compartment with some constant rate B, so we can write the probability master equation for the first compartment as

$$M_1(t+\Delta t) = \left(1 - \frac{D\Delta t}{\Delta x_2 m_1 h}\right) M_1(t) + \frac{D\Delta t}{\Delta x_2 m_2 h} M_2(t) + B\Delta t. \tag{4.58}$$

We can then rearrange equation (4.58), using the strategies from Chapter 2, to obtain

$$\frac{M_1(t+\Delta t) - M_1(t)}{\Delta t} = \frac{D}{\Delta x_2}\left[\frac{M_2(t)}{m_2 h} - \frac{M_1(t)}{m_1 h}\right] + B. \tag{4.59}$$

The right-hand terms are already arranged in the form of concentrations (particle numbers divided by the width of the compartments); to find the left-hand side in the form of a concentration, we divide both sides by $m_1 h$, and then multiply by $\sqrt{\Delta t}$, arriving at

$$\sqrt{\Delta t}\frac{c(x_1, t+\Delta t) - c(x_1, t)}{\Delta t} = \frac{D\sqrt{\Delta t}}{m_1 h}\left[\frac{c(x_1+\Delta x_2, t) - c(x_1, t)}{\Delta x_2}\right] + B\frac{\sqrt{\Delta t}}{m_1 h}.$$

Taking the diffusive limit, so that $\Delta t \to 0$, with the compartment widths also going to zero such that the ratio $\Delta t/h^2$ remains constant, we find

$$0 = D\left.\frac{\partial c}{\partial x}\right|_{x=0} + B, \tag{4.60}$$

$$\Rightarrow \frac{\partial c}{\partial x} = -\frac{B}{D}, \tag{4.61}$$

so simple flux boundary conditions can be implemented the same way on an irregular, Voronoi lattice as on a uniform one.

4.6.2 Robin boundaries for a Voronoi partitioned lattice

On a regular lattice, the removal of a particle was handled by a combination of an absorption probability, Ph, and a jump rate, D/h^2. It is not clear what jump rate should be used here at the boundary of an irregular lattice.

However, we do not need to know the individual form of either the jump rate or the absorption probability since they are used exclusively as a product. Making the assumption that the jump rate will scale with the diffusion constant D, and inversely with the width of the first compartment, $1/m_1$, we therefore write the

combined absorption probability and jump probability as

$$PT_1^- = \frac{D\Delta t}{m_1} r, \tag{4.62}$$

for some r. We wish to match the PDE boundary condition,

$$D\frac{\partial c}{\partial x}\bigg|_{x=0} = Rc(0,t), \tag{4.63}$$

and therefore write

$$M_1(t+\Delta t) = \left(1 - \frac{D\Delta t}{\Delta x_2 m_1} - \frac{D\Delta t}{m_1} r\right) M_1(t) + \frac{D\Delta t}{\Delta x_2 m_2} M_2(t), \tag{4.64}$$

which, after rearranging, becomes

$$\begin{aligned} \frac{M_1(t+\Delta t) - M_1(t)}{\Delta t} + \frac{2D}{2x_1 + \Delta x_2} r M_1(t) \quad &= \quad \frac{2D}{\Delta x_2(\Delta x_2 + \Delta x_3)} M_2(t) \\ &\quad - \frac{2D}{\Delta x_2(2x_1 + \Delta x_2)} M_1(t). \end{aligned} \tag{4.65}$$

After dividing both sides through by m_1, and using equation (4.55) to convert the mean values into concentrations, this becomes

$$\frac{c(x_1, t+\Delta t) - c(x_1,t)}{\Delta t} + \frac{D}{m_1} r c(x_1,t) = \frac{D}{m_1}\left(\frac{c(x_1+\Delta x_2, t) - c(x_1,t)}{\Delta x_2}\right). \tag{4.66}$$

We then multiply through by $\sqrt{\Delta t}$ and take the diffusive limit so that the time derivative term vanishes, leaving

$$Drc(0,t) = D\,\frac{\partial c}{\partial x}\bigg|_{x=0}, \tag{4.67}$$

so to match the PDE boundary condition, equation (4.63), we require

$$r = \frac{R}{D}, \tag{4.68}$$

which provides a particle absorption rate to replicate a Robin boundary condition.

As an aside, we note that this conception of the Robin boundary condition, as a rate at which particles are removed from the compartment, rather than as a combination of a jump rate and an absorption probability, makes it possible to implement a Robin boundary condition with larger values of R, since we are not constrained by the requirement to keep the absorption probability equal to or less than unity (as discussed in Section 2.3.2).

4.7 Discussion

In this chapter, we have presented two methods for the simulation of volume-excluding compartment-based models on non-uniform lattices. We have presented analytic arguments for the match of aggregated mean particle distribution in the uniform model with $m > 1$ and in both hybrid models (i.e. $M^{(m)}$ $\mu^{(v)}$ and $\mu^{(c)}$, respectively) with the aggregated mean particle distribution in the 'accurate' model with $m = 1$ ($\mu^{(m)}$). Numerical investigations of three single-species test cases confirm that all four models generally agree on the mean and variance of particle numbers within each compartment. We have further presented a simple multi-species system, where the results of uniform $m > 1$ models deviate from those of the accurate fully-excluding model, but the results of hybrid models match those of the fully-excluding model and can be generated in a fraction of the time. This is a valuable development for researchers working with multi-scale diffusion systems, as it enables computationally efficient partially-excluding compartments to be used where possible, while using fully-excluding compartments elsewhere in the domain when necessary.

Time savings of nearly a factor of seven relative to the fully-excluding model were observed for the Voronoi method in the multi-species system, and significant savings were also observed in other cases, such as the morphogen gradient, where the test system was conducive to hybrid modelling. The time savings in other situations could be even more significant. Hybrid methods may prove valuable in systems where most of the particles in the system spend the majority of the simulation occupying coarse compartments where jump propensities are lower; when this is not the case

(such as in the uniform steady-state test case) any time savings will only be minor.

Furthermore, in this chapter we have obtained additional results for volume exclusion on non-uniform Voronoi lattices, matching the mean occupancy of Voronoi compartments, $M^{(v)}$, to the mean occupancy of appropriate aggregations of fully-excluding compartments, $\mu^{(gv)}$, and similarly matching variance and covariance steady-state values. The results of the previous chapter, derived for uniformly partitioned volume-excluding LBPJ models, can therefore be considered as a special case of more general results for Voronoi-partitioned lattices.

In the next chapter, we will address the question of reactions for the first time, demonstrating how interactions between particles in partially-excluding compartments can be defined so that the resulting reaction rates match those observed between particles in a corresponding, contiguous grouping of fully-excluding compartments. We investigate the circumstances under which inter-reaction times in different models converge, or not, as the diffusion rate increases.

Chapter 5

Scaling reaction rates in crowded systems

In the previous chapters we have considered models of particles that are non-reactive, or undergo only simple reactions such as decay. This final research chapter considers how reactions can be implemented in a volume-excluding model so that behaviour is conserved across scales, and what assumptions this implementation requires.

5.1 Reactions and diffusion

Biological cells use reactions to sustain and propagate life, performing millions of reactions per second [43]. Many models of reactions, such as the chemical master equation (CME), do not track the positions of reactants, but only the total number of each reactant species in the system [109]. In many cases, however, particle concentrations vary across the region of interest, and incorporating spatial information can lead to different behaviour from that observed using the CME [110]. For example, in a bistable system, distinct spatial regions of opposite phases may emerge within the domain of a spatial model, while a non-spatial model would predict the entire system adopting a single phase [7].

5.1.1 Reaction diffusion master equations

The reaction-diffusion master equation (RDME) framework is a well-established tool for describing a system where the concentrations of interacting particles vary spatially [111]. The domain is divided into compartments, and particles interact exclusively with other particles sharing the same compartment, with rates for bimolecular reactions that vary with the number of possible pairings of reactants, divided by the size of the compartment (we do not generally consider simultaneous reactions between three or more particles in this chapter) [112]. Compartment sizes for the RDME must be chosen such that the particles within them can be treated as well-mixed on the time scale of the fastest bimolecular reaction [53]. The rate of diffusion is important: when D is large, the results of a spatial model can approach those of a non-spatial model, for example in predicting the mean number of proteins observed at steady-state [113], or in erasing spatial inhomogeneities in bistable systems [7].

A related framework is known as patch dynamics: as in the RDME particles are located at a series of discrete locations, but in this case a pair of particles are chosen from each location at discrete time steps with some probability and permitted to react [114].

5.1.2 Convergent and generalised reaction diffusion master equations

For purely diffusive simulations, refining compartment sizes leads to greater accuracy, but for RDME models incorporating bimolecular reactions the story is more complicated. In travelling-wave models, wave speeds can be affected by the choice of compartment size [102]. Furthermore, as the compartment size is reduced, an initial increase in accuracy (relative to equivalent off-lattice models) is often observed, but as compartment size $\Delta x \to 0$, bimolecular reactions are lost in two and three dimensional models [115, 116].

One response to this has been the convergent reaction-diffusion master equation (CRDME), which converges to the Doi model [56]. Within the Doi model, particles

are modelled as points undergoing Brownian motion: when one particle is within a specified reaction radius of another suitable reactant, a reaction will occur with fixed rate. By treating point particles as the ground truth, the CRDME does not incorporate volume-excluding effects.

A similar approach to the CRDME which does include volume-excluding effects is the generalised reaction-diffusion master equation (gRDME) [117, 118]. In this case, the model is designed to converge to a Smoluchowski model. The Smoluchowski model represents particles as hard spheres undergoing Brownian motion, and reactions occur with fixed probability when two particles collide.

5.1.3 Excluded volume RDME

Of particular relevance to our work are the existing models of reactions and volume exclusion within lattice-based frameworks. A recent paper introduced volume-excluding variations on the CME and RDME, termed the excluded volume chemical master equation (vCME) and excluded volume reaction-diffusion master equation (vRDME) [119]. The vRDME is lattice-based with only one particle permitted per voxel, which we would describe as fully-excluding.

In this chapter, we refer to a fully-excluding model incorporating reactions between adjacent particles as the fully-excluding reaction-diffusion master equation (feRDME). Our feRDME corresponds to the vRDME [119]. We chose to adopt the acronym feRDME instead of vRDME, however, to avoid confusion with the partially-excluding model, which is also volume-excluding. As in Chapters 3 and 4, we treat this fully-excluding model as our ground truth, and use it to obtain reaction rates for corresponding partially-excluding models, the partially-excluding reaction-diffusion master equation (peRDME), and for a spatially-homogeneous model, the vCME. We study the circumstances in which the feRDME, peRDME and vCME agree, or disagree, in predicting the time it will take a system of reacting particles to reach a steady-state.

5.1.4 Chapter outline

In Section 5.2 we discuss the possible reactions to be considered, and how they can be implemented in an feRDME model. We then use the feRDME reaction rates to obtain reactions rates for peRDME and vCME models in Section 5.3, observing that, in the case of the peRDME, it is necessary to allow for reactions both within and between partially-excluding compartments.

Having obtained reaction rates for volume-excluding models, in the remainder of this chapter we examine how closely the results of peRDME and vCME models capture the behaviour of our fundamental feRDME model. We compare the models analytically in Section 5.4, obtaining expressions for the mean time to reaction for a pair of particles, and demonstrating that all three models predict the same mean time in the limit as diffusion becomes infinitely fast.

In Sections 5.5, 5.6 and 5.7 we investigate the different modelling regimes numerically in cases where there are more than one pair of particles in the systems, comparing the mean time taken to reach a steady-state. The three example reactions considered in these three sections are, in order: (i) a single-species mutual annihilation reaction; (ii) a two-species mutual annihilation reaction; and (iii) a two-species conversion reaction (where a particle of one species may cause another particle to change its species). We observe that the feRDME, peRDME and vCME models agree well when only one particle species is present, at least in systems where diffusion is relatively rapid, but that care must be taken when applying peRDME and vCME in one spatial dimension when multiple species are present. We discuss these caveats in Section 5.8, which concludes the chapter.

5.2 Reaction propensities for fully-excluding systems

In this chapter we consider two distinct species of particle, denoted A and B, though the results presented are generalisable to more complex systems. Particles of both species are assumed to be of the same size. This is a common assumption in the literature [113, 119], though some models do incorporate diffusing entities of sig-

nificantly different size, such as biological cells and much smaller chemoattractant molecules [80]. Throughout this chapter, we will write A_j and B_j to denote a particle in the j^{th} compartment of species A or B, respectively, for the purpose of defining reactions. In addition, we will use E_j to denote available space within the j^{th} compartment. We will continue to use $n_j^{(m)}$ to refer to the total number of particles within a compartment of capacity m; when we wish to refer exclusively to the number of A or B particles, we will write $a_j^{(m)}$ and $b_j^{(m)}$, respectively. In a two species system, we therefore note that $a_j^{(m)} + b_j^{(m)} = n_j^{(m)}$. For ease of reading, it will sometimes be convenient to write $e_j^{(m)} = m - n_j^{(m)}$ to denote the unused capacity.

Reactions are commonly classified by their order. A reaction that occurs at a constant rate, and requires no reactants, is zeroth order; a reaction involving a single reactant is first order; a reaction involving two reactants is second order and so on [120]. This is complicated slightly by volume-exclusion. We treat empty space as a reactant, so that a propagation event for a single particle, creating a new particle in an adjacent space, is considered to be a second-order reaction between the particle and the empty space [119]. As a consequence, zeroth order events do not occur in a volume-excluding framework. For example, one zeroth order reaction in a non-excluding model would be particle production at a constant rate, but in a volume-excluding model this would be a first-order reaction with empty space as the reactant.

5.2.1 First order events

Consider a fully-excluding creation/decay system, in which unoccupied compartments may spawn a new particle of species A with propensity k_1^c, and particles of species A may decay with propensity k_1^d. We write these reactions

$$E_j \xrightarrow{k_1^c} A_j, \tag{5.1}$$

$$A_j \xrightarrow{k_1^d} E_j. \tag{5.2}$$

This is an example of a system where all events are of first order. The other possible first order reaction in a two species system would be the transformation of one particle species into the other with constant propensity per particle, i.e.

$$A_j \xrightarrow{k_1^t} B_j. \tag{5.3}$$

5.2.2 Second order events

The category of second order reactions includes bimolecular reactions, whether between two particles of the same species, or between two particles of different species. For example, we might consider a mutual annihilation reaction between two particles of species A, occurring with propensity k_2^d,

$$A_i + A_j \xrightarrow{k_2^d} E_i + E_j, \tag{5.4}$$

or a similar mutual annihilation reaction occurring between one particle of species A and another of species B,

$$A_i + B_j \xrightarrow{k_2^d} E_i + E_j, \tag{5.5}$$

where compartments i and j are adjacent. We study both single-species and two-species mutual annihilation reactions in Sections 5.5 and 5.6, respectively. Another example would be a particle of species A reacting with one of species B with propensity k_2^t, and one particle changing its species to that of the other

$$A_i + B_j \xrightarrow{k_2^t} \begin{cases} A_i + A_j & \text{with probability } p, \\ B_i + B_j & \text{with probability } (1-p). \end{cases} \tag{5.6}$$

We term the reaction described in expression (5.6) a two-species conversion reaction, and study it in detail in Section 5.7. The reactions described so far would also be termed second order in a non-excluding model. In a volume-excluding model, however, we must also treat as second order propagation events which might be

considered first order in a non-excluding context, e.g. a particle producing a new particle of the same species in an adjacent empty space,

$$A_i + E_j \xrightarrow{k_2^c} A_i + A_j, \tag{5.7}$$

where compartments i and j are again adjacent. All references to 'second order' reactions in the remainder of this chapter refer exclusively to reactions which are second order in a volume-excluding model.

Some studies conceive reactions for feRDME models slightly differently, so that when a particle attempts to move into another fully-excluding compartment occupied by a suitable particle they may react with some probability [121]. Our implementation is less restricted, however, as it allows for the modelling of reactions that occur between adjacent particles with a rate higher than the rate at which the particles attempt to move between compartments.

5.2.3 Third order events and higher

Reactions involving more than two reactants in a single step are rare in nature, as the probability of three or more entities interacting simultaneously is vanishingly small [122]. In chemistry, only a few elementary termolecular reactions (involving three molecules in a single step) are known, and no elementary reactions requiring more than three molecules to interact simultaneously are currently known [123]. For this reason, reactions involving three or more reactants are generally modelled stochastically as multi-stage processes, e.g. trimerisation is represented by two particles coming together in a dimerisation reaction, then a further reaction between the resulting dimer and a third particle [120].

Although we do not further consider third order reactions in this chapter, we note that second-order bimolecular reactions would need to be treated as effectively third-order if they require empty space to create a new particle. For example, we might consider a particle of species A, which may interact with a catalyst of species

B to produces a new particle of species A in an adjacent empty space,

$$A_i + B_j + E_k \xrightarrow{k_3^c} A_i + B_j + A_k. \tag{5.8}$$

In implementing such a reaction, care should be taking in specifying possible valid combinations i, j and k: it seems clear that the voxels i and j should be adjacent to allow for the initial interaction, but it is not so clear whether the voxel indexed k must be adjacent to that indexed i (i.e. the reproducing A particle), or whether it is sufficient to be adjacent to voxel j, where the catalyst, B, is located. This decision will depend on the physical details of the interaction (it may be that both choices can be appropriate in the right circumstances) and will affect the form taken by the mesoscopic reaction propensity.

5.3 Reaction propensities for partially-excluding systems

In Chapters 3 and 4, we assumed that mean particle numbers on fully-excluding lattices could be linearly interpolated from the particle numbers in partially-excluding compartments. To incorporate reactions however, and in common with the standard RDME, we need to make the assumption that particles are well-mixed within compartments in order to calculate reaction rates. These two models of particle distribution are not equivalent in all circumstances but, in the cases considered for this thesis, both are reasonable approximations. In cases where the well-mixed assumption cannot be made, it would be necessary to use a fully-excluding model, or a hybrid method of the types discussed in Chapter 4.

5.3.1 First order events

Recalling the decay and creation rates from Section 5.2.1, we intuitively expect creation and decay events in a partially-excluding compartment to occur with rates proportional to the quantity of unused capacity and the quantity of particles in the compartment, respectively. More precisely, we expect new particles to be created

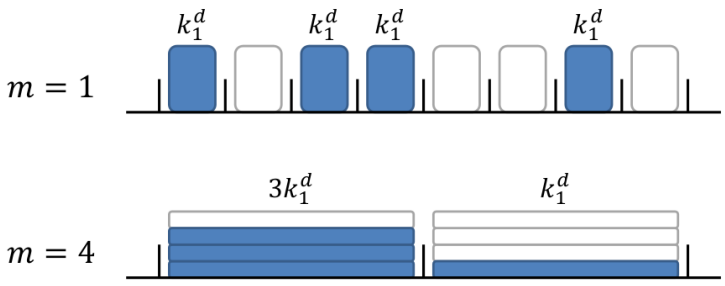

Figure 5.1: In this figure we illustrate a simple reaction-diffusion system where individual particles may decay with propensity k_1^d. Particles are represented by blue cells, while unused capacity is represented by white cells. The rate with which first order decay reactions occur within partially-excluding compartments scales linearly with the number of particles.

with propensity $k_1^d e_j^{(m)} = k_1^d \left(m - n_j^{(m)}\right)$, and similarly expect to see particles decay with propensity $k_1^d n_j^{(m)}$. A comparison of decay in fully- and partially-excluding models is shown in Figure 5.1. It can be seen that reconciling first order reactions between the models is straight-forward, since the rate at which first order events will occur within each aggregated coarse compartment is determined solely by the number of particles within it. This is in contrast to second order reactions, where it is necessary to make assumptions about the probable locations of particles within the partially-excluding compartments.

5.3.2 Second order events within compartments

To obtain reaction propensities for particles within partially-excluding compartments of capacity m in one spatial dimension, we assume that the particles within the compartments are uniformly distributed over a contiguous block of m fully-excluding compartments. A comparison of fully-excluding and partially-excluding models is given in Figure 5.2. It is then possible to calculate the expected total reaction propensity for the entire block using combinatorial arguments which we present in this section, first in one spatial dimension then generalised to d spatial dimensions. As can be seen in Figure 5.2, it is also necessary to consider reactions occurring between adjacent partially-excluding compartments, and we address this in Section 5.3.3.

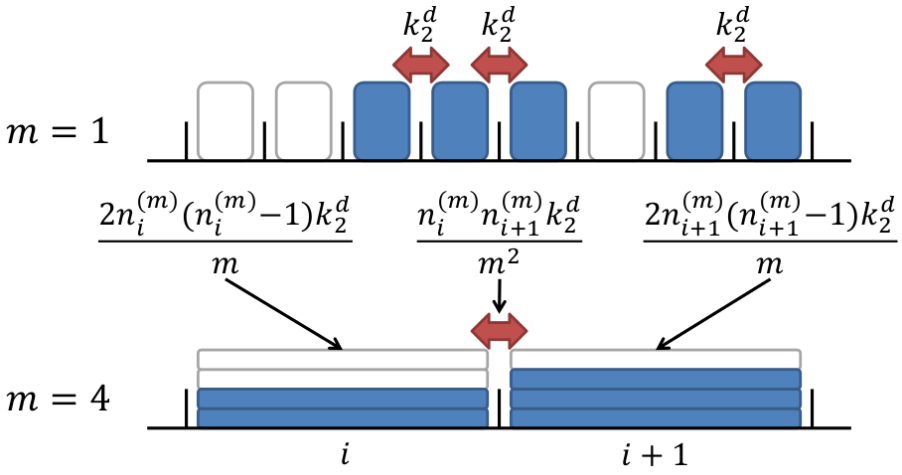

Figure 5.2: In this figure we illustrate a reaction-diffusion system where pairs of adjacent particles may react with propensity k_2^d. Particles are represented by blue cells. The upper figure shows a fully-excluding model, where potential reaction pairings are denoted with red arrows. To match the average behaviour of the fully-excluding model, the partially-excluding model must include not only reactions between particles sharing the same compartment, but also reactions between particles in adjacent compartments. The rates for reactions within and between compartments, shown in the figure, are obtained in Sections 5.3.2 and 5.3.3, respectively.

Consider a single partially-excluding compartment, which we label i, of capacity m. The compartment contains $a_i^{(m)}$ particles of type A, and $b_i^{(m)}$ of type B, which we assume to be well-mixed. Suppose that the two species react with propensity k_2 when occupying adjacent fully-excluding compartments (for the purposes of this derivation the outcome of the reaction is immaterial). In the standard, non-excluding RDME framework, the reaction propensity would take the form

$$k_{RDME}\frac{a_i^{(m)}b_i^{(m)}}{m}, \tag{5.9}$$

where k_{RDME} is a constant, reflecting the reaction rate and size of particles. To obtain propensities for the peRDME, we begin by determining the number of ways in which the volume-excluding particles could be arranged in the compartment. When randomizing the location of these particles over m fully-excluding compartments,

the number of possible arrangements is given by the standard result

$$\frac{m!}{a_i^{(m)}!b_i^{(m)}!\left(m-a_i^{(m)}-b_i^{(m)}\right)!}=\frac{m!}{a_i^{(m)}!b_i^{(m)}!e_i^{(m)}!}. \tag{5.10}$$

To determine the probability that a given pair of adjacent fully-excluding compartments contain one particle of species A and one of species B, we need to know how many possible arrangements have this property (i.e. how many ways there are to distribute the remaining $(a_i^{(m)}-1)$ A particles and $(b_i^{(m)}-1)$ particles over the other $(m-2)$ compartments). This is of a similar form to expression (5.10):

$$2\frac{(m-2)!}{\left(a_i^{(m)}-1\right)!\left(b_i^{(m)}-1\right)!\left(m-a_i^{(m)}-b_i^{(m)}\right)!}=2\frac{(m-2)!}{\left(a_i^{(m)}-1\right)!\left(b_i^{(m)}-1\right)!e_i^{(m)}!}, \tag{5.11}$$

where the factor of two is introduced because there are two valid ways for the initial pair of particles to be arranged: AB or BA. We can then find the probability that a given pair of compartments are occupied by one A and one B particle by dividing expression (5.11) by expression (5.10):

$$2\frac{\left(\frac{(m-2)!}{\left(a_i^{(m)}-1\right)!\left(b_i^{(m)}-1\right)!e_i^{(m)}!}\right)}{\left(\frac{m!}{a_i^{(m)}!b_i^{(m)}!e_i^{(m)}!}\right)} \quad = \quad 2\frac{a_i^{(m)}b_i^{(m)}}{m(m-1)}. \tag{5.12}$$

This can be interpreted as the number of pairings of A and B particles, divided by the number of pairings between compartments. To obtain the expected total reaction propensity within the partially-excluding compartment, we multiply this expression by the reaction rate, k_2, and by the number of pairs of adjacent compartments, $(m-1)$, to arrive at

$$2k_2\frac{a_i^{(m)}b_i^{(m)}}{m}. \tag{5.13}$$

We note that this recovers the form of the reaction propensity typically used in

RDME type systems, as stated in equation (5.9): a product of the two reactants, divided by the size of the compartment, and multiplied through by some constant coefficient (in this case $2k_2$) [124].

This approach generalises easily to higher dimensions. For a two-dimensional model, with a coarse square compartment of capacity m^2, the probability of any given pair of compartments being occupied by one A and one B particle is

$$2\frac{\left(\dfrac{(m^2-2)!}{\left(a_i^{(m)}-1\right)!\left(b_i^{(m)}-1\right)!\left(m^2-a_i^{(m)}-b_i^{(m)}\right)!}\right)}{\left(\dfrac{(m^2)!}{a_i^{(m)}!b_i^{(m)}!\left(m^2-a_i^{(m)}-b_i^{(m)}\right)!}\right)} \quad = \quad 2\frac{a_i^{(m)}b_i^{(m)}}{m^2(m^2-1)}. \tag{5.14}$$

By multiplying expression (5.14) by $2m(m-1)$, i.e. the number of possible pairings of adjacent fully-excluding compartments, and by the reaction constant k_2, we find the reaction propensity for reactions within the coarse compartment to be

$$\left(4\frac{m}{m+1}\right)k_2\frac{a_i^{(m)}b_i^{(m)}}{m^2}, \tag{5.15}$$

which again gives us the product of reactant numbers divided by the coarse compartment size, with constant coefficient $4k_2m/(m+1)$. We can further generalise this result to a d-dimensional hypercube, in which case there will be $dm^{d-1}(m-1)$ possible pairings to consider (Figure 5.3 illustrates how the number of pairings scales with m and d for $d = 1, 2$ and 3) and we can obtain an expected reaction propensity

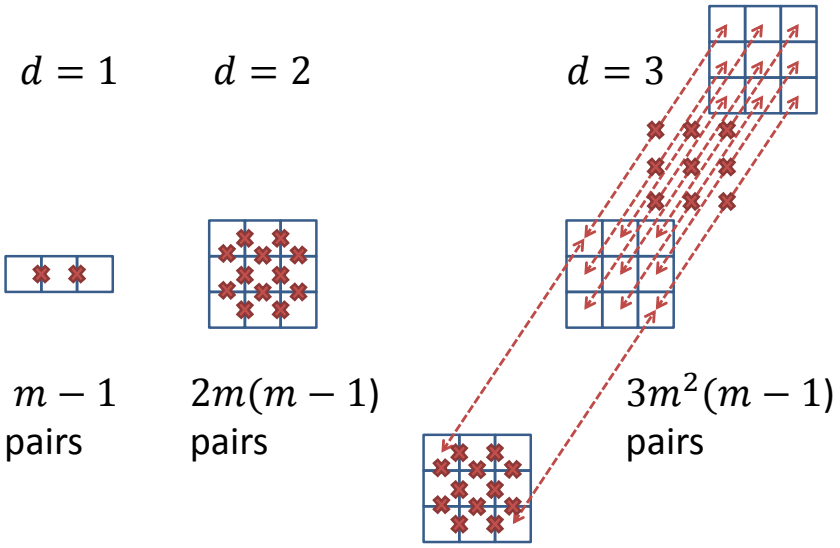

Figure 5.3: The number of possible pairings between adjacent compartments in a regular d-dimensional array of m^d compartments is $dm^{d-1}(m-1)$. Connections between adjacent compartments are highlighted with red crosses. In the interests of clarity, only a representative sample of connections are highlighted in the case $d = 3$.

for the coarse compartment:

$$\begin{aligned} 2k_2 \quad dm^{d-1} \quad (m-1)\frac{\left(\dfrac{\left(m^d-2\right)!}{\left(a_i^{(m)}-1\right)!\left(b_i^{(m)}-1\right)!\left(m^d-a_i^{(m)}-b_i^{(m)}\right)!}\right)}{\left(\dfrac{\left(m^d\right)!}{a_i^{(m)}!b_i^{(m)}!\left(m^d-a_i^{(m)}-b_i^{(m)}\right)!}\right)} \\ = \quad 2dk_2m^{d-1}(m-1)\frac{a_i^{(m)}b_i^{(m)}}{m^d\left(m^d-1\right)}, \\ = \quad \left(2d\frac{m^{d-1}}{\sum_{i=0}^{d-1}m^i}\right)k_2\frac{a_i^{(m)}b_i^{(m)}}{m^d}. \end{aligned} \tag{5.16}$$

This expression can be modified for other reactants. For example, rates for a propagation reaction between a species A particle and an empty space can be obtained by substituting $e_i^{(m)}$ for $b_i^{(m)}$, and for a reaction between two particles of species A we write

$$\left(d\frac{m^{d-1}}{\sum_{i=0}^{d-1}m^i}\right)k_2\frac{a_i^{(m)}\left(a_i^{(m)}-1\right)}{m^d}. \tag{5.17}$$

In the next section, we apply similar reasoning to obtain propensities for reactions occurring between partially-excluding compartments.

5.3.3 Second order events between compartments

We have derived expected rates for reactions occurring within a single partially-excluding compartment, but in Figure 5.2 we observed that it is also possible for reactions to occur between particles contained within adjacent partially-excluding compartments. Using the same arguments employed in the preceding section we can obtain expected rates with which such reactions will occur.

We consider again a partially-excluding compartment indexed i, and an adjacent partially-excluding compartment indexed (without loss of generality) $i+1$. We assume that both compartments are composed of m^d fully-excluding compartments, arranged into a regular d-dimensional array.

There will be m^{d-1} fully-excluding compartments in compartment i that border onto fully-excluding compartments in compartment $i+1$. Assuming well-mixedness, each will be occupied by an A or B particle with probabilities $a_i^{(m)}/m^d$ or $b_i^{(m)}/m^d$, respectively, while the neighbouring box in compartment $i+1$ will be occupied by an A or B particle with probabilities $a_{i+1}^{(m)}/m^d$ or $b_{i+1}^{(m)}/m^d$, respectively. We therefore expect reactions to occur between particles of different species, each occupying adjacent but distinct partially-excluding compartments, to occur with rate

$$k_2 m^{d-1} \frac{a_i^{(m)}}{m^d} \frac{b_{i+1}^{(m)}}{m^d} + k_2 m^{d-1} \frac{a_{i+1}^{(m)}}{m^d} \frac{b_i^{(m)}}{m^d} = k_2 \frac{1}{m} \frac{a_i^{(m)} b_{i+1}^{(m)}}{m^d} + k_2 \frac{1}{m} \frac{a_{i+1}^{(m)} b_i^{(m)}}{m^d}. \tag{5.18}$$

This can be adapted for other second order reactions. For example, to describe a reaction between two particles of species A, or between a particle of species A and an empty space, we simply substitute the $b^{(m)}$ terms for $a^{(m)}$ or $e^{(m)}$, respectively.

5.3.4 Comparison to the traditional RDME

Combining the results of Sections 5.3.3 and 5.3.2, we can write the total rate at which reactions occur, involving at least one particle within a given one-dimensional

compartment of size m, as

$$2k_2\frac{a_i^{(m)}b_i^{(m)}}{m}+\frac{1}{m}\left[\frac{a_i^{(m)}b_{i-1}^{(m)}}{m}+\frac{a_{i-1}^{(m)}b_i^{(m)}}{m}+\frac{a_i^{(m)}b_{i+1}^{(m)}}{m}+\frac{a_{i+1}^{(m)}b_i^{(m)}}{m}\right]. \tag{5.19}$$

It is clear that as m becomes large this rate is dominated by the term

$$2k_2\frac{a_i^{(m)}b_i^{(m)}}{m}, \tag{5.20}$$

and we thus recover the traditional RDME reaction rates. When m is smaller, however, it will be important to account for the possibility of reactions occurring between compartments. The limiting case of this is the fully-excluding model where $m = 1$, and hence reactions can only occur between compartments as no compartment can hold two particles simultaneously.

We note that existing work in the field has also found that the RDME must include reactions between compartments in order to incorporate second order reactions when compartment sizes are small [56, 118]. As in these previous works, our approach also recovers the conventional RDME formulation as the asymptotic limit of large box sizes. To conclude this section, we consider the special case when $m = \kappa$, i.e. a non-spatial model where every particle is located in a single domain-sized compartment.

5.3.5 The volume excluding chemical master equation

This thesis focuses on diffusion, and hence spatial modelling. It is also useful to consider a non-spatial model of reactions in a volume-excluding system, the vCME, which can be used later in this chapter for comparisons with the feRDME and peRDME models [119].

In one spatial dimension, the reaction rate for a bimolecular reaction between A and B particles can be obtained for a non-periodic domain by substituting $m = \kappa$ into equation (5.13), i.e. assuming that particles are well-mixed across the whole

domain, obtaining

$$2k_2\frac{a^{(\kappa)}b^{(\kappa)}}{\kappa}, \tag{5.21}$$

where $a^{(\kappa)}$ and $b^{(\kappa)}$ describe the total number of particles of species A and B, respectively, in the entire system. Similarly, for a single-species reaction the reaction rate will be

$$k_2\frac{a^{(\kappa)}\left(a^{(\kappa)}-1\right)}{\kappa}. \tag{5.22}$$

On a periodic domain, equation (5.21) can be modified slightly to obtain

$$2k_2\frac{a^{(\kappa)}b^{(\kappa)}}{\kappa-1}. \tag{5.23}$$

The reaction propensity for the periodic domain is slightly higher to represent the possibility of reactions occurring between particles at the left and right edges of the domain. Similar rates can be obtained for vCME models in two or more spatial dimensions. For example, by substituting $m = \sqrt{\kappa}$ into expression (5.15) (using $\sqrt{\kappa}$ since the expression was derived for a compartment of capacity m^2) we can arrive at the reaction rate for reactions between particles of species A and B in a two-dimensional vCME model:

$$\left(4\frac{\sqrt{\kappa}}{\sqrt{\kappa}+1}\right)k_2\frac{a_i^{(m)}b_i^{(m)}}{\kappa}. \tag{5.24}$$

To ensure that our derived reaction rates preserve reaction behaviour between scales, in the next section we obtain analytically expected times for two particles to meet and react using these rates.

5.4 Expected time for two particles to meet and react

In order to obtain an expected time until reaction for two particles in a reaction-diffusion system, we choose a deliberately simple system in which two particles diffuse on a one-dimensional periodic lattice of $K = 2n$ compartments of capacity m, where $n \in \mathbb{N}$. Each particle may jump to adjacent compartments with propensity $T^{\pm}$, with

a blocking probability of $1/m$ for attempts to jump into an occupied compartment (since this is a two particle system, there will be at most one particle occupying any adjacent compartment). In addition, when the two particles occupy the same compartment they may react with rate $R = 2k_2/m$, as obtained from expression (5.13); when they occupy adjacent compartments they may react with rate $R/2m$, as obtained from expression (5.18).

5.4.1 Expected time until reaction on a periodic grid

We write $E(k)$ for the expected time until a reaction between two particles moving on this domain, where $0 \leq k \leq n$ describes how far the two particles are from one another; values of k can be interpreted as the minimum number of jumps necessary for the two particles to reach one another. $E(0)$ is the expected time until reaction for two particles sharing the same box, and $E(n)$ the expected time until reaction for two particles as far away from one another as is possible on the periodic domain.

For even-valued K, this leads to the system of equations

$$\begin{aligned}
E(0) &= \frac{4T^{\pm}}{4T^{\pm}+R}E(1) + \frac{1}{4T^{\pm}+R}, && (5.25)\\
E(1) &= \frac{2(1-\frac{1}{m})T^{\pm}}{(4-\frac{2}{m})T^{\pm}+\frac{R}{2m}}E(0) + \frac{2T^{\pm}}{(4-\frac{2}{m})T^{\pm}+\frac{R}{2m}}E(2) \\
&\quad + \frac{1}{(4-\frac{2}{m})T^{\pm}+\frac{R}{2m}}, && (5.26)\\
E(k) &= \frac{1}{2}E(k-1) + \frac{1}{2}E(k+1) + \frac{1}{4T^{\pm}}, \text{ for } 1 < k < n, && (5.27)\\
E(n) &= E(n-1) + \frac{1}{4T^{\pm}}. && (5.28)
\end{aligned}$$

In the fully-excluding case where $m = 1$, we discard equation (5.25), and set $E(0) = 0$ in equation (5.26). We do not consider the case when $K = 2n + 1$ is odd, but note that it could be resolved easily by changing equation (5.28) of the above system so that

$$\begin{aligned}
E(n) &= \frac{1}{2}E(n-1) + \frac{1}{2}E(n) + \frac{1}{4T^{\pm}} && (5.29)\\
&= E(n-1) + \frac{1}{2T^{\pm}}. && (5.30)
\end{aligned}$$

In the interests of brevity we consider only the case where $K(=2n)$ is even valued, as the method for odd valued K is almost identical. By means of a proof by induction, it can be shown that

$$E(n-l) = E(n-l-1) + \frac{2l+1}{4T^{\pm}}, \tag{5.31}$$

for $0 \leq l \leq n-2$. By setting $l = n-2$, we find

$$E(2) = E(1) + \frac{K-3}{4T^{\pm}}, \tag{5.32}$$

which we substitute into equation (5.26), arriving at

$$E(1) = \frac{2(1-\frac{1}{m})T^{\pm}}{2(1-\frac{1}{m})T^{\pm} + \frac{R}{2m}} E(0) + \frac{\frac{K-1}{2}}{2(1-\frac{1}{m})T^{\pm} + \frac{R}{2m}}. \tag{5.33}$$

We substitute equation (5.33) into equation (5.25) to finally arrive at

$$E(0) = \left[\frac{4T^{\pm}(Km-1)+R}{4mT^{\pm}R + R^2}\right]. \tag{5.34}$$

We note that when $T^{\pm} = 0$ this expression reduces to $E(0) = 1/R$ as expected (if diffusion away is impossible then two particles sharing the same box can only react with rate R, and hence the expected time to reaction is $1/R$). It is also instructive to note the behaviour of $E(0)$ in the limit as diffusion becomes fast, $T^{\pm} \to \infty$:

$$E(0) \to \frac{K-\frac{1}{m}}{R} = \frac{\kappa - 1}{2k_2}. \tag{5.35}$$

We note that this is the inverse of the reaction propensity derived for the vCME on a periodic lattice in equation (5.23), and discuss the significance of this further in Section 5.4.2. In the remainder of this section, we obtain expressions for $E(1)$, and for $E(k)$, where $1 < k < n$.

Using the expression for $E(0)$ given in equation (5.34), we can evaluate equation

(5.33) to obtain an expression for $E(1)$:

$$\begin{aligned} E(1) &= \frac{4(m-1)T^{\pm}\left[4T^{\pm}(Km-1)+R\right]+m(K-1)\left[4mT^{\pm}R+R^2\right]}{\left[4(m-1)T^{\pm}+R\right]\left[4mT^{\pm}R+R^2\right]} \\ &= \frac{4T^{\pm}(Km-1)+mR(K-1)}{4mT^{\pm}R+R^2}. \end{aligned} \tag{5.36}$$

Note that, as expected, this has the same limit as $E(0)$ when $T^{\pm} \to \infty$. We can extend the result using the relationship given in equation (5.31), which we restate here for convenience

$$E(n-l) = E(n-l-1) + \frac{2l+1}{4T^{\pm}},$$

for $0 \leq l \leq n-2$. By applying equation (5.31) recursively, it is possible to write $E(n-l)$ in terms of $E(1)$,

$$E(n-l) = E(1) + \sum_{i=l}^{n-2} \frac{2i+1}{4T^{\pm}} \tag{5.37}$$

$$\begin{aligned} &= E(1) + \frac{1}{4T^{\pm}}\left[(n-2)-l+1\right] + \frac{2}{4T^{\pm}}\sum_{i=l}^{n-2} i \\ &= E(1) + \frac{1}{4T^{\pm}}\left[(n-2)-l+1\right] + \frac{2}{4T^{\pm}}\sum_{i=1}^{n-2} i - \frac{2}{4T^{\pm}}\sum_{i=1}^{l-1} i \\ &= E(1) + \frac{1}{4T^{\pm}}\left[(n-2)-l+1\right] + \frac{2}{4T^{\pm}}\left[\frac{(n-1)(n-2)}{2} - \frac{(l-1)l}{2}\right] \\ &= E(1) + \frac{1}{4T^{\pm}}\left[(n-1)^2 - l^2\right]. \end{aligned} \tag{5.38}$$

This is an awkward form, so we set $l = n - j$, then write

$$\begin{aligned} E(j) &= E(1) + \frac{1}{4T^{\pm}}\left[(n-1)^2 - (n-j)^2\right] \\ &= E(1) + \frac{1}{4T^{\pm}}\left[2n(j-1) - j^2 + 1\right] \\ &= E(1) + \frac{1}{4T^{\pm}}\left[K(j-1) - j^2 + 1\right]. \end{aligned} \tag{5.39}$$

Clearly this formula will match the values of $E(0)$ and $E(1)$, in the limit $T^{\pm} \to \infty$. We now consider the interpretation of this limit, before further studying the case where $T^{\pm}$ is finite in Section 5.4.3.

5.4.2 Limiting values and agreement between scales

Recall from equation (5.35) that, as $T^{\pm} \to \infty$, we found

$$E(0) \to \frac{\kappa - 1}{2k_2}, \tag{5.40}$$

and that in Section 5.4.1 we demonstrated that all other $E(j)$ expressions have the same limit. This agreement of $E(j)$ terms makes intuitive sense, since as the movement rates of particles become arbitrarily large their starting positions become irrelevant, and the expected time until reaction should be independent of their initial separation. We also note that the limiting value depends only on the system capacity κ and reaction coefficient k_2: the predictions of the feRDME will agree with those of a peRDME for any possible choice of m when $T^{\pm}$ is sufficiently large.

We have already noted that the expected time until reaction in equation (5.35) agrees with the expected time until reaction given by a vCME model (as obtained by inverting the vCME reaction propensity in equation (5.23)).

Having found that our derived reaction rates at varying spatial scales agree when $T^{\pm}(= D/m^2h^2)$ is arbitrarily large, it is natural to ask how well they agree for smaller values of $T^{\pm}$. We explore the effect of varying D and m in the following section, studying a pair of particles that are initially uniformly distributed on the domain.

5.4.3 Expected time until reaction from initial uniform distribution

Suppose two particles are initialised so as to be uniformly distributed across a periodic lattice consisting of $K = 2n$ compartments, where $n \in \mathbb{N}$. In this section we obtain an expression for the expected time until they react. We discuss our interpretation of uniform distributions for volume-excluding models in Appendix D.1, and present an algorithm to generate uniform distributions.

For a two particle model on a uniform grid, we initialise the first particle in a randomly selected compartment, where each compartment is equally likely to be selected. We then select an initial compartment for the second particle, weighting the possibility of choosing the first particle's compartment by $(m-1)/m$, and the

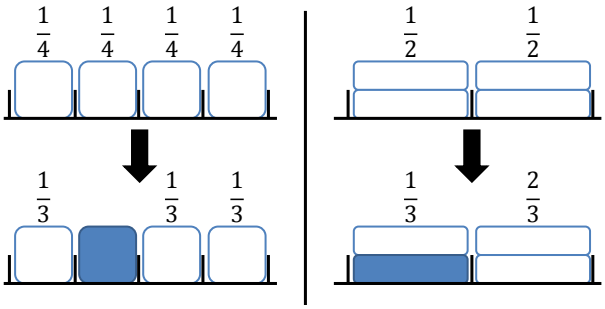

Figure 5.4: When the empty, each compartment is equally likely to be chosen as the initial location of the first particle, with the probabilities shown above each compartment. Once the first particle has been positioned, it is impossible (in the fully-excluding case on the left) or less likely (in the partially-excluding case on the right) for the second uniformly particle to be located in the same compartment, and the probabilities are reweighted accordingly.

possibility of choosing all other compartments by unity. We divide each of these values by a normalising factor of $(K - 1/m)$, representing the sum of all weightings, to obtain a probability for each choice of compartment. A simple example for $m = 1$ and $m = 2$ is shown in Figure 5.4. We will write $E(:)$ to denote the expected time until reaction between two particles that begin uniformly distributed on the domain, and obtain

$$E(:) = \frac{1}{K - \frac{1}{m}} \left(\frac{m-1}{m} E(0) + 2 \sum_{j=1}^{n-1} E(j) + E(n) \right), \tag{5.41}$$

where $(m-1)/m$ represents the lower probability of two volume-excluding particles being initialised in the same compartment, and the fraction outside of the brackets is a normalising term for the probabilities of each possible position. We evaluate equation (5.41) in Appendix D.2, and eventually obtain

$$\begin{aligned} E(:) &= \frac{Dh^2(\kappa - 1)}{2Dh^2 k_2 + k_2^2} \\ &+ \frac{1}{\kappa - 1} \left(\frac{m(m-1) + m(\kappa - m)^2}{4Dh^2 + 2k_2} + \frac{1}{4Dh^2} \left[\frac{1}{6}\kappa^3 - \kappa^2 m + \frac{11}{6}\kappa m^2 - m^3 \right] \right). \end{aligned} \tag{5.42}$$

In the limit as $D \to \infty$, we recover equation (5.35), as expected. For finite D, since not all m and K terms can be arranged into scale invariant κ terms, we will

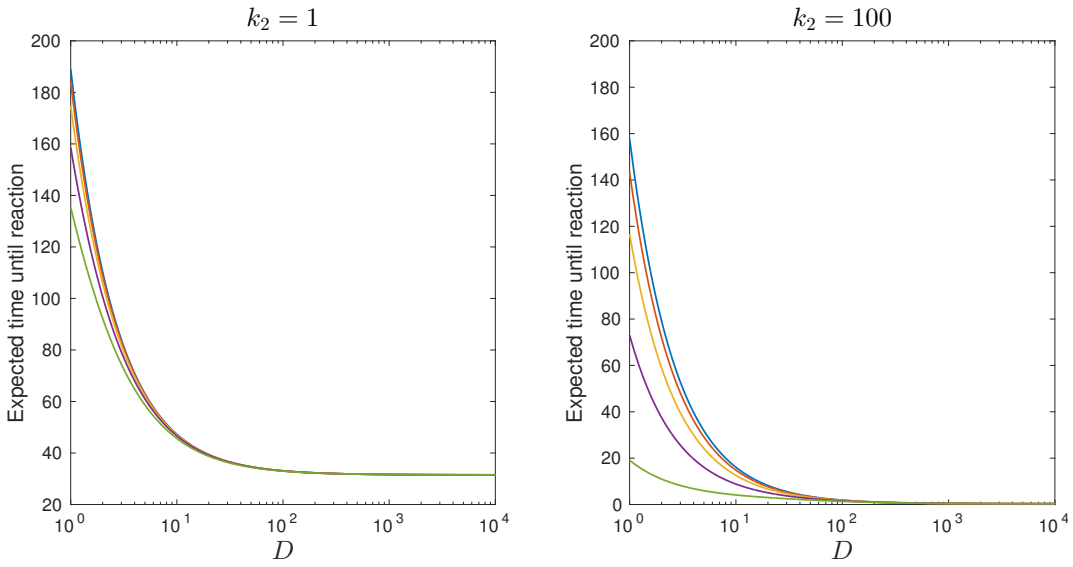

Figure 5.5: In this figure the dependence of equation (5.42) on choices of D, k_2 and m is illustrated. The total capacity of the system is set to $\kappa = 64$, with $h = 1$, and we plot expected times to reaction for $m = 1, 2, 4, 8$ and 16 in blue, red, yellow, purple and green, respectively. As D increases, we observe the expected time to reaction for each choice of m converging, as expected. For large D, the time until reaction is determined primarily by the reaction propensity, k_2. By contrast, when D is small, different choices of m lead to significant different expected reaction times. In this case, the time until a reaction occurs is primarily determined by the time taken for the two particles to diffuse to within reaction distance, and this happens more quickly when m is large.

see differences in the expected time to reaction depending on the choice of m, as illustrated in Figure 5.5. We tested these predictions by comparing the predictions for $m = 1, 4$ and 16, where $k_2 = 100$ and $\kappa = 64$, to the average time to reaction observed in stochastic simulations. For each realisation, we initialised two particles in the domain, as discussed in Appendix D.1, and allowed them to diffuse until a reaction occurred. This was repeated 10,000 times for each choice of parameters, recording the average time to reaction. The results are shown in Figure 5.6, where we observe strong agreement between the expected times to reaction obtained from simulation, and the predictions from equation (5.42).

For systems including more than two particles, deriving general results for either the feRDME or peRDME models becomes infeasible, although we do obtain analytic results for the vCME. In the following sections, we simulate feRDME or peRDME

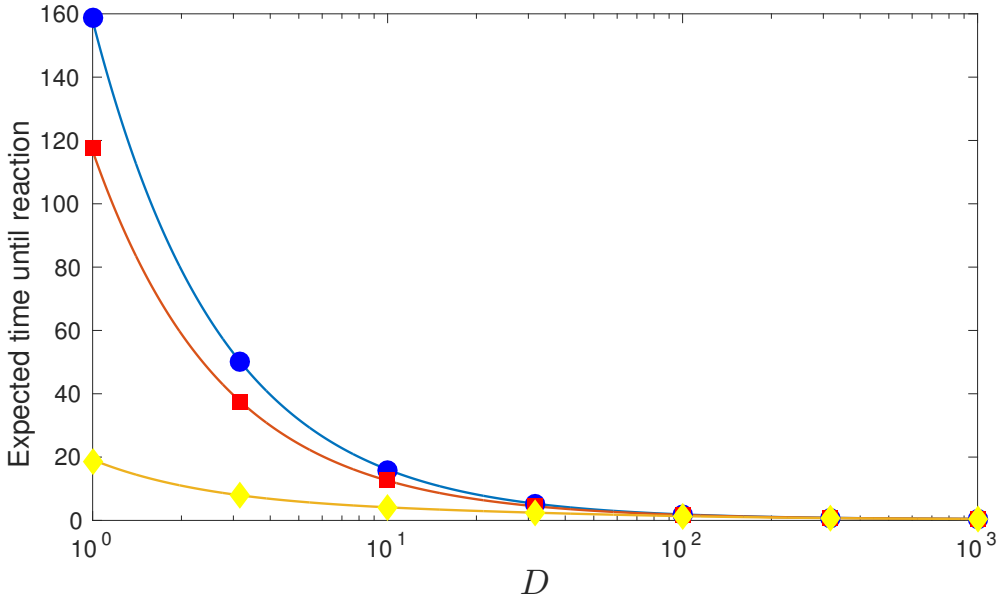

Figure 5.6: We compare the predictions of equation (5.42) to the results of simulation, using $\kappa = 64$ and $k_2 = 100$. Predictions for $m = 1, 4$ and 16 as D varies are shown as blue, red and yellow lines, respectively. The mean time observed before a reaction occurs in a stochastic simulation is represented by discrete markers for seven values of D. We observe very close agreement between the values obtained from simulation and our derived equations.

models of three reactions: i) single-species mutual annihilation; ii) two-species mutual annihilation; and iii) two-species conversion. In each case, we simulate the model until a steady-state is reached, and compare the mean time taken to achieve this steady-state in the feRDME model to the mean time observed in the peRDME models, and to the predictions of the corresponding vCME model.

5.5 Single-species mutual annihilation

The single-species mutual annihilation reaction was defined in expression (5.4), which we restate for convenience:

$$A_i + A_j \xrightarrow{k_2^d} E_i + E_j,$$

where k_2^d is the reaction coefficient for a mutual annihilation reaction. We assume that the system contains an even number N of particles, all of which are of species A. In Section 5.5.1 we obtain the mean and variance of time to reaction, as predicted by the vCME model, which we compare to simulation results in Section 5.5.2.

5.5.1 Analytic predictions for vCME

In equation (5.22) we obtained a rate for single-species reactions on a non-periodic domain that, with reaction coefficient k_2^d, can be written

$$\frac{a^{(\kappa)}(a^{(\kappa)}-1)}{\kappa} k_2^d. \tag{5.43}$$

The time until the next reaction will be exponentially distributed with parameter $\lambda = a^{(\kappa)}(a^{(\kappa)}-1)k_2^d/\kappa$. By standard results, the mean and variance of an exponentially distributed random number are $1/\lambda$ and $1/\lambda^2$, respectively [120].

In the vCME model, the times between reactions will be independent of one another. We therefore expect the mean time until the system reaches the steady-

state, i.e. total annihilation, will be the sum of mean inter-reaction times:

$$\left[\frac{\kappa}{N(N-1)k_2^d} + \frac{\kappa}{(N-2)(N-3)k_2^d} + \cdots + \frac{\kappa}{2\cdot 1 k_2^d}\right] = \sum_{n=1}^{N/2} \frac{\kappa}{2n(2n-1)k_2^d}, \quad (5.44)$$

where we recall that N is the initial number of particles. Similarly, by independence, the variance of the time to steady-state can be written as the sum of variances of each inter-reaction time:

$$\sum_{n=1}^{N/2} \left(\frac{\kappa}{2n(2n-1)k_2^d}\right)^2. \quad (5.45)$$

We test these results with numerical simulation in Section 5.5.2. For both fully-excluding and partially-excluding models, the results confirm that the means and variances of times taken to reach total annihilation agree with expressions (5.44) and (5.45) as the diffusion constant, D, becomes large.

5.5.2 Numerical investigations

In each simulation, we initialised eight uniformly-distributed particles of length $h = 1$, all of species A, on a domain of capacity $\kappa = 32$. For $m = 1, 4$ and 16, we performed 10,000 repeats of each model at different choices of D and k_2^d and recorded the time taken to reach steady-state (i.e. all particles removed from the system). The means of times taken to reach total annihilation were then compared to the predictions obtained for the vCME in Section 5.5.1 in Figure 5.7.

It can be seen that, as D increases, the mean times to reach total annihilation observed in the feRDME and peRDME models agree with the predictions of the vCME, and with each other. Similar agreement can be observed between the variances of times taken to reach steady-state. We will not generally plot the variances of time to steady-state in this chapter, as the figures produced are very similar to the corresponding figures describing mean time to steady-state, but include results here in Figure 5.8 as a representative example. With only one species of particle present it is relatively easy to maintain a well-mixed state, as well-mixed in this context refers only to particle positions rather than the orderings of particles.

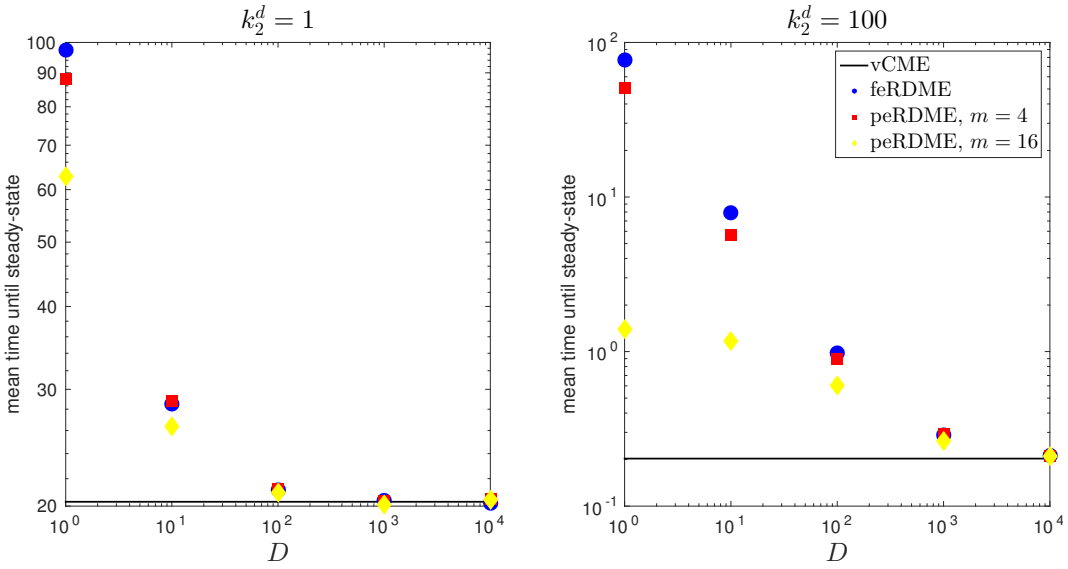

Figure 5.7: An initial eight uniformly-distributed particles, all of the same species, diffused on a domain of capacity $\kappa = 32$ until they had all mutually-annihilated, and thus a steady-state was reached. The mean times taken for the feRDME model to reach total annihilation are compared to the mean times observed for the peRDME models with $m = 4$ and $m = 16$ and the prediction of the corresponding vCME. As the diffusion constant D becomes large, all models are seen to agree, though mean times vary at lower levels of D.

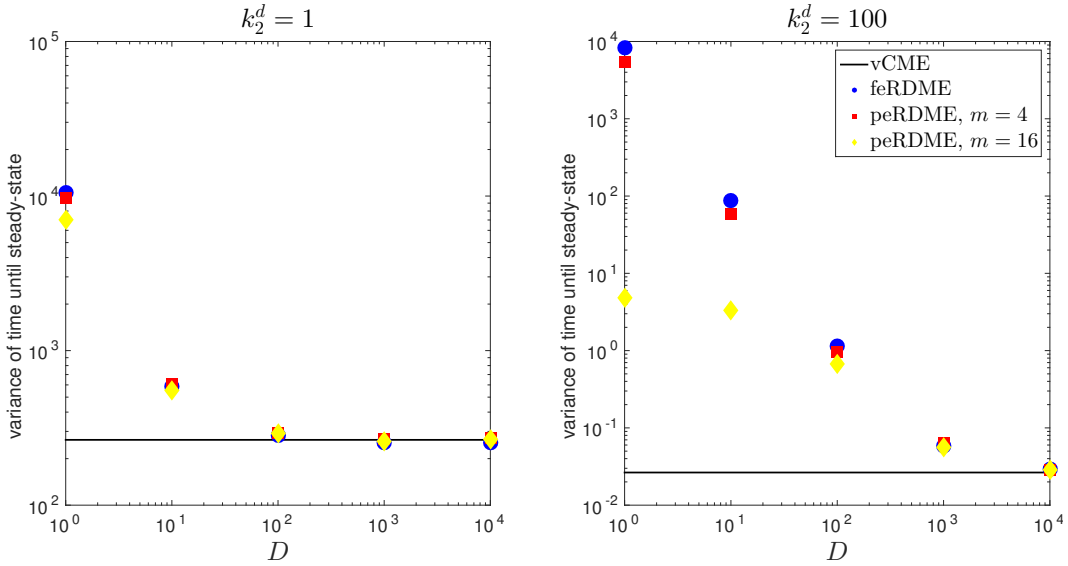

Figure 5.8: An initial eight uniformly-distributed particles, all of the same species, diffused on a domain of capacity $\kappa = 32$ until they had all mutually-annihilated, and thus a steady-state was reached. The variance of times taken for the feRDME model to reach total annihilation are compared to the variance of times observed for the peRDME models with $m = 4$ and $m = 16$ and the prediction of the corresponding vCME. As the diffusion constant D increases, all models are seen to agree.

5.6 Two-species mutual annihilation

The two-species mutual annihilation was defined in expression (5.5), which we restate for convenience:

$$A_i + B_j \xrightarrow{k_2^d} E_i + E_j.$$

In this section, we consider the case where $a = b$, i.e. there are equal numbers of species A and B particles, though similar results could be obtained in cases where one species outnumbers the other. In Section 5.6.1 we obtain analytic predictions for the mean and variance of the time until the steady-state is reached, in the limit as D becomes large. In Section 5.6.2 we test these predictions against the results of simulation. It is shown that the results obtained by simulation are close to the analytic predictions, but differ due to insufficient mixing, especially in the fully-excluding model.

5.6.1 Analytic predictions for vCME

In equation (5.21) we obtained a rate for two-species reactions on a non-periodic domain, which with reaction coefficient k_2^d, can be written:

$$2k_2^d \frac{a^{(\kappa)} b^{(\kappa)}}{\kappa}.$$

We assume again that there are initially N particles at time $t = 0$, of which half are of species A, and half are of species B. The steady-state for this system is then an empty state, where every particle has been removed. Using the same method applied in Section 5.5.1, the expected time until steady-state will be

$$\left[\frac{\kappa}{(N/2)^2 k_2^d} + \frac{\kappa}{(N/2-1)^2 k_2^d} + \cdots + \frac{\kappa}{(1)^2 k_2^d}\right] = \sum_{n=1}^{N/2} \frac{\kappa}{n^2 k_2^d}. \tag{5.46}$$

Similarly, the variance of the time to steady-state will be

$$\sum_{n=1}^{N/2} \left(\frac{\kappa}{n^2 k_2^d}\right)^2. \tag{5.47}$$

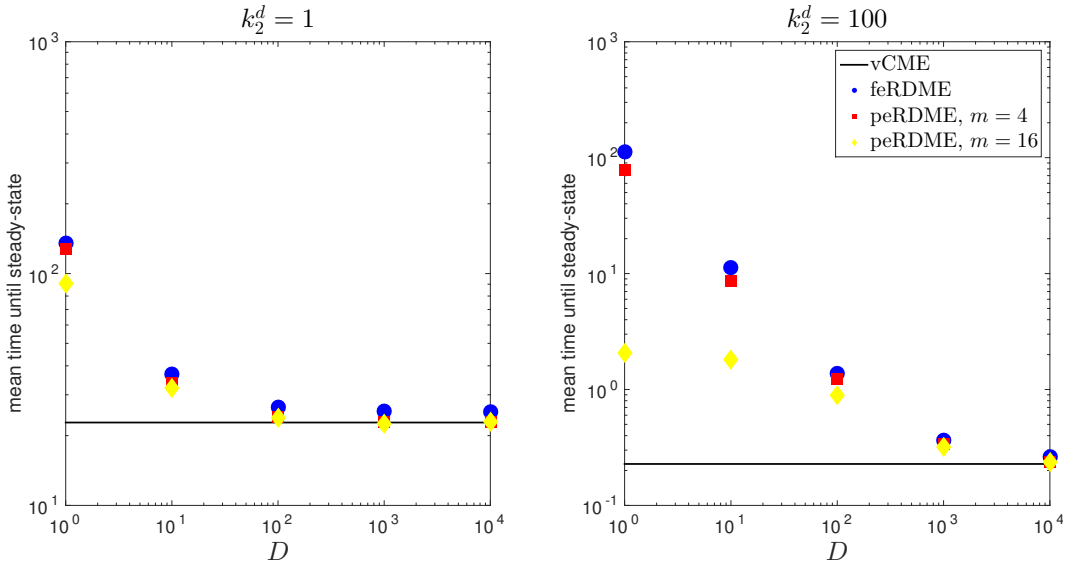

Figure 5.9: An initial eight uniformly-distributed particles, four of species A and four of species B, diffused on a domain of capacity $\kappa = 32$ until they had all mutually-annihilated, and thus a steady-state was reached. This simulation was repeated 10,000 times, and the times taken to reach total annihilation recorded. As the diffusion constant, D, becomes large, the vCME and peRDME models are seen to agree, though the mean time for the feRDME model remains slightly higher. This can be seen more clearly in the left-hand plot, where $k_2^d = 1$, though similar differences can also be observed in the right-hand plot, where $k_2^d = 100$.

We test these results with numerical simulation in Section 5.6.2. Although the partially-excluding models are seen to agree with the predictions given in expressions (5.46) and (5.47) as D becomes large, we observe that the fully-excluding model does not converge to the same mean values (see Figure 5.9).

5.6.2 Numerical investigations

In each simulation, we initialised eight uniformly-distributed particles of length $h = 1$, four of species A and four of species B, on a domain of capacity $\kappa = 32$. For $m = 1, 4$ and 16, we performed 10,000 repeats of each model for different choices of D and k_2^d and recorded the time taken to reach steady-state (i.e. all particles removed from the system). The means of times taken to reach steady-state were then compared to the predictions obtained for the vCME in Section 5.5.1 in Figure 5.9.

It can be seen that, as D becomes large, the mean times to total annihilation

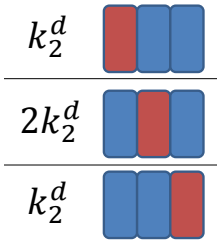

Figure 5.10: Suppose there are two particles of species A, and one of species B (represented in blue and red, respectively) in a domain of capacity $\kappa = 3$. This figure illustrates all possible arrangements, and the corresponding reaction rates.

observed in the peRDME models agree with the predictions of the vCME, and with each other, but the results of the feRDME model are slightly different. Similar disagreement can be observed between the variances of times taken to reach steady-state, which are not presented here. This is a result of the inability of particles of different species to mix in an feRDME model.

As an explanatory example, consider a simple system of capacity $\kappa = 3$, containing two particles of species A, and one of species B. The three possible arrangements for such as system are illustrated in Figure 5.10, along with the reaction rate associated with each arrangement. The well-mixed assumption, and our derivation of peRDME reaction rates in Section 5.3.2, presumes that the system is continuously fluctuating between these three equiprobable arrangements. The reaction rate of the system would then be the average of the three rates, $4k_2^d/3$, and so the expected time until a reaction occurs is

$$\frac{3}{4k_2^d} = \frac{9}{12k_2^d}. \tag{5.48}$$

In the feRDME, however, the system will assume one of these equiprobable arrangements and then maintain it until a reaction occurs. The expected time until reaction will then be the average of each arrangement's expected time to reaction:

$$\frac{1}{3}\left(\frac{1}{k_2^d} + \frac{1}{2k_2^d} + \frac{1}{k_2^d}\right) = \frac{10}{12k_2^d}, \tag{5.49}$$

which is slightly different from the rate obtained in equation (5.48). This explains why the feRDME results in Figure 5.9 are close to those of the vCME and peRDMEs

as D grows large, but differ slightly. Similar results were observed for the variances of times to total annihilation, but are not plotted here. In the following section, we examine a different reaction where the problem of mixing in an feRDME model is even more pronounced.

5.7 Two-species conversion

The two-species conversion reaction was defined in expression (5.6), which we restate for convenience:

$$A_i + B_j \xrightarrow{k_2^t} \begin{cases} A_i + A_j & \text{with probability } p, \\ B_i + B_j & \text{with probability } (1-p). \end{cases}$$

Particles of species A may react with particles of species B, with the result that one of the reactant particles will switch species. We exclusively consider the symmetric case where 1/2. This system will eventually reach an absorbing state, populated exclusively with either A or B particles, and in Section 5.7.1 we obtain analytic predictions for the mean and variance of the time until the steady-state is reached, in the limit as D becomes large. In Section 5.7.2 we test these predictions against the results of simulation. It is shown that the results obtained by simulation differ significantly from the analytic predictions, especially for the fully-excluding model.

5.7.1 Analytic predictions for vCME

Consider a system of N particles in a single compartment of capacity κ. As in the previous section, we seek to find the expected time until a steady-state is reached. In the case of the conversion reaction, however, the steady-states are not an empty domain, but a domain occupied by a single species. We denote the expected waiting time until a steady-state is reached as $E_s(a)$, where a denotes the number of particles of species A.

When $p = 1/2$, the number of A particles can be modelled as a symmetric one-dimensional random walk, where the time between steps scales inversely with the

reaction rate. The probability that a system containing a particles of species A will eventually reach an absorbing state where all particles are of species A or B will thus be a/N or $(N-a)/N$, respectively [83].

When there are a particles of species A (and thus $b = N - a$ particles of species B) then the expected time taken until the next reaction occurs will be the inverse of the total reaction propensity. For a model in one spatial dimension, for $0 < a < N$, we can write a recursive relation

$$E_s(a) = \frac{1}{2}E_s(a-1) + \frac{1}{2}E_s(a+1) + \frac{\kappa}{2k_2^t a(N-a)}. \tag{5.50}$$

To complete the resulting system of equations, we only need to define the two absorbing cases:

$$E_s(0) = 0; \tag{5.51}$$

$$E_s(N) = 0. \tag{5.52}$$

In Appendix D.3, we show that, for $a \leq (N/2)$,

$$E_s(a) = \frac{\kappa}{2k_2^t}\sum_{i=1}^{a}\left[\sum_{j=i}^{N-i}\frac{1}{j(N-j)}\right], \tag{5.53}$$

while for $a > (N/2)$ we can obtain a solution by symmetry by finding $E_s(N-a)$.

Similar results can be obtained for vCME models in two or more spatial dimensions. Recalling the reaction rates for two-dimensional models from expression (5.24), which we reproduce here for convenience

$$\left(4\frac{\sqrt{\kappa}}{\sqrt{\kappa}+1}\right)k_2\frac{a_i^{(m)}b_i^{(m)}}{\kappa},$$

it is straightforward to obtain an expression for the expected time to reaction for a

vCME model in two dimensions:

$$E_s(a) = \frac{\kappa}{4k_2^t}\frac{\sqrt{\kappa}+1}{\sqrt{\kappa}}\sum_{i=1}^{a}\left[\sum_{j=i}^{N-i}\frac{1}{j(N-j)}\right]. \tag{5.54}$$

Recall that the vCME models assume that all particles in the system are well-mixed. This assumption does not hold for the feRDME in one spatial dimension. It will be seen in Section 5.7.2 that the mean and variance of feRDME models of this conversion reaction do not converge to the results of the vCME in one spatial dimension as D becomes large, because particle mixing is impossible in single-file diffusion. The results of the peRDME models are seen to match those of the vCME as D becomes large, since partially-excluding compartments allow for particle mixing. In Section 5.7.3 we simulate a conversion reaction in two spatial dimensions, demonstrating that, when mixing is possible, the feRDME does agree with the vCME and peRDME when D is large.

5.7.2 Numerical investigations: one spatial dimension

In each simulation, we initialised six uniformly-distributed particles of length $h = 1$, three of species A and three of species B, on a domain on capacity $\kappa = 16$. For $m = 1, 4$ and 8, we performed 10,000 repeats of each model for different choices of D and k_2^d and recorded the time taken to reach steady-state (i.e. all particles become the same species). The mean of times taken to reach steady-state were then compared to the predictions obtained for the vCME (in Section 5.7.1) in Figure 5.11. The variance of times for the vCME to reach steady-state are challenging to obtain analytically, so instead we simulated the vCME 1,000,000 times and computed the variance of times to reach steady-state.

In Figure 5.11, we observe that the results of the peRDME converge to those of the vCME as D becomes large, but the results of the feRDME do not. This is because particles in a conversion reaction in one spatial dimension do not remain well-mixed: instead the reaction leads to particles being grouped with others of the same species as illustrated in Figure 5.12. As a result, the reaction rate in the feRDME model

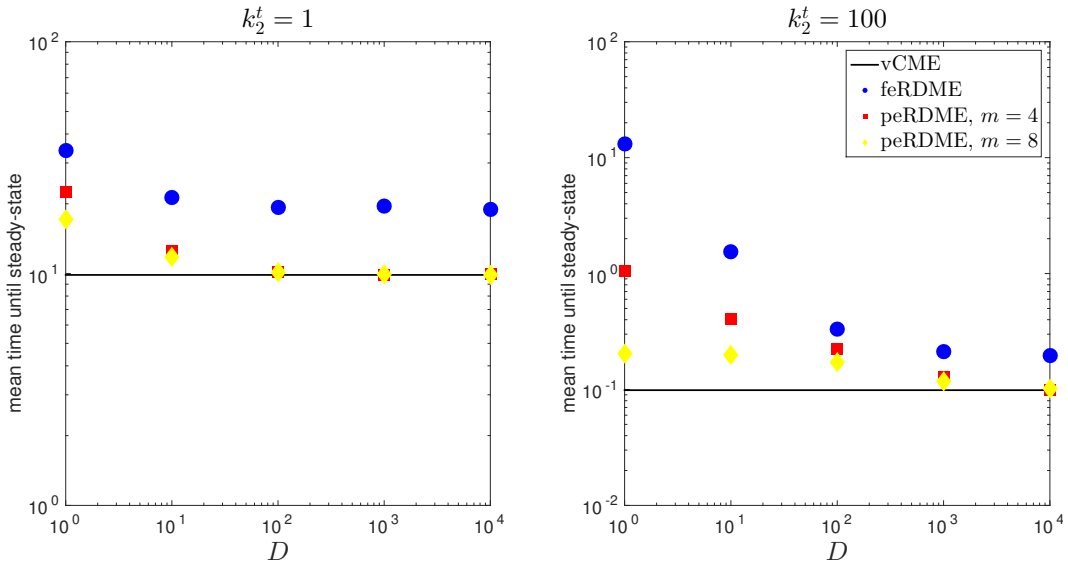

Figure 5.11: An initial three A particles and three B particles diffuse on a domain of total capacity $\kappa = 16$. The particles interact in a conversion reaction, and we simulate the model until all particles are of the same species, recording the time taken to reach this steady-state. The mean time taken to reach steady-state by the peRDME models, as estimated by observing 10,000 instantiations of each model, agree with the predictions of the vCME model as D increases, but the mean time for the feRDME remains higher due to the inability of particles to mix.

will be smaller than that for the corresponding vCME. Similar disagreement can be observed between the variances of times taken to reach steady-state, which are not presented here.

Together with the non-reactive multi-species model considered in Section 4.4 of the previous chapter, this example demonstrates that the different mixing behaviour in one-dimensional fully-excluding and partially-excluding models lead the models to make irreconcilable predictions in situations where mixing is important. To demonstrate that the disagreement between models results from a lack of mixing, in the next section we simulate the same reaction in two spatial dimensions, where mixing becomes possible for the feRDME.

5.7.3 Numerical investigations: two spatial dimensions

In Section 5.7.2 we saw that the results of the feRDME do not match those of the vCME, even as D grows large, because the particles cannot mix in one spatial

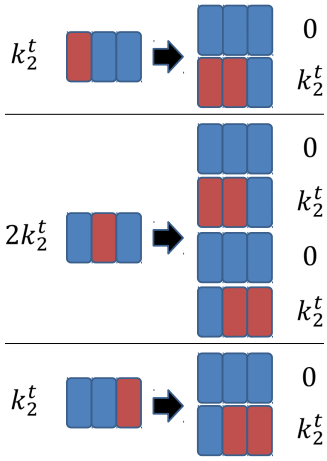

Figure 5.12: In one spatial dimension the conversion reaction does not lead to a well-mixed system, instead it causes particles to be grouped with other particles of the same species. The left-hand side of this figure shows the three possible arrangements of two A particles and one B particle, shown in blue and red, respectively, on a fully-excluding domain of total capacity $\kappa = 3$, and the corresponding reaction rates. The right-hand side shows the possible arrangements after a single conversion reaction, with the corresponding (lower) reaction rates: it is impossible to recover the middle arrangement from the left-hand side, which has the highest reaction rate. The vCME model will therefore overestimate reaction rates for an feRDME model.

dimension. In this section we simulate the same reaction in two spatial dimensions, to show that the results of the feRDME do match those of the vCME when mixing is possible (in the limit of large D).

We consider a two-dimensional square domain of capacity $\kappa = 36$, and compare four models: i) an feRDME model; ii) a peRDME model with $m = 2$ (and hence compartment capacity 2^2); iii) a peRDME model with $m = 3$ (and hence compartment capacity 3^2); and iv) a vCME model. These four models are illustrated in Figure 5.13; in all cases we impose no-flux conditions at the domain boundaries.

As in Section 5.7.2, at time $t = 0$ we initialise three particles of species A, and three particles of species B. Each feRDME and peRDME model was then simulated 10,000 times, and the time taken to reach a steady-state recorded. For the vCME model, we use the analytical results from Section 5.7.1 to find the mean time to steady-state, while the variance of time to steady-state is calculated from the results of 1,000,000 repeats of a vCME simulation.

The mean times to reach steady-states in each model, for varying values of k_2^t

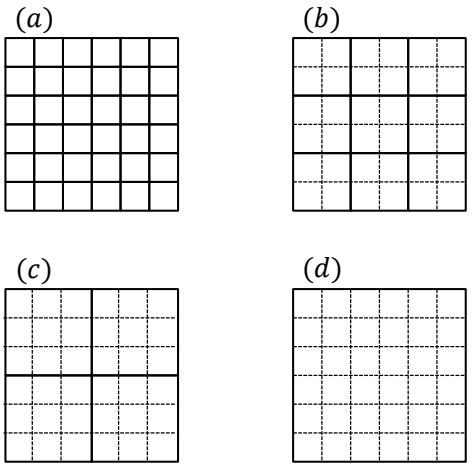

Figure 5.13: We compare four models for reactions on a two-dimensional square domain with capacity $\kappa = 36$. The feRDME in this case consists of a six by six lattice of fully-excluding compartments (a). We consider two peRDME models, where the partially-excluding compartments have capacities 2^2 and 3^2, shown in (b) and (c), respectively. We also consider a vCME model, which does not track the spatial position of particles (d). The boundaries between compartments are denoted with solid lines; dotted lines denote a notional fully-excluding partition to illustrate the capacity of each compartment.

and D, are plotted in Figure 5.14. In previous sections we compared $k_2^t = 1$ and $k_2^t = 100$, but in this case simulating the model with $k_2^t = 1$ is too computationally demanding to be feasible, so we use $k_2^t = 10$ instead.

As expected, the results for the feRDME in two spatial dimensions agree with the results of the peRDMEs and vCME models as D grows large. Similar agreement can be observed between the variances of times taken to reach steady-state, which are not presented here. This confirms that the differences observed in Section 5.7.2 resulted from an inability for particles to mix and change their order in one spatial dimension.

5.8 Discussion

In this chapter, we have considered how to implement reactions in partially-excluding models (peRDMEs). We began by briefly reviewing the state of the field in Section 5.1, and defining reaction rates for an feRDME model in Section 5.2. We then

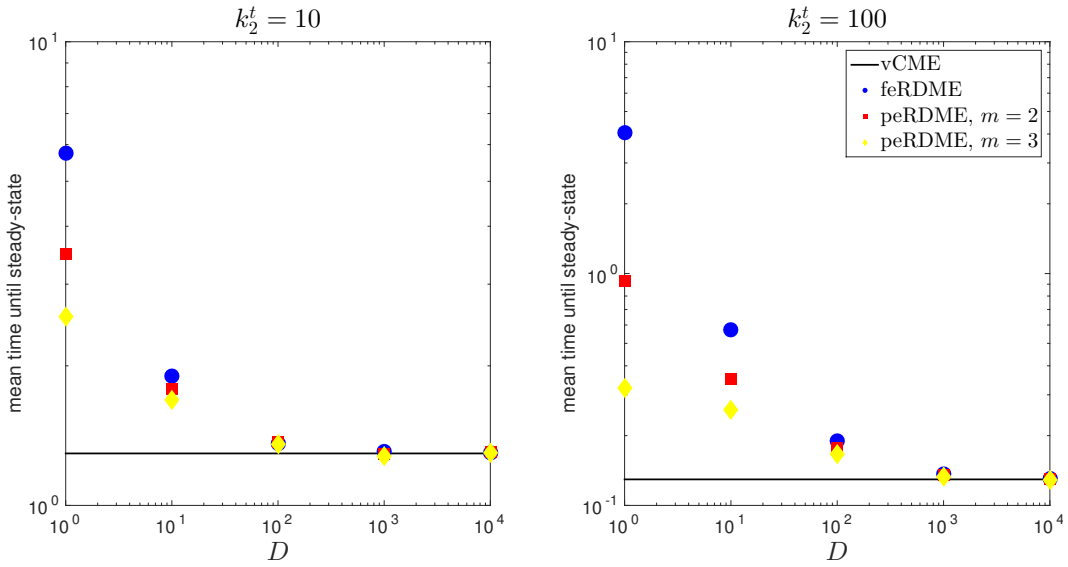

Figure 5.14: An initial three A particles and three B particles diffuse on a two-dimensional domain of total capacity $\kappa = 36$, and interact in a conversion reaction. The mean time to steady-state observed from 10,000 repeats of the feRDME (plotted as blue datapoints) and peRDME models (plotted as red and yellow datapoints for $m = 4$ and $m = 8$, respectively) agree with the vCME (plotted as a black line) as D becomes large, as expected.

proceeded to apply combinatorial arguments in Section 5.3 to obtain reaction rates for peRDMEs from an underlying fully-excluding model. We tested these rates analytically for a single pair of particles in Section 5.4, and numerically for a single-species mutual annihilation system in Section 5.5. In both cases, we observe that the feRDME, peRDME and vCME models all make similar predictions of expected times to reaction, and the mean and variance of times to reach steady-state when diffusion is sufficiently rapid.

Having derived reaction rates under the assumption that particles are well-mixed, we have seen that this assumption is problematic when trying to match the results of multi-species feRDME models in one spatial dimension, observing minor disagreements with peRDME and vCME models in Section 5.6.2 and more serious disagreements in Section 5.7.2. In both cases, we explained why the well-mixed assumption failed to describe the feRDME models, and in Section 5.7.3 we used simulations in two spatial dimensions to show that our derivations are accurate for multi-species reaction systems when mixing is possible.

It is also valuable to consider the constraints that the assumption of well-mixedness places on our choice of m. A simple scaling argument can be used to obtain an approximate constraint for a dilute system. By standard diffusive results, the expected length of time taken for a particle starting in the centre of a partially-excluding compartment to reach the compartment boundaries will be

$$\frac{m^2(\Delta x)^2}{4D}, \tag{5.55}$$

i.e. the inverse of the rate at which a particle would jump half the width of the compartment, $m\Delta x/2$. Let us assume, as an approximation of a dilute system, that there is one other particle in the compartment, capable of reacting with the first. The expected time until this reaction occurs will be $m/2k$ by the results obtained in this chapter. For the well-mixed assumption to be reasonable, we require that the expected time taken to reach the compartment boundaries should be less than that taken to react with another particle,

$$\frac{m^2(\Delta x)^2}{4D} < \frac{m}{2k}. \tag{5.56}$$

After rearranging, we obtain a constraint for the maximum compartment capacity m in terms of the diffusion constant D, reaction coefficient k, and particle length Δx:

$$m < \frac{2D}{k(\Delta x)^2}. \tag{5.57}$$

This constraint captures the behaviour observed in earlier numerical investigations, i.e. that the results of feRDME and peRDME agree as D becomes large, and that higher values of D are required for agreement when the reaction coefficient k is larger. We do not consider less dilute systems here, as the movement of a single tagged particle is known to be subdiffusive in crowded environments, and thus a more complicated scaling argument would be required.

Our implementation of reaction rates for peRDME models may not lead directly to substantially reduced computational costs. Since we have explicitly sought to

make reaction rates in peRDME models agree with those in feRDME models, we would expect the same mean number of reaction events to occur in each (although determining where a reaction has occurred will be slightly faster in a peRDME model with fewer compartments). This work will lead to significant indirect savings, however, by expanding the range of scenarios in which efficient, partially-excluding models (involving fewer diffusive jump events) can be applied. In Chapters 3 and 4, we demonstrated that partially-excluding models (including hybrid fully/partially-excluding models) can lead to large savings in computational time when modelling non-reactive particles. In many reaction-diffusion models, diffusion events greatly outnumber reaction events, and in such cases peRDME models can be expected to run up to m^2 faster than the more computationally intensive feRDME models due to the lower number of diffusion events occuring [70].

We have not reported the times taken to run each simulation in this chapter because the examples are not conducive to fair comparison, especially when diffusion is relatively slow. For example, the feRDME model in Section 5.7.2 requires more computational resources than the corresponding peRDME models: the relative speed of the peRDME models is partly a result of simulating fewer diffusion events per unit time, but is also due to the feRDME model reaching a steady-state later (on average) than the corresponding peRDME models, and therefore being required to simulate a longer time interval. However, in non-pathological examples, such as those presented in Sections 5.5.2 and 5.7.3, we observed peRDME models running approximately m^2 times faster than the corresponding feRDME models for large values of D, as expected. For smaller values of D, observed time savings can be even more significant, but this is partly an artefact of the peRDME models reaching a steady-state and finishing earlier.

In the following chapter we conclude this thesis with a discussion of the results obtained, and of the possibilities for future work.

Chapter 6

Discussion

Reactions and diffusion are fundamental to biology, but can be computationally expensive to simulate stochastically. In this thesis we have formulated and validated techniques to reduce the computational cost of simulating diffusive movement.

6.1 Conclusions

We begin this chapter by revisiting the conclusions of each preceding research chapter, considering both what has been achieved and the limitations on our work at present.

6.1.1 Coarse-graining jump lengths

In Chapter 2, we asked whether it was possible to observe similar mean particle numbers by replacing frequent, short jumps with a distribution of rarer, longer jumps. Surprisingly, this was relatively straightforward to achieve on the majority of the domain, however, the boundary conditions had to be carefully derived to avoid introducing errors into the model. This chapter combines lengthy proofs by induction, to obtain boundary condition implementations, with numerous numerical investigations, to validate our results. We paid particularly close attention to the correspondence of our LBPJ models to PDE models in this chapter, in order to test our novel LBPJ boundary conditions against established methods (in the later chap-

ters, we considered fully-excluding models to be the ground truth, and so reduced our reliance on PDEs).

The reductions in computational cost observed in this chapter were significant, though not as large as those demonstrated for partially-excluding models in the following chapters. It remains to be seen whether researchers will find non-local jumping, and its associated reductions in computational cost, useful enough to incorporate into their own models. However, our results on boundary conditions are novel and often counter-intuitive. For example, prior to our work on flux boundary conditions, there would have been no reason to think that particles would have to be added with particular weightings to a group of compartments near the boundary. The intuitive approach, simply adding all new particles to the first compartment, as would be appropriate in a local jumping model, was shown to lead to errors.

6.1.2 Coarse-graining volume-excluding box sizes

As noted in Chapter 3, partially-excluding models have previously been used by researchers in mathematical biology [80]. Our work makes novel contributions, however, in deriving a connection between fully- and partially-excluding models, and hence explicitly proposing that partially-excluding models can be used in place of fully-excluding models to save computational time. Previous work has also attempted to relate the transition rates of fully- and partially-excluding models by simulating particle movement on a fully-excluding lattice, and tracking the rate with which notional, superimposed partially-excluding lattice boundaries are crossed [91]. We have shown how this approach overestimates the transition rate for partially-excluding models, and proposed more appropriate techniques.

Of particular interest in this chapter is the derivation of equations for the variances of particle numbers in each compartment. To the best of our knowledge, this is the first time these have been obtained for a volume-excluding LBPJ model. Moreover, models of single-file diffusion typically focus on mean particle numbers, and the displacement of a single tagged particle (see, for a recent example, [40]) so demonstrating a connection between variances of particle numbers within fully- and

partially-excluding models is a very satisfying result.

It would be relatively straightforward to extend our arguments in this chapter to diffusion in two spatial dimensions, at least for the equations describing mean particle numbers. The linear interpolation arguments used in one spatial dimension generalise elegantly to barycentric weightings, interpolating the occupancies of fully-excluding compartments from those of the surrounding partially-excluding compartments. The reasoning applied to the evolution of the variances and covariances could also, in principle, be generalised to two spatial dimensions, though the necessary reasoning would be very convoluted. It may also be possible, though challenging, to obtain results for hexagonal lattices in two spatial dimensions. Many studies prefer to tessellate the domain with hexagons due to their lower anisotropy, so this would be a valuable development [125, 126, 127].

6.1.3 Hybrid exclusion systems

Chapter 3 considered partially-excluding models in an idealised setting, and the example simulation we presented showed the partially-excluding model performing very well. There are, nonetheless, situations in which partially-excluding models are not a suitable replacement for fully-excluding models, particularly when more than one species of particle is present. Examples of such situations were considered in Chapters 4 and 5.

Chapter 4 is primarily concerned with formulating and justifying hybrid methods to connect spatial regions of fully-excluding compartments to spatial regions of partially-excluding compartments, although we do also obtain some more general results for partially-excluding Voronoi partitions. We test these hybrid methods in a variety of settings. The first examples are used to test the accuracy of the hybrid methods, and the final example demonstrates their potential to deliver reduced computational costs while maintaining accuracy in a system where a uniform partially-excluding model deviates from the results of a uniform fully-excluding model. Together with our work on reactions in the following chapter, these hybrid methods serve to increase the range of scenarios in which partially-excluding models

can be usefully applied to models of biological systems, increasing their value to researchers.

Our work on non-uniform lattices could potentially be extended to two spatial dimensions, however, this would only be practical for fully-excluding compartments that are square, and hence partially-excluding compartments which are square or rectangular. Furthermore, any such extension of the Voronoi method to two spatial dimensions would have to be justified by numerical experiment rather than the analytical reasoning used in this chapter, as interpolating the occupancies of fully-excluding compartments is not always practical on non-uniform lattices.

6.1.4 Particle interaction and mixing

Particle mixing is central to Chapter 5. We derive reaction rates for peRDME models, on the assumption that the particles in each partially-excluding compartment can be treated as well-mixed. Our derived rates were seen to predict similar behaviour at different scales when the well-mixed assumption held, whether because the system only contained a single pair of particles (and hence expected times until a reaction occurred could be obtained analytically) or because all particles were of the same species.

We also investigated cases in which the well-mixed assumption failed, to a greater or lesser degree. Mutual annihilation reactions between particles of two different species provided a particularly interesting example, emphasising that averaging over all possible fixed arrangements of particles is not an exact substitute for actual mixing, although the impact on predicted times to reaction remained small. A much larger disagreement was observed between feRDME and peRDME models in the case of two species conversion in one spatial dimension. With particles unable to mix, the reaction was seen to lead to particles of the same species being grouped together, and hence predicted much lower total reaction propensities. As with the multispecies example in Chapter 4, we must conclude that there are some circumstances in which fully- and partially-excluding models are fundamentally irreconcilable, and cannot be expected to produce similar results.

A question not addressed in the current work is to what extent volume exclusion inhibits mixing in two and three spatial dimensions. The only two-dimensional model considered (in Section 5.7.3) is relatively dilute, and it is not obvious how our results would change if particles occupied a large fraction of the available space, as this has been shown to obstruct mixing [108]. It seems likely that agreement would still be observed between models as the diffusion coefficient, D, tends to infinity, but that disagreement would be seen at large but finite values of D. Unfortunately the implementation of feRDME models is computationally expensive, especially for large values of D, making this hypothesis difficult to test.

6.1.5 Developing partially-excluding LBPJ models

As three of the four research chapters in this thesis concern the development of partially-excluding LBPJ models in particular, we provide a summary of our contributions to the field here, before proceeding to discuss directions for future research.

There are three significant papers by other authors which use partially-excluding models. Painter and Hillen, and more recently Anguige and Schmeiser, consider partially-excluding compartment based models, incorporating volume exclusion as a linearly scaling blocking probability [80, 81]. Painter and Hillen's model also includes quorum sensing and chemotaxis, while Anguige and Schmeiser use cell to cell adhesion as an additional inhibitor of jumping. In contrast to our own work, however, these papers exclusively consider deterministic models with continuous particle densities, using the partially-excluding framework as ODEs or to obtain PDEs, rather than as a stochastic system of discrete particles.

Our work has more in common with that of Khain et al, who use a stochastic, partially-excluding framework to study the probability of spontaneous particle clustering [91]. There are important differences between our approach and that of Khain et al however, the most significant being that the jump rates for partially-excluding compartments in their model are much higher than those we obtained. They consider every fully-excluding jump which crosses partially-excluding compartment boundaries to be a transition, an approach which we rejected for reasons discussed in

Appendix B.1. It should also be noted that Khain et al use their partially-excluding framework to obtain probabilities of particular clusters forming, and do not attempt to use it as a more general framework for efficient stochastic simulation.

Our work on partially-excluding models is therefore a significant departure from existing applications, in that we work with variances and covariances of discrete particle numbers throughout, rather than restricting our work to mean particle concentrations, and have been able to find and justify jump rates and blocking properties which lead to agreement between fully-excluding and partially-excluding models, a reconciliation which has never previously been attempted. Using the properties of partially-excluding models to save computational time is also a novel application: as noted previously, a partially-excluding model will only be required to simulate $1/m^2$ as many diffusive jump events as an equivalent fully-excluding model. For applications where diffusive jump events are the most common event to occur, partially-excluding models can therefore deliver very significant reductions in computational time.

Our initial investigations of partially-excluding models in Chapter 3 were limited to simple scenarios, with uniform lattices occupied by a single species of non-reactive particles. Partially-excluding models on non-uniform lattices, and the theory needed to justify their correspondence to an equivalent fully-excluding, were then developed in Chapter 4, where we considered a multi-species model for the first time. The results of the multi-species model demonstrated that, at least in one spatial dimension, partially-exluding and fully-excluding models may generate different results due to the inability of particles in a single file diffusion model to mix. The significance of mixing was then further explored in Chapter 5, where we also derived peRDME reaction rates to match reaction rates in feRDME, subject to the fully-excluding model permitting mixing.

Taken together, these three chapters on volume exclusion develop a versatile partially-excluding modelling framework, capable of modelling reaction-diffusion systems on both uniform and non-uniform lattices. The correspondence of these partially-excluding models to the corresponding fully-excluding models has been supported

by both analytical work and numerical investigations. In the course of the numerical investigations, increases in simulation speed up to a factor of m^2 were observed, permitting large savings in CPU time to be made. The only situation in which the results of partially-excluding models have been observed to deviate from those of fully-excluding models in this work has been in cases of single-file diffusion containing multiple particle species, where the ability of particles to mix within partially-excluding compartments has led to qualitatively different results. For models containing a single species of particles, or taking place in two or three spatial dimensions, partially excluding models have been shown to be a valuable addition to the toolbox of theoretical biology.

6.2 Further work

The work in this thesis suggests a number of promising directions for future work, and we discuss a selection here.

6.2.1 Improved Robin boundary conditions

The mathematical core of Chapter 2 is the derivation of Robin and flux boundary conditions for non-locally jumping LBPJ models, for both unbiased and biased particle movement. The implementations of these boundary conditions were simulated, and we observed good agreement between mean particles in both locally and non-locally jumping models compared to the solutions of the corresponding PDEs. In all cases, however, we note that the HDE metrics for models with Robin boundary conditions were not as good as those obtained for flux boundary conditions, for both locally and non-locally jumping models. A possible explanation for the increased error is that the Robin condition depends not only on the gradient at the boundary, but also on the concentration at the boundary. For a non-zero gradient and non-infinitesimal box size, Δx, the PDE will therefore use a boundary value smaller than that predicted by the first compartment of the LBPJ model. The resulting error is small, but if future work could eliminate it through a different implementation of

boundary conditions this would be valuable contribution to the field.

6.2.2 Alternative non-local jump distributions

Our non-local jumping work in Chapter 2 uses the expression given in equation (2.9) to determine jump-length distribution for a simulation, i.e.

$$T^q = \frac{T}{Qq^2},$$

where T is the rate of jumping in the locally jumping system. We chose this expression because it is relatively simple, can be used for any maximum jump length, Q, and follows naturally from the the condition, given in equation (2.7), which we restate for convenience:

$$T = \sum_{q=1}^{Q} q^2 T^q.$$

We noted, however, that are many other possible choices for T^q. Let us refer to our chosen distribution as the non-linear distribution. A more comprehensive study of non-local jumping could consider a range of possible distributions, and identify the most suitable ones to balance error with acceleration. To demonstrate the scope for improvements, we briefly consider two more possible distributions here, that we shall refer to as the linear and uniform jump distributions (denoted by subscripted l and u in equations (6.1) and (6.2), respectively). For the former, we specify that our jump rates should scale with $1/q$ rather than $1/q^2$, and obtain the expression

$$T_l^q = \frac{2T}{qQ(Q+1)}. \tag{6.1}$$

Similarly, if we specify that each rate for jumping any distance $q \leq Q$ should be equal, we obtain the expression

$$T_u^q = \frac{6T}{Q(Q+1)(2Q+1)}, \tag{6.2}$$

giving the uniform jump distribution. It can be seen by inspection that both of these satisfy condition (2.7), despite giving very different distributions of jump lengths. We have performed some basic error analysis (following the same approach used in Section 2.7) and also calculated the maximum possible acceleration each distribution could provide for a given value of Q (by dividing the total jump propensity of a particle in the equivalent locally-jumping system by the total jump propensity of a non-locally jumping particle). In practice, it may not be possible to attain this maximum possible speed up, since it does not account for the extra time which non-local simulations will take to search through the increased number of possible events, but it is a useful metric nonetheless.

Table 6.1: Relative error and potential acceleration of different distributions

		Q			
		2	3	4	5
Non-linear distribution	Relative Error	2.50	4.67	7.50	11.0
	Acceleration	1.60	2.20	2.81	3.42
	Acceleration/Error	0.64	0.47	0.37	0.31
Linear distribution	Relative Error	3.00	6.00	10.0	15.0
	Acceleration	2.00	3.27	4.80	6.57
	Acceleration/Error	0.67	0.55	0.48	0.44
Uniform distribution	Relative Error	3.40	7.00	11.8	17.8
	Acceleration	2.50	4.67	7.50	11.0
	Acceleration/Error	0.74	0.67	0.64	0.62

The relative error and accelerations are given in Table 6.1. The uniform and linearly distributed jump-lengths produce larger error terms than the non-linearly distributed one for any given Q, but also offer the possibility of much larger time savings. The results also suggest that it may be possible to decrease both error and run-time by moving to a different jump-length distribution with a smaller value of Q. For example, linearly distributed jump-lengths with $Q = 4$ will give an error term 10 times larger than that of the local system, and will run up to 4.8 times faster, while non-linearly distributed jump-lengths with $Q = 5$ give an error term 11 times larger than that of the local system, and will run at most 3.4 times faster.

It seems likely that there will not be a single, optimum distribution, since the

balancing of error with speed-savings will depend on the system being simulated. It may be, however, that for a given maximum permissible error value a distribution could be derived that maximises the speed of the simulation without its error term exceeding this maximum error. Conversely, a method could be sought to select a distribution that provides a specified degree of acceleration with the smallest possible error.

These suppositions form an interesting research question in themselves, and would also require an extension of the existing work on boundary conditions, as the results we have derived so far all assume a particular distribution of jump lengths. It would be necessary to derive these boundary conditions for other jump length distributions, and if possible find a generalised result for any arbitrary distribution of jump lengths.

6.2.3 Elaborating on volume exclusion

We have devoted two chapters to the development of diffusive models incorporating volume exclusion, but some of the assumptions we made in these chapters could be altered in future work. For example, throughout this thesis we have assumed that all particles are of the same size, but for many applications of interest this is not physically realistic. By reconciling fully- and partially-excluding models, we are in a strong position to model particles of varying sizes: a fully-excluding lattice could be defined such that compartment length Δx is the size of the smallest particle in the system, and larger particles would then occupy contiguous blocks of fully-excluding compartments. Another situation of interest to theoretical biologists is one in which motile particles are obstructed by immobile obstacles of varying sizes, and attempting to replicate such systems with partially-excluding models would be a natural next step [128].

Another assumption we have made throughout our work on volume exclusion is that attempted jumps into occupied compartments should be ignored. This is not the only possible treatment of volume exclusion, however. One recent paper has instead implemented pushing, so that an obstructed particle may move by dis-

placing the particles in its path [129]. Our work on both reactions and diffusion in volume-excluding models has relied upon on assumptions about the distribution of particles within partially-excluding compartments. It would therefore be interesting to apply these assumptions to a model that incorporates pushing, to determine whether partially-excluding models can still be designed to agree with the results of fully-excluding models when volume-exclusion is implemented differently.

6.2.4 Developing volume-excluding RDME models

All of the test cases we considered in Chapter 5 reached absorbing states in which no further reactions could occur, and compared the mean times taken to reach these states. It would be instructive to examine other examples with non-absorbing steady-states to examine the impact of varying compartment capacity, m, and the diffusion coefficient, D [113].

Another promising line of research would be to apply feRDME and peRDME models to systems in which we expect relatively stable spatial inhomogeneities to emerge, such as a bistable system where different spatial regions may reach different equilibria [7]. We could then investigate to what extent the feRDME and peRDME models agree on metrics such as overall particle concentrations, the average size of spatial regions adopting one or other equilibria, and the average times taken to transition from one equilibrium state to the other. It seems likely that, for large compartment capacity, m, spatial inhomogeneities will be lost, as particles are spread across large, partially-excluding compartments. For intermediate values of m, however, it may be possible to preserve the bistable properties of the system while making large savings in computational time.

6.3 Summary

The work in this thesis contributes to a growing literature on the efficient stochastic simulation of spatially-extended systems. The diversity of available methods benefits modellers working at the interface of mathematics and biology, who can access an

increasing variety of methods for accelerating their simulations. These techniques enable studies which would otherwise be impractically computationally intensive, while the diversity of approaches affords modellers freedom to choose techniques appropriate to the biological realities of their subject.

The preceding chapters began with two simple ideas, then explored the complexities that arose during the implementation of these ideas. The first idea, contained within Chapter 2, was to approximate frequent, short jumps on a lattice with fewer, longer jumps. We showed that non-locally jumping models could replicate the mean particle densities predicted by locally jumping models (as well as by PDEs), but that boundary conditions had to be imposed in a novel way. Boundary conditons in non-locally jumping models directly affect a region of compartments close to the boundary, rather than exclusively the compartment closest to the boundary.

The second idea running through this thesis is that the mean and variance of particle numbers within contiguous groups of fully-excluding compartments can be accurately approximated by the mean and variance of particle numbers in larger, partially-excluding compartments. Both fully-excluding and partially-excluding models have previously been used in the literature, but our work in Chapter 3 was the first to explicitly connect the two modelling frameworks, develop arguments justifying their equivalence, and demonstrate the potential of partially-excluding models for accelerating stochastic simulations.

We developed our work on volume exclusion further in Chapter 4, generalising the original results to non-uniform lattices, and considering the circumstances in which partially-excluding models become inappropriate. A similar theme runs through Chapter 5, where we investigate the implementation of reactions in partially-excluding models, and determine the situations where the inability to mix leads to one-dimensional fully- and partially-excluding models displaying differing reaction rates.

There is potential to explore these ideas still further, as discussed earlier in this chapter. By investigating fundamental questions, such as the impact of particle crowding on mixing, additional contributions could be made to the literature on

stochastic lattice-based models of diffusion. We leave such work for the future.

Appendix A

Appendices for Chapter 2

A.1 Proofs by induction: reflecting terms

In this and the two following appendices, we rearrange long summations of $M_i(t)$ terms (for various i) into an expression in terms of $M_1(t)$ and $M_2(t)$, representing the gradient at the boundary $x = 0$, and a series of terms collected into the form of second derivatives. We begin by writing our equation so that all expressions are grouped with some variable $M_i(t)$, then we take the highest value of i and rearrange all $M_i(t)$ terms, along with the appropriate values of M_{i-1} and $M_{i-2}(t)$, into a second derivative that will vanish in the diffusive limit. This step is repeated until only terms of $M_1(t)$ and $M_2(t)$ have not been rearranged into second derivatives.

A.1.1 Case when $k = 1$

When $k = 1$, the first line of equation (2.29) can be written as

$$\frac{D\sqrt{\Delta t}}{Q(\Delta x)^2}\left\{-\left[\sum_{j=2}^{Q}\frac{1}{j^2}\right]M_1(t)+\sum_{j=2}^{Q}\left[\frac{1}{j^2}M_j(t)\right]\right\}. \tag{A.1}$$

We apply the method described above to this expression, removing one variable at a time by rearranging it into a second derivative that will vanish in the diffusive limit. To begin the proof by induction, we assume that after $s \leq Q-4$ steps of this

method the expression will be of the form

$$\frac{D\sqrt{\Delta t}}{Q(\Delta x)^2}\left\{-\left[\sum_{j=2}^{Q}\frac{1}{j^2}\right]M_1(t)+\sum_{j=2}^{Q-s-2}\left[\frac{1}{j^2}M_j(t)\right]\right.$$
$$+\left[\frac{1}{(Q-s-1)^2}-\sum_{j=Q-s+1}^{Q}\left[\frac{j-Q+s}{j^2}\right]\right]M_{Q-s-1}(t)$$
$$+\left[\sum_{j=Q-s}^{Q}\left[\frac{j-Q+s+1}{j^2}\right]\right]M_{Q-s}(t)$$
$$\left.+(\Delta x)^2\sum_{j=Q-s+1}^{Q}\left[\sum_{i=j}^{Q}\left[\frac{i-j+1}{i^2}\right]\frac{(M_{j-2}(t)-2M_{j-1}(t)+M_j(t))}{(\Delta x)^2}\right]\right\}. \quad \text{(A.2)}$$

Assume this conjecture holds true for some value of s, then rearrange so that M_{Q-s} is only present inside a second derivative term, i.e.

$$\frac{D\sqrt{\Delta t}}{Q(\Delta x)^2}\left\{-\left[\sum_{j=2}^{Q}\frac{1}{j^2}\right]M_1(t)+\sum_{j=2}^{Q-s-3}\left[\frac{1}{j^2}M_j(t)\right]\right.$$
$$\left[\frac{1}{(Q-s-2)^2}-\sum_{j=Q-sc}^{Q}\left[\frac{j-Q+s+1}{j^2}\right]\right]M_{Q-s-2}(t)$$
$$\left[\frac{1}{(Q-s-1)^2}+2\sum_{j=Q-s}^{Q}\left[\frac{j-Q+s+1}{j^2}\right]-\sum_{j=Q-s+1}^{Q}\left[\frac{j-Q+s}{j^2}\right]\right]M_{Q-s-1}(t)$$
$$+(\Delta x)^2\sum_{j=Q-s}^{Q}\left[\frac{j-Q+s+1}{j^2}\right]\left(\frac{M_{Q-s-2}(t)-2M_{Q-s-1}(t)+M_{Q-s}(t)}{(\Delta x)^2}\right)$$
$$\left.+(\Delta x)^2\sum_{j=Q-s+1}^{Q}\left[\sum_{i=j}^{Q}\left[\frac{i-j+1}{i^2}\right]\frac{(M_{j-2}(t)-2M_{j-1}(t)+M_j(t))}{(\Delta x)^2}\right]\right\}. \quad \text{(A.3)}$$

It is clear that the first and second lines match our conjecture for $s+1$, while the fourth line can be incorporated into the fifth to satisfy our conjecture again. Checking the coefficients of the third line then, we find

$$\frac{1}{(Q-s-1)^2}+2\sum_{j=Q-s}^{Q}\left[\frac{j-Q+s+1}{j^2}\right]-\sum_{j=Q-s+1}^{Q}\left[\frac{j-Q+s}{j^2}\right]$$
$$=\frac{1}{(Q-s-1)^2}+2\frac{1}{(Q-s)^2}+\sum_{j=Q-s+1}^{Q}\left[\frac{j-Q+s+2}{j^2}\right]$$
$$=\sum_{j=Q-s-1}^{Q}\left[\frac{j-Q+s+2}{j^2}\right], \quad \text{(A.4)}$$

which matches our conjecture. We complete our proof by induction by noting that our conjecture is true for $s = 1$. We can then use it by setting $s = Q - 4$, the last value for which our induction is valid due to the summation from $j = 2$ to $Q - s - 2$, and write expression (A.1) in the form

$$\frac{D\sqrt{\Delta t}}{Q(\Delta x)^2}\left\{-\left[\sum_{j=2}^{Q}\frac{1}{j^2}\right]M_1(t)+\frac{1}{2^2}M_2(t)\right.$$
$$+\left(\frac{1}{3^2}-\sum_{j=5}^{Q}\left[\frac{j-4}{j^2}\right]\right)M_3(t)+\left(\sum_{j=4}^{Q}\left[\frac{j-3}{j^2}\right]\right)M_4(t)$$
$$\left.+(\Delta x)^2\sum_{j=5}^{Q}\left[\sum_{i=j}^{Q}\left[\frac{i-j+1}{i^2}\right]\frac{(M_{j-2}(t)-2M_{j-1}(t)+M_j(t))}{(\Delta x)^2}\right]\right\}. \tag{A.5}$$

Twice more we rearrange this expression to form second derivatives, leaving an expression entirely in terms of $M_1(t)$ and $M_2(t)$,

$$\frac{D\sqrt{\Delta t}}{Q(\Delta x)^2}\left\{-\left[\sum_{j=2}^{Q}\frac{1}{j^2}\right]M_1(t)+\left(\frac{1}{2^2}-\sum_{j=4}^{Q}\left[\frac{j-3}{j^2}\right]\right)M_2(t)\right.$$
$$+\left(\sum_{j=3}^{Q}\left[\frac{j-2}{j^2}\right]\right)M_3(t)$$
$$\left.+(\Delta x)^2\sum_{j=4}^{Q}\left[\sum_{i=j}^{Q}\left[\frac{i-j+1}{i^2}\right]\frac{(M_{j-2}(t)-2M_{j-1}(t)+M_j(t))}{(\Delta x)^2}\right]\right\}, \tag{A.6}$$
$$=\frac{D\sqrt{\Delta t}}{Q(\Delta x)^2}\left\{-\left(\sum_{j=2}^{Q}\left[\frac{1}{j^2}\right]+\sum_{j=3}^{Q}\left[\frac{j-2}{j^2}\right]\right)M_1(t)+\left(\sum_{j=2}^{Q}\left[\frac{j-1}{j^2}\right]\right)M_2(t)\right.$$
$$\left.+(\Delta x)^2\sum_{j=3}^{Q}\left[\sum_{i=j}^{Q}\left[\frac{i-j+1}{i^2}\right]\frac{(M_{j-2}(t)-2M_{j-1}(t)+M_j(t))}{(\Delta x)^2}\right]\right\}. \tag{A.7}$$

Taking the diffusive limit, all the second derivative terms go to zero, while $M_1(t)$ and $M_2(t)$ form a first derivative, so that expression (A.7) simplifies to

$$\frac{D\sqrt{\Delta t}}{Q\Delta x}\left(\sum_{j=2}^{Q}\left[\frac{j-1}{j^2}\right]\right)\left(\frac{M_2(t)-M_1(t)}{\Delta x}\right). \tag{A.8}$$

In the diffusive limit this becomes

$$\frac{D}{Q}\left(\sum_{j=2}^{Q}\left[\frac{j-1}{j^2}\right]\right)\left.\frac{\partial u}{\partial x}\right|_{x=0}. \tag{A.9}$$

A.1.2 Case when $k > 1$, but $2k - 1 \geq Q$

We begin by noting that $2k-1$ is the length of jump required for a particle to travel left from compartment k and be returned to the same compartment by reflection. We therefore begin by considering the case $2k - 1 \geq Q$, where only compartments to the left of x_k will contribute reflecting particles to the total number in k, and later combine this with the case $2k - 1 < Q$, where we must also consider particles reflecting into compartment k that started from compartments to the right.

We therefore begin by considering the following reflecting terms,

$$\frac{D\sqrt{\Delta t}}{Q(\Delta x)^2}\left\{\sum_{j=1}^{Q-k+1}\left[\frac{1}{(j+k-1)^2}M_j(t)\right] - \left[\sum_{j=1}^{Q-k+1}\frac{1}{(j+k-1)^2}\right]M_k(t)\right\}. \quad \text{(A.10)}$$

If $Q < 2k-2$ then there will be values of l, $Q-k+1 < l < k$, such that the coefficients of $M_l(t)$ are zero. We then use our established iteration $2k-1-Q$ times, so that all remaining M terms from $M_1(t)$ to M_{Q-k+1} have no zero coefficients, i.e.

$$\begin{aligned}\frac{D\sqrt{\Delta t}}{Q(\Delta x)^2}&\left\{\sum_{j=1}^{Q-k-1}\left[\frac{1}{(j+k-1)^2}M_j(t)\right]\right.\\ &+\left[\frac{1}{(Q-1)^2}-(2k-Q-1)\sum_{j=1}^{Q-k+1}\frac{1}{(j+k-1)^2}\right]M_{Q-k}(t)\\ &\left.-\left[\frac{1}{Q^2}-(2k-Q)\sum_{j=1}^{Q-k+1}\frac{1}{(j+k-1)^2}\right]M_{Q-k+1}(t)\right\}. \quad \text{(A.11)}\end{aligned}$$

In the case $Q = k-1$ this yields

$$-\frac{AD}{Q}\left\{\frac{(k-1)}{k^2}+\frac{k-2}{(k+1)^2}\right\}. \quad \text{(A.12)}$$

Otherwise, after a further $Q-k-1$ iterations, we have

$$\begin{aligned}\frac{D\sqrt{\Delta t}}{Q(\Delta x)^2}&\left\{\left[\frac{1}{k^2}-\sum_{j=3}^{Q-k+1}\left[\frac{j-2}{(j+k-1)^2}\right]+(k-2)\sum_{j=1}^{Q-k+1}\left[\frac{1}{(j+k-1)^2}\right]\right]M_1(t)\right.\\ &\left.-\left[\frac{1}{(k+1)^2}+\sum_{j=3}^{Q-k+1}\left[\frac{j-1}{(j+k-1)^2}\right]-(k-1)\sum_{j=1}^{Q-k+1}\left[\frac{1}{(j+k-1)^2}\right]\right]M_2(t)\right\}.\end{aligned}$$

In the diffusive limit this becomes

$$\frac{D}{Q}\left(\sum_{j=k}^{Q}\left[\frac{j-2k+1}{j^2}\right]\right)\left.\frac{\partial u}{\partial x}\right|_{x=0}, \tag{A.13}$$

which is consistent with our result for $k=1$.

A.1.3 Case when $k>1$, but $2k-1<Q$

Considering the case where $2k-1<Q$, the contribution of reflection to the master equation can be divided into two parts,

$$\begin{aligned}\frac{D\sqrt{\Delta t}}{Q(\Delta x)^2}\Bigg\{&\sum_{j=1}^{k}\left[\frac{1}{(j+k-1)^2}M_j(t)\right]-\left[\sum_{j=1}^{k}\frac{1}{(j+k-1)^2}\right]M_k(t)\\&-\left[\sum_{j=k+1}^{Q-k+1}\frac{1}{(j+k-1)^2}\right]M_k(t)+\sum_{j=k+1}^{Q-k+1}\left[\frac{1}{(j+k-1)^2}M_j(t)\right]\Bigg\}.\end{aligned} \tag{A.14}$$

From our previous result, it is clear that the first line of this expression will end up contributing

$$\frac{D}{Q}\left(\sum_{j=k}^{2k-1}\frac{j-2k+1}{j^2}\right)\left.\frac{\partial u}{\partial x}\right|_{x=0}, \tag{A.15}$$

to the value of B_k, so we can concentrate on the second line. After $Q-2k$ iterations this can be reduced to

$$-\left[\sum_{j=k+1}^{Q-k+1}\left[\frac{1}{(j+k-1)^2}\right]+\sum_{j=2k+1}^{Q}\left[\frac{j-2k}{j^2}\right]\right]M_k(t)+\left[\sum_{j=2k}^{Q}\left[\frac{j-2k+1}{j^2}\right]\right]M_{k+1}(t). \tag{A.16}$$

After a further $k-1$ iterations all terms of M_i, $i > 2$, have been rearranged into second derivatives and will vanish in the diffusive limit. We are left with

$$\frac{D\sqrt{\Delta t}}{Q(\Delta x)^2} \left\{ - \left[(k-1) \sum_{j-2k}^{Q} \left[\frac{j-2k+1}{j^2} \right] - (k-2) \sum_{j=2k+1}^{Q} \left[\frac{j-2k}{j^2} \right] \right. \right. \\ \left. -(k-2) \sum_{j=k+1}^{Q-k+1} \left[\frac{1}{(j+k-1)^2} \right] \right] M_1(t) \\ + \left[k \sum_{j-2k}^{Q} \left[\frac{j-2k+1}{j^2} \right] - (k-1) \sum_{j=2k+1}^{Q} \left[\frac{j-2k}{j^2} \right] \right. \\ \left. \left. -(k-1) \sum_{j=k+1}^{Q-k+1} \left[\frac{1}{(j+k-1)^2} \right] \right] M_2(t) \right\}. \tag{A.17}$$

After rearranging and taking the diffusive limit, it can be seen that the expression resolves to

$$\frac{D}{Q} \sum_{j=2k}^{Q} \left[\frac{j-2k+1}{j^2} \right] \left. \frac{\partial u}{\partial x} \right|_{x=0}. \tag{A.18}$$

Adding the terms from equations (A.15) and (A.18), we obtain

$$\frac{D}{Q} \sum_{j=k}^{Q} \left[\frac{j-2k+1}{j^2} \right] \left. \frac{\partial u}{\partial x} \right|_{x=0}, \tag{A.19}$$

which has been shown to hold for all values of k.

A.2 Proofs by induction: non-reflecting terms

In this appendix, we examine the second line of equation (2.29).

A.2.1 Case when $k = 1$

The non-reflecting jumping terms describing transitions in to and out of the first compartment are given by

$$\frac{D\sqrt{\Delta t}}{Q(\Delta x)^2} \left\{ - \left[\sum_{j=1}^{Q} \frac{1}{j^2} \right] M_1(t) + \sum_{j=1}^{Q} \left[\frac{1}{j^2} M_{j+1}(t) \right] \right\}. \tag{A.20}$$

As in Appendix A, the $M_{Q+1}(t)$ term can be removed from this expression by re-arranging it, together with some other terms, into a second derivative, which will vanish as $\Delta t \to 0$. The resulting expression is given by

$$\frac{D\sqrt{\Delta t}}{Q(\Delta x)^2}\left\{-\left[\sum_{j=1}^{Q}\frac{1}{j^2}\right]M_1(t)+\sum_{j=1}^{Q-3}\left[\frac{1}{j^2}M_{j+1}(t)\right]+\left[\frac{1}{(Q-2)^2}-\frac{1}{Q^2}\right]M_{Q-1}(t)\right.$$
$$\left.+\left[\frac{1}{(Q-1)^2}+2\frac{1}{Q^2}\right]M_Q(t)\right\}$$
$$+\left(\frac{1}{Q^2}\frac{D\sqrt{\Delta t}}{Q}\frac{M_{Q-1}(t)-2M_Q(t)+M_{Q+1}(t)}{(\Delta x)^2}\right). \tag{A.21}$$

This is the expression after one step (i.e. the conversion of the last term into a second derivative) so we conjecture that after s steps, for $s \leq (Q-3)$, it will be of the form

$$\frac{D\sqrt{\Delta t}}{Q(\Delta x)^2}\left\{-\left[\sum_{j=1}^{Q}\frac{1}{j^2}\right]M_1(t)+\sum_{j=1}^{Q-s-2}\left[\frac{1}{j^2}M_{j+1}(t)\right]\right.$$
$$+\left[\frac{1}{(Q-s-1)^2}-\sum_{j=Q-s+1}^{Q}\left((j-Q+s)\frac{1}{j^2}\right)\right]M_{Q-s}(t)$$
$$\left.+\left[\sum_{j=Q-s}^{Q}(j-Q+s+1)\frac{1}{j^2}\right]M_{Q-s+1}(t)\right\} \tag{A.22}$$
$$+\frac{D\sqrt{\Delta t}}{Q}\sum_{j=Q-s+1}^{Q}\left(\sum_{i=j}^{Q}\left[\frac{i-j+1}{i^2}\right]\frac{M_{Q-1}(t)-2M_Q(t)+M_{Q+1}(t)}{(\Delta x)^2}\right),$$

where the terms on the last line will vanish in the diffusive limit. This holds for $s = 1$, so we use a proof by induction again (not shown here). The next step is to remove the $M_{Q-s+1}(t)$ term by separating it out into another vanishing second

derivative, so the expression becomes

$$
\begin{aligned}
& \frac{D\sqrt{\Delta t}}{Q(\Delta x)^2}\left\{-\left[\sum_{j=1}^{Q}\frac{1}{j^2}\right]M_1(t)+\sum_{j=1}^{Q-s-3}\left[\frac{1}{j^2}M_{j+1}(t)\right]\right. \qquad \text{(A.23)}\\
+ & \left[\frac{1}{(Q-s-2)^2}-\sum_{j=Q-s}^{Q}\left((j-Q+s+1)\frac{1}{j^2}\right)\right]M_{Q-s-1}(t)\\
& +\left[\frac{1}{(Q-s-1)^2}-\sum_{j=Q-s+1}^{Q}\left((j-Q+s)\frac{1}{j^2}\right)\right.\\
+ & \left.2\sum_{j=Q-s}^{Q}\left((j-Q+s+1)\frac{1}{j^2}\right)\right]M_{Q-s}(t)\Bigg\}\\
+ & \left(\sum_{j=Q-s}^{Q}(j-Q+s+1)\frac{1}{j^2}\frac{D\sqrt{\Delta t}}{Q}\frac{M_{Q-s-1}(t)-2M_{Q-s}(t)+M_{Q-s+1}(t)}{(\Delta x)^2}\right)\\
+ & \frac{D\sqrt{\Delta t}}{Q}\sum_{j=Q-s+1}^{Q}\left(\sum_{i=j}^{Q}\left[\frac{i-j+1}{i^2}\right]\frac{M_{Q-1}(t)-2M_Q(t)+M_{Q+1}(t)}{(\Delta x)^2}\right).
\end{aligned}
$$

It is clear that the first and second lines of this expression recapitulate the postulated general form after $s+1$ steps, as do the fourth and fifth when taken in combination. Rearranging the coefficients of M_{Q-s}, we can rewrite them as

$$
\begin{aligned}
& \frac{1}{(Q-s-1)^2}+\sum_{j=Q-s+1}^{Q}\left[-(j-Q+s)\frac{1}{j^2}+2(j-Q+s+1)\frac{1}{j^2}\right]+2\frac{1}{(Q-s)^2}\\
& \quad =\frac{1}{(Q-s-1)^2}+2\frac{1}{(Q-s)^2}+\sum_{j=Q-s+1}^{Q}\left[(j-Q+s+2)\frac{1}{j^2}\right]\\
& \quad =\sum_{j=Q-s-1}^{Q}\left[(j-Q+s+2)\frac{1}{j^2}\right], \qquad \text{(A.24)}
\end{aligned}
$$

which matches the general form again, completing our proof by induction. When $s = Q - 3$, we can write

$$\begin{aligned}\frac{D\sqrt{\Delta t}}{Q(\Delta x)^2} & \left\{ -\left[\sum_{j=1}^{Q}\frac{1}{j^2}\right] M_1(t) + \frac{1}{1^2}M_2(t) + \left(\frac{1}{2^2} - \sum_{j=4}^{Q}\left[\frac{j-3}{j^2}\right]\right) M_3(t) \right. \\ & \left. + \left(\sum_{j=3}^{Q}\left[\frac{j-2}{j^2}\right]\right) M_4(t) \right\} \\ + \frac{D\sqrt{\Delta t}}{Q} & \sum_{j=4}^{Q}\left(\sum_{i=j}^{Q}\left[\frac{i-j+1}{i^2}\right]\left.\frac{\partial^2 u}{\partial x^2}\right|_{x=x_{j-1}}\right), \end{aligned} \tag{A.25}$$

and hence remove $M_4(t)$ from the expression as before, subsuming it into the second derivative term,

$$\begin{aligned}\frac{D\sqrt{\Delta t}}{Q(\Delta x)^2} & \left\{ -\left[\sum_{j=1}^{Q}\frac{1}{j^2}\right] M_1(t) + \left[\frac{1}{1^2} - \sum_{j=3}^{Q}\left[\frac{j-2}{j^2}\right]\right] M_2(t) \right. \\ & \left. + \left(\frac{1}{2^2} - \sum_{j=4}^{Q}\left[\frac{j-3}{j^2}\right] + 2\sum_{j=3}^{Q}\left[\frac{j-2}{j^2}\right]\right) M_3(t) \right\} \\ & + \frac{D\sqrt{\Delta t}}{Q}\sum_{j=3}^{Q}\left(\sum_{i=j}^{Q}\left[\frac{i-j+1}{i^2}\right]\left.\frac{\partial^2 u}{\partial x^2}\right|_{x=x_{j-1}}\right). \end{aligned} \tag{A.26}$$

Noting that the coefficients of $M_3(t)$ can be consolidated as $\sum_{j=2}^{Q}[j-1]/Q$ we then do the same to $M_3(t)$ and are left with an expression in terms of $M_1(t)$ and $M_2(t)$ alone:

$$\begin{aligned}\frac{D\sqrt{\Delta t}}{Q(\Delta x)^2} & \left\{ -\left[\sum_{j=1}^{Q}\left(\frac{1}{j^2}\right) + \sum_{j=2}^{Q}\left(\frac{j-1}{j^2}\right)\right] M_1(t) \right. \\ & \left. + \left[\frac{1}{1^2} - \sum_{j=3}^{Q}\left[\frac{j-2}{j^2}\right] + 2\sum_{j=2}^{Q}\left(\frac{j-1}{j^2}\right)\right] M_2(t) \right\} \\ & + \frac{D\sqrt{\Delta t}}{Q}\sum_{j=2}^{Q}\left(\sum_{i=j}^{Q}\left[\frac{i-j+1}{i^2}\right]\left.\frac{\partial^2 u}{\partial x^2}\right|_{x=x_{j-1}}\right). \end{aligned} \tag{A.27}$$

Then rearranging, and discarding the second derivative terms (as we know they will vanish in the diffusive limit), gives us

$$\frac{D\sqrt{\Delta t}}{Qh}\left(\sum_{j=1}^{Q}\frac{1}{j}\right)\left(\frac{M_2(t)-M_1(t)}{\Delta x}\right), \tag{A.28}$$

so in the diffusive limit, keeping the ratio $\sqrt{\Delta t}/\Delta x$ constant, we arrive at

$$\frac{D}{Q}\left(\sum_{j=1}^{Q}\frac{1}{j}\right)\left.\frac{\partial u}{\partial x}\right|_{x=0}. \tag{A.29}$$

A.2.2 Case when $k \neq 1$

Having found this expression for the the first compartment, we now generalise this to derive an expression for the k^{th} compartment. The relevant expressions are

$$\frac{D\sqrt{\Delta t}}{Q(\Delta x)^2}\left\{\left(\sum_{j=1}^{k-1}\frac{1}{(k-j)^2}M_j(t)\right)-\left(\sum_{j=1}^{k-1}\frac{1}{(k-j)^2}+\sum_{j=1}^{Q}\frac{1}{j^2}\right)M_k(t)\right.$$
$$\left.+\sum_{j=1}^{Q}\left(\frac{1}{j^2}M_{k+j}(t)\right)\right\}, \tag{A.30}$$

where the four summations represent particles jumping in from the left, out to the left, out to the right and in from the right, respectively.

We notice that, taken together, the terms for jumping in from and out to the right are the same as the whole expression for the first compartment, except defined for M_k and M_{k+j} rather than for M_1 and M_{k+1}. We therefore know that after $Q-1$ steps, using the same approach as before, these terms will reduce to

$$-\left(\sum_{j=1}^{Q}\frac{1}{j}\right)M_k(t)+\left(\sum_{j=1}^{Q}\frac{1}{j}\right)M_{k+1}(t), \tag{A.31}$$

plus some second derivative terms that will vanish in the diffusive limit. Discarding

these derivative terms for simplicity, the system becomes

$$\frac{D\sqrt{\Delta t}}{Q(\Delta x)^2} \quad \left\{ \left(\sum_{j=1}^{k-1} \frac{1}{(k-j)^2} M_j(t) \right) - \left(\sum_{j=1}^{k-1} \frac{1}{(k-j)^2} + \sum_{j=1}^{Q} \frac{1}{j} \right) M_k(t) + \sum_{j=1}^{Q} \left(\frac{1}{j} \right) M_{k+1}(t) \right\}. \tag{A.32}$$

Taking another step to eliminate $M_{k+1}(t)$, and discarding the resulting second derivative again, we obtain

$$0 = \frac{D\sqrt{\Delta t}}{Q(\Delta x)^2} \quad \left\{ \left(\sum_{j=1}^{k-2} \frac{1}{(k-j)^2} M_j(t) \right) + \left(\frac{1}{1^2} - \sum_{j=1}^{Q} \frac{1}{j} \right) M_{k-1}(t) + \left(\sum_{j=1}^{Q} \frac{1}{j} - \sum_{j=1}^{k-1} \frac{1}{(k-j)^2} \right) M_k(t) \right\}. \tag{A.33}$$

In the case where $k = 2$, the first term is zero, and in the diffusive limit this expression becomes

$$\frac{D}{Q} \left(\sum_{j=2}^{Q} \frac{1}{j} \right) \left. \frac{\partial u}{\partial x} \right|_{x=0}. \tag{A.34}$$

After another iteration of the method we arrive at the expression (discarding the second derivative again)

$$0 = \frac{D\sqrt{\Delta t}}{Q(\Delta x)^2} \quad \left\{ \left(\sum_{j=1}^{k-3} \frac{1}{(k-j)^2} M_j(t) \right) + \left(\frac{1}{2^2} - \sum_{j=1}^{Q} \frac{1}{j} + \sum_{j=1}^{k-1} \frac{1}{(k-j)^2} \right) M_{k-2}(t) + \left(\frac{1}{1^2} + \sum_{j=1}^{Q} \frac{1}{j} - 2 \sum_{j=1}^{k-1} \frac{1}{(k-j)^2} \right) M_{k-1}(t) \right\}. \tag{A.35}$$

In the case where $k = 3$, the first term is zero again, and in the diffusive limit this expression becomes

$$\frac{D}{Q} \left(\sum_{j=3}^{Q} \frac{1}{j} \right) \left. \frac{\partial u}{\partial x} \right|_{x=0}. \tag{A.36}$$

For $k > 3$, it can be shown by induction that the general form for this equation after

a total of $s > Q+1$ steps is

$$\frac{D\sqrt{\Delta t}}{Q(\Delta x)^2}\left\{\left(\sum_{j=1}^{Q+k-s-2}\frac{1}{(k-j)^2}M_j(t)\right)\right.$$
$$+\left(\frac{1}{(s-Q+1)^2}-\sum_{j=1}^{s-Q-1}\frac{k-3-j}{j^2}-\sum_{j=1}^{Q}\frac{1}{j}+(s-Q)\sum_{j=1}^{k-1}\frac{1}{j^2}\right)M_{Q+k-s-1}(t)$$
$$\left.+\left(\sum_{j=1}^{s-Q}\frac{s-Q+1-j}{j^2}+\sum_{j=1}^{Q}\frac{1}{j}-(s-Q+1)\sum_{j=1}^{k-1}\frac{1}{j^2}\right)M_{Q+k-s}(t)\right\}, \quad \text{(A.37)}$$

plus some vanishing second derivative terms. It therefore follows that after $s = Q+k-2$ steps the remaining terms will be

$$\frac{D\sqrt{\Delta t}}{Q(\Delta x)^2}\quad\left\{\left(\frac{1}{(k-1)^2}-\sum_{j=1}^{k-3}\frac{k-2-j}{j^2}-\sum_{j=1}^{Q}\frac{1}{j}+(k-2)\sum_{j=1}^{k-1}\frac{1}{j^2}\right)M_1(t)\right.$$
$$\left.+\left(\sum_{j=1}^{k-2}\frac{k-1-j}{j^2}+\sum_{j=1}^{Q}\frac{1}{j}-(k-1)\sum_{j=1}^{k-1}\frac{1}{j^2}\right)M_2(t)\right\}, \quad \text{(A.38)}$$

which can be consolidated in the diffusive limit to yield

$$\frac{D}{Q}\left(\sum_{j=k}^{Q}\frac{1}{j}\right)\frac{M_2(t)-M_1(t)}{\Delta x}=\frac{D}{Q}\left(\sum_{j=k}^{Q}\frac{1}{j}\right)\left.\frac{\partial u}{\partial x}\right|_{x=0}. \quad \text{(A.39)}$$

A.3 Proof by induction: adsorption terms

We wish to evaluate the third line of equation (2.29),

$$\frac{D\sqrt{\Delta t}}{Q\Delta x}\sum_{j=1}^{Q-k+1}\left[\frac{P_{j+k-1,Q}}{(j+k-1)^2}M_j(t)\right]. \quad \text{(A.40)}$$

We separate terms out into second derivatives as before, until the only terms which will not vanish in the diffusive limit are M_1 and M_2,

$$\frac{D\sqrt{\Delta t}}{Q\Delta x}\left\{\left(\frac{P_{k,Q}}{k^2}-\sum_{j=k+2}^{Q}\left[\frac{(j-1-k)P_{j,Q}}{j^2}\right]\right)M_1(t)+\sum_{j=k+1}^{Q}\left[\frac{(j-k)P_{j,Q}}{j^2}\right]M_2(t)\right.$$
$$\left.+\sum_{j=3}^{Q-k+1}\left[\left(\sum_{i=j}^{Q-k+1}\frac{(i+1-j)P_{i+k-1,Q}}{i^2}\right)\frac{M_{j-2}(t)-2M_{j-1}(t)+M_j(t)}{(\Delta x)^2}\right]\right\}.$$

As our final step, we separate these terms into an expression in terms of $M_1(t)$ alone, and a first derivative term,

$$\begin{aligned}
&\frac{D\sqrt{\Delta t}}{Q\Delta x}\left\{\left(\sum_{j=k}^{Q}\left[\frac{P_{j,Q}}{j^2}\right]\right)M_1(t)\right. \\
&\quad+\sum_{j=k+1}^{Q}\left[\frac{(j-k)P_{j,Q}}{j^2}\right]\Delta x\left(\frac{M_2(t)-M_1(t)}{\Delta x}\right) \\
&\left.+\sum_{j=3}^{Q-k+1}\left[\left(\sum_{i=j}^{Q-k+1}\frac{(i+1-j)P_{i+k-1,Q}}{i^2}\right)\frac{M_{j-2}(t)-2M_{j-1}(t)+M_j(t)}{(\Delta x)^2}\right]\right\}.
\end{aligned} \tag{A.41}$$

The extra value of Δx means that first derivative terms also vanish in the diffusive limit, so taking that limit this expression will tend to

$$\frac{D\sqrt{\Delta t}}{Q\Delta x}\left(\sum_{j=k}^{Q}\left[\frac{P_{j,Q}}{j^2}\right]\right)u(0,t), \tag{A.42}$$

as stated in the main text.

Appendix B

Appendices for Chapter 3

B.1 Exit locations and expected leaving times for a 2D lattice

Previous work has attempted to reconcile fully- and partially-excluding LBPJ models by superimposing a fine lattice onto a coarser one, simulating a random walk on the fine lattice, and obtaining jump rates for the coarse lattice by counting the number of times the walk crosses the borders of the coarse compartments [91]. Figure B.1 illustrates this approach, and in this section we will show why it overestimates transition rates on the coarse lattice.

We begin by defining a coarse two-dimensional 2×2 lattice of compartments with periodic boundary conditions, where each coarse compartment is formed from a finer lattice of $m \times m$ sites. The size of each fine lattice site is fixed to be $h \times h$, so that each coarse compartment is of size $mh \times mh$. We are interested in the relation of random walks on these two levels of lattices. In particular, when a particle performs a random walk of fixed length on the fine lattice, we are interested in how the number of transitions between the compartments on the coarse lattice will vary with our choice of m.

It is easy to show, using either martingales and Doob's optional stopping theorem [130], or a recursion argument, that a one-dimensional random walk process on

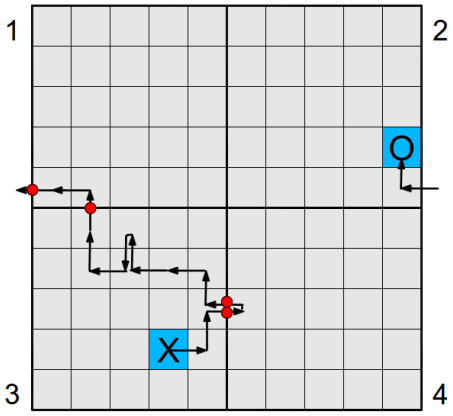

Figure B.1: This example illustrates one possible walk on a periodic lattice, composed of four 5×5 notional compartments (i.e. $m = 5$). In the course of fifteen steps on the fine lattice, the particle starts from the site marked with an 'X' in the third compartment, and transitions between compartments four times (these transitions are marked with red dots). It moves from the third to the fourth compartment, then back to the third compartment, then from the third to the first compartment, and finally from the first to the second. It finishes its walk in the second compartment, at the site marked with an 'O'.

a lattice of length m, starting from the first or m^{th} site, will exit (i.e. move left from the first lattice site or right from the m^{th} one) after an expected time $m\Delta t$, where Δt is the expected time taken by each jump.

We have extended this result to higher dimensions, showing that a particle that starts uniformly distributed across a given edge of a square lattice (as illustrated in Figure B.2(a)), or across a given face of a cubic lattice, will also have expected exit time $m\Delta t$. Furthermore, we have studied the exit location of particles, that start uniformly distributed across a given edge or face of a square or cubic lattice, respectively. It can be shown that the exit position is also, after accounting for reflective symmetries, uniformly distributed (see Figure B.2(c) for an illustration). Our proofs for the distribution of exit positions, and for the expected time before leaving, in the two-dimensional case are given in Sections B.1.1 and B.1.2, respectively.

Taken together, these two results explain why a walker on the fine lattice will average a transition between coarse compartments every m steps, rather than every m^2 steps as would be necessary to recapitulate the expected coarse lattice transition rates. We note that a large variance in this average is to be expected: a walker

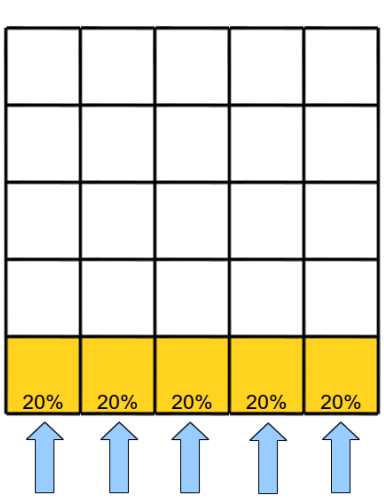

(a) Entrance probabilities

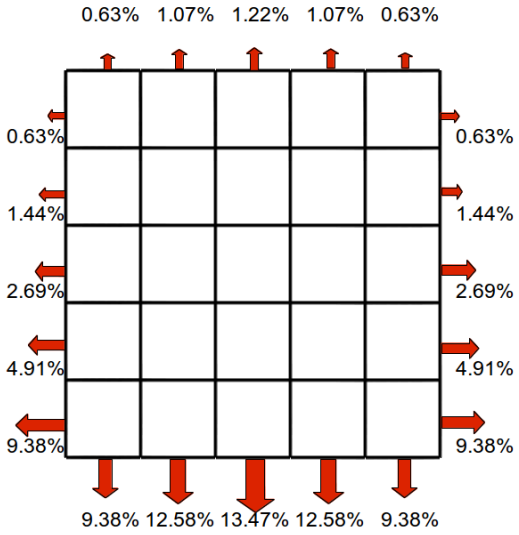

(b) Exit probabilities

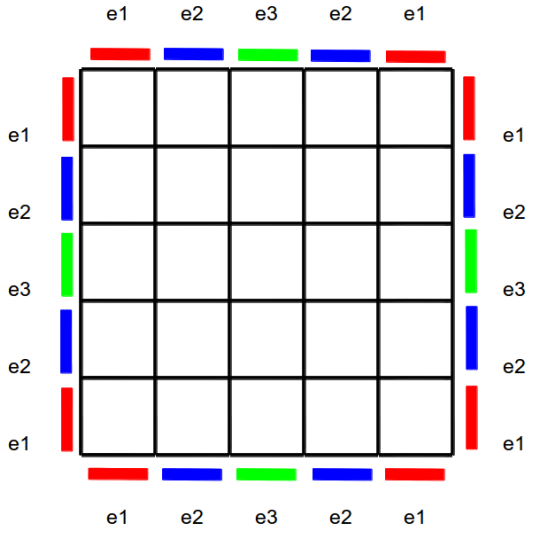

(c) Exit locations under reflectional symmetry

Figure B.2: Panel (a) shows a particle entering the square lattice, with its starting position uniformly distributed over one side. Panel (b) shows the probabilities, derived from simulation, of that particle then exiting through any given point on the boundary of the lattice, given the uniform starting distribution. Panel (c) illustrates what it means for the probability distribution of the particle's exit position relative to the corners to be uniform: it will leave through one of the edges labeled $e1$ (highlighted in red) with probability 0.4, through $e2$ (blue) with probability 0.4, and through $e3$ (green) with probability 0.2.

will typically either move over the boundary it begins adjacent to very quickly, or move away from the boundary and spend longer in the coarse compartment before leaving. In Section B.2 we discuss how this result is linked to the connection between Brownian motion and LBPJ descriptions of diffusion.

B.1.1 Exit point along edge is uniformly distributed

Consider an $m \times m$ square lattice of compartments, as illustrated in Figure B.2. Define the probability that a particle in the i^{th} compartment up and the j^{th} compartment along will exit through the e^{th} edge of the lattice from a corner as $P^e_{i,j}$. We assume symmetry, i.e.

$$P^e_{i,j} = P^e_{j,i} = P^e_{i,m+1-j} = P^{m+1-e}_{i,j}, \tag{B.1}$$

where the exit points considered are also treated symmetrically, e.g. when considering $e = 1$, the edge of a corner compartment, then we are interested in the probability of leaving by any of the eight corner compartment edges.

Note that, if a particle enters a compartment with position uniformly distributed over one edge, the odds of leaving through the e^{th} edge from a corner is given by

$$\frac{1}{m}\sum_{i=1}^{m} P^e_{i,1}. \tag{B.2}$$

For simplicity, we will only consider the case where $e = 1$ here, though the following proof generalises easily to all other choices of exit point. We note the following posssibilities for $P^1_{i,j}$:

$$P^1_{i,j} = \begin{cases} \frac{1}{2} + \frac{1}{4}P^1_{1,2} + \frac{1}{4}P^1_{2,1} & \text{if } i = 1, j = 1, \\ \frac{1}{4}P^1_{1,j-1} + \frac{1}{4}P^1_{1,j+1} + \frac{1}{4}P^1_{2,j} & \text{if } i = 1, 1 < j < m, \\ \frac{1}{4}P^1_{i,j-1} + \frac{1}{4}P^1_{i,j+1} + \frac{1}{4}P^1_{i-1,j} + \frac{1}{4}P^1_{i+1,j} & \text{if } 1 < i < m, 1 < j < m. \end{cases} . \tag{B.3}$$

Using these values, we can write

$$\sum_{i=1}^{m}\sum_{j=1}^{m} P^1_{i,j} = \sum_{i=2}^{m-1}\sum_{j=2}^{m-1} P^1_{i,j} + \frac{3}{4}\sum_{i=2}^{m-1} P^1_{i,1} + \frac{3}{4}\sum_{i=2}^{m-1} P^1_{i,m} + \frac{3}{4}\sum_{j=2}^{m-1} P^1_{1,j} + \frac{3}{4}\sum_{j=2}^{m-1} P^1_{m,j} + \frac{1}{2}P^1_{1,1} + \frac{1}{2}P^1_{1,m} + \frac{1}{2}P^1_{m,1} + \frac{1}{2}P^1_{m,m} + \frac{1}{2}4, \quad \text{(B.4)}$$

where the right-hand side was obtained by evaluating each term from the summation on the left-hand side using the expressions given by equation (B.3). Subtracting $\sum_{i=2}^{m-1}\sum_{j=2}^{m-1} P^1_{i,j}$ from each side, we obtain

$$2P^1_{1,1} + 4\sum_{i=2}^{m-1} P^1_{i,1} + 2P^1_{m,1} = \frac{3}{4}\sum_{i=2}^{m-1} P^1_{i,1} + \frac{3}{4}\sum_{i=2}^{m-1} P^1_{i,m} + \frac{3}{4}\sum_{j=2}^{m-1} P^1_{1,j} + \frac{3}{4}\sum_{j=2}^{m-1} P^1_{m,j} + \frac{1}{2}P^1_{1,1} + \frac{1}{2}P^1_{1,m} + \frac{1}{2}P^1_{m,1} + \frac{1}{2}P^1_{m,m} + 2, \quad \text{(B.5)}$$

where we have used the symmetries from equation (B.1) to simplify the remaining terms on the left-hand side. We can use these same symmetries to simplify the right-hand side:

$$2P^1_{1,1} + 4\sum_{i=2}^{m-1} P^1_{i,1} + 2P^1_{m,1} = P^1_{1,1} + 3\sum_{i=2}^{m-1} P^1_{i,1} + P^1_{m,1} + 2, \quad \text{(B.6)}$$

which becomes, after rearranging and dividing both sides by m,

$$\frac{1}{m}\sum_{i=1}^{m} P^1_{i,1} = \frac{2}{m}. \quad \text{(B.7)}$$

Recalling equation (B.2), this shows that the probability of exiting from a corner compartment, given an initial position uniformly distributed across an edge of the array, will be $2/m$.

A similar argument can be used to show that the probability of leaving through any other point (and its reflections) will be $2/m$, with the exception of the central compartment when m is odd, which particles will leave through with probability $1/m$. Therefore, if a particle's starting position along the edge of the compartment is uniformly distributed then its leaving position along the exit edge will also be

uniformly distributed (after accounting for symmetry).

B.1.2 Expected leaving time is $m\Delta t$

It can be shown that the expected exit time is $m\Delta t$ using a very similar argument, writing the expected exit time from the square lattice of compartments for a particle in the i^{th} compartment up and the j^{th} compartment along as $E_{i,j}$. We note that the same symmetries outlined for the probability of particular exit locations in equation (B.1) apply equally to expected leaving times. We then define

$$E_{i,j} = \begin{cases} \frac{1}{4}E_{1,2} + \frac{1}{4}E_{2,1} + \Delta t & \text{if } i = 1, j = 1, \\ \frac{1}{4}E_{1,j-1} + \frac{1}{4}E_{1,j+1} + \frac{1}{4}E_{2,j} + \Delta t & \text{if } i = 1, 1 < j < m, \\ \frac{1}{4}E_{i,j-1} + \frac{1}{4}E_{i,j+1} + \frac{1}{4}E_{i-1,j} + \frac{1}{4}E_{i+1,j} + \Delta t & \text{if } 1 < i < m, 1 < j < m. \end{cases} \tag{B.8}$$

We note again that, if the particle's initial position is uniformly distributed over one edge, its expected leaving time will be given by $\sum_{i=1}^{m} E_{i,1}/m$. Using these definitions, we can write

$$\begin{aligned} \sum_{i=1}^{m}\sum_{j=1}^{m} E_{i,j} &= \sum_{i=2}^{m-1}\sum_{j=2}^{m-1} E_{i,j} + \frac{3}{4}\sum_{i=2}^{m-1} E_{i,1} + \frac{3}{4}\sum_{i=2}^{m-1} E_{i,m} + \frac{3}{4}\sum_{j=2}^{m-1} E_{1,j} + \frac{3}{4}\sum_{j=2}^{m-1} E_{m,j} \\ &\quad + \frac{1}{2}E_{1,1} + \frac{1}{2}E_{1,m} + \frac{1}{2}E_{m,1} + \frac{1}{2}E_{m,m} + m^2\Delta t. \end{aligned} \tag{B.9}$$

Using the same approach used in Section B.1.1, we can subtract $\sum_{i=2}^{m-1}\sum_{j=2}^{m-1} E_{i,j}$ from both sides of equation (B.9), and exploit symmetries to rearrange the remaining terms into the form

$$\sum_{i=1}^{m} E_{i,1} = m^2\Delta t. \tag{B.10}$$

Dividing both sides by m completes the proof that a particle with initial position uniformly distributed along the edge of the lattice will have an expected leaving time of $m\Delta t$.

Together with the result from Section B.1.1, this explains the relationship observed between the number of transitions between coarse compartments, and the number of fine compartments each compartment is subdivided into. Connections

between this result and the properties of Brownian motion are briefly explored in the following section.

B.2 Connections to Brownian motion

Recall that lattice jump rates can be derived from the first passage time of a Brownian motion, and also that a Brownian motion can be constructed from the limit of a lattice-based random walk as the size of each lattice site tends to zero. Set $h = 1/m$, so that our coarse compartments are of constant size 1×1, and $D/m^2h^2 = D$. Our expression for transitions between coarse compartments should then be independent of the choice of m, so as to maintain this constant transition rate between coarse compartments. The derived relationship between compartment transitions and the choice of m (in Section B.1) therefore shows that it is not possible to use the crossings between coarse compartments of a walker on a fine lattice to recover the dynamics of a walker on the coarse lattice, as the coarse lattice behaviour would vary depending on the choice of m: specifically, the transition rate between coarse compartments would be $D/(mh^2) = Dm$. As we take the continuum limit, $h \to 0$, to recover a Brownian motion, we require $m = 1/h \to \infty$, and hence Dm grows to infinity, so we observe infinite numbers of transitions between coarse compartments, even in arbitrarily small time intervals.

This argument recovers a fundamental result for Brownian motion: that a one-dimensional Brownian motion starting from the origin at time $t = 0$ will return to the origin an infinite number of times in the interval $t \in (0, \epsilon]$ for arbitrarily small ϵ. We present a sketch of the proof for this result in Section B.2.1).

B.2.1 Brownian motion returns to its origin infinitely often

Let the process B_t, where $t \geq 0$ and B_0, be a Brownian motion, and T a stopping time. The reflection principle states that the process

$$B_t^* = \begin{cases} 2B_T - B_t & \text{if } t \geq T; \\ B_t & \text{if } t < T. \end{cases} \tag{B.11}$$

is also a Brownian motion. We define

$$T_a = \inf(t \geq 0 | B_t = a), \tag{B.12}$$

i.e. the first time at which a Brownian motion starting from zero will hit a, and note that it is a stopping time. We further define the maximal process of B_t to be

$$M_t = \max_{0<s\leq t}(B_s), \tag{B.13}$$

that is to say the largest value reached by the Brownian motion by time t. We can then write

$$P(M_t > a) = P(B_t > a) + P(B_t \leq a \text{ and } M_t > a). \tag{B.14}$$

Recalling our reflected Brownian motion equation (B.11), we note that the probability that both $B_t \leq a$ and $M_t > a$ is equivalent to the probability that $B_t^* > a$. We can therefore write

$$\begin{aligned} P(M_t > a) &= P(B_t > a) + P(B_t^* > a) & \text{(B.15)} \\ &= 2P(B_t > a), & \text{(B.16)} \end{aligned}$$

by symmetry. Now, in the interval $(0, \epsilon]$, we can write

$$P(M_\epsilon > 0) = 2P(B_\epsilon > 0) = 1, \tag{B.17}$$

for any $\epsilon > 0$, because Brownian motion is a symmetric process, so we must have $P(B_\epsilon > 0) = P(B_\epsilon < 0) = 1/2$.

In other words, a Brownian motion starting from zero will take a positive value at some point in any arbitrarily small time interval. By the same reasoning, it must also take a negative value in that time interval. Since the motion is continuous, the Intermediate Value theorem requires that its position must be zero at some point, therefore there is at least one zero in $t \in (0, \epsilon]$. This result can be applied recursively to show that the Brownian motion must return to zero an infinite number of times in the interval [131].

B.3 Physical interpretation of the linear interpolation assumption

Having established in Sections B.1 and B.2 that crossing the boundary between aggregated compartments is not an appropriate measure to relate jump rates on a fine-grained lattice to those on a coarse-grained lattice, it may seem strange that we have apparently relied on exactly this approach in Section 3.3.2. In this section, we will argue that the use of linear interpolation to estimate mean particle numbers at the compartment boundaries can instead be interpreted as a means of extrapolating the chance of a particle reaching the centre of a neighbouring compartment. We begin by considering how transitions between compartments for a single random walker could be defined, and then use this definition to provide a different interpretation of the linear interpolation argument.

B.3.1 Defining the exit from a compartment

When deriving lattice transition rates from an off-lattice Brownian motion, we interpret the move to a new compartment as being the first time at which the random walk reaches the residence point of that compartment (see the discussion in Section 4.2.1). Suppose we wished to derive a similar result for transition rates between coarse-grained compartments, using an unbiased random walk over a fine-grained

lattice, such that each coarse-grained compartment is divided into m fine-grained boxes. Note that, to avoid ambiguity in this section, and to aid readability, for the remainder of this appendix we use 'compartment' exclusively to refer to coarse-grained, partially-excluding sites on a lattice, and 'box' to refer to fine-grained, fully-excluding sites. Suppose the expected time between steps on the fine-grained lattice is Δt. When $m = 2n + 1$ is odd-valued it is easy to proceed: we suppose the random walk begins from the box at the centre of a compartment, and simply need to determine the expected time until it has travelled m steps away from its starting position (as illustrated in Figure B.3). We denote the expected time until the walker achieves this, given that it is currently s steps from the starting position, as $E(s)$. Then we can write

$$\begin{aligned} E(0) &= E(1) + \Delta t, && \text{(B.18)} \\ E(s) &= \frac{1}{2}E(s-1) + \frac{1}{2}E(s+1) + \Delta t, \ \forall\, 0 < s < m, && \text{(B.19)} \\ E(m) &= 0. && \text{(B.20)} \end{aligned}$$

It is then easy to show by induction that

$$E(m-k) = \frac{k}{k+1}E(m-(k+1)) + k\Delta t, \qquad \text{(B.21)}$$

and hence we can write

$$\begin{aligned} E(0) &= E(1) + \Delta t \\ &= E(m-(m-1)) + \Delta t \\ &= \frac{m-1}{m}E(0) + (m-1)\Delta t + \Delta t \\ &= m^2\Delta t, && \text{(B.22)} \end{aligned}$$

as expected. It seems that we should be able to derive a similar result for even values of m, but here there are two boxes flanking the centre of each compartment, so there is no clear criterion for changing compartment (Figure B.3 illustrates this

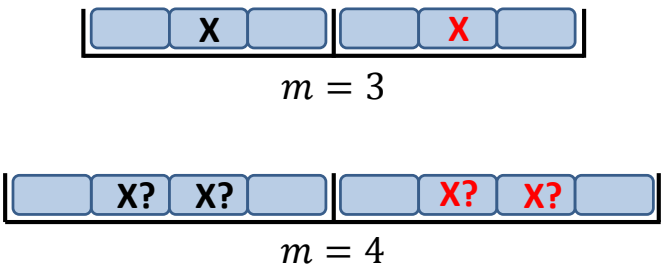

Figure B.3: When each compartment has odd-valued capacity, m, it is simple to define residence points at the centre of each compartment. In the first diagram above, a particle could start at the box marked with a black X, and would be judged to have changed compartment when it reached the box marked with a red X. When the capacity m is even valued, it is less clear when a particle should be considered to have changed compartment.

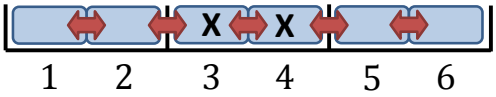

Figure B.4: Starting from the central compartment, i.e. boxes 3 and 4, we want an expected leaving time of $4\Delta t$, and seek to find a rule for leaving the compartment which fits this requirement.

ambiguity). One option is to simply track the expected time to travel m steps from their starting point, but this is unsatisfying, and in a real simulation would lead to a non-Markovian system, where the particle's starting position had to be recorded as well as its current location. For clarity, we will discuss the case $m = 2$, as illustrated in Figure B.4, though it can be seen that the principles behind our result generalise to any even valued m.

Two more options to define the exit from the central compartment (boxes 3 and 4 in Figure B.4) are to consider the particle to have changed compartment as soon as the walker reaches one of the neighbouring boxes, indexed 2 and 5, but this gives an expected leaving time of slightly less than $m^2\Delta$ (since the walker will always start two steps from one exit point, but only one from the other). Another option is to require that the walk must actually cross the central point of a neighbouring compartment (hence reaching boxes 1 or 6), but this gives an expected leaving time greater than $m^2\Delta$ (since the walker starts two steps from one exit point, but three

from the other).

To solve this problem, we suppose that a walker reaching either either box 1 or 6 is always deemed to have transitioned to the neighbouring compartment; in addition, each time a walker enters either box 2 or box 5, it may be deemed to have changed compartment with probability ρ, but will be considered to remain within its starting compartment with probability $(1-\rho)$. We therefore write

$$\begin{aligned} E(0) &= \frac{1}{2}E(0) + \frac{1-\rho}{2}E(1) + \Delta t \\ &= (1-\rho)E(1) + 2\Delta t, \qquad \text{(B.23)} \\ E(1) &= \frac{1}{2}E(0) + \frac{1}{2}E(2) + \Delta t \\ &= \frac{1}{2}E(0) + \Delta t, \qquad \text{(B.24)} \\ E(2) &= 0. \qquad \text{(B.25)} \end{aligned}$$

Here, $E(0)$ corresponds to the expected leaving time from boxes 3 and 4, and $E(1)$ from boxes 2 and 5 (given that the particle has not already been deemed to have changed compartment). We can now seek a value of ρ such that $E(0) = 4\Delta t$, and it is easy to see that we must have $\rho = 1/3$. To add a physical interpretation to this value, this has the effect that a walker deemed to have transitioned to a new compartment will be equally likely to be in either of the two boxes that comprise it (i.e. the probability of completing a walk in box 5 is equal to that of completing it in box 6, and similarly for boxes 1 and 2).

This result can be generalised to any even valued m, so that a random walk starts from either of the two central boxes i and $i+1$, it will be considered to have changed compartment with probability $1/3$ each time it enters the closer of the two central boxes of a neighbouring compartment (boxes $i-m+1$ and $i+m$) and with probability 1 if it enters the more distant of the central boxes (boxes $i-m$ and $i+m+1$). This then gives us the expected leaving time $E(0) = m^2\Delta t$ which we anticipated.

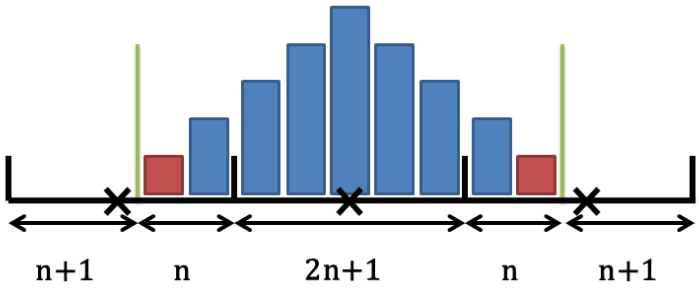

Figure B.5: An example of particle distributions for $m = 2n + 1 = 5$. Particles located in the boxes shown in red are the only ones that can change compartment by moving to the centre of a neighbouring compartment. The compartment centres are denoted with crosses, and the green lines shown the point beyond which a particle will be deemed to have left the compartment. The estimated occupation of each of these locations is $1/5^2 = 1/m^2$ of the total occupancy of the compartment, hence recovering the compartment level jump rates.

B.3.2 Implications for the interpolation

Having found a definition for compartment transitions for a random walker on a fine-grained lattice in the preceding section, we now use this definition to explain why linear interpolation is appropriate for matching mean master equations between scales. Let us use linear interpolation to approximate the likelihood of finding particles in a position to reach the centre of the neighbouring compartment.

When $m = 2n + 1$ is odd, this means being adjacent to the central box of a neighbouring compartment. The interpolation tells us that to expect a given particle to be present there with probability $1/m^2$, which then leads to matching the transition rates (note that we are only using half of the terms from the interpolation, as we are interested in a particle *from a different compartment* being close to the compartment centre, not in any particular particle being there). An example for $m = 5$ is shown in Figure B.5.

When $m = 2n$ is even, we must consider both the nearer of the two boxes that flank the centre of the compartment, and the box before it. The interpolation estimates that each particle will have a probability of $1/2m^2$ to be in the closer central box, and a probability of $3/2m^2$ to be in the box adjacent to it. We know that one third of the particles in this second group will count as transitioning if they

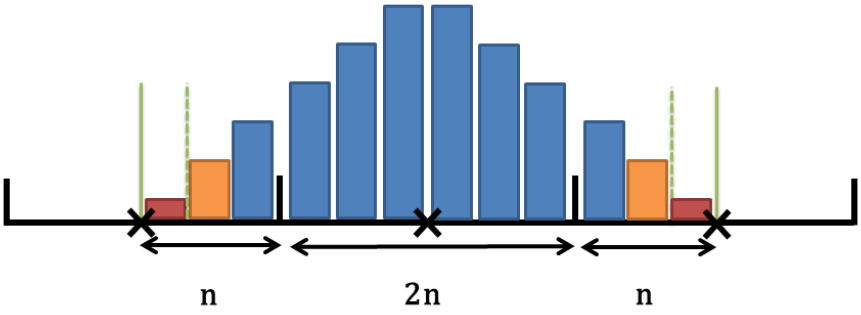

Figure B.6: An example of particle distributions for $m = 2n = 6$. Particles located in the boxes shown in red can change compartment by crossing the solid green line and moving beyond the centre of a neighbouring compartment; particles located in the orange boxes can cross the dashed green lines, and in doing so have a 1/3 chance of leaving the compartment. The interpolated occupations of each of the red and orange locations are $1/72 = 1/2m^2$ and $1/24 = 3/2m^2$ of the total occupancy of the compartment, respectively, hence (taking the 1/3 leaving probability for the orange location into account) we recover the expected compartment transition rate rate.

jump towards the centre of the compartment, and that all of those in the first group will, so together this matches the transition rates. An example for $m = 6$ is shown in Figure B.6.

We can therefore conclude that our linear interpolation at the boundary between compartments works because it is establishing the values that will be found further away, at the centres of the neighbouring compartments.

Appendix C

Appendices for Chapter 4

C.1 Outline of transition rate derivations

Transition rates between compartments can be obtained from standard first passage process results [55]. Consider a particle undergoing Brownian motion, starting from x_j, the residence point of the j^{th} compartment. The probability distribution for its position, $p(x,t)$, evolves in time following the diffusion equation,

$$\frac{\partial p}{\partial t} = D\frac{\partial^2 p}{\partial x^2}. \tag{C.1}$$

To calculate transition rates between compartments, we consider a first passage process on the interval $x \in [x_{j-1}, x_{j+1}]$ to determine the expected time until a particle starting from one residence point reaches one of its neighbouring residence points. For the diffusion equation, this means defining boundary conditions $p(x_{j-1},t) = p(x_{j+1},t) = 0$, and initial condition $p(x,0) = \delta(x - x_j)$. By applying a Laplace transform, it is possible to obtain the eventual hitting probabilities describing the likelihood of the particle leaving to either side of the interval [83]

$$\epsilon_-(x_j) = \frac{x_{j+1} - x_j}{x_{j+1} - x_{j-1}}, \tag{C.2}$$

$$\epsilon_+(x_j) = \frac{x_j - x_{j-1}}{x_{j+1} - x_{j-1}}. \tag{C.3}$$

Combining these values with the conditional mean exit times

$$\begin{aligned}\langle t(x_j)\rangle_- &= \frac{(x_j - x_{j-1})(2x_{j+1} - x_j - x_{j-1})}{6D}, &\text{(C.4)}\\ \langle t(x_j)\rangle_+ &= \frac{(x_{j+1} - x_j)(x_{j+1} + x_j - 2x_{j-1})}{6D}, &\text{(C.5)}\end{aligned}$$

we can then obtain the unconditional exit time

$$\begin{aligned}\langle t(x_j)\rangle &= \epsilon_-(x_j)\langle t(x_j)\rangle_- + \epsilon_+(x_j)\langle t(x_j)\rangle_+\\ &= \frac{(x_j - x_{j-1})(x_{j+1} - x_j)\left([2x_{j+1} - x_j - x_{j-1}] + [x_{j+1} + x_j - 2x_{j-1}]\right)}{6D(x_{j+1} - x_{j-1})}\\ &= \frac{(x_j - x_{j-1})(x_{j+1} - x_j)\,(3x_{j+1} - 3x_{j-1})}{6D(x_{j+1} - x_{j-1})}\\ &= \frac{(x_j - x_{j-1})(x_{j+1} - x_j)}{2D}. &\text{(C.6)}\end{aligned}$$

Inverting the unconditional exit times gives the unconditional exit rate, and by multiplying this value by the hitting probabilities we obtain the transition rates

$$\begin{aligned}T_j^- &= \frac{\epsilon_-(x_j)}{\langle t(x_j)\rangle} = \frac{2D}{(x_j - x_{j-1})(x_{j+1} - x_{j-1})} = \frac{Dh}{\Delta x_j m_j},\\ T_j^+ &= \frac{\epsilon_+(x_j)}{\langle t(x_j)\rangle} = \frac{2D}{(x_{j+1} - x_j)(x_{j+1} - x_{j-1})} = \frac{Dh}{\Delta x_{j+1} m_j}. &\text{(C.7)}\end{aligned}$$

It is also possible to derive these values using a finite element approach [52]. Transition rates for the two boundary compartments, $j = 1, K$, can be derived similarly using the reflection principle of Brownian motion. For example, if we define a notional point $x_0 = -x_2$, the unconditional expected exit time for the first compartment is

$$\langle t(x_1)\rangle = \frac{(x_1 - x_0)(x_2 - x_1)}{2D} = \frac{(x_1 + x_2)(x_2 - x_1)}{2D}. \quad \text{(C.8)}$$

Clearly $\epsilon_+(x_1) = 1$, hence we write

$$T_1^+ = \frac{Dh}{\Delta x_2 m_1}. \quad \text{(C.9)}$$

We can similarly derive T_K^- by reflecting x_{K-1} about $x = L$.

C.2 Variance of the last partially-excluding compartment

To recap Section 3.2.3, the variance master equations for a one-dimensional diffusion process are normally obtained by first writing

$$\begin{aligned}\frac{\mathrm{d}}{\mathrm{d}t}\sum^{\mathcal{N}} n_j^2 = \quad & T^+_{j-1} \quad \left(2\langle n_{j-1}n_j\rangle - \frac{2}{m_j}\langle n_{j-1}n_jn_j\rangle + M_{j-1} - \frac{1}{m_j}\langle n_{j-1}n_j\rangle\right) \\ + \quad & T^+_{j} \quad \left(-2\langle n_jn_j\rangle + \frac{2}{m_{j+1}}\langle n_jn_jn_{j+1}\rangle + M_{j} - \frac{1}{m_{j+1}}\langle n_jn_{j+1}\rangle\right) \\ + \quad & T^-_{j} \quad \left(-2\langle n_jn_j\rangle + \frac{2}{m_{j-1}}\langle n_{j-1}n_jn_j\rangle + M_{j} - \frac{1}{m_{j-1}}\langle n_{j-1}n_j\rangle\right) \\ + \quad & T^-_{j+1} \quad \left(2\langle n_jn_{j+1}\rangle - \frac{2}{m_j}\langle n_jn_jn_{j+1}\rangle + M_{j+1} - \frac{1}{m_j}\langle n_jn_{j+1}\rangle\right),\end{aligned}$$

then using $V_j = \langle n_j^2\rangle - M_j^2$.

For compartment p, this requires some modification, as particles are exchanged with all m compartments within the pseudo-compartment, so instead we write

$$\begin{aligned}\frac{\mathrm{d}}{\mathrm{d}t}\sum^{\mathcal{N}} n_p^2 = \quad & T^+_{p-1} \quad \left(2\langle n_{p-1}n_p\rangle - \frac{2}{m_p}\langle n_{p-1}n_pn_p\rangle + M_{p-1} - \frac{1}{m_p}\langle n_{p-1}n_p\rangle\right) \\ + \quad & \frac{T^+_p}{m}\sum_{i=p+1}^{p+m} \quad \left(-2\langle n_pn_p\rangle + \frac{2}{m_i}\langle n_pn_pn_i\rangle + M_{p} - \frac{1}{m_i}\langle n_pn_i\rangle\right) \\ + \quad & T^-_{p} \quad \left(-2\langle n_pn_p\rangle + \frac{2}{m_{p-1}}\langle n_{p-1}n_pn_p\rangle + M_{p} - \frac{1}{m_{p-1}}\langle n_{p-1}n_p\rangle\right) \\ + \quad & \sum_{i=p+1}^{p+m} T'^-_i \quad \left(2\langle n_pn_i\rangle - \frac{2}{m_p}\langle n_pn_pn_i\rangle + M_{i} - \frac{1}{m_p}\langle n_pn_i\rangle\right),\end{aligned}$$

where we have omitted to include the superscript (c) in the interests of brevity. Note that $m_{p-1} = m_p = m$, and that for $i > p$ we have $m_i = 1$. We use T'^- to denote jumps from the pseudo-compartment into compartment p. $T_i^\pm$ for all the transition

rates in the equation above, so after making these substitutions we can write

$$\begin{aligned}
\frac{\mathrm{d}}{\mathrm{d}t}\sum^{\mathcal{N}} n_p^2 = \quad & \frac{D}{(mh)^2} \quad \Bigg[2\langle n_{p-1}n_p\rangle - \frac{2}{m}\langle n_{p-1}n_pn_p\rangle + M_{p-1} - \frac{1}{m}\langle n_{p-1}n_p\rangle \\
& + \frac{1}{m}\sum_{i=p+1}^{p+m}\left(-2\langle n_pn_p\rangle + 2\langle n_pn_pn_i\rangle + M_p - \langle n_pn_i\rangle\right) \\
& + -2\langle n_pn_p\rangle + \frac{2}{m}\langle n_{p-1}n_pn_p\rangle + M_p - \frac{1}{m}\langle n_{p-1}n_p\rangle \\
& + \sum_{i=p+1}^{p+m}\left(2\langle n_pn_i\rangle - \frac{2}{m}\langle n_pn_pn_i\rangle + M_i - \frac{1}{m}\langle n_pn_i\rangle\right)\Bigg] \\
= \quad & \frac{D}{(mh)^2} \quad \Bigg[2\langle n_{p-1}n_p\rangle + M_{p-1} - \frac{1}{m}\langle n_{p-1}n_p\rangle \\
& + \frac{1}{m}\sum_{i=p+1}^{p+m}\left(-2\langle n_pn_p\rangle + M_p - \langle n_pn_i\rangle\right) \\
& + -2\langle n_pn_p\rangle + M_p - \frac{1}{m}\langle n_{p-1}n_p\rangle \\
& + \sum_{i=p+1}^{p+m}\left(2\langle n_pn_i\rangle + M_i - \frac{1}{m}\langle n_pn_i\rangle\right)\Bigg]. \qquad \text{(C.10)}
\end{aligned}$$

After consolidating terms and rearranging, this can be written

$$\begin{aligned}
\frac{\mathrm{d}}{\mathrm{d}t}\sum^{\mathcal{N}} n_p^2 = \quad & \frac{D}{(mh)^2} \quad \Bigg[2\frac{m-1}{m}\langle n_{p-1}n_p\rangle - 4\langle n_pn_p\rangle + 2\frac{m-1}{m}\sum_{i=p+1}^{p+m}\langle n_pn_i\rangle \\
& + M_{p-1} + 2M_p + \sum_{i=p+1}^{p+m} M_i\Bigg] \\
= \quad & \frac{D}{(mh)^2} \quad \Bigg[2\frac{m-1}{m}(V_{p-1,p} + M_{p-1}M_p) - 4(V_p + M_p^2) \qquad \text{(C.11)} \\
& + 2\frac{m-1}{m}\sum_{i=p+1}^{p+m}(V_{p,i} + M_pM_i) + M_{p-1} + 2M_p + \sum_{i=p+1}^{p+m} M_i\Bigg].
\end{aligned}$$

Recalling equation (4.22) from the main text, we can also write

$$\begin{aligned}
\frac{\mathrm{d}}{\mathrm{d}t}M_p^2 &= 2M_p\frac{\mathrm{d}M_p}{\mathrm{d}t} \\
&= 2M_p\frac{D}{(mh)^2}\left(M_{p-1} - 2M_p + \sum_{i=p+1}^{p+m} M_i\right). \qquad \text{(C.12)}
\end{aligned}$$

Subtracting equation (C.12) from equation (C.11), we arrive at

$$\begin{aligned}\frac{\mathrm{d}V_p^{(c)}}{\mathrm{d}t} = \frac{D}{(mh)^2} & \left[2\frac{m-1}{m}V_{p-1,p}^{(c)} - 4V_p^{(c)} + 2\frac{m-1}{m}v_{p,p+1}^{(c)}\right. \\ & + M_p^{(c)}\left(1-\frac{\mu_{p+1}^{(c)}}{m}\right) + M_p^{(c)}\left(1-\frac{M_{p-1}^{(c)}}{m}\right) \\ & \left. + M_{p-1}^{(c)}\left(1-\frac{M_p^{(c)}}{m}\right) + \mu_{p+1}^{(c)}\left(1-\frac{M_p^{(c)}}{m}\right)\right] \end{aligned} \tag{C.13}$$

where we have used the definitions from equation (4.27) to note

$$\mu_{p+1}^{(c)} = \sum_{i=p+1}^{p+m} M_i, \tag{C.14}$$

$$v_{p,p+1}^{(c)} = \sum_{i=p+1}^{p+m} v_{p,i}. \tag{C.15}$$

We complete this argument by noting that equation (C.13) matches equation (3.24) as expected, i.e.

$$\begin{aligned}\frac{\mathrm{d}V_p^{(m)}}{\mathrm{d}t} = \frac{D}{(mh)^2} & \left[2\frac{m-1}{m}V_{p-1,p}^{(m)} - 4V_p^{(m)} + 2\frac{m-1}{m}V_{p,p+1}^{(m)}\right. \\ & + M_p^{(m)}\left(1-\frac{M_{p+1}^{(m)}}{m}\right) + M_p^{(m)}\left(1-\frac{M_{p-1}^{(m)}}{m}\right) \\ & \left. + M_{p-1}^{(m)}\left(1-\frac{M_p^{(m)}}{m}\right) + M_{p+1}^{(m)}\left(1-\frac{M_p^{(m)}}{m}\right)\right]. \end{aligned} \tag{C.16}$$

C.3 Variance of the pseudo-compartment

Using equation (4.27), we can write

$$v_{p+1} = \sum_{i=p+1}^{p+m}\sum_{j=p+1}^{p+m} V_{i,j}^{(c)}. \tag{C.17}$$

We divide the terms from the right-hand side of equation (C.17) into three groupings: (i) variance terms, $V_j^{(c)}$ for $p < j \leq p+m$; (ii) covariance terms for adjacent compartments, $V_{j,j+1}^{(c)}$ for $p < j < p+m$; and (iii) covariance terms for non-adjacent

compartments, $V_{i,j}^{(c)}$ for $p < i, j \leq p + m$, such that $|i - j| > 1$. We consider each of these cases in Sections C.3.1, C.3.2, and C.3.3, respectively, then combine them in Section C.3.4 to obtain an expression for the evolution of the variance of particle number in the pseudo-compartment.

We treat V_{p+1} and $V_{p+1,p+2}$ separately as they are slightly different: compartment $p{+}1$ only exchanges particles with the fine jump rate with compartment $p{+}2$, whereas all the other compartments exchange with fine compartments to the left and right.

C.3.1 Variance terms

By standard reasoning, it is possible to obtain the following equation for the evolution of the variance in each of the compartments that collectively comprise the pseudo-compartment

$$\begin{aligned}
\frac{\mathrm{d}}{\mathrm{d}t}\sum^{\mathcal{N}} n_j^2 = \quad & \frac{1}{m}T_p^+ \quad \left(2\langle n_p n_j\rangle - \frac{2}{m_j}\langle n_p n_j n_j\rangle + M_p - \frac{1}{m_j}\langle n_p n_j\rangle\right) \\
+ \quad & T_{j-1}^+ \quad \left(2\langle n_{j-1} n_j\rangle - \frac{2}{m_j}\langle n_{j-1} n_j n_j\rangle + M_{j-1} - \frac{1}{m_j}\langle n_{j-1} n_j\rangle\right) \\
+ \quad & T_j^+ \quad \left(-2\langle n_j n_j\rangle + \frac{2}{m_{j+1}}\langle n_j n_j n_{j+1}\rangle + M_j - \frac{1}{m_{j+1}}\langle n_j n_{j+1}\rangle\right) \\
+ \quad & T_j^- \quad \left(-2\langle n_j n_j\rangle + \frac{2}{m_{j-1}}\langle n_{j-1} n_j n_j\rangle + M_j - \frac{1}{m_{j-1}}\langle n_{j-1} n_j\rangle\right) \\
+ \quad & T_j'^- \quad \left(-2\langle n_j n_j\rangle + \frac{2}{m_p}\langle n_p n_j n_j\rangle + M_j - \frac{1}{m_p}\langle n_p n_j\rangle\right) \\
+ \quad & T_{j+1}^- \quad \left(2\langle n_j n_{j+1}\rangle - \frac{2}{m_j}\langle n_j n_j n_{j+1}\rangle + M_{j+1} - \frac{1}{m_j}\langle n_j n_{j+1}\rangle\right),
\end{aligned}$$

where, as in Section C.2, we write T'^- to denote jumps from the pseudo-compartment into compartment p. It is useful to distinguish between the case $j = p{+}1$, in which the only leftward movements to be considered are jumps into the coarse compartment, and the cases $j > p{+}1$, where we must also account for short jumps into compartment $j - 1$.

When $j = p+1$, we set $T^+_{j-1} = T^-_j = 0$, and write

$$\begin{aligned}
\frac{\mathrm{d}}{\mathrm{d}t}\sum^{\mathcal{N}} n^2_{p+1} = \quad & \frac{1}{m}\frac{D}{(mh)^2}\left(2\langle n_p n_{p+1}\rangle - 2\langle n_p n_{p+1} n_{p+1}\rangle + M_p - \langle n_p n_{p+1}\rangle\right) \\
+ \quad & \frac{D}{h^2}\left(-2\langle n_{p+1} n_{p+1}\rangle + 2\langle n_{p+1} n_{p+1} n_{p+2}\rangle + M_{p+1} - \langle n_{p+1} n_{p+2}\rangle\right) \\
+ \quad & \frac{D}{(mh)^2}\left(-2\langle n_{p+1} n_{p+1}\rangle + \frac{2}{m}\langle n_p n_{p+1} n_{p+1}\rangle + M_{p+1} - \frac{1}{m}\langle n_p n_{p+1}\rangle\right) \\
+ \quad & \frac{D}{h^2}\left(2\langle n_{p+1} n_{p+2}\rangle - 2\langle n_{p+1} n_{p+1} n_{p+2}\rangle + M_{p+2} - \langle n_{p+1} n_{p+2}\rangle\right) \\
= \quad & \frac{1}{m}\frac{D}{(mh)^2}\left((V_{p,p+1} + M_p M_{p+1}) + M_p\right) \\
+ \quad & \frac{D}{h^2}\left(-2(V_{p+1} + M^2_{p+1}) + M_{p+1} - (V_{p+1,p+2} + M_{p+1} M_{p+2})\right) \\
+ \quad & \frac{D}{(mh)^2}\left(-2(V_{p+1} + M^2_{p+1}) + M_{p+1} - \frac{1}{m}(V_{p,p+1} + M_p M_{p+1})\right) \\
+ \quad & \frac{D}{h^2}\left((V_{p+1,p+2} + M_{p+1} M_{p+2}) + M_{p+2}\right),
\end{aligned}$$

where for ease of reading we have highlighted in red those terms that can immediately be cancelled out. From this expression, we subtract

$$\frac{\mathrm{d}M^2_{p+1}}{\mathrm{d}t} = 2M_{p+1}\left(\frac{1}{m}\frac{D}{(mh)^2}M_p - \left[\frac{D}{(mh)^2} + \frac{D}{h^2}\right]M_{p+1} + \frac{D}{h^2}M_{p+2}\right),$$

and obtain

$$\begin{aligned}
\frac{\mathrm{d}V_{p+1}}{\mathrm{d}t} = \quad & - \quad 2\left(\frac{D}{h^2} + \frac{D}{(mh)^2}\right)V_{p+1} \\
& + \quad \frac{D}{(mh)^2}M_{p+1}\left(1 - \frac{M_p}{m}\right) + \frac{D}{h^2}M_{p+1}\left(1 - M_{p+2}\right) \\
& + \quad \frac{1}{m}\frac{D}{(mh)^2}M_p\left(1 - M_{p+1}\right) + \frac{D}{h^2}M_{p+2}\left(1 - M_{p+1}\right).
\end{aligned} \tag{C.18}$$

Now, consider the case $j = p+2, \ldots, p+m$. In this case, we write

$$\begin{aligned}
\frac{\mathrm{d}}{\mathrm{d}t}\sum^{\mathcal{N}} n_j^2 = \quad & \frac{1}{m}\frac{D}{(mh)^2}\left(2\langle n_p n_j\rangle - 2\langle n_p n_j n_j\rangle + M_p - \langle n_p n_j\rangle\right) \\
+ \quad & \frac{D}{h^2}\left(2\langle n_{j-1} n_j\rangle - 2\langle n_{j-1} n_j n_j\rangle + M_{j-1} - \langle n_{j-1} n_j\rangle\right) \\
+ \quad & \frac{D}{h^2}\left(-2\langle n_j n_j\rangle + 2\langle n_j n_j n_{j+1}\rangle + M_j - \langle n_j n_{j+1}\rangle\right) \\
+ \quad & \frac{D}{h^2}\left(-2\langle n_j n_j\rangle + 2\langle n_{j-1} n_j n_j\rangle + M_j - \langle n_{j-1} n_j\rangle\right) \\
+ \quad & \frac{D}{(mh)^2}\left(-2\langle n_j n_j\rangle + \frac{2}{m}\langle n_p n_j n_j\rangle + M_j - \frac{1}{m_p}\langle n_p n_j\rangle\right) \\
+ \quad & \frac{D}{h^2}\left(2\langle n_j n_{j+1}\rangle - 2\langle n_j n_j n_{j+1}\rangle + M_{j+1} - \langle n_j n_{j+1}\rangle\right),
\end{aligned}$$

where we have again used red to denote terms that can be immediately cancelled. From this expression, we subtract

$$\frac{\mathrm{d}M_j^2}{\mathrm{d}t} = 2M_j\left(\frac{1}{m}\frac{D}{(mh)^2}M_p + \frac{D}{h^2}M_{j-1} - \left[\frac{D}{(mh)^2} + 2\frac{D}{h^2}\right]M_j + \frac{D}{h^2}M_{j+1}\right),$$

and hence obtain

$$\begin{aligned}
\frac{\mathrm{d}V_j^{(c)}}{\mathrm{d}t} = \quad & -2\left(2\frac{D}{h^2} + \frac{D}{(mh)^2}\right)V_j^{(c)} \\
& + \frac{D}{(mh)^2}M_j^{(c)}\left(1 - \frac{M_p^{(c)}}{m}\right) + \frac{D}{h^2}M_j^{(c)}\left(1 - M_{j-1}^{(c)}\right) + \frac{D}{h^2}M_j^{(c)}\left(1 - M_{j+1}^{(c)}\right) \\
& + \frac{1}{m}\frac{D}{(mh)^2}M_p^{(c)}\left(1 - M_j^{(c)}\right) + \frac{D}{h^2}M_{j-1}^{(c)}\left(1 - M_j^{(c)}\right) + \frac{D}{h^2}M_{j+1}^{(c)}\left(1 - M_j^{(c)}\right).
\end{aligned} \tag{C.19}$$

Together, equations (C.18) and (C.19) describe the evolution of variances for each of the fully-excluding compartments that collectively comprise the pseudo-compartment. We therefore turn our attention to the relevant covariance terms.

C.3.2 Covariances of adjacent compartments

For $p < j < p + m$, we can obtain by the usual method

$$\begin{aligned}
\frac{\mathrm{d}}{\mathrm{d}t}\sum^{\mathcal{N}} n_j n_{j+1} = \quad & \frac{1}{m}T_p^+ \quad \left(\langle n_p n_{j+1}\rangle - \frac{1}{m_j}\langle n_p n_j n_{j+1}\rangle\right) \\
& +\frac{1}{m}T_p^+ \quad \left(\langle n_p n_j\rangle - \frac{1}{m_{j+1}}\langle n_p n_j n_{j+1}\rangle\right) \\
& +T_{j-1}^+ \quad \left(\langle n_{j-1} n_{j+1}\rangle - \frac{1}{m_j}\langle n_{j-1} n_j n_{j+1}\rangle\right) \\
& +T_j^+ \quad \left(\langle n_j n_j\rangle - \frac{1}{m_{j+1}}\langle n_j n_j n_{j+1}\rangle - \langle n_j n_{j+1}\rangle\right. \\
& \qquad \left. +\frac{1}{m_{j+1}}\langle n_j n_{j+1} n_{j+1}\rangle - M_j + \frac{1}{m_{j+1}}\langle n_j n_{j+1}\rangle\right) \\
& +T_{j+1}^+ \quad \left(-\langle n_j n_{j+1}\rangle + \frac{1}{m_{j+2}}\langle n_j n_{j+1} n_{j+2}\rangle\right) \\
& +T_j^- \quad \left(-\langle n_j n_{j+1}\rangle + \frac{1}{m_{j-1}}\langle n_{j-1} n_j n_{j+1}\rangle\right) \\
& +T_j'^- \quad \left(-\langle n_j n_{j+1}\rangle + \frac{1}{m_p}\langle n_p n_j n_{j+1}\rangle\right) \\
& +T_{j+1}^- \quad \left(\langle n_{j+1} n_{j+1}\rangle - \frac{1}{m_j}\langle n_j n_{j+1} n_{j+1}\rangle - \langle n_j n_{j+1}\rangle\right. \\
& \qquad \left. +\frac{1}{m_j}\langle n_j n_j n_{j+1}\rangle - M_{j+1} + \frac{1}{m_j}\langle n_j n_{j+1}\rangle\right) \\
& +T_{j+1}'^- \quad \left(-\langle n_j n_{j+1}\rangle + \frac{1}{m_p}\langle n_p n_j n_{j+1}\rangle\right) \\
& +T_{j+2}^- \quad \left(\langle n_j n_{j+2}\rangle - \frac{1}{m_{j+1}}\langle n_j n_{j+1} n_{j+2}\rangle\right). \qquad \text{(C.20)}
\end{aligned}$$

We begin by considering the case $j = p+1$, setting $T^+_{j-1} = T^-_j = 0$, and writing

$$\begin{aligned}
\frac{\mathrm{d}}{\mathrm{d}t}\sum^{\mathcal{N}} n_{p+1}n_{p+2} = \quad & \frac{1}{m}\frac{D}{(mh)^2} && \Big(\langle n_p n_{p+2}\rangle - \langle n_p n_{p+1} n_{p+2}\rangle\Big) \\
& + \frac{1}{m}\frac{D}{(mh)^2} && \Big(\langle n_p n_{p+1}\rangle - \langle n_p n_{p+1} n_{p+2}\rangle\Big) \\
& + \frac{D}{h^2} && \Big(\langle n_{p+1} n_{p+1}\rangle - \langle n_{p+1} n_{p+1} n_{p+2}\rangle - \langle n_{p+1} n_{p+2}\rangle \\
& && + \langle n_{p+1} n_{p+2} n_{p+2}\rangle - M_{p+1} + \langle n_{p+1} n_{p+2}\rangle\Big) \\
& + \frac{D}{h^2} && \big(-\langle n_{p+1} n_{p+2}\rangle + \langle n_{p+1} n_{p+2} n_{p+3}\rangle\big) \\
& + \frac{D}{(mh)^2} && \Big(-\langle n_{p+1} n_{p+2}\rangle + \frac{1}{m}\langle n_p n_{p+1} n_{p+2}\rangle\Big) \\
& + \frac{D}{h^2} && \Big(\langle n_{p+2} n_{p+2}\rangle - \langle n_{p+1} n_{p+2} n_{p+2}\rangle - \langle n_{p+1} n_{p+2}\rangle \\
& && + \langle n_{p+1} n_{p+1} n_{p+2}\rangle - M_{p+2} + \langle n_{p+1} n_{p+2}\rangle\Big) \\
& + \frac{D}{(mh)^2} && \Big(-\langle n_{p+1} n_{p+2}\rangle + \frac{1}{m}\langle n_p n_{p+1} n_{p+2}\rangle\Big) \\
& + \frac{D}{h^2} && \Big(\langle n_{p+1} n_{p+3}\rangle - \langle n_{p+1} n_{p+2} n_{p+3}\rangle\Big) \\
= \quad & -\left(2\frac{D}{(mh)^2} + \frac{D}{h^2}\right) && \langle n_{p+1} n_{p+2}\rangle + \frac{D}{h^2}\langle n_{p+2} n_{p+2}\rangle + \frac{D}{h^2}\langle n_{p+1} n_{p+3}\rangle \\
& + \frac{D}{h^2} && \langle n_{p+1} n_{p+1}\rangle + \frac{1}{m}\frac{D}{(mh)^2}\langle n_p n_{p+1}\rangle \\
& + \frac{1}{m}\frac{D}{(mh)^2} && \langle n_p n_{p+2}\rangle - \frac{D}{h^2}M_{p+1} - \frac{D}{h^2}M_{p+2}, \qquad \text{(C.21)}
\end{aligned}$$

where once again we use red font to highlight those terms that can be immediately cancelled. From this expression we subtract

$$\begin{aligned}
\frac{\mathrm{d}}{\mathrm{d}t}(M_{p+1}M_{p+2}) \quad = \quad & M_{p+1}\left(\frac{1}{m}\frac{D}{(mh)^2}M_p + \frac{D}{h^2}M_{p+1} - \left[2\frac{D}{h^2} + \frac{D}{(mh)^2}\right]M_{p+2} + \frac{D}{h^2}M_{p+3}\right) \\
& + \left(\frac{1}{m}\frac{D}{(mh)^2}M_p - \left[\frac{D}{h^2} + \frac{D}{(mh)^2}\right]M_{p+1} + \frac{D}{h^2}M_{p+2}\right)M_{p+2}, \qquad \text{(C.22)}
\end{aligned}$$

and hence obtain

$$\begin{aligned}\frac{\mathrm{d}V^{(c)}_{p+1,p+2}}{\mathrm{d}t} = &- \left(2\frac{D}{(mh)^2}+\frac{D}{h^2}\right)V^{(c)}_{p+1,p+2}+\frac{D}{h^2}V^{(c)}_{p+2}+\frac{D}{h^2}V^{(c)}_{p+1,p+3}\\ &+ \frac{D}{h^2}V^{(c)}_{p+1}+\frac{1}{m}\frac{D}{(mh)^2}V^{(c)}_{p,p+1}+\frac{1}{m}\frac{D}{(mh)^2}V^{(c)}_{p,p+2}\\ &- \frac{D}{h^2}M^{(c)}_{p+1}\left(1-M^{(c)}_{p+2}\right)-\frac{D}{h^2}M^{(c)}_{p+2}\left(1-M^{(c)}_{p+1}\right). \qquad \text{(C.23)}\end{aligned}$$

For the cases where $(p+1)<j\leq(p+m-1)$, we write

$$\begin{aligned}\frac{\mathrm{d}}{\mathrm{d}t}\sum^{\mathcal{N}} n_j n_{j+1} = &\quad \frac{1}{m}\frac{D}{(mh)^2} && \left(\langle n_p n_{j+1}\rangle - \langle n_p n_j n_{j+1}\rangle\right)\\ &+\frac{1}{m}\frac{D}{(mh)^2} && \left(\langle n_p n_j\rangle - \langle n_p n_j n_{j+1}\rangle\right)\\ &+\frac{D}{h^2} && \left(\langle n_{j-1} n_{j+1}\rangle - \langle n_{j-1} n_j n_{j+1}\rangle\right)\\ &+\frac{D}{h^2} && \Big(\langle n_j n_j\rangle - \langle n_j n_j n_{j+1}\rangle - \langle n_j n_{j+1}\rangle\\ & && + \langle n_j n_{j+1} n_{j+1}\rangle - M_j + \langle n_j n_{j+1}\rangle\Big)\\ &+\frac{D}{h^2} && \left(-\langle n_j n_{j+1}\rangle + \langle n_j n_{j+1} n_{j+2}\rangle\right)\\ &+\frac{D}{h^2} && \left(-\langle n_j n_{j+1}\rangle + \langle n_{j-1} n_j n_{j+1}\rangle\right)\\ &+\frac{D}{(mh)^2} && \left(-\langle n_j n_{j+1}\rangle + \frac{1}{m}\langle n_p n_j n_{j+1}\rangle\right)\\ &+\frac{D}{h^2} && \Big(\langle n_{j+1} n_{j+1}\rangle - \langle n_j n_{j+1} n_{j+1}\rangle - \langle n_j n_{j+1}\rangle\\ & && + \langle n_j n_j n_{j+1}\rangle - M_{j+1} + \langle n_j n_{j+1}\rangle\Big)\\ &+\frac{D}{(mh)^2} && \left(-\langle n_j n_{j+1}\rangle + \frac{1}{m}\langle n_p n_j n_{j+1}\rangle\right)\\ &+\frac{D}{h^2} && \left(\langle n_j n_{j+2}\rangle - \langle n_j n_{j+1} n_{j+2}\rangle\right) \qquad \text{(C.24)}\\ = &-\left(2\frac{D}{(mh)^2}+2\frac{D}{h^2}\right) && \langle n_j n_{j+1}\rangle + \frac{D}{h^2}\langle n_{j+1} n_{j+1}\rangle + \frac{D}{h^2}\langle n_j n_{j+2}\rangle\\ &+\frac{D}{h^2} && \langle n_j n_j\rangle + \frac{1}{m}\frac{D}{(mh)^2}\langle n_p n_j\rangle + \frac{1}{m}\frac{D}{(mh)^2}\langle n_p n_{j+1}\rangle\\ &+\frac{D}{h^2} && \langle n_{j-1} n_{j+1}\rangle - \frac{D}{h^2}M_j - \frac{D}{h^2}M_{j+1}, \qquad \text{(C.25)}\end{aligned}$$

where the terms in red can be immediately cancelled. From this expression we subtract

$$\begin{aligned}\frac{\mathrm{d}}{\mathrm{d}t}(M_jM_j) &= M_j\left(\frac{1}{m}\frac{D}{(mh)^2}M_p+\frac{D}{h^2}M_j-\left[2\frac{D}{h^2}+\frac{D}{(mh)^2}\right]M_{j+1}+\frac{D}{h^2}M_{j+2}\right)\\ &+\left(\frac{1}{m}\frac{D}{(mh)^2}M_p+\frac{D}{h^2}M_{j-1}-\left[2\frac{D}{h^2}+\frac{D}{(mh)^2}\right]M_j+\frac{D}{h^2}M_{j+1}\right)M_{j+1},\end{aligned}$$

and arrive at

$$\begin{aligned}\frac{\mathrm{d}V^{(c)}_{j,j+1}}{\mathrm{d}t} = &-\left(2\frac{D}{(mh)^2}+2\frac{D}{h^2}\right)V^{(c)}_{j,j+1}+\frac{D}{h^2}V^{(c)}_{j+1}+\frac{D}{h^2}V^{(c)}_{j,j+2}\\ &+\frac{D}{h^2}V^{(c)}_{j}+\frac{D}{h^2}V^{(c)}_{j-1,j+1}+\frac{1}{m}\frac{D}{(mh)^2}V^{(c)}_{p,j}+\frac{1}{m}\frac{D}{(mh)^2}V^{(c)}_{p,j+1}\\ &-\frac{D}{h^2}M^{(c)}_j\left(1-M^{(c)}_{j+1}\right)-\frac{D}{h^2}M^{(c)}_{j+1}\left(1-M^{(c)}_j\right).\end{aligned}\tag{C.26}$$

Equations (C.23) and (C.26) describe the evolution of covariances between adjacent compartments. The final case to consider is the evolution of covariances between non-adjacent compartments within the pseudo-compartment.

C.3.3 Covariances of non-adjacent compartments

The derivations for used for covariances of non-adjacent compartments are extremely similar to those applied to the covariances of adjacent compartments in Section C.3.2, so we do not show it here. In general, when $p < i, j \leq p + m$, such that $|i - j| > 1$, we can write

$$\begin{aligned}\frac{\mathrm{d}V^{(c)}_{i,j}}{\mathrm{d}t} &= -\left(4\frac{D}{h^2}+2\frac{D}{(mh)^2}\right)V^{(c)}_{i,j}+\frac{1}{m}\frac{D}{(mh)^2}V^{(c)}_{p,i}+\frac{1}{m}\frac{D}{(mh)^2}V^{(c)}_{p,j}\\ &+\frac{D}{h^2}V^{(c)}_{i-1,j}+\frac{D}{h^2}V^{(c)}_{i,j-1}+\frac{D}{h^2}V^{(c)}_{i+1,j}+\frac{D}{h^2}V^{(c)}_{i,j+1}.\end{aligned}\tag{C.27}$$

The only special case is when $i = p+1$ (or equivalently $j = p+1$, since $V_{i,j} = V_{j,i}$) in which case we write

$$\begin{aligned}\frac{\mathrm{d}V^{(c)}_{p+1,j}}{\mathrm{d}t} &= -\left(3\frac{D}{h^2} + 2\frac{D}{(mh)^2}\right)V^{(c)}_{p+1,j} + \frac{1}{m}\frac{D}{(mh)^2}V^{(c)}_{p,p+1} + \frac{1}{m}\frac{D}{(mh)^2}V^{(c)}_{p,j} \\ &\quad + \frac{D}{h^2}V^{(c)}_{p+1,j-1} + \frac{D}{h^2}V^{(c)}_{p+2,j} + \frac{D}{h^2}V^{(c)}_{p+1,j+1}. \end{aligned} \tag{C.28}$$

We now have variance and covariance master equations for all compartments within the pseudo-compartment. By combining all of these equations, we can find an equation for the evolution of the variance of particle number in the pseudo-compartment.

C.3.4 Combining variance and covariance equations

Recall that we have defined

$$v^{(c)}_{p+1} = \sum_{i=p+1}^{p+m}\sum_{j=p+1}^{p+m} V^{(c)}_{i,j}, \tag{C.29}$$

and hence

$$\frac{\mathrm{d}v^{(c)}_{p+1}}{\mathrm{d}t} = \sum_{i=p+1}^{p+m}\sum_{j=p+1}^{p+m} \frac{\mathrm{d}V^{(c)}_{i,j}}{\mathrm{d}t}. \tag{C.30}$$

We therefore combine the results of the three preceding subsections to obtain:

$$\begin{aligned}\frac{\mathrm{d}v_{p+1}}{\mathrm{d}t} &= -2\frac{D}{(mh)^2}v_{p+1} - 2\frac{D}{h^2}\sum_{i=p+1}^{p+m} V_{i,p+m} \\ &\quad + \frac{1}{m}\frac{D}{(mh)^2}\sum_{i=p+1}^{p+m-1} V_{p,i} + \frac{1}{m}\frac{D}{(mh)^2}\sum_{i=p+2}^{p+m} V_{p,i} \\ &\quad + 2\frac{D}{h^2}\sum_{i=p+1}^{p+m-1} V_{i,p+m+1} \\ &\quad + \frac{D}{(mh)^2}M_p\left(1 - \frac{\mu_{p+1}}{m}\right) + \frac{D}{(mh)^2}\mu_{p+1}\left(1 - \frac{M_p}{m}\right) \\ &\quad + \frac{D}{h^2}M_{p+m}\left(1 - M_{p+m+1}\right) + \frac{D}{h^2}M_{p+m+1}\left(1 - M_{p+m}\right). \end{aligned} \tag{C.31}$$

Using similar assumptions to those we used in Section 3.3.3, we assume that

$$-2\frac{D}{h^2}\sum_{i=p+1}^{p+m} V_{i,p+m} \approx -2\frac{D}{(mh)^2}v_{p+1}, \tag{C.32}$$

$$2\frac{D}{h^2}\sum_{i=p+1}^{p+m-1} V_{i,p+m+1} \approx -2\frac{m-1}{m}\frac{D}{(mh)^2}v_{p+1,p+2}, \tag{C.33}$$

and

$$\begin{aligned}\frac{D}{h^2}M_{p+m}\left(1-M_{p+m+1}\right)+\frac{D}{h^2}M_{p+m+1}\left(1-M_{p+m}\right) &\approx \frac{D}{(mh)^2}\mu_{p+1}\left(1-\frac{\mu_{p+2}}{m}\right)\\ &\quad+\frac{D}{(mh)^2}\mu_{p+2}\left(1-\frac{\mu_{p+1}}{m}\right).\end{aligned}$$

Using these approximations, we can write

$$\begin{aligned}\frac{\mathrm{d}v_{p+1}^{(c)}}{\mathrm{d}t} &\approx \frac{D}{(mh)^2}\left[2\frac{m-1}{m}v_{p,p+1}^{(c)}-4v_{p+1}^{(c)}+2\frac{m-1}{m}v_{p+1,p+2}^{(c)}\right.\\ &\quad+M_{p+1}^{(c)}\left(1-\frac{\mu_{p+2}^{(c)}}{m}\right)+\mu_{p+1}^{(c)}\left(1-\frac{M_p^{(c)}}{m}\right)\\ &\quad\left.+M_p^{(c)}\left(1-\frac{\mu_{p+1}^{(c)}}{m}\right)+\mu_{p+2}^{(c)}\left(1-\frac{\mu_{p+1}^{(c)}}{m}\right)\right],\end{aligned} \tag{C.34}$$

which matches the expected general form equation (3.24):

$$\begin{aligned}\frac{\mathrm{d}V_j^{(c)}}{\mathrm{d}t} &= \frac{D}{(mh)^2}\left[2\frac{m-1}{m}V_{j-1,j}^{(c)}-4V_j^{(c)}+2\frac{m-1}{m}V_{j,j+1}^{(c)}\right.\\ &\quad+M_j\left(1-\frac{M_{j+1}^{(c)}}{m}\right)+M_j^{(c)}\left(1-\frac{M_{j-1}^{(c)}}{m}\right)\\ &\quad\left.+M_{j-1}^{(c)}\left(1-\frac{M_j^{(c)}}{m}\right)+M_{j+1}^{(c)}\left(1-\frac{M_j^{(c)}}{m}\right)\right].\end{aligned} \tag{C.35}$$

Having matched the variance master equations for the pseudo-compartment to the variance master equations of the partially-excluding system, we consider as a final case the covariance between the final partially-excluding compartment and the pseudo-compartment.

C.4 Covariance between the partially-excluding compartment and the pseudo-compartment

In equation (C.15), we noted that the covariance between particle numbers in compartment p and the pseudo-compartment is given by

$$v^{(c)}_{p,p+1} = \sum_{j=p+1}^{p+m} V^{(c)}_{p,j}. \tag{C.36}$$

To find an equation describing the evolution of $v^{(c)}_{p,p+1}$ in time, we consider two cases: (i) $V^{(c)}_{p,p+1}$; and (ii) $V^{(c)}_{p,j}$, $p+1 < j \leq p+m$.

C.4.1 Case $V^{(c)}_{p,p+1}$

Using the same methods employed earlier in these appendices, we begin with

$$\begin{aligned}
\frac{\mathrm{d}}{\mathrm{d}t}\sum^{\mathcal{N}} n_p n_{p+1} = \quad & T^+_{p-1} \quad \left(\langle n_{p-1}n_{p+1}\rangle - \frac{1}{m_p}\langle n_{p-1}n_p n_{p+1}\rangle\right) \\
+ \quad & \frac{1}{m}T^+_p \quad \left(\langle n_p n_p\rangle - \frac{1}{m_{p+1}}\langle n_p n_p n_{p+1}\rangle - \langle n_p n_{p+1}\rangle \right. \\
& \qquad \left. + \frac{1}{m_{p+1}}\langle n_p n_{p+1} n_{p+1}\rangle - M_p + \frac{1}{m_{p+1}}\langle n_p n_{p+1}\rangle\right) \\
+ \quad & \frac{1}{m}T^+_p \quad \sum_{i=p+2}^{p+m}\left(-\langle n_p n_{p+1}\rangle + \frac{1}{m_i}\langle n_p n_{p+1} n_i\rangle\right) \\
+ \quad & T^+_{p+1} \quad \left(-\langle n_p n_{p+1}\rangle + \frac{1}{m_{p+2}}\langle n_p n_{p+1} n_{p+2}\rangle\right) \\
+ \quad & T^-_p \quad \left(-\langle n_p n_{p+1}\rangle + \frac{1}{m_{p-1}}\langle n_{p-1} n_p n_{p+1}\rangle\right) \\
+ \quad & T^-_{p+1} \quad \left(-\langle n_p n_{p+1}\rangle + \frac{1}{m_p}\langle n_p n_p n_{p+1}\rangle + \langle n_{p+1} n_{p+1}\rangle \right. \\
& \qquad \left. - \frac{1}{m_p}\langle n_p n_{p+1} n_{p+1}\rangle - M_{p+1} + \frac{1}{m_p}\langle n_p n_{p+1}\rangle\right) \\
+ \quad & T^-_{p+2} \quad \left(\langle n_p n_{p+2}\rangle - \frac{1}{m_{p+1}}\langle n_p n_{p+1} n_{p+2}\rangle\right) \\
+ \sum_{i=p+2}^{p+m} \quad & T'^-_i \quad \left(\langle n_{p+1} n_i\rangle - \frac{1}{m_p}\langle n_p n_{p+1} n_i\rangle\right).
\end{aligned} \tag{C.37}$$

Substituting in the appropriate jump rates and capacities, this equation becomes

$$\begin{aligned}
\frac{\mathrm{d}}{\mathrm{d}t}\sum^{\mathcal{N}} n_p n_{p+1} = \quad & \frac{D}{(mh)^2} \quad \Big(\langle n_{p-1}n_{p+1}\rangle - \frac{1}{m}\langle n_{p-1}n_p n_{p+1}\rangle\Big) \\
+ \quad & \frac{1}{m}\frac{D}{(mh)^2} \quad \Big(\langle n_p n_p\rangle - \langle n_p n_p n_{p+1}\rangle - \langle n_p n_{p+1}\rangle \\
& \qquad\qquad + \langle n_p n_{p+1} n_{p+1}\rangle - M_p + \langle n_p n_{p+1}\rangle\Big) \\
+ \quad & \frac{1}{m}\frac{D}{(mh)^2} \quad \sum_{i=p+2}^{p+m}\Big(-\langle n_p n_{p+1}\rangle + \langle n_p n_{p+1} n_i\rangle\Big) \\
+ \quad & \frac{D}{h^2} \quad \Big(-\langle n_p n_{p+1}\rangle + \langle n_p n_{p+1} n_{p+2}\rangle\Big) \\
+ \quad & \frac{D}{(mh)^2} \quad \Big(-\langle n_p n_{p+1}\rangle + \frac{1}{m}\langle n_{p-1} n_p n_{p+1}\rangle\Big) \\
+ \quad & \frac{D}{(mh)^2} \quad \Big(-\langle n_p n_{p+1}\rangle + \frac{1}{m}\langle n_p n_p n_{p+1}\rangle + \langle n_{p+1} n_{p+1}\rangle \\
& \qquad\qquad - \frac{1}{m}\langle n_p n_{p+1} n_{p+1}\rangle - M_{p+1} + \frac{1}{m}\langle n_p n_{p+1}\rangle\Big) \\
+ \quad & \frac{D}{h^2} \quad \Big(\langle n_p n_{p+2}\rangle - \langle n_p n_{p+1} n_{p+2}\rangle\Big) \\
+ \sum_{i=p+2}^{p+m} \quad & \frac{D}{(mh)^2} \quad \Big(\langle n_{p+1} n_i\rangle - \frac{1}{m}\langle n_p n_{p+1} n_i\rangle\Big)
\end{aligned} \tag{C.38}$$

where once again we have highlighted in red those terms which can be cancelled out immediately. Consolidating the remaining terms, the equation can be written

$$\begin{aligned}
\frac{\mathrm{d}}{\mathrm{d}t}\sum^{\mathcal{N}} n_p n_{p+1} = \quad & \frac{D}{(mh)^2} \quad \langle n_{p-1}n_{p+1}\rangle + \frac{D}{(mh)^2}\langle n_{p+1}n_{p+1}\rangle + \frac{D}{h^2}\langle n_p n_{p+2}\rangle \\
- \quad & \frac{1}{m}\frac{D}{(mh)^2} \quad M_p - \left(2\frac{m-1}{m}\frac{D}{(mh)^2} + \frac{D}{(mh)^2} + \frac{D}{h^2}\right)\langle n_p n_{p+1}\rangle \\
& + \quad \sum_{i=p+2}^{p+m} \frac{D}{(mh)^2}\langle n_{p+1} n_i\rangle + \frac{1}{m}\frac{D}{(mh)^2}\langle n_p n_p\rangle - \frac{D}{(mh)^2} M_{p+1},
\end{aligned} \tag{C.39}$$

or, when rewritten in terms of means, variances and covariances:

$$\begin{aligned}\frac{\mathrm{d}}{\mathrm{d}t}\sum^{\mathcal{N}} n_p n_{p+1} = \quad & \frac{D}{(mh)^2} \quad (V_{p-1,p+1} + M_{p-1}M_{p+1}) + \frac{D}{(mh)^2}(V_{p+1} + M_{p+1}^2) \\ & + \quad \frac{D}{h^2}(V_{p,p+2} + M_p M_{p+2}) + \frac{1}{m}\frac{D}{(mh)^2}(V_p + M_p^2) \\ & - \quad \frac{1}{m}\frac{D}{(mh)^2}M_p - \frac{D}{(mh)^2}M_{p+1} \\ & - \quad \left(2\frac{m-1}{m}\frac{D}{(mh)^2} + \frac{D}{(mh)^2} + \frac{D}{h^2}\right)(V_{p,p+1} + M_p M_{p+1}) \\ & + \quad \sum_{i=p+2}^{p+m} \frac{D}{(mh)^2}(V_{p+1,i} + M_{p+1}M_i). \end{aligned} \tag{C.40}$$

From this equation, we subtract

$$\begin{aligned}\frac{\mathrm{d}}{\mathrm{d}t}(M_p M_{p+1}) &= \frac{\mathrm{d}M_p}{\mathrm{d}t}M_{p+1} + M_p\frac{\mathrm{d}M_{p+1}}{\mathrm{d}t}, \\ &= \left(\frac{D}{(mh)^2}M_{p-1} - 2\frac{D}{(mh)^2}M_p + \sum_{i=p+1}^{p+m}\frac{D}{(mh)^2}M_i\right)M_{p+1} \\ &\quad + M_p\left(\frac{1}{m}\frac{D}{(mh)^2}M_p - \left(\frac{D}{(mh)^2} + \frac{D}{h^2}\right)M_{p+1} + \frac{D}{h^2}M_{p+2}\right),\end{aligned} \tag{C.41}$$

to arrive at

$$\begin{aligned}\frac{\mathrm{d}V_{p,p+1}^{(c)}}{\mathrm{d}t} = \quad & \frac{D}{(mh)^2} \quad V_{p-1,p+1}^{(c)} + \frac{D}{h^2}V_{p,p+2}^{(c)} + \frac{1}{m}\frac{D}{(mh)^2}V_p^{(c)} + \sum_{i=p+1}^{p+m}\frac{D}{(mh)^2}V_{p+1,i}^{(c)} \\ & - \quad \frac{1}{m}\frac{D}{(mh)^2}M_p^{(c)}\left(1 - M_{p+1}^{(c)}\right) - \frac{D}{(mh)^2}M_{p+1}^{(c)}\left(1 - \frac{M_p^{(c)}}{m}\right) \\ & - \quad \left(2\frac{m-1}{m}\frac{D}{(mh)^2} + \frac{D}{(mh)^2} + \frac{D}{h^2}\right)V_{p,p+1}^{(c)}.\end{aligned}$$

C.4.2 Case $V_{p,j}^{(c)}$, where $(p+1) < j \leq (p+m)$

By standard techniques, we initially obtain

$$\begin{aligned}
\frac{\mathrm{d}}{\mathrm{d}t}\sum^{\mathcal{N}} n_p n_j = \quad & T_{p-1}^{+} \quad \left(\langle n_{p-1}n_j\rangle - \frac{1}{m_p}\langle n_{p-1}n_p n_j\rangle\right) \\
+ \quad & \frac{1}{m}T_p^{+} \quad \left(\langle n_p n_p\rangle - \frac{1}{m_j}\langle n_p n_p n_j\rangle - \langle n_p n_j\rangle\right. \\
& \qquad \left. + \frac{1}{m_j}\langle n_p n_j n_j\rangle - M_p + \frac{1}{m_j}\langle n_p n_j\rangle\right) \\
+ \quad & \frac{1}{m}T_p^{+} \quad \sum_{i=p+1, i\neq j}^{p+m}\left(-\langle n_p n_j\rangle + \frac{1}{m_i}\langle n_p n_j n_i\rangle\right) \\
+ \quad & T_{j-1}^{+} \quad \left(\langle n_{j-1}n_p\rangle - \frac{1}{m_j}\langle n_{j-1}n_p n_j\rangle\right) \\
+ \quad & T_{j}^{+} \quad \left(-\langle n_p n_j\rangle + \frac{1}{m_{j+1}}\langle n_p n_j n_{j+1}\rangle\right) \\
+ \quad & T_{p}^{-} \quad \left(-\langle n_p n_j\rangle + \frac{1}{m_{p-1}}\langle n_{p-1}n_p n_j\rangle\right) \\
+ \quad & T_{j}^{-} \quad \left(-\langle n_p n_j\rangle + \frac{1}{m_{j-1}}\langle n_p n_{j-1}n_j\rangle\right) \\
+ \quad & T_{j}'^{-} \quad \left(-\langle n_p n_j\rangle + \frac{1}{m_p}\langle n_p n_p n_j\rangle + \langle n_j n_j\rangle\right. \\
& \qquad \left. - \frac{1}{m_p}\langle n_p n_j n_j\rangle - M_j + \frac{1}{m_p}\langle n_p n_j\rangle\right) \\
+ \sum_{i=p+1, i\neq j}^{p+m} \quad & T_{i}'^{-} \quad \left(\langle n_j n_i\rangle - \frac{1}{m_p}\langle n_p n_j n_i\rangle\right) \\
+ \quad & T_{j+1}^{-} \quad \left(\langle n_p n_{j+1}\rangle - \frac{1}{m_j}\langle n_p n_j n_{j+1}\rangle\right). \qquad \text{(C.42)}
\end{aligned}$$

Substituting in transition rates and capacities, this becomes

$$\begin{aligned}
\frac{\mathrm{d}}{\mathrm{d}t}\sum^{\mathcal{N}} n_p n_j = \quad & \frac{D}{(mh)^2} && \left(\langle n_{p-1}n_j\rangle - \frac{1}{m}\langle n_{p-1}n_p n_j\rangle\right) \\
+ \quad & \frac{1}{m}\frac{D}{(mh)^2} && (\langle n_p n_p\rangle - \langle n_p n_p n_j\rangle - \langle n_p n_j\rangle \\
& && + \langle n_p n_j n_j\rangle - M_p + \langle n_p n_j\rangle) \\
+ \quad & \frac{1}{m}\frac{D}{(mh)^2} && \sum_{i=p+1, i\neq j}^{p+m} (-\langle n_p n_j\rangle + \langle n_p n_j n_i\rangle) \\
+ \quad & \frac{D}{h^2} && (\langle n_{j-1}n_p\rangle - \langle n_p n_{j-1} n_j\rangle) \\
+ \quad & \frac{D}{h^2} && (-\langle n_p n_j\rangle + \langle n_p n_j n_{j+1}\rangle) \\
+ \quad & \frac{D}{(mh)^2} && \left(-\langle n_p n_j\rangle + \frac{1}{m}\langle n_{p-1}n_p n_j\rangle\right) \\
+ \quad & \frac{D}{h^2} && (-\langle n_p n_j\rangle + \langle n_p n_{j-1} n_j\rangle) \\
+ \quad & \frac{D}{(mh)^2} && \left(-\langle n_p n_j\rangle + \frac{1}{m}\langle n_p n_p n_j\rangle + \langle n_j n_j\rangle\right. \\
& && \left. - \frac{1}{m}\langle n_p n_j n_j\rangle - M_j + \frac{1}{m}\langle n_p n_j\rangle\right) \\
+ \sum_{i=p+1, i\neq j}^{p+m} \quad & \frac{D}{(mh)^2} && \left(\langle n_j n_i\rangle - \frac{1}{m}\langle n_p n_j n_i\rangle\right) \\
+ \quad & \frac{D}{h^2} && (\langle n_p n_{j+1}\rangle - \langle n_p n_j n_{j+1}\rangle)\,,
\end{aligned} \tag{C.43}$$

where the terms in red can be cancelled immediately. After rearranging, this equation can be written

$$\begin{aligned}
\frac{\mathrm{d}}{\mathrm{d}t}\sum^{\mathcal{N}} n_p n_j = \quad & \frac{D}{(mh)^2}\langle n_{p-1}n_j\rangle + \frac{D}{h^2}\langle n_p n_{j-1}\rangle + \frac{1}{m}\frac{D}{(mh)^2}\langle n_p n_p\rangle \\
+ \quad & \frac{D}{h^2}\langle n_p n_{j+1}\rangle + \sum_{i=p+1}^{p+m}\frac{D}{(mh)^2}\langle n_j n_i\rangle \\
- \quad & \frac{1}{m}\frac{D}{(mh)^2}M_p - \frac{D}{(mh)^2}M_j \\
- \quad & \left(2\frac{D}{h^2} + \frac{D}{(mh)^2} + 2\frac{m-1}{m}\frac{D}{(mh)^2}\right)\langle n_p n_j\rangle.
\end{aligned} \tag{C.44}$$

From this equation, we subtract

$$\begin{aligned}\frac{\mathrm{d}}{\mathrm{d}t}(M_pM_j) &= \frac{\mathrm{d}M_p}{\mathrm{d}t}M_j + M_p\frac{\mathrm{d}M_j}{\mathrm{d}t} \\ &= \left(\frac{D}{(mh)^2}M_{p-1} - 2\frac{D}{(mh)^2}M_p + \sum_{i=p+1}^{p+m}\frac{D}{(mh)^2}M_i\right)M_j \qquad \text{(C.45)} \\ &\quad + M_p\left(\frac{1}{m}\frac{D}{(mh)^2}M_p + \frac{D}{h^2}M_{j-1} - \left[\frac{D}{(mh)^2} + 2\frac{D}{h^2}\right]M_j + \frac{D}{h^2}M_{j+1}\right),\end{aligned}$$

to arrive at

$$\begin{aligned}\frac{\mathrm{d}V^{(c)}_{p,j}}{\mathrm{d}t} &= \frac{D}{(mh)^2}V^{(c)}_{p-1,j} + \frac{D}{h^2}V^{(c)}_{p,j-1} + \frac{1}{m}\frac{D}{(mh)^2}V^{(c)}_p \\ &\quad + \frac{D}{h^2}V^{(c)}_{p,j+1} + \sum_{i=p+1}^{p+m}\frac{D}{(mh)^2}V^{(c)}_{j,i} \\ &\quad - \frac{1}{m}\frac{D}{(mh)^2}M^{(c)}_p\left(1 - M^{(c)}_j\right) - \frac{D}{(mh)^2}M^{(c)}_j\left(1 - \frac{M^{(c)}_p}{m}\right) \\ &\quad - \left(2\frac{D}{h^2} + \frac{D}{(mh)^2} + 2\frac{m-1}{m}\frac{D}{(mh)^2}\right)V^{(c)}_{p,j}. \qquad \text{(C.46)}\end{aligned}$$

We now have all the terms necessary to analyse the evolution of $v^{(c)}_{p,p+1}$.

C.4.3 Combining covariance equations

Recalling that

$$\frac{\mathrm{d}v_{p,p+1}}{\mathrm{d}t} = \sum_{j=p+1}^{p+m}\frac{\mathrm{d}V_{p,j}}{\mathrm{d}t}, \qquad \text{(C.47)}$$

we can therefore write, after much scribbling and crying,

$$\begin{aligned}\frac{\mathrm{d}v_{p,p+1}}{\mathrm{d}t} &= \frac{D}{(mh)^2}\sum_{i=p+1}^{p+m}\sum_{j=p+1}^{p+m}V_{i,j} + \frac{D}{(mh)^2}\sum_{j=p+1}^{p+m}V_{p-1,j} + \frac{1}{m}\frac{D}{(mh)^2}\sum_{j=p+1}^{p+m}V_p \\ &\quad - \frac{1}{m}\frac{D}{(mh)^2}\sum_{j=p+1}^{p+m}M_p(1 - M_j) - \frac{D}{(mh)^2}\sum_{j=p+1}^{p+m}M_j\left(1 - \frac{M_p}{m}\right) \\ &\quad + \frac{D}{h^2}\sum_{j=p+1}^{p+m}V_{p,j+1} + \frac{D}{h^2}\sum_{j=p+2}^{p+m}V_{p,j-1} - \frac{D}{h^2}\sum_{j=p+1}^{p+m}V_{p,j} - \frac{D}{h^2}\sum_{j=p+2}^{p+m}V_{p,j} \\ &\quad - \left(2\frac{m-1}{m} + 1\right)\frac{D}{(mh)^2}\sum_{j=p+1}^{p+m}V_{p,j}. \qquad \text{(C.48)}\end{aligned}$$

We cancel out most of the terms from the third line of the equation above, and for the rest rewrite in terms of v and μ where possible, to obtain

$$\begin{aligned}\frac{\mathrm{d}v^{(c)}_{p,p+1}}{\mathrm{d}t} &= \frac{D}{(mh)^2}\left[v^{(c)}_{p+1} + v^{(c)}_{p-1,p+1} + V^{(c)}_{p} + m^2 V^{(c)}_{p,p+m+1}\right. \\ &\quad -M^{(c)}_{p}\left(1-\frac{\mu^{(c)}_{p+1}}{m}\right) - \mu^{(c)}_{p+1}\left(1-\frac{M^{(c)}_{p}}{m}\right) \\ &\quad \left.-\left(2\frac{m-1}{m}+1\right)v^{(c)}_{p,p+1} - m^2 V^{(c)}_{p,p+m}\right]. \end{aligned} \tag{C.49}$$

We recall that, on uniform lattices, the covariance equation is given by equation (3.27):

$$\begin{aligned}\frac{\mathrm{d}V_{j,j+1}}{\mathrm{d}t} &= \frac{D}{(mh)^2}\left[V^{(m)}_{j+1} + V^{(m)}_{j-1,j+1} + V^{(m)}_{j} + V^{(m)}_{j,j+2}\right. \\ &\quad -M^{(m)}_{j}\left(1-\frac{M^{(m)}_{j+1}}{m}\right) - M^{(m)}_{j+1}\left(1-\frac{M^{(m)}_{j}}{m}\right) \\ &\quad \left.-\left(2\frac{m-1}{m}+2\right)V^{(m)}_{j,j+1}\right], \end{aligned}$$

so equating the exchange $(D/h^2)(V_{p,p+m+1}-V_{p,p+m})$ with $(D/m^2h^2)(v_{p,p+2}-v_{p,p+1})$, by analogy to the linear interpolation arguments we used for the means, these equations match.

Appendix D

Appendices for Chapter 5

D.1 Uniformly distributing particles in volume-excluding systems

Several sections in Chapter 5 rely on randomising uniformly distributed initial particle positions, by which we mean that each possible starting configuration is equally likely. To clarify how this can be implemented in the context of a volume-excluding model, this appendix outlines the simple algorithm that we have used.

Let there be N particles to distribute over K compartments, each of capacity m_i where i is the compartment index. The total capacity of the system is therefore $\kappa = \sum_{i=1}^{K} m_i$. The algorithm is as follows:

1. Set $r_{lim} = \kappa$.
2. Initialise an array of length κ, within which the number 1 appears m_1 times, the number 2 appears m_2 times, and so on, up to K appearing m_K times.
3. Initialise an empty lattice of K empty compartments.
4. Generate a uniformly distributed random integer in the range, $r = [1, r_{lim}]$.
5. Take the value of the r^{th} entry of the array, and add one particle to the compartment with this index value on the lattice.

6. Delete the r^{th} entry of the array, so that it is now one entry shorter than it was before.

7. Set $r_{lim} = r_{lim} - 1$.

8. Set $N = N - 1$.

9. If N is still greater than zero, return to Step 4 and repeat.

D.2 Expected time to reaction from an initial uniform distribution

We recall equations (5.34), (5.36) and (5.39), which are restated here for convenience

$$\begin{aligned} E(0) &= \frac{4T^{\pm}(Km-1)+R}{4mT^{\pm}R+R^2}, \\ E(1) &= \frac{4T^{\pm}(Km-1)+mR(K-1)}{4mT^{\pm}R+R^2}, \\ E(k) &= E(1)+\frac{1}{4T^{\pm}}\left[K(k-1)-k^2+1\right], \;\; 1<k\leq n. \end{aligned}$$

Substituting equations (5.34), (5.36) and (5.39) into equation (5.41), we find

$$\begin{aligned} E(:) = \;& \frac{1}{K-\frac{1}{m}} \left(\frac{m-1}{m}E(0)+2\sum_{k=1}^{n-1}E(k)+E(n)\right) \\ = \;& \frac{m}{Km-1} \left(\frac{m-1}{m}E(0)+(2n-1)E(1)\right. \\ & \left. +\frac{1}{4T^{\pm}}\left[2K\sum_{k=2}^{n-1}(k-1)-2\sum_{k=2}^{n-1}k^2+2\sum_{k=2}^{n-1}1+K(n-1)-n^2+1\right]\right). \end{aligned} \tag{D.1}$$

The first of the summations in equation (D.1) can be evaluated by writing

$$\begin{aligned} 2K\sum_{k=2}^{n-1}(k-1) &= 2K\sum_{k=2}^{n-1}k-2K(n-2) = 2K\sum_{k=1}^{n-1}k-2K(n-1) \\ &= 2K\frac{1}{2}(n-1)n-2K(n-1) \\ &= K(n-1)(n-2). \end{aligned} \tag{D.2}$$

By similarly reasoning, we can write

$$\begin{aligned} -2\sum_{i=2}^{n-1} k^2 &= 2 - 2\sum_{i=1}^{n-1} k^2 \\ &= 2 - 2\frac{(n-1)n(2n-1)}{6}. \end{aligned} \tag{D.3}$$

Substituting equations (D.2) and (D.3) into equation (D.1), we obtain

$$\begin{aligned} E(:) = \frac{m}{Km-1} & \left(\frac{m-1}{m} E(0) + (2n-1)E(1) \right. \\ & + \frac{1}{4T^{\pm}} \left[K(n-1)(n-2) + 2 - \frac{(n-1)n(2n-1)}{3} \right. \\ & \left. \left. + K(n-1) + (2n-3) - n^2 \right] \right) \end{aligned} \tag{D.4}$$

$$\begin{aligned} = \frac{m}{Km-1} & \left(\frac{m-1}{m} \frac{4T^{\pm}(Km-1)+R}{4mT^{\pm}R+R^2} + (2n-1)\frac{4T^{\pm}(Km-1)+mR(K-1)}{4mT^{\pm}R+R^2} \right. \\ & \left. + \frac{1}{4T^{\pm}} \left[K(n-1)^2 + 2 - \frac{(n-1)n(2n-1)}{3} + (2n-3) - n^2 \right] \right), \end{aligned} \tag{D.5}$$

where equations (5.34) and (5.36) were used to state $E(0)$ and $E(1)$ explicitly. For consistency, we use $K = 2n$ to replace all n terms, arriving at

$$\begin{aligned} E(:) = \frac{m}{Km-1} & \left(\frac{m-1}{m} \frac{4T^{\pm}(Km-1)+R}{4mT^{\pm}R+R^2} + (K-1)\frac{4T^{\pm}(Km-1)+mR(K-1)}{4mT^{\pm}R+R^2} \right. \\ & \left. + \frac{1}{4T^{\pm}} \left[\frac{1}{4}K(K-2)^2 + 2 - \frac{(K-2)K(K-1)}{12} + (K-3) - \frac{1}{4}K^2 \right] \right) \end{aligned}$$

$$\begin{aligned} = \frac{m}{Km-1} & \left(\frac{m-1}{m} \frac{4T^{\pm}(Km-1)+R}{4mT^{\pm}R+R^2} + (K-1)\frac{4T^{\pm}(Km-1)+mR(K-1)}{4mT^{\pm}R+R^2} \right. \\ & \left. + \frac{1}{4T^{\pm}} \left[\frac{1}{6}K^3 - K^2 + \frac{11}{6}K - 1 \right] \right) \end{aligned} \tag{D.6}$$

$$\begin{aligned} = \frac{1}{Km-1} & \left((Km-1)\frac{4T^{\pm}(Km-1)}{4mT^{\pm}R+R^2} + \frac{(m-1)R+(Km-m)^2R}{4mT^{\pm}R+R^2} \right. \\ & \left. + \frac{1}{4T^{\pm}} \left[\frac{1}{6}K^3 - K^2 + \frac{11}{6}K - 1 \right] \right). \end{aligned} \tag{D.7}$$

We can now make substitutions to put as much of this expression as possible in terms of the scale invariant variables, $\kappa = Km$, $D = T^{\pm}m^2h^2$, and $r = Rm/2$:

$$E(:) = \frac{1}{\kappa - 1}\left((\kappa - 1)\frac{Dh^2(\kappa - 1)}{2Dh^2r + r^2} + \frac{m(m-1)r + m(\kappa - m)^2r}{4Dh^2r + 2r^2} + \frac{1}{4Dh^2}\left[\frac{1}{6}\kappa^3 - \kappa^2 m + \frac{11}{6}\kappa m^2 - m^3\right]\right) \quad \text{(D.8)}$$

$$= \frac{Dh^2(\kappa - 1)}{2Dh^2r + r^2} + \frac{1}{\kappa - 1}\left(\frac{m(m-1) + m(\kappa - m)^2}{4Dh^2 + 2r} + \frac{1}{4Dh^2}\left[\frac{1}{6}\kappa^3 - \kappa^2 m + \frac{11}{6}\kappa m^2 - m^3\right]\right), \quad \text{(D.9)}$$

which is the result stated in equation (5.42).

D.3 Expected time to steady-state in a conversion reaction

Recall that the expected time taken for the vCME model to reach the steady-state for a conversion reaction in one-spatial dimension is described by equations (5.50)-(5.52), which we restate here for convenience:

$$\begin{aligned} E_s(a) &= \frac{1}{2}E_s(a-1) + \frac{1}{2}E_s(a+1) + \frac{\kappa}{2k_2^t a(N-a)}, \\ E_s(0) &= 0, \\ E_s(N) &= 0. \end{aligned}$$

We can therefore write

$$\sum_{a=1}^{N-1} E_s(a) = \frac{1}{2}E_s(1) + \sum_{a=2}^{N-2} E_s(a) + \frac{1}{2}E_s(N-1) + \sum_{a=1}^{N-1}\frac{\kappa}{2k_2^t a(N-a)}, \quad \text{(D.10)}$$

where the right-hand side is obtained by using equation (5.50) to evaluate each term on the left-hand side. We can now subtract the summation

$$\sum_{a=2}^{N-2} E_s(a), \quad \text{(D.11)}$$

from both sides of equation (D.10), leaving us with

$$E_s(1) + E_s(N-1) = \frac{1}{2}E_s(1) + \frac{1}{2}E_s(N-1) + \sum_{a=1}^{N-1} \frac{\kappa}{2k_2^t a(N-a)}. \tag{D.12}$$

Using $E_s(1) = E_s(N-1)$ due to symmetry, and rearranging, we find

$$E_s(1) = \sum_{a=1}^{N-1} \frac{\kappa}{2k_2^t a(N-a)}. \tag{D.13}$$

By similar reasoning, we obtain an expression for $E_s(2)$:

$$\begin{aligned}
\sum_{a=2}^{N-2} E_s(a) &= \frac{1}{2}E_s(1) + \frac{1}{2}E_s(2) + \sum_{a=3}^{N-3} E_s(a) + \frac{1}{2}E_s(N-2) + \frac{1}{2}E_s(N-1) \\
&\quad + \sum_{a=2}^{N-2} \frac{\kappa}{2k_2^t a(N-a)}, \\
E_s(2) &= E_s(1) + \sum_{a=2}^{N-2} \frac{\kappa}{2k_2^t a(N-a)} && \text{(D.14)} \\
&= \sum_{i=1}^{2} \left[\sum_{a=i}^{N-i} \frac{\kappa}{2k_2^t a(N-a)} \right] && \text{(D.15)} \\
&= \frac{\kappa}{2k_2^t} \sum_{i=1}^{2} \left[\sum_{j=i}^{N-i} \frac{1}{j(N-j)} \right]. && \text{(D.16)}
\end{aligned}$$

By induction, we find that, for $a \leq (N/2)$,

$$E_s(a) = \frac{\kappa}{2k_2^t} \sum_{i=1}^{a} \left[\sum_{j=i}^{N-i} \frac{1}{j(N-j)} \right], \tag{D.17}$$

while for $a > (N/2)$ we can obtain a solution by symmetry by finding $E_s(N-a)$.

To obtain results for reactions in more than one spatial dimension, we simply modify equation (5.50). For example, in two spatial dimensions we use the reaction rate from expression (5.24) to write

$$E_{s,2}(a) = \frac{1}{2}E_{s,2}(a-1) + \frac{1}{2}E_{s,2}(a+1) + \frac{\sqrt{\kappa}+1}{\sqrt{\kappa}} \frac{\kappa}{4k_2^t a(N-a)}, \tag{D.18}$$

where we use a subscripted 2 to distinguish the two-dimensional case from the one-dimensional case considered previously. By identical reasoning to that used in one spatial dimension, we then find

$$E_{s,2}(a) = \frac{\sqrt{\kappa}+1}{\sqrt{\kappa}} \frac{\kappa}{4k_2^t} \sum_{i=1}^{a} \left[\sum_{j=i}^{N-i} \frac{1}{j(N-j)} \right]. \tag{D.19}$$

Bibliography

[1] P. C. Bressloff. *Stochastic Processes in Cell Biology*. Springer, 2014.

[2] C. V. Pao. On nonlinear reaction-diffusion systems. *J. Math. Anal. Appl.*, 87(1):165–198, 1982.

[3] D. T. Gillespie, A. Hellander, and L. R. Petzold. Perspective: Stochastic algorithms for chemical kinetics. *J. Chem. Phys.*, 138(17):170901, 2013.

[4] M. Delbrück. Statistical fluctuations in autocatalytic reactions. *J. Chem. Phys.*, 8(1):120–124, 1940.

[5] H. H. McAdams and A. Arkin. Stochastic mechanisms in gene expression. *Proc. Natl. Acad. Sci. USA*, 94(3):814–819, 1997.

[6] R. J. Ellis and A. P. Minton. Cell biology: join the crowd. *Nature*, 425(6953):27–28, 2003.

[7] J. Elf and M. Ehrenberg. Spontaneous separation of bi-stable biochemical systems into spatial domains of opposite phases. *Syst. Biol.*, 1:230–236, 2004.

[8] T. Nakanishi. Stochastic analysis of an oscillating chemical reaction. *J. Phys. Soc. Jpn.*, 32(5):1313–1322, 1972.

[9] D. T. Gillespie. A general method for numerically simulating the stochastic time evolution of coupled chemical reactions. *J. Comput. Phys.*, 22:403–434, 1976.

[10] C. A. Yates and G. Klingbeil. Recycling random numbers in the stochastic simulation algorithm. *J. Chem. Phys.*, 138:094103, 2013.

[11] A. Arkin, J. Ross, and H. H. McAdams. Stochastic kinetic analysis of developmental pathway bifurcation in phage λ-infected escherichia coli cells. *Genetics*, 149(4):1633–1648, 1998.

[12] M. B. Elowitz, A. J. Levine, E. D. Siggia, and P. S. Swain. Stochastic gene expression in a single cell. *Science*, 297:1183–1186, 2002.

[13] M. Kærn, T. C. Elston, W. J. Blake, and J. J. Collins. Stochasticity in gene expression: from theories to phenotypes. *Nat. Rev. Genet.*, 6:451–464, 2005.

[14] N. Fedoroff and W. Fontana. Small numbers of big molecules. *Science*, 297(5584):1129–1131, 2002.

[15] H. Kuthan. Self-organisation and orderly processes by individual protein complexes in the bacterial cell. *Prog. Biophys. Mol. Biol.*, 75:1–17, 2001.

[16] E. M. Ozbudak, M. Thattai, I. Kurtser, A. D. Grossman, and A. van Oudenaarden. Regulation of noise in the expression of a single gene. *Nat. Genet.*, 31:69–73, 2002.

[17] M. D. McDonnell and D. Abbott. What is stochastic resonance? Definitions, misconceptions, debates, and its relevance to biology. *PLoS Comput. Biol.*, 5:e1000348, 2009.

[18] A. Danchin, P. M. Binder, and S. Noria. Antifragility and tinkering in biology (and in business) flexibility provides an efficient epigenetic way to manage risk. *Genes*, 2:998–1016, 2011.

[19] C. Blomberg. Fluctuations for good and bad: The role of noise in living systems. *Phys. Life Rev.*, 3(3):133 – 161, 2006.

[20] M. Samoilov, S. Plyasunov, and A. P. Arkin. Stochastic amplification and signaling in enzymatic futile cycles through noise-induced bistability with oscillations. *Proc. Natl. Acad. Sci. USA*, 102:2310–2315, 2005.

[21] L. M. Bishop and H. Qian. Stochastic bistability and bifurcation in a mesoscopic signalling system with autocatalytic kinase. *Biophys. J.*, 98:1–11, 2010.

[22] J. Paulsson, O. G. Berg, and M. Ehrenberg. Stochastic focusing: fluctuation-enhanced sensitivity of intracellular regulation. *Proc. Natl. Acad. Sci. USA*, 97:7148–7153, 2000.

[23] L. Gammaitoni, P. Hänggi, P. Jung, and F. Marchesoni. Stochastic resonance. *Rev. Mod. Phys.*, 70:223, 1998.

[24] Z. Hou and H. Xin. Internal noise stochastic resonance in a circadian clock system. *J. Chem. Phys.*, 119:11508, 2003.

[25] C. A. Yates, R. Erban, C. Escudero, I. D. Couzin, J. Buhl, I. G. Kevrekidis, P. K. Maini, and D. J. T. Sumpter. Inherent noise can facilitate coherence in collective swarm motion. *Proc. Natl. Acad. Sci. USA*, 106:5464–5469, 2009.

[26] C. Escudero, C. A. Yates, J. Buhl, I. D. Couzin, R. Erban, I. G. Kevrekidis, and P. K. Maini. Ergodic directional switching in mobile insect groups. *Phys. Rev. E*, 82:011926, 2010.

[27] A. J. McKane and T. J. Newman. Predator-prey cycles from resonant amplification of demographic stochasticity. *Phys. Rev. Lett.*, 94:218102, 2005.

[28] C. A. Lugo and A. J. McKane. Quasicycles in a spatial predator-prey model. *Phys. Rev. E*, 78:051911, 2008.

[29] A. J. Black and A. J. McKane. Stochastic formulation of ecological models and their applications. *Trends Ecol. Evol.*, 27(6):337–345, 2012.

[30] T. Lenormand, D. Roze, and F. Rousset. Stochasticity in evolution. *Trends Ecol. Evol.*, 24:157–165, 2009.

[31] J. D. Murray. Parameter space for turing instability in reaction diffusion mechanisms: a comparison of models. *J. Theor. Biol.*, 98:143–163, 1982.

[32] T. E. Woolley, R. E. Baker, E. A. Gaffney, and P. K. Maini. Power spectra methods for a stochastic description of diffusion on deterministic growing domains. *Phys. Rev. E*, 84:021915, 2011.

[33] T. E. Woolley, R. E. Baker, E. A. Gaffney, and P. K. Maini. Influence of stochastic domain growth on pattern nucleation for diffusive systems with internal noise. *Phys. Rev. E*, 84:041905, 2011.

[34] T. E. Woolley, R. E. Baker, E. A. Gaffney, and P. K. Maini. Stochastic reaction and diffusion on growing domains: understanding the breakdown of robust pattern formation. *Phys. Rev. E*, 84:046216, 2011.

[35] H. C. Berg. *Random Walks in Biology.* Princeton University Press, 1993.

[36] G. Kallianpur and P. Sundar. *Stochastic Analysis and Diffusion Processes.* Oxford University Press, 2014.

[37] R. E. Baker, C. A. Yates, and R. Erban. From microscopic to macroscopic descriptions of cell migration on growing domains. *Bull. Math. Biol.*, 72:719–762, 2010.

[38] N. M. Shnerb, Y. Louzoun, E. Bettelheim, and S. Solomon. The importance of being discrete: Life always wins on the surface. *Proc. Natl. Acad. Sci. USA*, 97:10322–10324, 2000.

[39] R. E. Baker and M. J. Simpson. Correcting mean-field approximations for birth-death-movement processes. *Phys. Rev. E*, 82:041905, 2010.

[40] S. G. Farrell, A. I. Brown, and A. D. Rutenberg. Single file diffusion into a semi-infinite tube. *Phys. Biol.*, 12(6):064001, 2015.

[41] A. S. Stern and H. C. Berg. Single-file diffusion of flagellin in flagellar filaments. *Biophys. J.*, 105(1):182 – 184, 2013.

[42] S. Y. Yang, J. Yang, E. Kim, G. Jeon, E. J. Oh, K. Y. Choi, S. K. Hahn, and J. K. Kim. Single-file diffusion of protein drugs through cylindrical nanochannels. *ACS Nano*, 4(7):3817–3822, 2010. PMID: 20507175.

[43] B. Alberts, A. Johnson, J. Lewis, M. Raff, K. Roberts, and P. Walter. *Molecular Biology of the Cell*. Garland Science, 2008.

[44] B. Bénazéraf, P. Francois, R. E. Baker, N. Denans, C. D. Little, and O. Pourquié. A random cell motility gradient downstream of FGF controls elongation of an amniote embryo. *Nature*, 466:248–252, 2010.

[45] R. N. Thompson, C. A. Yates, and R. E. Baker. Modelling cell migration and adhesion during development. *Bull. Math. Biol.*, 74:2793–809, 2012.

[46] M. J. Simpson, K. K. Treloar, B. J. Binder, P. Haridas, K. J. Manton, D. I. Leavesley, D. L. S. McElwain, and R. E. Baker. Quantifying the roles of cell motility and cell proliferation in a circular barrier assay. *J. Roy. Soc. Interface*, 10:20130007, 2013.

[47] T. Callaghan, E. Khain, L. M. Sander, and R. M. Ziff. A stochastic model for wound healing. *J. Stat. Phys.*, 122:909–924, 2006.

[48] D. C. Markham, M. J. Simpson, P. K. Maini, E. A. Gaffney, and R. E. Baker. Comparing methods for modelling spreading cell fronts. *J. Theor. Biol.*, 353(0):95 – 103, 2014.

[49] J. V. Ross and B. J. Binder. Approximating spatially exclusive invasion processes. *Phys. Rev. E*, 89:052709, 2014.

[50] H. G. Othmer, S. R. Dunbar, and W. Alt. Models of dispersal in biological systems. *J. Math. Biol.*, 26:263–298, 1988.

[51] F. Débarre, C. Hauert, and M. Doebeli. Social evolution in structured populations. *Nat. Commun.*, 5:3409, 2014.

[52] S. Engblom, L. Ferm, A. Hellander, and P. Lötstedt. Simulation of stochastic reaction-diffusion processes on unstructured meshes. *SIAM J. Sci. Comput.*, 31:1774–1797, 2009.

[53] S. A. Isaacson and C. S. Peskin. Incorporating diffusion in complex geometries into stochastic chemical kinetics simulations. *SIAM J. Sci. Comput.*, 28:47–74, 2006.

[54] C. A. Yates and R. E. Baker. Importance of the voronoi domain partition for position-jump reaction-diffusion processes on nonuniform rectilinear lattices. *Phys. Rev. E*, 88:054701, 2013.

[55] C. A. Yates, R. E. Baker, R. Erban, and P. K. Maini. Going from microscopic to macroscopic on nonuniform growing domains. *Phys. Rev. E*, 86:021921, 2012.

[56] S. A. Isaacson. A convergent reaction-diffusion master equation. *J. Chem. Phys.*, 139:054101, 2013.

[57] C. A. Yates and M. B. Flegg. The pseudo-compartment method for coupling partial differential equation and compartment-based models of diffusion. *J. Roy. Soc. Interface*, 12(106), 2015.

[58] M. B. Flegg, S. J. Chapman, L. Zheng, and R. Erban. Analysis of the two-regime method on square meshes. *SIAM J. Sci. Comput.*, 36:B561–588, 2014.

[59] T. Fricke and J. Schnakenberg. Monte-Carlo simulation of an inhomogeneous reaction-diffusion system in the biophysics of receptor cells. *Z. Phys. B - Condensed Matter*, 83:277–284, 1991.

[60] D. Bernstein. Simulating mesoscopic reaction-diffusion systems using the Gillespie algorithm. *Phys. Rev. E*, 71:041103, 2005.

[61] D. F Anderson and D. J. Higham. Multilevel monte carlo for continuous time markov chains, with applications in biochemical kinetics. *Multiscale. Model. Simul.*, 10(1):146–179, 2012.

[62] C. Lester, C. A. Yates, M. B. Giles, and R. E. Baker. An adaptive multi-level simulation algorithm for stochastic biological systems. *J. Chem. Phys.*, 142(2), 2015.

[63] C. Lester, R. E. Baker, M. B. Giles, and C. A. Yates. Extending the multi-level method for the simulation of stochastic biological systems. *Bull. Math. Biol.*, 2016.

[64] H. Kuwahara and I. Mura. An efficient and exact stochastic simulation method to analyze rare events in biochemical systems. *J. Chem. Phys.*, 129(16), 2008.

[65] D. T. Gillespie, M. Roh, and L. R. Petzold. Refining the weighted stochastic simulation algorithm. *J. Chem. Phys.*, 130(7), 2009.

[66] D. T. Gillespie. Approximate accelerated stochastic simulation of chemically reacting systems. *J. Chem. Phys.*, 115:1716–1733, 2001.

[67] M. Rathinam, L. Petzold, Y. Cao, and D. T. Gillespie. Stiffness in stochastic chemically reacting systems: the implicit tau-leaping method. *J. Chem. Phys.*, 119:12784–94, 2003.

[68] Y. Cao, D. T. Gillespie, and L. R. Petzold. Efficient step size selection for the tau-leaping simulation method. *J. Chem. Phys.*, 124:044109, 2006.

[69] A. Auger, P. Chatelain, and P. Koumoutsakos. R-leaping: Accelerating the stochastic simulation algorithm by reaction leaps. *J. Chem. Phys.*, 125(8), 2006.

[70] S. Lampoudi, D. T. Gillespie, and L. R. Petzold. The multinomial simulation algorithm for discrete stochastic simulation of reaction-diffusion systems. *J. Chem. Phys.*, 130:094104, 2009.

[71] F. Spill, P. K. Maini, and H. M. Byrne. Optimisation of simulations of stochastic processes by removal of opposing reactions. *J. Chem. Phys.*, 144(8), 2016.

[72] B. Bayati, P. Chatelain, and P. Koumoutsakos. Adaptive mesh refinement for stochastic reaction–diffusion processes. *J. Comput. Phys.*, 230:13–26, 2011.

[73] M. A. Gibson and J. Bruck. Efficient exact stochastic simulation of chemical systems with many species and many channels. *J. Phys. Chem. A*, 104:1876–1889, 2000.

[74] Y. Cao, H. Li, and L. Petzold. Efficient formulation of the stochastic simulation algorithm for chemically reacting systems. *J. Chem. Phys.*, 121:4059, 2004.

[75] J. M. McCollum, G. D. Peterson, C. D. Cox, M. L. Simpson, and N. F. Samatova. The sorting direct method for stochastic simulation of biochemical systems with varying reaction execution behavior. *Comp. Biol. Chem.*, 30(1):39 – 49, 2006.

[76] H. Li and L. Petzold. Logarithmic direct method for discrete stochastic simulation of chemically reacting systems. Technical report, Department of Computer Science, University of California Santa Barbara, 2006.

[77] A. Okubo. *Diffusion and Ecological Problems, Mathematical Models.* Springer-Verlag, 1980.

[78] F. J. R. Meysman, B. P. Boudreau, and J. J. Middelburg. Relations between local, nonlocal, discrete and continuous models of bioturbation. *J. Mar. Res.*, 61:391–410, 2003.

[79] P. R. Taylor, R. E. Baker, and C. A. Yates. Deriving appropriate boundary conditions, and accelerating position-jump simulations, of diffusion using non-local jumping. *Phys. Biol.*, 12(1):016006, 2015.

[80] K. Painter and T. Hillen. Volume-filling and quorum-sensing in models for chemosensitive movement. *Can. Appl. Math. Quart.*, 10:501–543, 2002.

[81] K. Anguige and C. Schmeiser. A one-dimensional model of cell diffusion and aggregation, incorporating volume filling and cell-to-cell adhesion. *J. Math. Biol.*, 58(3):395–427, 2009.

[82] M. Mourão, D. Kreitman, and S. Schnell. Unravelling the impact of obstacles in diffusion and kinetics of an enzyme catalysed reaction. *Phys. Chem. Chem. Phys.*, 16:4492, 2014.

[83] S. Redner. *A Guide to First-Passage Processes.* Cambridge University Press, 2001.

[84] Y. Cao and L. Petzold. Accuracy limitations and the measurement of errors in the stochastic simulation of chemically reacting systems. *J. Comput. Phys.*, 212:6–24, 2006.

[85] K. R. Swanson. Quantifying glioma cell growth and invasion in vitro. *Math. Comput. Model.*, 47(5–6):638 – 648, 2008.

[86] R. Zwanzig. Diffusion-controlled ligand binding to spheres partially covered by receptors: An effective medium treatment. *Proc. Natl. Acad. Sci. USA.*, 1990.

[87] R. Erban and S. J. Chapman. Reactive boundary conditions for stochastic simulations of reaction-diffusion processes. *Phys. Biol.*, 4:16–28, 2007.

[88] W. Alt. Biased random walk models for chemotaxis and related diffusion approximations. *J. Math. Biol.*, 9(2):147–177, 1980.

[89] S. Turner, J. A. Sherratt, and K. J. Painter. From a discrete to a continuous model of biological cell movement. *Phys. Rev. E*, 69:021910, 2004.

[90] P. R. Taylor, C. A. Yates, M. J. Simpson, and R. E. Baker. Reconciling transport models across scales: The role of volume exclusion. *Phys. Rev. E*, 92:040701(R), 2015.

[91] E. Khain, M. Khasin, and L. M. Sander. Spontaneous formation of large clusters in a lattice gas above the critical point. *Phys. Rev. E*, 90:062702, 2014.

[92] D. T. Gillespie and E. Seitaridou. *Simple Brownian Diffusion*. Oxford University Press, 2012.

[93] R. Erban, S. J. Chapman, and P. K. Maini. A practical guide to stochastic simulations of reaction-diffusion processes. arXiv, 2007.

[94] B. Franz, M. B. Flegg, S. J. Chapman, and R. Erban. Multiscale reaction-diffusion algorithms: PDE-assisted Brownian dynamics. *SIAM J. Appl. Math.*, 73:1224–1247, 2013.

[95] M. B. Flegg, S. Hellander, and R. Erban. Convergence of methods for coupling of microscopic and mesoscopic reaction-diffusion simulations. *J. Comput. Phys.*, 289(C):1–17, May 2015.

[96] M. Meier-Schellersheim, I. D. C. Fraser, and F. Klauschen. Multi-scale modeling in cell biology. *Wiley Interdiscip. Rev. Syst. Biol. Med.*, 1(1):4–14, 2009.

[97] P. R. Taylor, R. E. Baker, M. J. Simpson, and C. A. Yates. Coupling volume-excluding compartment-based models of diffusion at different scales: Voronoi and pseudo-compartment approaches. *J. Roy. Soc. Interface.*, 13(120), 2016.

[98] J. Walpole, J. A. Papin, and S. M. Peirce. Multiscale computational models of complex biological systems. *Annu. Rev. Biomed. Eng.*, 15:137–54, 2013.

[99] M. Klann, A. Ganguly, and H. Koeppl. Hybrid spatial Gillespie and particle tracking simulation. *Bioinformatics*, 28(18):i549–i555, 2012.

[100] M. B. Flegg, S. Rüdiger, and R. Erban. Diffusive spatio-temporal noise in a first-passage time model for intracellular calcium release. *J. Chem. Phys.*, 138(15), 2013.

[101] M. B. Flegg, S. J. Chapman, and R. Erban. The two-regime method for optimizing stochastic reaction-diffusion simulations. *J. Roy. Soc. Interface.*, 9:859–868, 2012.

[102] M. Robinson, M. B. Flegg, and R. Erban. Adaptive two-regime method: Application to front propagation. *J. Chem. Phys.*, 140(12):124109, 2014.

[103] L. Ferm, A. Hellander, and P. Lötstedt. An adaptive algorithm for simulation of stochastic reaction–diffusion processes. *J. Comput. Phys.*, 229(2):343 – 360, 2010.

[104] E. Moro. Hybrid method for simulating front propagation in reaction-diffusion systems. *Phys. Rev. E*, 69:060101, 2004.

[105] T. Bollenbach, K. Kruse, P. Pantazis, M. González-Gaitán, and F. Jülicher. Robust formation of morphogen gradients. *Phys. Rev. Lett.*, 94:018103, Jan 2005.

[106] F. Tostevin, P. R. ten Wolde, and M. Howard. Fundamental limits to position determination by concentration gradients. *PLoS Comput. Biol.*, 3(4):1–9, 2007.

[107] D. T. Gillespie. Exact stochastic simulation of coupled chemical reactions. *J. Phys. Chem.*, 81:2340–2361, 1977.

[108] M. J. Simpson, K. A. Landman, and B. D. Hughes. Multi-species simple exclusion processes. *Physica A*, 388(4):399–406, 2009.

[109] D. T. Gillespie. A rigorous derivation of the chemical master equation. *Physica A*, 188:404–425, 1992.

[110] K. Takahashi, S. Tănase-Nicola, and P. Rein ten Wolde. Spatio-temporal correlations can drastically change the response of a MAPK pathway. *Proc. Natl. Acad. Sci. USA*, 107(6):2473–2478, 2010.

[111] C. W. Gardiner, K. J. McNeil, D. F. Walls, and I. S. Matheson. Correlations in stochastic theories of chemical reactions. *J. Stat. Phys.*, 14(4):307–331, 1976.

[112] D. Fange and J. Elf. Noise-induced Min phenotypes in E. coli. *PLoS Comput. Biol.*, 2(6):e80, 2006.

[113] S. Smith, C. Cianci, and R. Grima. Analytical approximations for spatial stochastic gene expression in single cells and tissues. *J. Roy. Soc. Interface.*, 13(118), 2016.

[114] A. J. McKane and T. J. Newman. Stochastic models in population biology and their deterministic analogs. *Phys. Rev. E*, 70:041902, 2004.

[115] S. A. Isaacson. The reaction-diffusion master equation as an asymptotic approximation of diffusion to a small target. *SIAM J. Appl. Math.*, 70:77–111, 2009.

[116] S. Hellander, A. Hellander, and L. Petzold. Reaction-diffusion master equation in the microscopic limit. *Phys. Rev. E*, 85(4):042901, 2012.

[117] S. Hellander, A. Hellander, and L. Petzold. Reaction rates for mesoscopic reaction-diffusion kinetics. *Phys. Rev. E*, 91:023312, 2015.

[118] S. Hellander and L. Petzold. Reaction rates for a generalized reaction-diffusion master equation. *Phys. Rev. E*, 93:013307, 2016.

[119] C. Cianci, S. Smith, and R. Grima. Molecular finite-size effects in stochastic models of equilibrium chemical systems. *J. Chem. Phys.*, 144(8):084101, 2016.

[120] D. J. Wilkinson. *Stochastic Modelling for Systems Biology.* Chapman & Hall / CRC, 2006.

[121] L. Meinecke and M. Eriksson. Excluded volume effects in on- and off-lattice reaction-diffusion models. arXiv:1604.06660, 2016.

[122] C. G. Hill and T. W. Root. *Introduction to Chemical Engineering Kinetics and Reactor Design.* John Wiley & Sons, 2014.

[123] R. Chang. *Phyical Chemistry for the Biosciences.* University Science Books, 2005.

[124] N. G. van Kampen. *Stochastic Processes in Physics and Chemistry.* Elsevier, third edition, 2008.

[125] S. Succi. *The Lattice Boltzmann Equation, For Fluid Dynamics and Beyond.* Oxford University Press, 2001.

[126] R. Grima and S. Schnell. A systematic investigation of the rate laws valid in intracellular environments. *Biophys. Chem.*, 124(1):1–10, 2006.

[127] C. Deroulers, M. Aubert, M. Badoual, and B. Grammaticos. Modeling tumor cell migration: from microscopic to macroscopic models. *Phys. Rev. E*, 79:031917, 2009.

[128] A. J. Ellery, R. E. Baker, S. W. McCue, and M. J. Simpson. Modeling transport through an environment crowded by a mixture of obstacles of different shapes and sizes. *Physica A*, 449:74–84, 2016.

[129] C. A. Yates, A. Parker, and R. E. Baker. Incorporating pushing in exclusion-process models of cell migration. *Phys. Rev. E*, 91:052711, 2015.

[130] G. Grimmett and D. Stirzaker. *Probability and Random Processes.* Oxford University Press, third edition, 2001.

[131] G. F. Lawler. *Introduction to Stochastic Processes.* Chapman and Hall/CRC, second edition, 2006.